

# SEISMIC SHEAR DEMAND IN HIGH-RISE CONCRETE WALLS

by

BABAK RAJAEI RAD

B.Sc., The University of Tehran, 2000

M.Sc., The University of Tehran, 2003

A THESIS SUBMITTED IN PARTIAL FULFILLMENT OF  
THE REQUIREMENTS FOR THE DEGREE OF

DOCTOR OF PHILOSOPHY

in

THE FACULTY OF GRADUATE STUDIES

(Civil Engineering)

THE UNIVERSITY OF BRITISH COLUMBIA

(Vancouver)

March 2009

© Babak Rajaei Rad, 2009

## **Abstract**

Concrete shear walls are used as the seismic force resisting system in many high-rise buildings in Western Canada. During earthquake, the response of a high-rise concrete wall as it undergoes severe cracking of concrete and yielding of reinforcement is very complex. In particular, the nonlinear shear behaviour of concrete shear walls is not well known; therefore available analysis programs generally use very primitive models for nonlinear shear behaviour. Gérin and Adebar (2004) quantified the observed experimental results on reinforced concrete membrane elements and presented a simple nonlinear shear model that included the influence of concrete diagonal cracking, yielding of horizontal reinforcement and ultimate shear capacity.

There are a number of important issues in the design of high-rise concrete shear walls where shear deformations play a very important role and hence nonlinear shear behaviour will have a significant influence. In this dissertation, three different seismic design issues where nonlinear shear response plays a significant role are investigated.

The first issue which is of considerable concern to designers is the large reverse shear force in high-rise concrete walls due to rigid diaphragms below the flexural plastic hinge. The nonlinear analyses that were carried out in this study show that diagonal cracking and yielding of horizontal reinforcement significantly reduce the magnitude of reverse shear force compared to what is predicted by using linear analysis procedures.

A second issue where nonlinear shear behaviour has a significant influence is associated with the shear force distribution between inter-connected high-rise walls of different lengths. The results presented in this work, show that when diagonal cracking is included in the analysis, significant redistribution of shear forces takes place between walls and all walls do not necessarily yield at the same displacement.

The third issue is related to the dynamic shear demand caused by influence of higher modes and the corresponding nonlinear action that takes place in tall cantilever walls. According to the nonlinear dynamic analyses that were performed, the influence of hysteretic shear response on the seismic demand of high-rise concrete walls was investigated.

# Table of Contents

Abstract .....	ii
Table of Contents .....	iii
List of Tables .....	vi
List of Figures .....	ix
List of Symbols and Abbreviations .....	xvii
Acknowledgments.....	xxii
Dedication .....	xxiii
<b>Chapter 1: Introduction .....</b>	<b>1</b>
1.1 High-rise concrete shear wall buildings.....	1
1.2 Seismic design of high-rise buildings .....	1
1.3 Nonlinear shear behaviour of concrete walls.....	3
1.4 Seismic shear demand issues in high-rise concrete buildings .....	5
1.5 Thesis objectives .....	10
1.6 Thesis organization .....	11
<b>Chapter 2: Literature review .....</b>	<b>13</b>
2.1 Nonlinear flexural response in reinforced concrete walls.....	13
2.2 Nonlinear shear response in reinforced concrete walls.....	16
2.3 Seismic shear force demand at levels below ground .....	27
2.4 Seismic shear force distribution between inter-connected walls .....	34
2.5 Dynamic shear force demand on cantilever concrete walls.....	37
<b>Chapter 3: Seismic shear demand in high-rise walls below ground .....</b>	<b>49</b>
3.1 Overview .....	49
3.2 Model definition.....	51
3.2.1 Diaphragm stiffness below ground .....	55
3.2.2 Foundation wall influence.....	58
3.2.3 Flexural and shear deformation of the wall .....	59

3.2.4 Effect of wall footing partial fixity .....	62
3.3 Dynamic response .....	64
3.3.1 Linear dynamic response .....	65
3.3.2 Nonlinear dynamic response.....	67
3.3.3 Shear-flexure interaction .....	82
3.4 Nonlinear static analysis .....	83
3.4.1 Nonlinear shear behaviour in concrete walls .....	84
3.4.2 Reversal shear solution through a design example .....	92
3.5 Nonlinear shear response of concrete floor diaphragms.....	101
3.6 Procedure for design of the shear wall below ground.....	102
3.7 Summary and Conclusions .....	105
 <b>Chapter 4: Seismic shear demand in inter-connected high-rise walls .....</b>	<b>106</b>
4.1 Overview.....	106
4.2 Model of two walls .....	108
4.3 Nonlinear analysis.....	111
4.3.1 Model assumptions .....	111
4.3.2 Moment to shear ratio at the base .....	114
4.3.2 Analysis parameters and results.....	115
4.4 Simplified effective stiffness approach .....	128
4.5 Conclusions.....	140
 <b>Chapter 5: Dynamic shear demand in high-rise concrete walls .....</b>	<b>143</b>
5.1 Overview.....	143
5.2 Model of high-rise wall in this study .....	144
5.3 Ground motions used for dynamic analysis.....	145
5.3.1 Ground motion scaling.....	147
5.3.2 Acceleration records used for analysis .....	151
5.4 Linear time history analysis (LTHA) vs. response spectrum analysis (RSA) .....	152
5.5 Nonlinear time history analysis .....	154
5.5.1 Model definition.....	155

5.5.2 Hysteretic models.....	156
5.6 Influence of flexural strength in the model of high-rise wall .....	156
5.7 Influence of effective shear stiffness due to diagonal cracking.....	160
5.8 Influence of degrading hysteretic shear response .....	179
5.8.1 Estimate of shear strength at cracking .....	180
5.8.2 Estimate of shear strength at yielding.....	181
5.9 Discussion of dynamic response due to hysteretic shear model .....	187
5.10 Summary and Conclusions .....	205
 <b>Chapter 6: Conclusions and recommendations for future studies.....</b>	<b>207</b>
6.1 Introduction.....	207
6.2 Summary and conclusions of present study.....	209
6.2.1 Seismic shear demand below grade in high-rise concrete walls.....	209
6.2.2 Seismic shear force distribution in connected high-rise walls.....	211
6.2.3 Dynamic shear demand on high-rise concrete walls.....	212
6.3 Recommendations for future studies .....	214
 <b>References.....</b>	<b>215</b>
 <b>Appendices.....</b>	<b>220</b>
Appendix A: Ground motions used for dynamic analysis .....	220
Appendix B: Response spectra for selected ground motions.....	230
Appendix C: Nonlinear time history analysis results for Section 3.3.2.....	234
Appendix D: Nonlinear time history analysis envelopes for Section 5.8 .....	240

## List of Tables

Table 2.1 Specification of PDV elements tested by Villani (1995).....	17
Table 2.2 Ratio of shear force at the first below-ground level to base shear for different analysis cases in study by Bevan-Pritchard, Man and Anderson (1983) ....	33
Table 2.3 Different procedures to determine dynamic shear amplification factor....	48
Table 3.1 Possible diaphragm stiffness used in practice (values in MN/mm).....	56
Table 3.2 Diaphragm stiffness used for analysis cases.....	56
Table 3.3 Wall sections used for analysis cases .....	59
Table 3.4 Ground motions used for NTHA .....	74
Table 3.5 Target overturning moment (kNm) at base of wall for different cases of nonlinear static analysis in this study.....	88
Table 4.1 Geometrical properties of the walls shown in Fig. 4.1 .....	109
Table 4.2 Summary of forces determined at base of walls from linear static analysis.....	113
Table 4.3 Nonlinear flexural model parameters used for concrete walls in example.....	113
Table 4.4 Nonlinear shear model parameters used for analysis.....	113
Table 4.5 Nonlinear flexure and shear models used for analysis .....	115
Table 4.6 Nonlinear states captured by Model 1 .....	117
Table 4.7 Nonlinear states captured by Model 2 .....	118
Table 4.8 Nonlinear states captured by Model 3 .....	120
Table 4.9 Nonlinear states captured by Model 4 .....	122
Table 4.10 Nonlinear states captured by Model 5 .....	124
Table 4.11 Nonlinear states captured according to Fig. 4.9.....	125
Table 4.12 Nonlinear states captured according to Fig. 4.10.....	126
Table 4.13 Section properties for walls shown in Fig. 4.12 .....	129
Table 4.14 Resulting moments and shear forces for $W1$ in Case 1.....	130
Table 4.15 Tri-linear flexural and shear models used for $W1$ in Case 1.....	130
Table 4.16 Resulting moments and shear forces for $W2$ in Case 1.....	130
Table 4.17 Tri-linear flexural and shear models used for $W2$ in Case 1.....	130
Table 4.18 Nonlinear states captured by Case 1 according to Fig. 4.12.....	132
Table 4.19 Nonlinear states captured by Case 1-2 according to Fig. 4.13 .....	134

Table 4.20 Resulting moments and shear forces for $W1$ in Case 2.....	135
Table 4.21 Tri-linear flexural and shear models used for $W1$ in Case 2.....	135
Table 4.22 Resulting moments and shear forces for $W2$ in Case 2.....	135
Table 4.23 Tri-linear flexural and shear models used for $W2$ in Case 2.....	135
Table 4.24 Nonlinear states captured by Case 2 according to Fig. 4.14.....	137
Table 4.25 Tri-linear flexural and shear models for $W1$ and $W2$ in Case 3.....	138
Table 4.26 Nonlinear states captured by Case 2 according to Fig. 4.15.....	139
Table 4.27 Shear force distribution between walls relative to their initial uncracked case .....	139
Table 5.1 Set of recorded earthquakes used in <i>FEMA-440 (ATC-2005)</i> for site class C .....	146
Table 5.2 Selected subduction records from Tokachi-Oki earthquake .....	147
Table 5.3 Final selection of records used for analysis.....	152
Table 5.4 Scaling factors used for final selection of records .....	152
Table 5.5 Parameters used to define tri-linear moment-curvature response.....	157
Table 5.6 Shear demand obtained from nonlinear dynamic analysis (values in kN) .....	168
Table 5.7 Amount of shear demand increase in Case SH with respect to Case MH .....	169
Table 5.8 Dynamic shear amplification for nonlinear response history analysis vs. RSA .....	169
Table 5.9 Dynamic shear force demand at the base obtained from crustal events for different effective shear stiffness (values in kN) .....	176
Table 5.10 Dynamic shear force demand at the base obtained from subduction events for different effective shear stiffness (values in kN) .....	177
Table 5.11 Mean dynamic shear force demand at the base obtained from different earthquake events for different effective shear stiffness (values in kN).....	177
Table 5.12 Mean dynamic shear force amplification at the base with respect to shear force demand obtained from RSA.....	178
Table 5.13 Ratios of $h'/H$ for walls according to RSA of different design spectra .....	182
Table 5.14 Ratios of $h'/H$ for walls according to LTHA for different earthquakes ..	183
Table 5.15 Nonlinear shear model used in the example of wall.....	186
Table 5.16 Shear force demand at different sections of wall for $R=2.0$ and $SF=1.0$ .....	191

Table 5.17 Shear force demand at different section of wall for $R=3.5$ and $SF=1.0$ .....	192
Table 5.18 Shear force demand at different sections of wall for $R=5.0$ and $SF=1.0$ .....	195
Table 5.19 Shear force demand at different sections of wall for $R=3.5$ and $SF=1.5$ .....	197
Table 5.20 Shear force demand at different sections of wall for $R=5.0$ and $SF=1.5$ .....	198
Table 5.21 Shear force demand at different sections of wall for $R=5.0$ and $SF=2.0$ .....	201



## List of Figures

Figure 1.1 Structural system in a typical high-rise concrete shear wall building including the underground portion of the building .....	2
Figure 1.2 – Shear stress versus shear strain response of a reinforced concrete element tested by Villani (1995) (from Gérin, 2003) .....	4
Figure 1.3 – Commonly assumed brittle shear behaviour (dashed line) versus the actual shear behaviour of concrete shear walls according to the Gérin-Adebar model (solid line) .....	5
Figure 1.4 Seismic shear force demand below base level .....	6
Figure 1.5 Regions where flexure and shear stiffnesses influence the shear force distribution in inter-connected high-rise walls, and self-equilibrating forces resulting from flexural yielding in the longer wall .....	8
Figure 1.6 Shear force distributions in a cantilever high-rise concrete wall .....	10
Figure 2.1 Moment-curvature response of a typical high-rise core wall .....	15
Figure 2.2 Shear stress-shear strain responses for shear wall elements: a) PDV1, b) PDV2, c) PDV3 (from Gérin, 2003) .....	18
Figure 2.3 Simplified prediction response as bi-linear and tri-linear envelopes: a) PDV1, b) PDV2, c) PDV3 (from Gérin, 2003) .....	19
Figure 2.4 Contribution to shear strain at yield for typical shear walls (from Gérin, 2004) .....	22
Figure 2.5 Shear strain ductility with respect to developed shear stress (from Gérin, 2004) .....	22
Figure 2.6 Comparison between different estimates of shear stress at cracking .....	24
Figure 2.7 Proposed load-deformation curve for nonlinear static analysis by Gérin (2004), shown for membrane element SE8 tested by Stevens et al. 1991 .....	25
Figure 2.8 Proposed simplified hysteretic model by Gérin (2004), shown for membrane element test SE8 (Stevens et al. 1991) .....	26

Figure 2.9 Plan and elevation section of the subgrade structure which include core wall, perimeter walls and parking slabs (from Bevan-Pritchard, Man and Anderson 1983).....	27
Figure 2.10 Model used to study force demand at subgrade structure by Bevan-Pritchard, Man and Anderson (1983).....	28
Figure 2.11 Moment distribution for applied concentrated moment at grade for Rigid perimeter walls (a) fixed footing (b) pinned footing (from Bevan-Pritchard, Man and Anderson 1983). ....	29
Figure 2.12 Influence of diaphragm stiffness on moment and shear force distribution (from Bevan-Pritchard, Man and Anderson 1983).....	30
Figure 2.13 Influence of diaphragm stiffness on moment and shear force distribution for simultaneously applied concentrated moment and shear at grade (from Bevan-Pritchard, Man and Anderson 1983).....	31
Figure 2.14 Example of building studied by Rutenberg (2004) .....	34
Figure 2.15 Moment and shear force distribution between structural walls in the model shown in Fig. 2.14 by Rutenberg (2004) .....	36
Figure 2.16 Proposed envelope for dynamic shear demand by Rutenberg and Nsieri (2006) .....	46
Figure 2.17 Dynamic shear amplification factor $\omega$ for the presented example .....	48
Figure 3.1 Model of two typical high-rise with foundation walls and the corresponding simplified 2-D model .....	50
Figure 3.2 Reversal shear phenomenon in high-rise concrete walls and the corresponding moment and shear distribution.....	51
Figure 3.3 Diagram of forces at the below-ground section of wall .....	53
Figure 3.4 Simplified model to determine the diaphragm stiffness.....	55
Figure 3.5 Diaphragm stiffness effect on the shear force distribution for a 30-storey wall.....	57
Figure 3.6 Foundation wall stiffness effect on the shear force distribution.....	58
Figure 3.7 Influence of flexural rigidity of wall below ground on the reverse shear force .....	60

Figure 3.8 Increase in reversal shear due to reduction in effective flexural stiffness .....	61
Figure 3.9 Influence of shear rigidity of wall below ground on the reverse shear force .....	62
Figure 3.10 Effect of number of stories below ground and the footing fixity on reverse shear force at the first below-ground level.....	63
Figure 3.11 Left: Cantilever model of wall (Model 1), Right: the simplified wall and below-ground diaphragms (Model 2) .....	64
Figure 3.12 RSA results for normalized shear force and overturning moment over the height of a cantilever wall (Model 1).....	65
Figure 3.13 Moment to shear ratio at the base of cantilever wall having different fundamental periods obtained from RSA (Model 1) .....	66
Figure 3.14 Figure 3.15 Response spectrum analysis vs. linear time history-analysis (Model 2) .....	67
Figure 3.15 Nonlinear Takeda model (1970) for the plastic hinge at the base of wall .....	68
Figure 3.16 Normalized bending moment and shear force history at base of a cantilever wall with $T_I=1$ sec (Model 1).....	70
Figure 3.17 Normalized bending moment and shear force history at base of a cantilever wall with $T_I=2$ sec (Model 1).....	71
Figure 3.18 Normalized bending moment and shear force history at base of a cantilever wall with $T_I=3$ sec (Model 1).....	72
Figure 3.19 Normalized bending moment and shear force history at base of a cantilever wall with $T_I=4$ sec (Model 1).....	73
Figure 3.20 Normalized shear force in the wall section and the diaphragm at yielding for $T_I=4$ sec (Model 2) .....	76
Figure 3.21 Normalized shear force in the wall section and the diaphragm at yielding for $T_I=1$ sec (Model 2).....	76
Figure 3.22 Normalized shear force and bending moment in the wall section during Northridge event for $T_I=4$ sec (Model 2) .....	77

Figure 3.23 Normalized shear force: a) wall section below-grade (top), b) base of wall (middle), c) diaphragm at ground level (bottom) for $T_I=4$ sec (Model 2).....	79
Figure 3.24 Normalized shear force: a) wall section below-grade (top), b) base of wall (middle), c) diaphragm at ground level (bottom) for $T_I=1$ sec (Model 2).....	80
Figure 3.25 Normalized overturning moment to shear force ratio at the base of wall during flexural yielding (Model 2).....	81
Figure 3.26 Shear-flexure interaction for the example of the core wall (Response-2000).....	82
Figure 3.27 Proposed tri-linear model for shear in shear walls (Gérin and Adebar 2003) .....	85
Figure 3.28 Tri-linear shear force- shear strain ( $V-\gamma$ ) Curves in present study .....	86
Figure 3.29 Model of wall below ground to perform nonlinear static analysis.....	87
Figure 3.30 Shear strain vs. shear strength of wall below ground at target moment for different $h^*/h$ ratio and for diaphragm stiffness $K30$ .....	89
Figure 3.31 Shear strain vs. shear strength of wall below ground at target moment for different $h^*/h$ ratio and for diaphragm stiffness $K10$ .....	90
Figure 3.32 Shear strain vs. shear strength of wall below ground at target moment for different $h^*/h$ ratio and for diaphragm stiffness $K1$ .....	90
Figure 3.33 Flanged section core walls considered in the present example (Left: Section $I3$ , Right: Section $I4$ ) .....	92
Figure 3.34 Bending moment at the base vs. shear strain for section $I4$ (Alternative I).....	93
Figure 3.35 Shear strain vs. shear strength of wall below ground (Alternative I): a) Section $I3$ , b) Section $I4$ .....	94
Figure 3.36 Bending moment at the base vs. shear strain for section $I4$ (Alternative II) .....	95
Figure 3.37 Shear strain vs. shear strength of wall section below ground (Alternative II): a) Section $I3$ , b) Section $I4$ .....	96
Figure 3.38 Shear force in the below-ground section vs. overturning moment at the base of wall (Alternative II) .....	98

Figure 3.39 Shear stain in the wall section below ground vs. diaphragm stiffness at the base level: a) Section <i>I3</i> , b) Section <i>I4</i> ) .....	99
Figure 3.40 Results from four nonlinear static analyses showing reduction in reverse shear force demand due to shear strain from diagonal cracking of wall, and yielding of horizontal wall reinforcement. ....	101
Figure 4.1 Example of two-wall model used in the present study.....	109
Figure 4.2 Comparison of bending moment and shear force distributions over lower floors from RSA (dashed lines) and linear static analysis (solid lines) .....	112
Figure 4.3 a) Flexural models and b) Shear models used in the present study.....	115
Figure 4.4 Normalized shear and flexure demand predicted by Model 1.....	117
Figure 4.5 Normalized shear and flexure demand predicted by Model 2.....	118
Figure 4.6 Normalized shear and flexure demand predicted by Model 3.....	119
Figure 4.7 Normalized shear and flexure demand predicted by Model 4.....	121
Figure 4.8 Normalized shear and flexure demand predicted by Model 5.....	123
Figure 4.9 Influence of 10% flexural overstrength of W2 according to Model 1 ....	125
Figure 4.10 Influence of 10% flexural overstrength of W2 according to Model 3 ..	126
Figure 4.11 Sections of walls considered in the present example .....	128
Figure 4.12 Moment and shear force demand according to Case 1.....	131
Figure 4.13 Reduction of moment and shear force demand according to Case 1-2..	133
Figure 4.14 Moment and shear force demand according to Case 2.....	136
Figure 4.15 Moment and shear force demand according to Case 3.....	138
Figure 5.1 Section of the core wall used in dynamic analysis .....	144
Figure 5.2 Scaled spectra within period range of 0.5 sec and 4.5 sec corresponding to crustal earthquakes given in Table 5.1.....	150
Figure 5.3 Scaled spectra within period range of 0.5 sec and 4.5 sec corresponding to subduction earthquakes given in Table 5.2.....	150

Figure 5.4 Scaled spectra within period range of 0.5 sec and 4.5 sec corresponding to selected earthquakes and their corresponding average spectrum ..	151
Figure 5.5 Bending moment envelopes obtained from LTHA and RSA.....	153
Figure 5.6 Shear force envelopes obtained from LTHA and RSA .....	153
Figure 5.7 2-D Link element used in SAP-2000 (CSI 2006).....	155
Figure 5.8 Moment-curvature backbone used for hysteretic flexural response.....	157
Figure 5.9 Flexural limits over the height in the model of high-rise wall .....	158
Figure 5.10 Envelopes for bending moment over the height (Case SH- $R=2.0$ ) .....	162
Figure 5.11 Envelopes for bending moment over the height (Case MH- $R=2.0$ ).....	162
Figure 5.12 Envelopes for shear force over the height (Case SH- $R=2.0$ ).....	163
Figure 5.13 Envelopes for shear force over the height (Case MH- $R=2.0$ ) .....	163
Figure 5.14 Envelopes for bending moment over the height (Case SH- $R=5.0$ ) .....	164
Figure 5.15 Envelopes for bending moment over the height (Case MH- $R=5.0$ ).....	164
Figure 5.16 Envelopes for shear force over the height (Case SH- $R=5.0$ ).....	165
Figure 5.17 Envelopes for shear force over the height (Case MH- $R=5.0$ ) .....	165
Figure 5.18 Envelopes for curvature demand over the height (Case MH- $R=2.0$ ) .....	167
Figure 5.19 Envelopes for curvature demand over the height (Case MH- $R=2.0$ ) .....	167
Figure 5.20 Use of equivalent area approach to estimate the effective shear stiffness .....	170
Figure 5.21 Influence of effective shear stiffness on shear force demand (Average for all earthquakes, $R=2.0$ ).....	172
Figure 5.22 Influence of effective shear stiffness on shear force demand (Average for all earthquakes, $R=5.0$ ).....	172
Figure 5.23 Influence of effective shear stiffness on curvature demand (Average for all earthquakes, $R=2.0$ ).....	173

Figure 5.24 Influence of effective shear stiffness on curvature demand (Average for all earthquakes, $R=5.0$ ).....	174
Figure 5.25 Dynamic shear demand at the base for nonlinear response history analysis, $R=2.0$ .....	175
Figure 5.26 Dynamic shear demand at the base for nonlinear response history analysis, $R=5.0$ .....	175
Figure 5.27 Hysteretic shear models in walls a) Experimental data (from Gérin, 2003) b) Simplified Model used in this study using NLINK element (SAP-2000, CSI 2006).....	179
Figure 5.28 Hysteretic shear comparisons between experimental data and simplified model used in this study.....	180
Figure 5.29 Shear at cracking for concrete walls predicted by ACI 318-05.....	181
Figure 5.30 Scaled design response spectra used for RSA.....	182
Figure 5.31 Ratios of $h'/H$ for walls according to RSA of different design spectra.....	183
Figure 5.32 RSA prediction of bending moment and shear force over the wall height with $T_f=3.0$ sec .....	184
Figure 5.33 Shear strength envelopes over the height of 30-storey wall model.....	185
Figure 5.34 Shear force-shear strain envelope used for hysteretic shear response ...	185
Figure 5.35 a) Model of the 30-storey wall and b) the nonlinear springs used to simulate nonlinear flexure and shear model. ....	186
Figure 5.36 Envelope of bending moment for NTHA ( $R=2.0$ , $SF=1.0$ ).....	188
Figure 5.37 Envelope of curvature for NTHA( $R=2.0$ , $SF=1.0$ ).....	188
Figure 5.38 Envelope of shear force for NTHA ( $R=2.0$ , $SF=1.0$ ) .....	189
Figure 5.39 Envelope of shear strain for NTHA ( $R=2.0$ , $SF=1.0$ ) .....	189
Figure 5.40 Envelope of bending moment for NTHA ( $R=5.0$ , $SF=1.0$ ).....	193
Figure 5.41 Envelope of curvature for NTHA ( $R=5.0$ , $SF=1.0$ ).....	193
Figure 5.42 Envelope of shear force for NTHA ( $R=5.0$ , $SF=1.0$ ) .....	194

Figure 5.43 Envelope of shear strain for NTHA ( $R=5.0$ , $SF=1.0$ ) .....	194
Figure 5.44 Envelope of bending moment for NTHA ( $R=5.0$ , $SF=2.0$ ).....	199
Figure 5.45 Envelope of curvature for NTHA ( $R=5.0$ , $SF=2.0$ ).....	199
Figure 5.46 Envelope of shear force for NTHA ( $R=5.0$ , $SF=2.0$ ) .....	200
Figure 5.47 Envelope of shear strain for NTHA ( $R=5.0$ , $SF=2.0$ ) .....	200
Figure 5.48 Shear strain vs. shear strength factor applied on initial design base shear for $R=3.5$ .....	202
Figure 5.49 Shear strain vs. shear strength factor applied on initial design base shear for $R=5.0$ .....	203
Figure 5.50 Design shear force ratio vs. uniform effective stiffness over height used in the simplified analysis .....	203



## List of Symbols and Abbreviations

$ACI$	American concrete institute
$ATC$	applied technology council
$A_e$	peak ground acceleration
$A_g$	gross area of section
$A_v$	shear area of section
$A_{ve}$	effective shear area of section
$A_{vg}$	gross shear area of section
$a_{gmax}$	peak ground acceleration
$b_w$	effective width of section
$C_a$	seismic coefficient ( <i>UBC97</i> )
$C_v$	seismic coefficient ( <i>UBC97</i> )
$CSA$	cement association of Canada
$c$	compression depth of section
$d$	effective depth of section
$d_v$	effective shear depth of section
$D_m$	coefficient used in Eberhard and Sozen study (1993)
$E$	modulus of elasticity
$E_c$	modulus of elasticity for concrete
$E_s$	modulus of elasticity for steel
$FEMA$	federal emergency management agency
$F_a$	seismic acceleration coefficient
$F_v$	seismic velocity coefficient
$f'_c$	compressive strength of concrete
$f_t$	tensile strength of concrete
$f_y$	yielding strength of steel reinforcement
$G_c$	shear modulus for concrete (also referred to as $G$ )
$G_{cracked}$	shear modulus for cracked concrete
$G_{gross}$	shear modulus for uncracked concrete
$h$	height of storey

$H$	total height
$h^*$	ratio of flexural to shear strength at the base of wall
$h'$	ratio of flexural to shear force demand at the base of wall
$h_n$	total height of structure
$h_w$	total height of wall
$I$	moment of inertia
$I_c$	cracked moment of inertia
$I_e$	effective moment of inertia
$I_g$	uncracked moment of inertia
$k$	shear strain post yield state coefficient
$K1$	diaphragm with equivalent axial stiffness of 1MN/mm
$K10$	diaphragm with equivalent axial stiffness of 10MN/mm
$K30$	diaphragm with equivalent axial stiffness of 30MN/mm
$K_s$	diaphragm stiffness
$LTHA$	linear time history analysis
$L$	length of wall
$L_f$	length of wall flange
$l_w$	length of wall
$L_w$	length of wall
$M_f$	factored moment demand
$M_l$	bending moment demand corresponding to first mode
$M_p$	probable bending moment
$M_s$	moment magnitude of earthquake
$M_y$	bending moment at yielding of longitudinal reinforcements
$n$	compressive stress on section, number of stories
$N$	compressive force on section
$LTHA$	linear time history analysis
$NBCC$	national building code of Canada
$NTHA$	nonlinear time history analysis
$N_u$	factored axial force in the concrete section

$N_x$	axial force in x-direction
$N_y$	axial force in y-direction
$P$	axial force in the section
$P1$	first underground level
$P2$	second underground level
$P3$	third underground level
$P4$	fourth underground level
$PGA$	peak ground acceleration
$q$	behaviour factor or ductility factor
$R$	ductility factor
$R_d$	ductility factor corresponding to <i>NBCC-2005</i>
$RC$	reinforced concrete
$RSA$	response spectrum analysis
$S_{ad}$	design value of response spectra
$T$	fundamental period
$T_1$	fundamental period
$UBC$	uniform building code
$V$	shear force
$V_{1st}$	shear force at first underground level
$V_a$	amplified shear force
$V_b$	shear force at base
$V_c$	shear force at cracking of concrete
$V_{cr}$	shear force at cracking of concrete
$V_d$	shear force in the diaphragm at ground level
$V_{ds}$	shear force evaluated by pseudo-static method
$V_f$	factored shear force
$V_i$	shear force at level i
$V_k$	peak shear force demand
$V_{max}$	peak shear force demand
$V_n$	nominal shear strength

$V_r$	reverse shear force at below-ground level
$V_{rf}$	reverse shear force demand for fixed footing
$V_{rp}$	reverse shear force demand for pinned footing
$V_u$	shear force at ultimate failure
$V_{xy}$	shear force at xy-plane
$V_y$	shear force at yielding of horizontal reinforcement
$W$	weight of structure
$Z_a$	zonal acceleration coefficient
$Z_v$	zonal velocity coefficient
$\alpha$	post yielding coefficient
$\gamma_{cr}$	shear strain at cracking of concrete
$\gamma_e$	elastic shear strain
$\gamma_p$	plastic shear strain
$\gamma_u$	shear strain at ultimate failure
$\gamma_y$	shear strain at yielding of horizontal reinforcement
$\varepsilon$	normal strain
$\varepsilon_{45}$	strain at 45°
$\varepsilon_{cu}$	normal strain at ultimate failure of concrete
$\varepsilon_h$	normal strain in horizontal direction
$\varepsilon_v$	normal strain in vertical direction
$\mu$	ductility
$\mu_y$	shear strain ductility
$v$	shear stress
$v_{cr}$	shear stress at cracking of concrete
$v_u$	ultimate shear stress
$v_y$	shear stress at yielding of horizontal reinforcement
$\rho$	reinforcement ratio
$\rho_n$	horizontal reinforcement ratio
$\rho_v$	vertical reinforcement ratio
$\rho_h$	horizontal reinforcement ratio

$\rho_x$	reinforcement ratio in x-direction
$\rho_y$	reinforcement ratio in y-direction
$\emptyset$	curvature
$\emptyset_y$	curvature at yielding of longitudinal reinforcement
$\omega_v$	dynamic shear amplification factor

## **Acknowledgments**

I would like to express my sincere gratitude to my supervisor, Dr. Perry Adebar for his invaluable comments and suggestions. This thesis would not have been possible without his kind support.

I am very thankful to my parents, family and friends for their love and support throughout my studies. I would not have come this far without their support in all my endeavours.

The funding provided by the Cement Association of Canada to support this research is gratefully acknowledged.

*To My Parents*

## Introduction

### 1.1 High-rise concrete shear wall buildings

Most high-rise buildings in Western Canada are constructed of reinforced concrete, and contain concrete shear walls as the seismic force resisting system. A typical concrete high-rise building has core shear walls located near the centre of the building plan, and has perimeter columns to support the flat plate floor slabs (see Fig. 1.1).

There are a number of architectural advantages of concrete shear wall buildings over concrete frame buildings. For example, the absence of large moment-resisting frames on the outside of the building means that larger windows can be provided around the entire exterior of shear wall buildings. The construction of concrete shear wall buildings is also known to be very competitive because simpler formwork and less congested reinforcement lead to lower labour costs and generally faster construction.

### 1.2 Seismic design of high-rise concrete buildings

Concrete shear walls generally provide very good lateral drift control during earthquakes. The seismic response of high-rise concrete walls during earthquakes – as it undergoes



severe cracking and localized damage – is very complex. For design, the response of concrete shear walls is approximated using different analysis procedures.

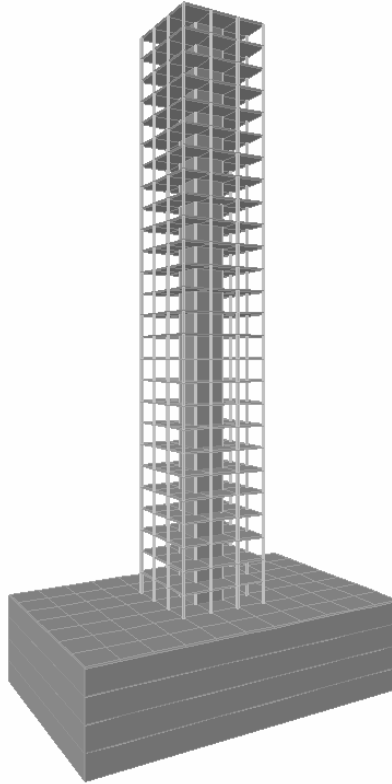


Figure 1.1 Structural system in a typical high-rise concrete shear wall building including the underground portion of the building.

Response spectrum analysis (RSA), which is a linear dynamic analysis procedure, is commonly used in design to determine the global displacement demands and force demands on individual components of concrete shear walls. In Canada, RSA is commonly the only seismic analysis that is done for concrete shear wall buildings.

Nonlinear dynamic analysis, commonly called nonlinear time history analysis (NTHA), is the most complete and sophisticated procedure to estimate the seismic response of structures. Changes in stiffness of members due to material nonlinearity and local damage caused by cracking of concrete and yielding of reinforcement can all be accounted for when performing nonlinear time history analysis

Although nonlinear time history analysis is now more commonly used for design of high-rise concrete wall buildings in the western U.S., it is rarely, if ever, used for design in Canada. There are a number of issues regarding the use of nonlinear time history analysis for design. NTHA is known to be record sensitive and therefore it is crucial to use the appropriate ground motions based on the seismicity and soil characteristics of the site. The results are also very depended on the nonlinear models that are used for the structural members. Finally, considerable effort is needed to correctly interpret the large amount of output results.

The nonlinear flexural behaviour of concrete shear walls is generally well known. This behaviour can be defined in terms of bending moment-rotation or bending moment-curvature response while accounting for axial force-bending moment interaction. Available analysis programs that use fibre-section models for reinforced concrete walls are able to accurately model the effects of cracking and reinforcement yielding, and are capable of considering the interaction between bending moment and axial compression. In comparison to flexure, the nonlinear shear behaviour of concrete shear walls is generally much less well known, and available nonlinear time history analysis programs use very primitive models for shear behaviour.

### **1.3 Nonlinear shear behaviour of concrete walls**

It is commonly thought that the shear behaviour of reinforced concrete is linear until the shear strength is reached, and that shear failure is always brittle. Tests on reinforced concrete membrane elements subjected to shear at the University of Toronto by for example Villani (1995), Stevens et al. (1991), Meyboom (1987) and Vecchio (1982), have demonstrated that this is not the case. Membrane elements are similar to a portion of a concrete shear wall.

Figure 1.2 shows the results obtained by Villani (1995) from testing of an element with 1% vertical and horizontal reinforcement under reverse cyclic loading. The results are presented in terms of average shear stress (shear force per unit area) and average shear strain (shear displacement per unit length).

The initial shear stiffness of the element is approximately equal to the shear modulus of the concrete  $G_c = 10,200$  MPa. After diagonal cracks form, the shear stiffness of the element reduces. Before yielding of the reinforcement, the shear stiffness has reduced to about 10% of the initial shear stiffness due to diagonal cracking.

Figure 1.2 is a close-up of the response prior to reinforcement yielding. Thus the shear strain capacity of the element after reinforcement yielding is not shown. Tests on membrane elements have demonstrated that reinforced concrete subjected to shear will deform in a ductile manner after yielding of the reinforcement as long as there is an appropriate amount of reinforcement. Reinforced concrete with inadequate reinforcement will fail due to concrete diagonal tension at first cracking, whereas reinforced concrete with too much reinforcement will fail due to diagonal compression in concrete. Typical reinforced concrete shear walls will have considerable shear strain ductility.

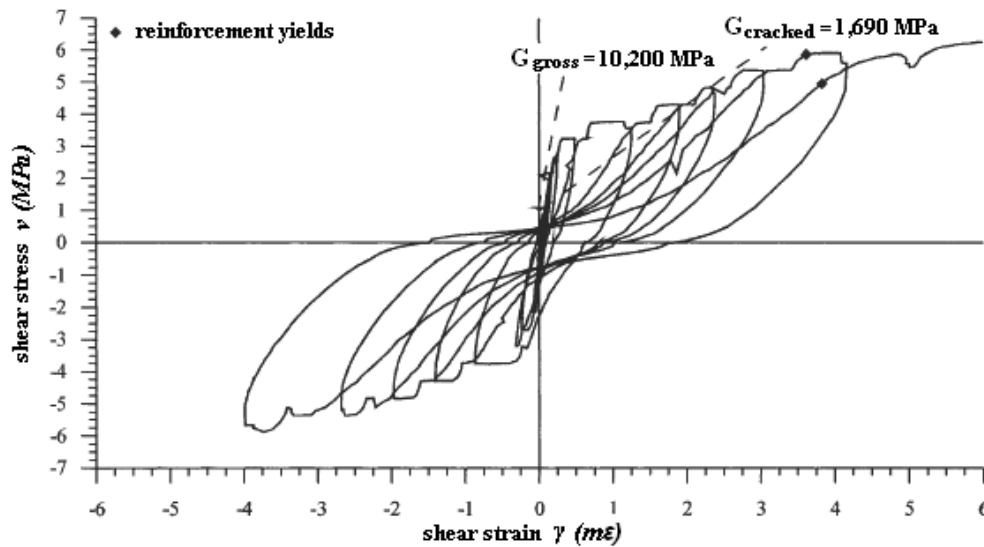


Figure 1.2 Shear stress versus shear strain response of a reinforced concrete element tested by Villani (1995) (from Gérin, 2003).

Gérin and Adebar (2004) quantified the observed experimental results on reinforced concrete membrane elements and presented a simple nonlinear shear model for reinforced concrete walls that includes the influence of concrete cracking, yielding of reinforcement, and maximum shear strain capacity. Figure 1.3 summarizes the simplified envelope for nonlinear shear response of concrete walls. The shear force at concrete cracking is called  $V_{cr}$  and the corresponding shear strain is  $\gamma_{cr}$ . The shear force capacity of

the element is called  $V_n$ , while the shear strain at yielding of the reinforcement and the shear strain capacity of the element are called  $\gamma_y$  and  $\gamma_u$ , respectively.

The commonly assumed linear–brittle behaviour in shear is labelled as Line 1 (dashed line) in Fig. 1.3. The slope of this line is equal to the gross shear stiffness of the wall  $G_c A_{vg}$ . Line 2 represents the effective shear stiffness of a fully cracked element. The slope of this line can be determined from the shear strength of the element and the shear strain at yielding. Gérin and Adebar (2004) presented a simplified procedure to estimate the shear strain at yielding. A comparison between Line 1 and Line 2 shows the significance of accounting for diagonal cracking in reinforced concrete walls. Gérin and Adebar (2004) also presented an expression for shear strain capacity of reinforced concrete. For a typical shear wall, the shear strain capacity is two to four times the shear strain at yielding.

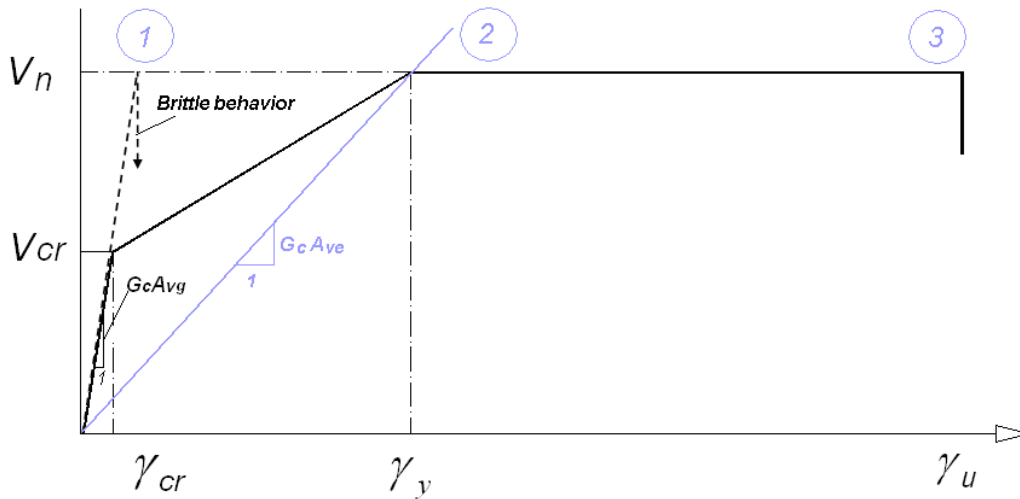


Figure 1.3 Commonly assumed brittle shear behaviour (dashed line) versus the actual shear behaviour of concrete shear walls according to the Gérin-Adebar model (solid line).

Different models for nonlinear shear response of concrete walls have been proposed (i.e., Ozcebe and Saatcioglu 1989) and different models to simulate shear response are also used in some computer programs such as Response-2000 (Bentz 2000). The advantage of using the tri-linear shear model proposed by Gérin (2003) in this study is the significance of considering three distinctive parameters associated with cracking of concrete, yielding of horizontal reinforcement and ultimate shear strain capacity to address important design issues in seismic design of high-rise concrete walls.

## 1.4 Seismic shear demand issues in high-rise concrete buildings

The nonlinear shear response of reinforced concrete is very important whenever shear deformations are significant. There are a number of important issues in the design of high-rise concrete shear walls where shear deformations play a very important role, and hence nonlinear shear behaviour will have a significant influence.

One example is the maximum shear force demand on concrete walls below the base level during lateral ground motion (see Fig. 1.4). The perimeter foundation walls of a typical high-rise building are orders of magnitude stiffer than the central core (tower) walls extending to the top of the building. As a result, the lateral seismic forces in high-rise walls are transferred to the perimeter foundation walls by interconnecting floor diaphragms below the base. The multiple levels of floor diaphragms also transfer the over-turning moments from the high-rise walls to the perimeter foundation walls. The reduction in bending moment in the high-rise walls is accompanied by a corresponding reverse shear force in the wall section below ground. When a building has tall walls connected to large perimeter foundation walls by rigid floor diaphragms, linear analysis, such as RSA, may indicate a reverse shear force that is many times larger than the base shear force above the foundation walls. Figure 1.4 shows a simplified model of high-rise wall including diaphragms and foundation wall below base level. Lateral seismic loads corresponding to earthquake are also shown over the height of the wall.

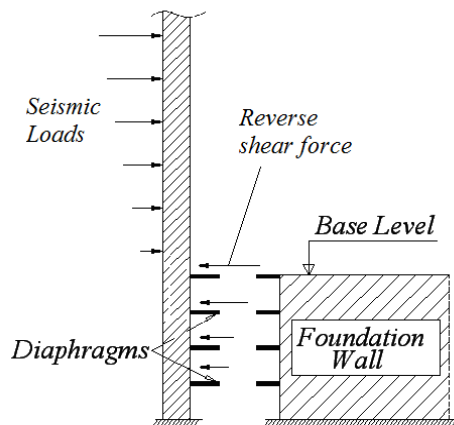


Figure 1.4 Seismic shear force demand below base level.

Different approaches are currently used to design high-rise walls for the large reverse shear force below ground. One approach that has been used is to design the concrete walls and floor diaphragms for the forces calculated in a linear analysis. Another approach that is used is to completely ignore the reverse shear force altogether, and design the entire below-ground portion of the wall for the base shear force and corresponding bending moment calculated above the base. A third approach is to use cracked-section stiffnesses for the diaphragm or the wall (or both) in order to reduce the magnitude of the reverse shear force, and depending on what is assumed, this will give a solution somewhere between the first two solutions.

The reverse shear force is the result of the compatibility of deformations. Thus, when a concrete wall is designed for a higher shear force, the effective shear stiffness of the wall will be larger and the reverse shear force demand will be larger. On the other hand, if the wall is designed for a lower shear force, the effective shear stiffness of the wall will be smaller and the reverse shear force will be smaller. While it is obvious that the latter approach will result in a less expensive structure, what is not known is which of these approaches will result in a better performance. To assess the performance of these different design approaches requires a nonlinear analysis using an appropriate shear model for the concrete walls as shear deformation is quite significant at the section of core wall below ground level and hence consideration of nonlinear shear behaviour is very important.

A second seismic shear demand issue where nonlinear shear response is expected to have a significant influence is the distribution of shear forces between inter-connected high-rise walls. In high-rise buildings, concrete walls are tied together over the height of the wall by rigid floor plates at every floor level as shown in Fig. 1.5. At the upper levels of the structure, the shear force distribution between walls depends primarily on the relative flexural rigidity of the walls. In the lower levels of the building, the shear force distribution depends more on the relative shear rigidity of the walls.

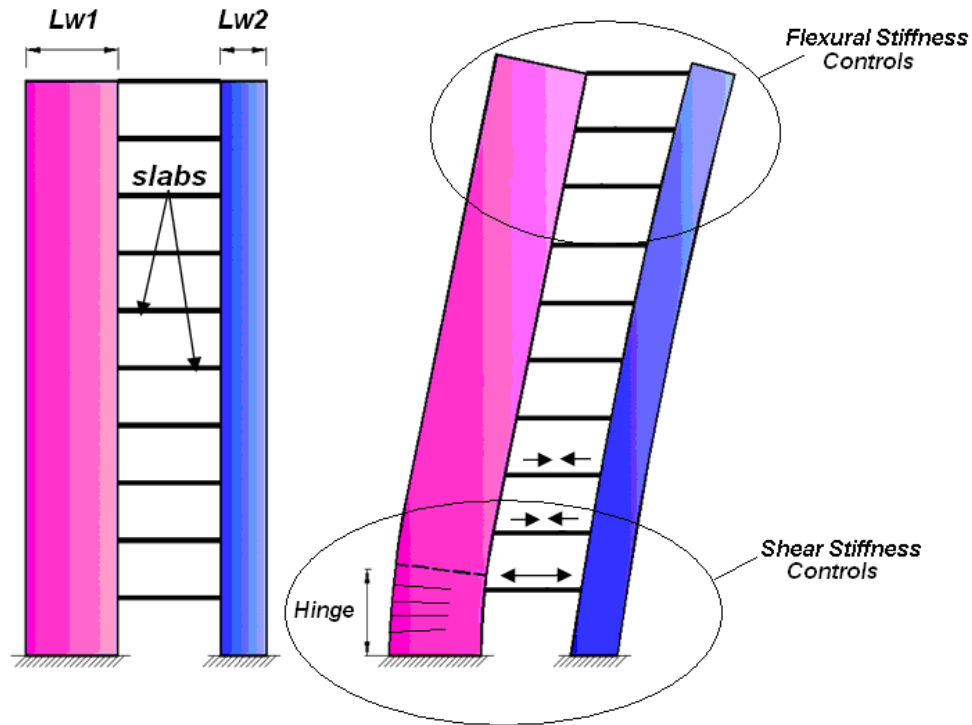


Figure 1.5 Regions where flexure and shear stiffnesses influence the shear force distribution in inter-connected high-rise walls, and self-equilibrating forces resulting from flexural yielding in the longer wall.

Simple stiffness properties are usually used in a linear seismic analysis to account for the presence of cracked regions of concrete members. The effective flexural rigidity  $E_c I_e$  is normally a portion of the gross section flexural rigidity  $E_c I_g$  of the walls. For simplicity, one reduction factor, such as 70%, is normally used for all elements in the structure. The effective shear rigidity of concrete walls is usually assumed to equal the gross section shear rigidity  $G_c A_{ve}$ . That is, the effect of shear cracking is usually not accounted for. While these simple assumptions about effective member rigidities lead to reasonable estimates of overall structural displacement, such as the displacement at the top of concrete walls, they may result in poor estimates of shear force distribution between concrete walls.

When one wall begins to yield prior to the other wall as shown in Fig. 1.5, significant redistribution of shear forces will occur in the vicinity of the hinge. The yielding wall will try to rotate as a rigid body about the hinge, while the non-yielding wall will try to deform elastically. As a result, a set of self-equilibrating forces will be transmitted between the walls causing the shear force distribution to change significantly.

To predict the shear force distribution in two inter-connected walls from the initial uncracked state to when the system of walls fails, requires both a rigorous nonlinear flexural model and a rigorous nonlinear shear model.

The third and final seismic shear demand issue in which nonlinear shear response is expected to have a significant influence is shear force demand due to higher modes of vibration in cantilever walls. Flexural yielding at the base of the cantilever wall is the desired inelastic mechanism; however nonlinear dynamic analysis has shown that flexural yielding of the wall does not necessarily limit the shear force in the wall near the base. The shear force tends to increase as the magnitude of ground motion increases. This phenomenon is often referred to as “dynamic shear amplification” Ghosh (1990), Keintzel (1992), Eberhard and Sozen (1993), Priestley and Amaris (2003). The dynamic shear amplification factor is the ratio of shear force demand obtained from nonlinear analysis to shear demand obtained from a linear procedure such as the simplified code procedure. This amplification, which can be as large as 2.0 or 3.0, is caused by the effect of higher modes in tall structures.

Figure 1.6 shows a simple picture of the phenomenon. Deformation of a cantilever wall is shown in its second vibration mode. Influence of higher modes is significant for flexible structures with lower natural frequencies such as tall structural walls. Contribution of higher modes of vibration would lower the point of application for the resultant seismic loading. This means that a greater base shear is required to reach the wall flexural yielding at the base.

In all previous studies on dynamic shear amplification, the shear response of the concrete wall was assumed to be linear and the uncracked section shear rigidity was typically used. It is expected that significant shear deformation of a concrete wall due to diagonal cracking and yielding of horizontal reinforcement may reduce the dynamic shear amplification.



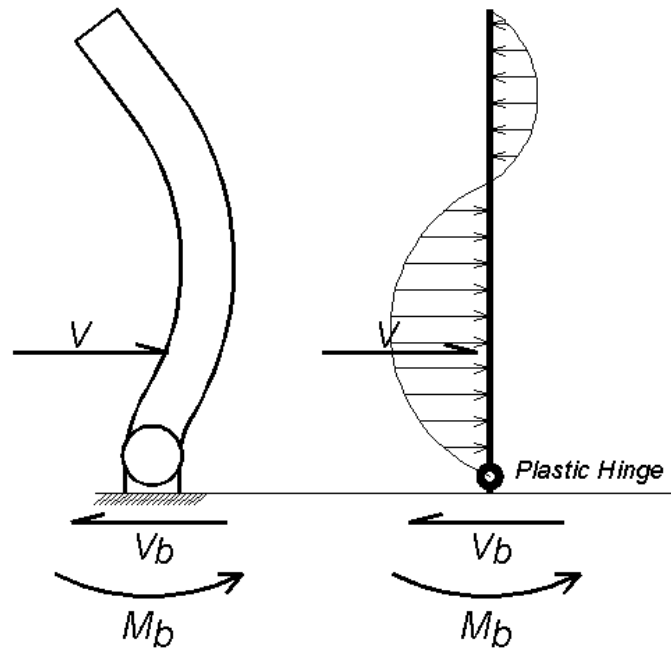


Figure 1.6 Shear force distributions in a cantilever high-rise concrete wall.

### 1.5 Thesis objectives

The objective of this thesis is to investigate how nonlinear shear response due to diagonal cracking and yielding of horizontal reinforcement influences the seismic shear demand in high-rise concrete structural walls.

Three specific seismic shear demand problems will be investigated:

1. The reverse shear force problem in high-rise concrete walls due to rigid diaphragms below the flexural plastic hinge. It is expected that diagonal cracking and yielding of horizontal reinforcement may significantly reduce the magnitude of reverse shear force compared to what is predicted using linear analysis.
2. The shear force distribution between different length high-rise concrete walls interconnected by floor slabs, including the redistribution that occurs due to flexural cracking

of walls and flexural yielding of walls. It is expected that diagonal cracking and yielding of horizontal reinforcement may significantly change the shear force distribution in walls, and may result in a very different failure mechanism of the wall system than is predicted using linear analysis.

3. The dynamic shear amplification due to higher modes in high-rise concrete walls. It is expected that the reduction in shear stiffness of concrete walls due to diagonal cracking and yielding of horizontal reinforcement may significantly reduce the maximum seismic shear demand in high-rise walls.

The approach taken throughout this research is to try to develop a simple understanding of the physical phenomenon, and to use this understanding to develop simplified procedures that can be used by design engineers. Where possible, procedures that can be used with linear seismic analysis will be developed.

## **1.6 Thesis organization**

Recent developments on nonlinear behaviour of high-rise walls during earthquake are presented in Chapter 2. Nonlinear models in concrete walls are discussed in terms of nonlinear flexural and nonlinear shear models. A brief summary of previous work on investigating nonlinear dynamic response of high-rise concrete walls are presented in this chapter.

Chapter 3 investigates the seismic shear demand on high-rise walls at below ground level. This problem is also referred to as “Shear reversal” on high-rise walls at levels below ground. The parameters which have significant influence on the magnitude of reverse shear demand on wall are examined with the most important ones to be addressed. Nonlinear dynamic response of the wall is studied and the findings are used to assess the nonlinear shear performance of the wall at levels below ground.

In Chapter 4, seismic shear force distribution between two connected walls in a high-rise is studied. Model definition for the problem is presented at the beginning, followed by discussion on the input parameters and the nonlinear models used. The

nonlinear analysis is performed for each case of analysis and the final results are compared at the end.

Chapter 5 focuses on dynamic shear demand on a realistic model of high-rise cantilever wall which is subjected to different earthquake events. Different cases for variation of flexural strength over the height of wall are considered to investigate the nonlinear effects on seismic shear force demand. A simplified method to account for degradation of shear stiffness during earthquake is presented to study the seismic response and finally the best available state of art hysteretic shear model for concrete walls is use to study the problem in further details.

Conclusions and recommendations for future studies are presented in Chapter 6. Ground motions used for nonlinear dynamic analysis and their corresponding response spectra are given in an appendix. Analyses information which is not addressed in the text is also presented in an appendix.

## **Literature review**

A brief introduction to available nonlinear models in reinforced concrete walls is presented in this chapter. A short discussion on a flexural model is followed by a more detailed explanation on the recent findings on nonlinear shear response of reinforced concrete walls. Literature review presented in this chapter focuses on the three seismic shear demand issues which were explained earlier as the scope of the present study. First, review of previous studies on shear demand at below-ground sections of a high-rise core wall is presented. Review of previous work on force distribution between inter-connected high-rise walls is discussed next and finally in the last section of this chapter, review of the past studies on dynamic shear demand in concrete walls during earthquake is presented.

### **2.1 Nonlinear flexural response in reinforced concrete walls**

During lateral motion caused by earthquake, a high-rise structural wall deforms mainly due to the bending behaviour. Flexural behaviour of concrete walls is known to be ductile and therefore it is rational to ensure nonlinear behaviour is controlled by hinging mechanism at the base of wall during ground motion.

In order to establish the nonlinear behaviour of structural walls, sectional analysis is used to determine the bending moment and corresponding curvature carried by a

reinforced concrete section under a certain axial loading. Several sectional analysis tools are available for modeling the flexural behaviour in a reinforced concrete section. Program Response-2000 (Bentz 2000) was used to build the moment-curvature response for the structural walls in this study.

Figure 2.1 shows the initial part (before ultimate failure) of moment-curvature diagram for a section of previously uncracked reinforced concrete wall at the base level. The values are shown for a typical high-rise core wall to provide a realistic moment-curvature relationship. Core wall considered has an I-shaped section with overall dimensions of 9.0 m and has a uniform thickness of 750 mm as shown in Fig. 2.1. The core wall has an average vertical reinforcement ratio of 1% in the flange area and an average vertical reinforcement ratio of 0.5% in the web area with  $f_y=400$  MPa. Concrete strength was assumed to be  $f'_c=50$  MPa and wall is subjected to an average axial compression of  $P/A_g=3.75$  MPa. Solid line in Fig. 2.1 presents the actual response obtained from Response-2000 using Vecchio-Collins model (1986) for compression softening and Bentz model (1999) for tension stiffening. Dashed line presents a corresponding simplified tri-linear model with an equal captured area under the moment-curvature curve in comparison to the actual response.

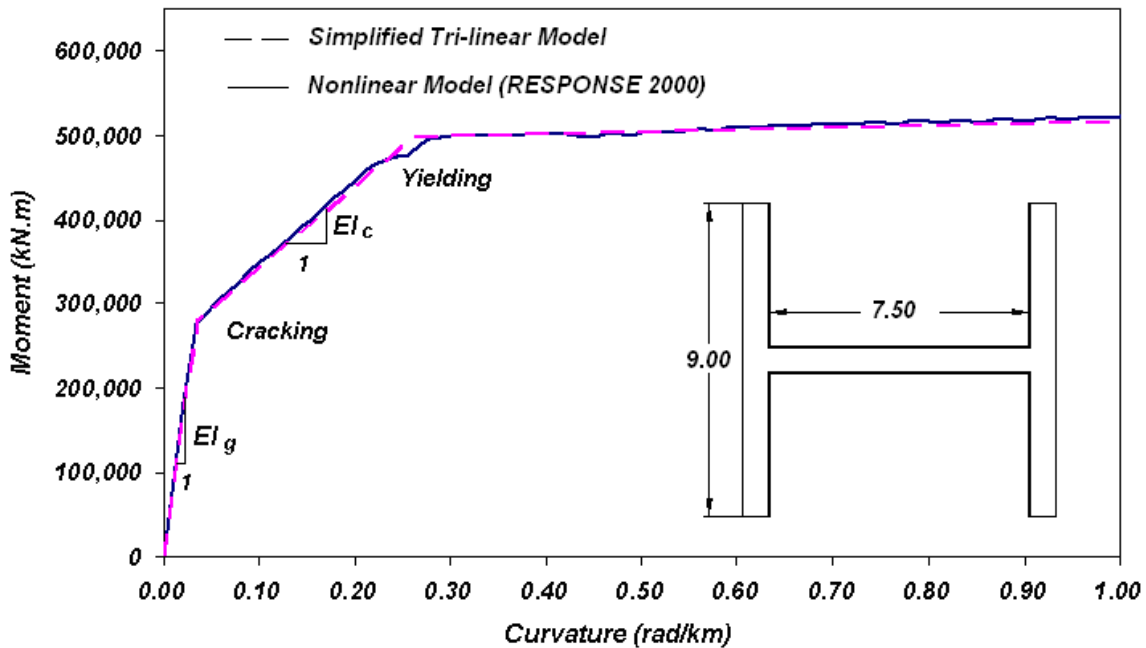


Figure 2.1 Moment-curvature response of a typical high-rise core wall.

Two important points where the slope of curves changes suddenly are associated with cracking of concrete and yielding of vertical reinforcement.

As illustrated in Fig. 2.1, the nonlinear flexural response of concrete walls can be simplified by using a tri-linear moment-curvature curve. Ibrahim (2000) presented a simplified method to estimate the moment-curvature response in the high-rise concrete wall without using sectional analysis. It was observed that the secondary slope of the moment-curvature curve beyond elastic portion of the curve is mainly dependent on the section geometry and the amount of vertical reinforcement. This slope is parallel to the well-known cracked-section stiffness which can be defined for two different states: one when the section is previously uncracked and the other when the member is severely cracked due to previous cycles of loading.

One important point on the moment-curvature curve is the point at which reinforced concrete section reaches the maximum curvature capacity (not shown on Fig. 2.1). The ultimate curvature capacity of the wall ( $\phi_y$ ) is inversely proportional to the depth of flexural compression zone. The depth of compression zone at maximum curvature can be easily calculated and consequently ultimate curvature in reinforced concrete walls can be estimated. Because of the ductile flexural behaviour, concrete walls can deform a significant amount beyond yielding of vertical reinforcement before the ultimate capacity is reached.

One of the major parameters affecting displacement ductility in walls is the length of plastic hinge which cannot be defined with great precision; however improvement of available fiber section models has led to a better estimate of nonlinear flexural response in concrete walls by accounting for spread of plasticity in the plastic hinge zone.

## **2.2 Nonlinear shear response in reinforced concrete walls**

In the past, very little was known about the nonlinear shear behaviour of reinforced concrete walls. Until recently (Gérin 2003), available models for reinforced concrete walls subjected to shear did not properly account for cracking of concrete and yielding of horizontal reinforcement. In order to investigate the nonlinear shear response of concrete walls, experimental tests were conducted on reinforced concrete panels subjected to pure shear loading at the University of Toronto (Stevens et al. 1991 and Villani 1995).

Gérin (2003) studied the results obtained from testing of membrane elements to investigate the nonlinear shear behaviour of reinforced concrete walls. He selected seven specimens taken from three different research projects at the University of Toronto. Three specimens, SE8, SE9 and SE10 which were heavily reinforced panels in horizontal direction were tested under reverse-cyclic shear by Stevens (1991). Another set of reinforced concrete wall elements namely PDV1, PDV2 and PDV3 were tested by Villani (1995) under monotonic shear, reverse-cyclic shear, and positive-only cyclic shear, respectively. All tests were stress controlled and the load was applied until the specified level of shear stress was reached. For monotonic tests, the load was gradually increased until the specimen failed. For reverse-cyclic tests, the load was gradually increased from zero until it reached a target stress level; then it was reduced to zero and the same loading was applied in the reverse direction to complete one full cycle. Typically, a number of cycles were performed at a stress level below yielding of reinforcement recognized as elastic cycles. The load was then cycled at a stress level causing yielding of the weaker reinforcement and the cycles were continued until the element failed. For the tested PDV elements weaker reinforcement ratio was 0.91%. This amount of horizontal reinforcement is close to the typical reinforcement ratio of an existing core wall at its base. Specifications of PDV elements are given in Table 2.1.

Table 2.1 Specification of PDV elements tested by Villani (1995).

Parameter	PDV1	PDV2	PDV3
size (mm)	890x890x70	890x890x70	890x890x70
shear load	monotonic	reverse-cyclic	cyclic
axial load	$N_x=N_y=-0.4V_{xy}$	$N_x=N_y=-0.4V_{xy}$	$N_x=N_y=-0.4V_{xy}$
$f'_c$ (MPa)	26.8	23.7	34.1
$E_c$ (MPa)	24480	23030	27620
$f_t$ (MPa)	1.7	1.6	1.9
Reinforcement			
x-dir	6 mm $\Phi$ @ 45mm	6 mm $\Phi$ @ 45mm	6 mm $\Phi$ @ 45mm
$\rho_x$	0.0182	0.0182	0.0182
y-dir	6 mm $\Phi$ @ 89mm	6 mm $\Phi$ @ 89mm	6 mm $\Phi$ @ 89mm
$\rho_y$	0.0091	0.0091	0.0091
$\rho_x:\rho_y$	2:1	2:1	2:1

Results of testing of specimens PDV1, PDV2 and PDV3 are presented in Fig. 2.2 in terms of shear stress – shear strain of a reinforced concrete wall element. As shown in Fig. 2.2 (a) for PDV1 element, the cracked shear modulus  $G_{cracked}$ , is approximately 10% of initial elastic shear modulus  $G_{gross}$ . The first visible crack forms roughly at  $45^\circ$  to the x-axis normal to the principal applied tension at the stress level of 2.6 MPa. As more cracks form and the cracks widen, reinforcement starts to carry more of the load. At a stress level of 6.2 MPa reinforcement yields and the shear strain increases more rapidly. Yielding of horizontal reinforcement in the PDV1 element takes place at a shear strain range between 0.003 and 0.004. Figure 2.2 (b) shows the reverse-cyclic response of PDV2 element. Most of loading cycles occur under the cracking state for element PDV2. For these cycles, the re-loading curve passes through the last point in the previous cycle in the same direction. First cracking was observed at a shear stress level of 2.8 MPa followed by development of more diagonal cracks until yielding of reinforcement occurred at shear stress of 6.2 MPa and a shear strain of approximately 0.0035. Results for PDV3 is shown in Fig. 2.2 (c) where the element is cycled in positive shear only and all but one cycle happened before yielding. Concrete shear cracking and yielding of reinforcement occurred at stress levels of 4.0 MPa and 6.5 MPa respectively.



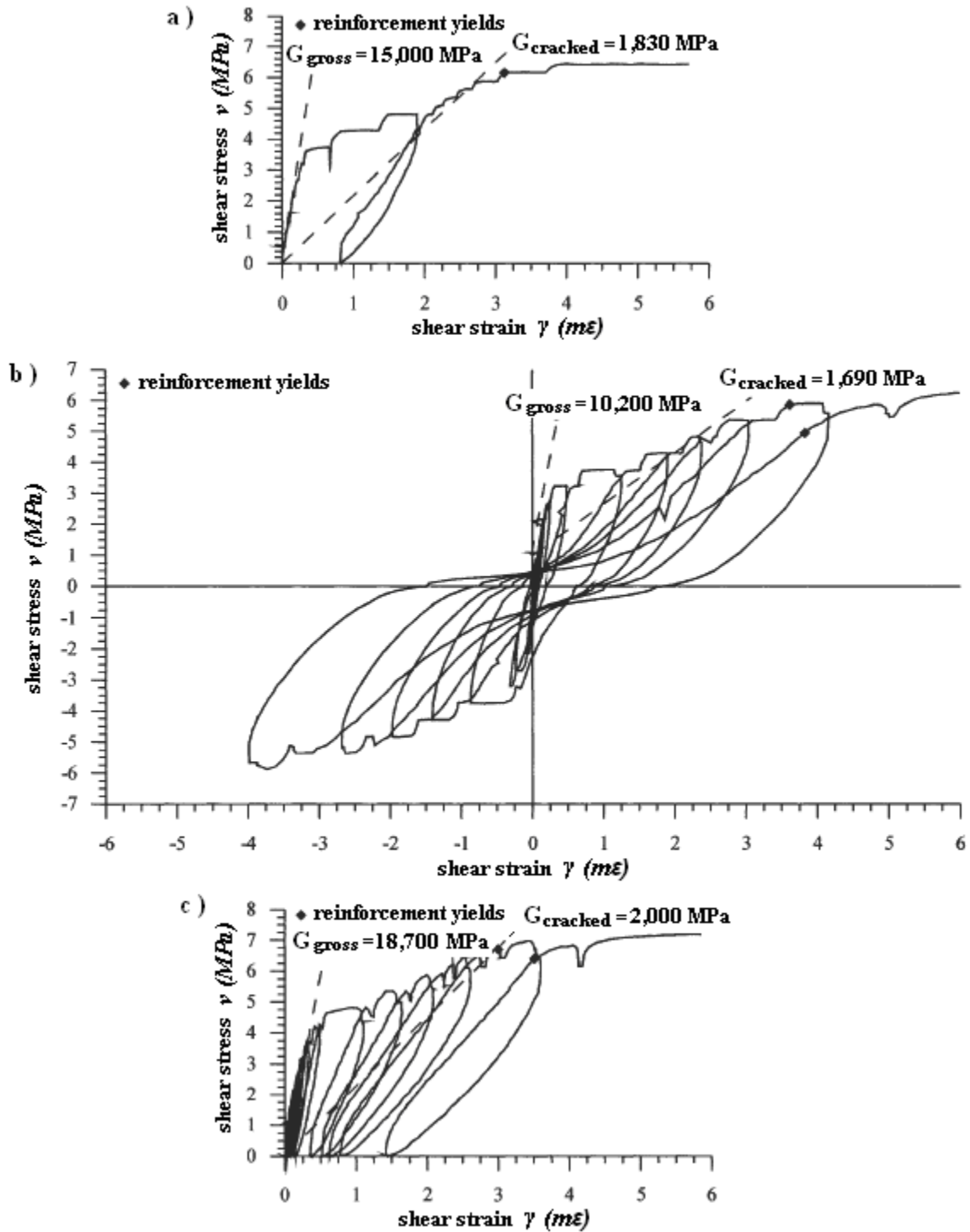


Figure 2.2 Shear stress-shear strain responses for shear wall elements:  
a) PDV1, b) PDV2, c) PDV3 (from G  rin, 2003).

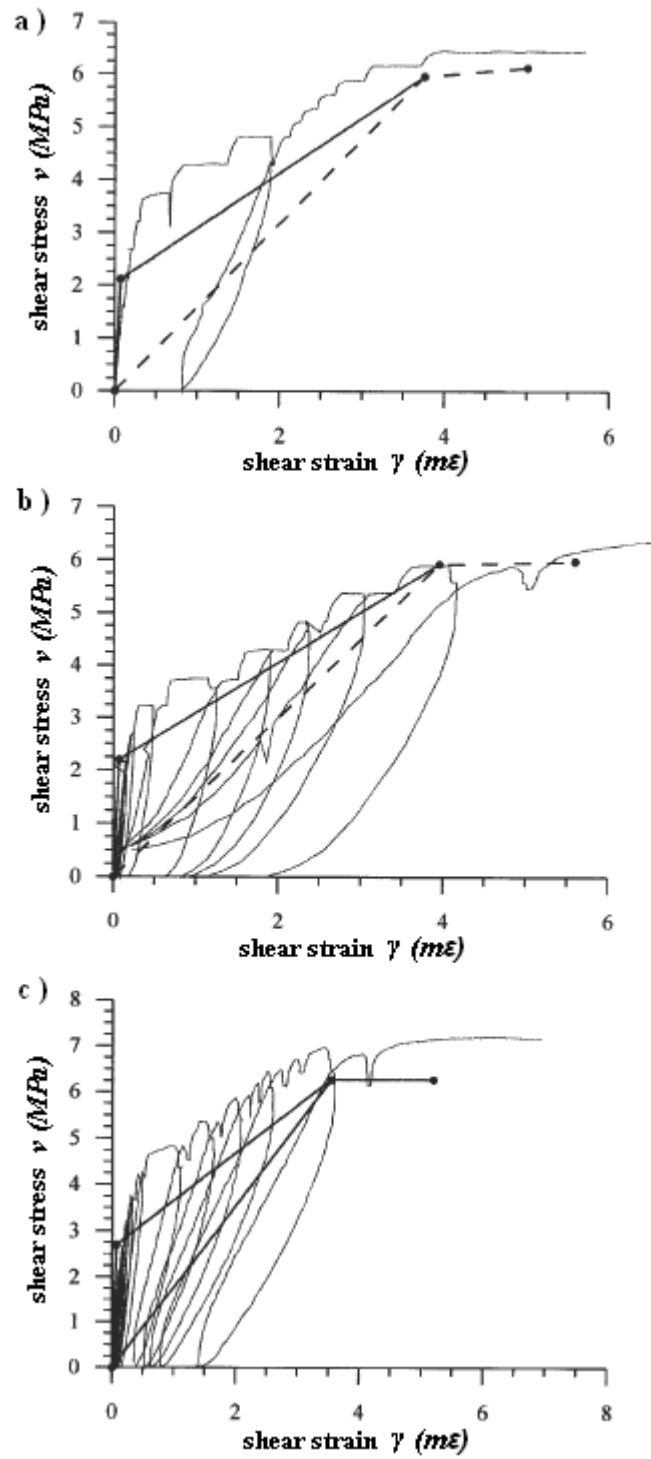


Figure 2.3 Simplified predicted response as bi-linear and tri-linear envelopes:  
a) PDV1, b) PDV2, c) PDV3 (from Gérin, 2003).

A simplified way of accounting for concrete cracking in shear is to use effective stiffness as a fraction of gross shear stiffness. Effective stiffness ( $G_e A_{vg}$ ) may range from a non-cracked state ( $G_g A_{vg}$ ) to a fully cracked state ( $G_{cr} A_{vg}$ ) as shown in Fig. 2.2. Gérin (2003) proposed a simplified model for the hysteretic shear response in terms of bi-linear and tri-linear envelopes to fit the cyclic response as shown in Fig. 2.3.

Gérin (2003) observed that there is a linear relationship between shear strain demand and the developed strain in the weaker reinforcement (first reinforcement to yield). Shear deformation increases proportionally when the weaker reinforcement yields. The pinching of the hysteretic loop was found to be a function of plastic strain in the horizontal reinforcement and it becomes more pronounced as additional plastic strain accumulates in the reinforcement.

A general model was formulated where deformations at cracks are separated from deformation of concrete in-between cracks. Gérin (2003) observed that the strains in concrete and reinforcement are directly related to the applied loads whereas strains at cracks are related to the maintaining strain compatibility between the concrete and the reinforcement. As proposed by Gérin (2003), the shear strain in reinforced concrete section can be determined from compatibility of concrete and reinforcement strain as given in Eq. 2.1.

$$\gamma_{hv} = \varepsilon_h + \varepsilon_v - 2\varepsilon_{45} \quad (2.1)$$

$\varepsilon_h$  and  $\varepsilon_v$  are the normal strains of reinforcement in the horizontal and vertical directions respectively and  $\varepsilon_{45}$  is the strain at  $45^\circ$  to the reinforcement and in the direction closest to the principal compression strain direction. Yielding of the element is defined as when the horizontal reinforcement reaches the yield point. For simplicity this strain is assumed to be equal the bare bar yield strain given by Eq. 2.2 where  $E_s$  is the elastic modulus of steel bars.

$$\varepsilon_h = \frac{f_y}{E_s} \quad (2.2)$$

For simplicity, Gérin (2003) assumed that the concrete stresses consist of uniaxial compression at 45° to the reinforcement and assumed a linear stress-strain relationship for the vertical reinforcement. The strain in vertical reinforcing bars is given by Eq. 2.3.

$$\varepsilon_v = \frac{v_y - n}{E_s \rho_v} \geq 0 \quad (2.3)$$

$v_y$  is the applied shear stress at yield,  $n$  is the axial compressive stress in the section and  $\rho_v$  is the vertical reinforcement ratio. The strain at 45° at yield is obtained from Eq. 2.4.

$$\varepsilon_{45} = \frac{-2v_y}{E_c} \quad (2.4)$$

In Eq. 2.4,  $E_c$  is the elastic modulus of concrete material. By combining previous expressions, the shear strain at yield can be obtained by:

$$\gamma_y = \frac{f_y}{E_s} + \frac{v_y - n}{E_s \rho_v} + \frac{4v_y}{E_c} \geq 0 \quad (2.5)$$

With the condition that:

$$0 \leq \frac{v_y - n}{E_s \rho_v} \leq \frac{f_y}{E_s} \quad (2.6)$$

Gérin (2003) observed that for typical design, developed shear strain at yield in a reinforced concrete wall section ranges from 0.0021 to 0.0047 as shown in Fig. 2.4. Gérin also investigated the fact that shear dominated elements with typical amount of reinforcement can deform significantly beyond yielding of the horizontal reinforcement. This suggests that shear walls possess considerable ductility in shear.

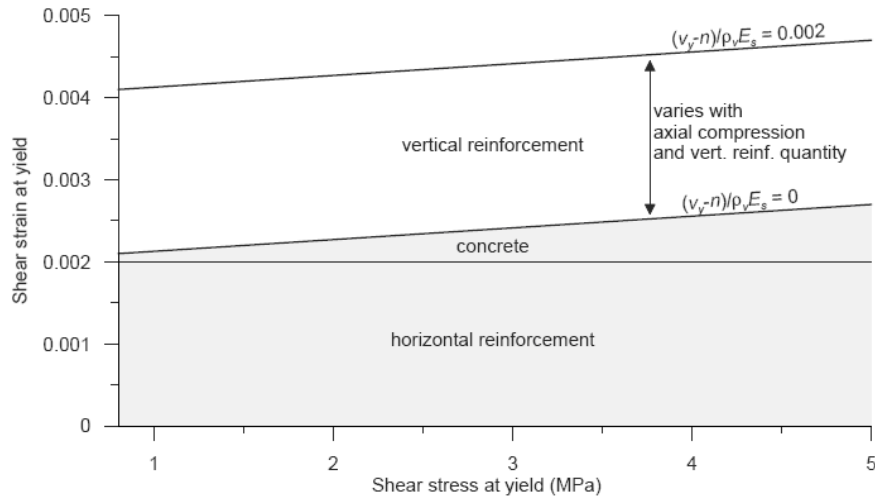


Figure 2.4 Contribution to shear strain at yield for typical shear walls (from Gérin, 2004)

Another investigation by Gérin (2003) was to obtain a relationship between shear strain ductility and applied shear stress. Figure 2.5 shows the relationship between shear strain ductility and the shear stress at yielding as proposed by Gérin (2003) based on results of experimental testing.

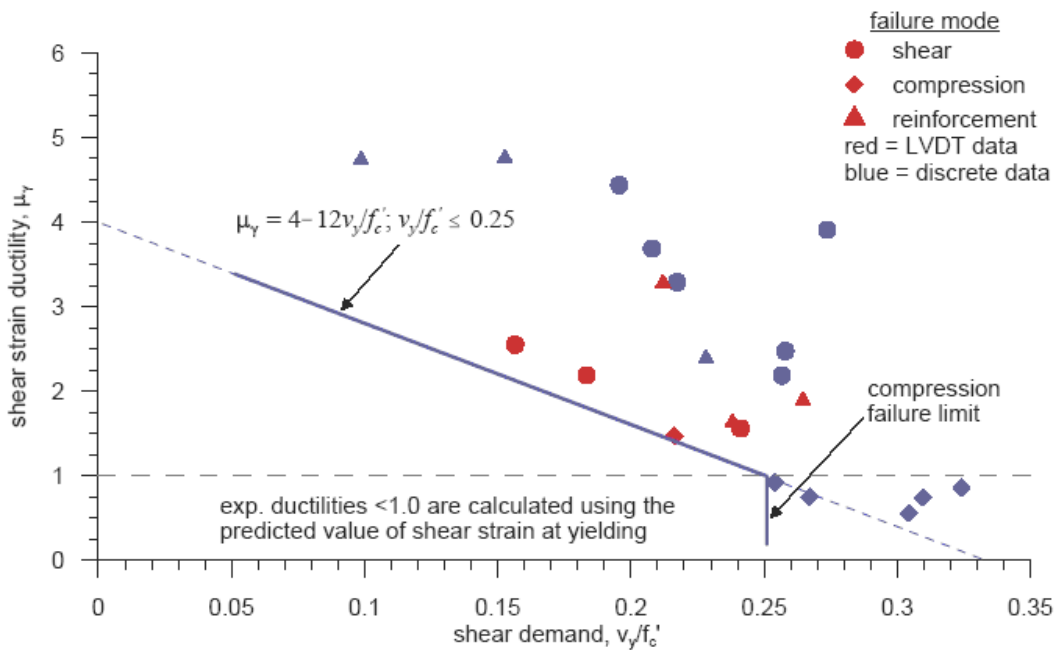


Figure 2.5 Shear strain ductility with respect to developed shear stress (from Gérin, 2004).

The expression for shear strain ductility is given by Eq. 2.7.

$$\mu_\gamma = 4 - 12 v_y / f'_c ; \quad v_y / f'_c \leq 0.25 \quad (2.7)$$

In order to construct the tri-linear shear stress – shear strain envelope for a given reinforced concrete wall, shear stress at diagonal cracking of concrete and yielding of horizontal reinforcement need to be determined. The shear force at cracking can be estimated by using the expressions suggested in *ACI 318-05* which are summarized below.

For members subjected to axial compression load  $N_u$ , shear strength provided by concrete alone and for non-prestressed members is given by Eq. 2.8:

$$V_c = \left(1 + \frac{N_u}{14A_g}\right) \left(\frac{\sqrt{f'_c}}{6}\right) b_w d : \text{(ACI 11-4)} \quad (2.8)$$

In the expressions above,  $N_u$  is the axial compressive force in the wall section,  $d$  is the total shear depth of the section and  $b_w$  is the thickness of section considered. Equation 2.8 gives a lower bound for shear strength provided by concrete. In order to obtain an upper bound estimate for shear strength, *ACI 318-05* suggests using Eq. 2.9.

$$V_c = 0.3\sqrt{f'_c} b_w d \sqrt{1 + \frac{0.3N_u}{A_g}} : \text{(ACI 11-7)} \quad (2.9)$$

Provisions given by *ACI318-05* for prestressed concrete members can be used for non-prestressed members with minor adjustments for axial compression instead of pre-stressing force as expressed by Eq. 2.10.

$$V_{cw} = 0.3\left(\sqrt{f'_c} + \frac{N_u}{A_g}\right) b_w d : \text{(ACI 11-12)} \quad (2.10)$$

The theoretical upper bound for strength of concrete at cracking based on basic principles is expressed in Eq. 2.11.

$$V_c = 0.33\sqrt{f'_c} \sqrt{1 + \frac{N_u}{0.33\sqrt{f'_c}A_g}} b_w d ; \text{ Upper bound limit} \quad (2.11)$$

Figure 2.6 compares each of the explained expressions to estimate shear strength of walls at cracking. The horizontal axis in Fig. 2.6 corresponds to axial compression stress while the vertical axis shows the shear stress level at cracking in the section of wall.

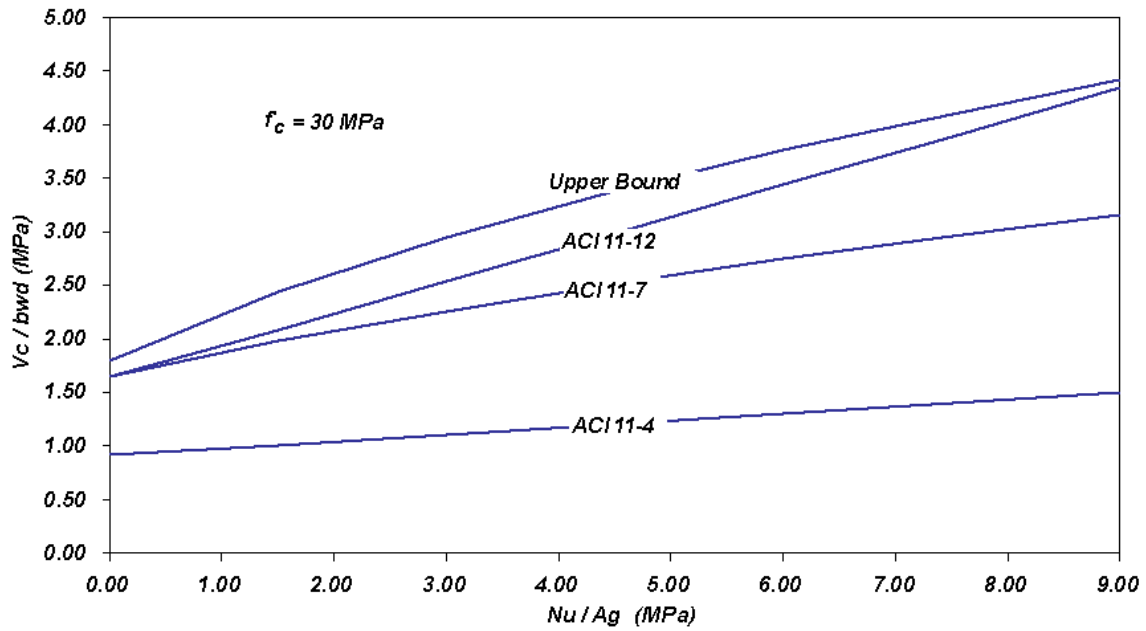


Figure 2.6 Comparison between different estimates of shear stress at cracking.

Shear force at yielding can be considered equal to nominal shear strength by assuming the strain hardening is insignificant. ACI318-05 recommends the upper limit for the nominal shear strength of structural walls as:

$$V_n = A_{cv} (\alpha_c \sqrt{f'_c} + \rho_n f_y) : \quad (\text{ACI 21-7-4}) \quad (2.12)$$

Where,  $A_{cv}$  is the effective shear area taken as  $b_w d$  and  $\rho_n$  is the horizontal steel ratio. Coefficient  $\alpha_c$  is taken as  $1/4$  for  $h_w/l_w \leq 1.5$  and is taken as  $1/6$  for  $h_w/l_w \geq 2.0$ .

Figure 2.7 shows the proposed tri-linear curve by G  rin (2004) and the corresponding cyclic shear stress-shear strain curve according to the testing of SE8 wall element. As shown, an envelope to fit the hysteretic response is defined by three specific points; initiating of diagonal cracking in concrete at stress level of  $v_{cr}$  at the corresponding shear strain of  $\gamma_{cr} = v_{cr}/G_{gross}$ , yielding of horizontal reinforcement at stress level of  $v_y$  at an associated shear strain of  $\gamma_y$  and point of ultimate shear failure at stress level of  $v_u$  at an associated ultimate shear strain of  $\gamma_u$ . Note that in Fig. 2.7 strain hardening was insignificant and therefore the shear stress value is assumed constant from point of yielding to the point of ultimate failure.

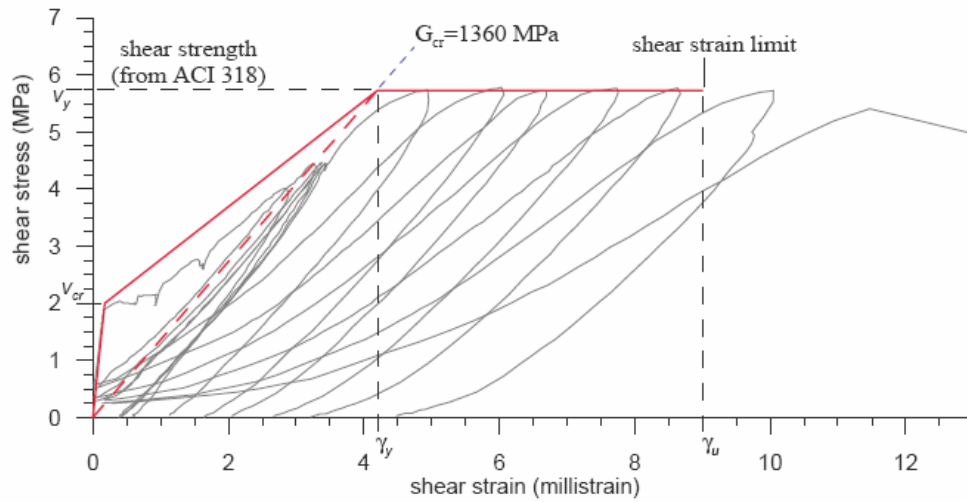


Figure 2.7 Proposed load-deformation curve for nonlinear static analysis by G  rin (2004), shown for membrane element SE8 tested by Stevens et al. 1991.

In order to study the nonlinear dynamic response of the reinforced concrete walls, a complete hysteretic behaviour is required for the stress-strain relationship in addition to the specified tri-linear backbone. A simplified hysteretic shear model that was proposed by G  rin (2004).



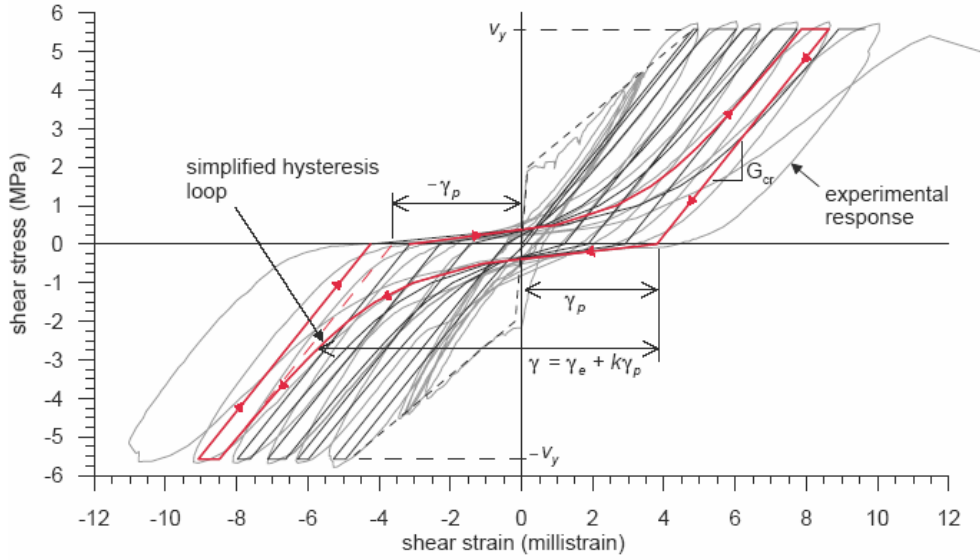


Figure 2.8 Proposed simplified hysteretic model by Gérin (2004), shown for membrane element SE8 (Stevens et al. 1991).

The simple hysteretic model shown in Fig. 2.8, assumes that yielding occurs at  $v_y$  for each cycle, unloading occurs at a constant slope equal to  $G_{cr}$ , and the plastic shear strain  $\gamma_p$  remaining at the end of each unloading segment is cumulative from one direction of loading to the other. The reloading curve accounts for the closing of diagonal cracks in one direction and the simultaneous opening of diagonal cracks in the other direction in a simple way. The shear strain at any applied shear stress level is computed by:

$$\gamma = \gamma_e + k\gamma_p \quad (2.13)$$

Where  $\gamma_e$  is the elastic shear strain equal to  $v / G_{cr}$  and  $k\gamma_p$  is the plastic portion of the shear strain. The response predicted by the simple model was compared to the experimental results from a large-scale membrane element test (Stevens et al. 1991) as shown in Fig. 2.8. Stiffness decay and pinching of the loops due to the accumulation of plastic strains in the reinforcement were both well represented by the proposed model.

### 2.3 Seismic shear force demand at levels below ground

There are a number of important issues in the design of high-rise concrete shear walls where shear deformations are significant and therefore the influence of the nonlinear shear response on the seismic force demand shall be investigated. The first topic of the present work which will be discussed in Chapter 3 will investigate the nonlinear shear response in the below-ground sections of a high-rise core wall where large reverse shear forces due to presence of rigid diaphragms and foundation walls, is of considerable concern to designers.

Bevan-Pritchard, Man and Anderson (1983) conducted a study on the force distribution in a core wall at the subgrade levels of a high-rise concrete building subjected to earthquake. Figure 2.9 shows the plan and elevation views of the model of building at levels below ground.

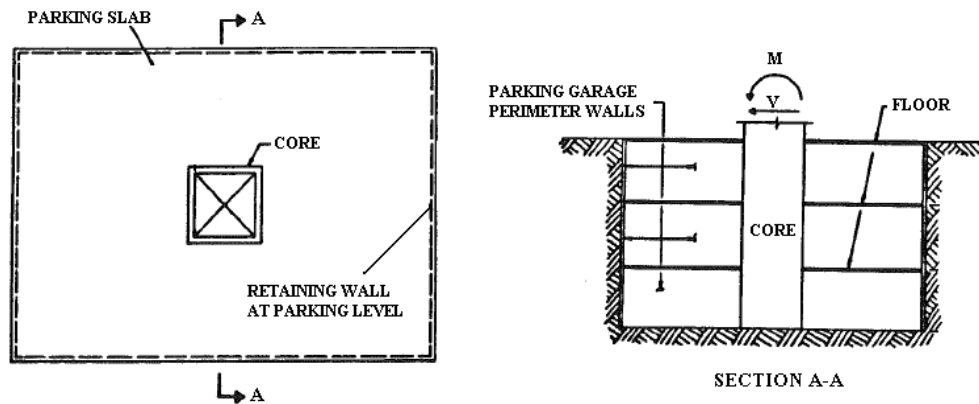


Figure 2.9 Plan and elevation section of the subgrade structure which include core wall, perimeter walls and parking slabs (from Bevan-Pritchard, Man and Anderson 1983).

The analytical model used for the subgrade structure is shown in Fig. 2.10. The core wall and foundation walls were modeled by frame elements accounting for both flexural and shear deformations. Line springs that attach the core wall to the foundation walls below ground were used to account for in-plane bending, axial and shear deformation of parking floor slabs.

As linear analysis was used, the shear force and bending moment could be applied separately, and the concept of applying a unit load was used. The applied base shear force used in all analyses was 1 k, while the bending moment applied at the base was 100 k-ft. Assuming a linearly varying lateral load, the value of moment to shear ratio used in analyses corresponds to a 150 ft high building.

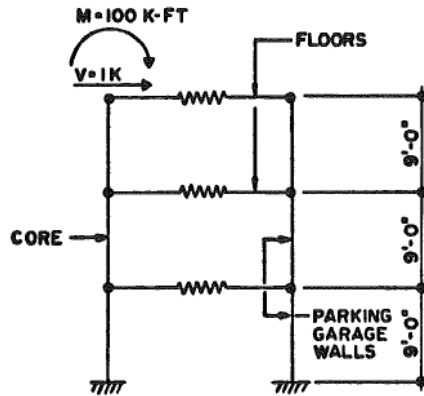


Figure 2.10 Model used to study force demand at subgrade structure by Bevan-Pritchard, Man and Anderson (1983).

Analyses were performed to identify the parameters which most influence the force distribution at subgrade levels of the core wall. In the first case, perimeter walls and the floor diaphragms below ground were assumed to be infinitely rigid neglecting any shear deformation in the core wall. Core wall had a  $30' \times 30'$  tubular section with an all around thickness of  $1'-0"$ , resulting in a moment of inertia of  $I=3.38 \times 10^8 \text{ in}^4$ . For this case, the shear force value in the core wall at the first level below ground was 14 kips, which is fourteen times the base shear associated with the applied bending moment.

In the next case, all the assumptions were similar to first case except that the shear deformation of the core wall was included in the model considering an effective shear area of  $A_v=8640 \text{ in}^2$ . The effect of shear deformation was examined in the core wall by reducing and increasing the initial effective shear area by a factor of 10.

Influence of degree of fixity at the core wall's footing was also examined by assuming an extreme case of fully pinned support. Results for bending moment and shear force at the core wall below ground are shown in Fig. 2.11.

The developed overturning moment and shear force in the core wall below ground showed that the influence of shear deformation was significant when perimeter foundation walls and the parking slabs were assumed infinitely rigid.

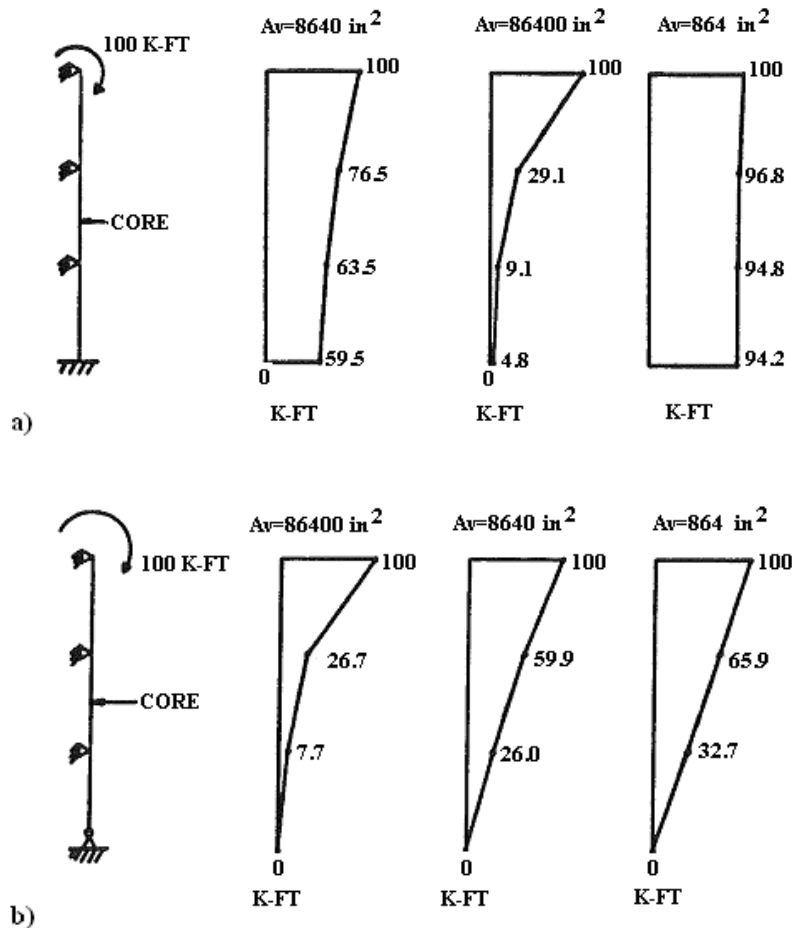


Figure 2.11 Moment distribution for applied concentrated moment at ground for rigid perimeter walls (a) fixed footing (b) pinned footing (from Bevan-Pritchard, Man and Anderson 1983).

Influence of flexibility of foundation walls and parking slabs on the magnitude of developed shear force in the core wall was also investigated. Perimeter foundation walls had a length of 100', a height of 9.0' floor to floor and a thickness of 8.0". Shear stiffness for the core wall was assumed infinite in the first run. Results obtained from analysis showed that due to the large stiffness of foundation walls relative to the core wall, flexural and shear stiffnesses of foundation walls have little influence on the magnitude shear force and bending moments developed in the core wall below ground.

Part of this study proposed a formula for determining the stiffness of the springs used to model the floor diaphragms. Upper and lower bounds equal to 100,000 kips/in and 3,000 kips/in were used for diaphragm stiffnesses to study the distribution of shear force and bending moment in the core wall below ground. Figure 2.12 shows the results for the case when the influence of shear deformation is included in the core wall by assuming  $A_v=8640 \text{ in}^2$ . Comparison of obtained results showed that major influence on shear force distribution was caused by diaphragm stiffness rather than the shear deformation of core wall.

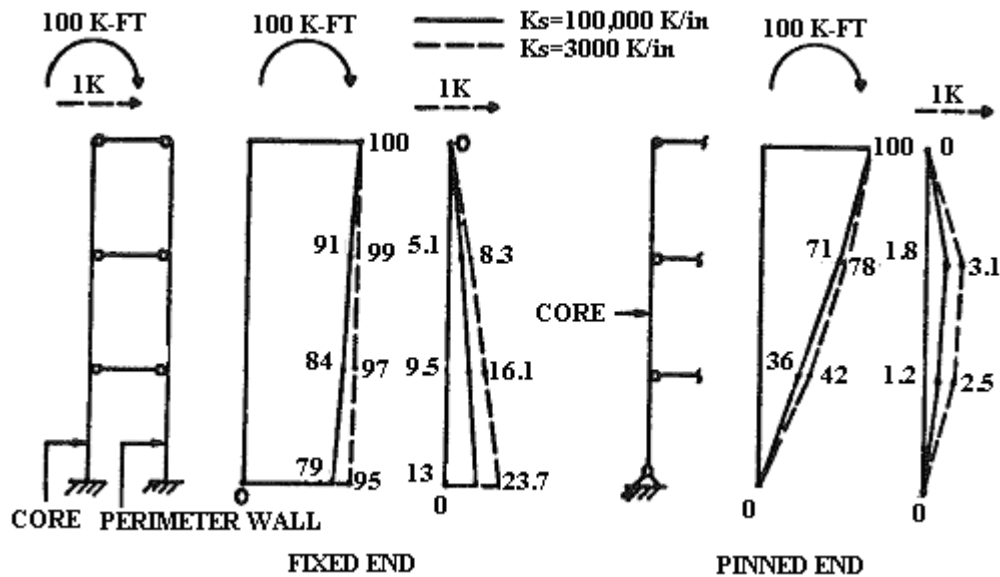


Figure 2.12 Influence of diaphragm stiffness on moment and shear force distribution (from Bevan-Pritchard, Man and Anderson 1983).

Finally 100 k-ft moment and 1k shear force at the base were applied simultaneously to a  $30' \times 30'$  core wall which represented a 20-storey building subjected to lateral motion. Results for this case are shown in Fig. 2.13. The degree of fixity at the core wall's footing found to be the most important parameter with the second most important parameter being the parking slab stiffness. Influence of core wall stiffness was also studied by using  $20' \times 20'$  and  $40' \times 40'$  core sections with different combination of applied moment and shear at the ground level to represent a 6-storey and a 35-storey

building respectively. According to the analyses performed, as the core wall gets stiffer, the effect of other parameters on the distribution of shear force and bending moment below ground becomes less pronounced.

Table 2.2 shows the ratios of developed shear force at the first below-ground level to the applied shear at the base ( $V_{1st}/V_b$ ) corresponding to different analysis cases conducted by Bevan-Pritchard, Man and Anderson (1983).

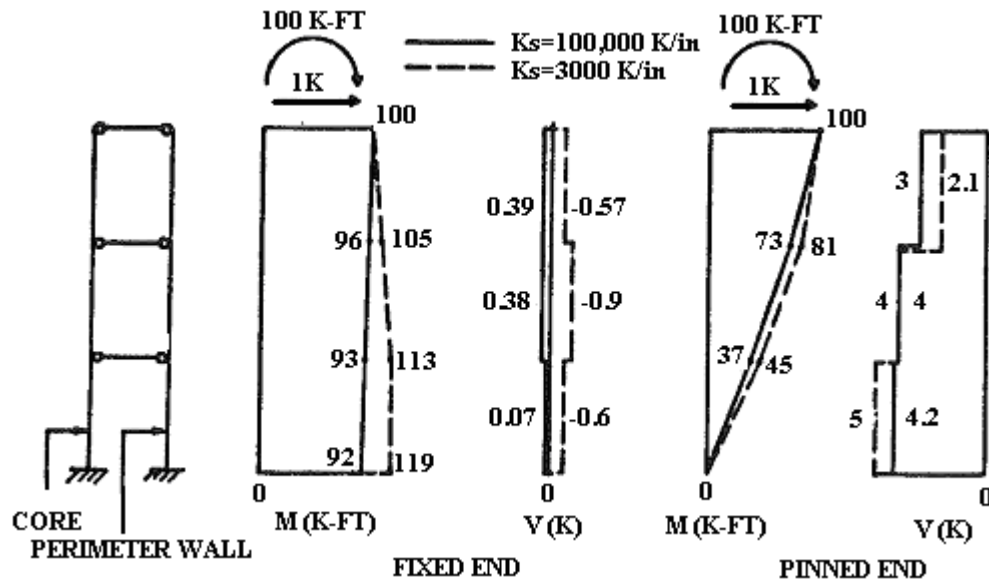


Figure 2.13 Influence of diaphragm stiffness on moment and shear force distribution for simultaneously applied concentrated moment and shear at ground (from Bevan-Pritchard, Man and Anderson 1983).

This study concluded that by using the assumption of rigid floor diaphragms, actual behaviour of the sub-grade structure cannot be captured properly. Parking diaphragm's stiffnesses and degree of fixity at the core wall's footing were found to be the most important parameters that influence the distribution of shear force below ground. It should be noted that the model used in this study was limited to only three stories below ground while the influence of number of stories below ground was not investigated. In fact most of high-rise buildings above 20 stories built today have more than three underground levels to accommodate vehicle's parking space.

The study conducted by Bevan-Pritchard, Man and Anderson (1983) lead to identify parameters that influence the seismic force demand at below-ground levels of the core wall; however their study did not include any nonlinearity in the analytical model. Nonlinear shear behaviour becomes important specially at below-ground levels where the shear stiffness is quite high, furthermore hinging due to large bending moment demand significantly influences the seismic response of core wall above ground.

The nonlinear flexural behaviour above ground as the plastic hinge forms at the base of wall also influences the shear force demand at levels below ground. In the present study, both nonlinear flexural response and nonlinear shear response will be used to investigate the seismic shear demand at below-ground levels of high-rise core walls.

Table 2.2 Ratio of shear force at the first below-ground level to base shear for different analysis cases in study by Bevan-Pritchard, Man and Anderson (1983).

Case	Core wall dimension	Perimeter walls dimension	Diaphragm stiffness	Core moment of inertia	Core wall shear area	Footing at Core	V1st / Vb
1	30'×30'×1'	infinitely rigid	infinitely rigid	$3.4 \times 10^8 \text{ in}^4$	infinite	fully fixed	14.1
2	30'×30'×1'	infinitely rigid	infinitely rigid	$3.4 \times 10^8 \text{ in}^4$	8640 in <sup>2</sup>	fully fixed	2.6
	30'×30'×1'	infinitely rigid	infinitely rigid	$3.4 \times 10^8 \text{ in}^4$	86400 in <sup>2</sup>	fully fixed	7.9
	30'×30'×1'	infinitely rigid	infinitely rigid	$3.4 \times 10^8 \text{ in}^4$	864 in <sup>2</sup>	fully fixed	0.3
3	30'×30'×1'	infinitely rigid	infinitely rigid	$3.4 \times 10^8 \text{ in}^4$	8640 in <sup>2</sup>	fully pinned	4.5
	30'×30'×1'	infinitely rigid	infinitely rigid	$3.4 \times 10^8 \text{ in}^4$	86400 in <sup>2</sup>	fully pinned	7.9
	30'×30'×1'	infinitely rigid	infinitely rigid	$3.4 \times 10^8 \text{ in}^4$	864 in <sup>2</sup>	fully pinned	3.8
4	30'×30'×1'	100'×8"	100,000 K/in	$3.4 \times 10^8 \text{ in}^4$	infinite	fully fixed	0.7
	30'×30'×1'	100'×8"	3,000 K/in	$3.4 \times 10^8 \text{ in}^4$	infinite	fully fixed	-0.8
	30'×30'×1'	100'×8"	100,000 K/in	$3.4 \times 10^8 \text{ in}^4$	infinite	fully pinned	2.8
	30'×30'×1'	100'×8"	3,000 K/in	$3.4 \times 10^8 \text{ in}^4$	infinite	fully pinned	2.1
5	30'×30'×1'	100'×8"	100,000 K/in	$3.4 \times 10^8 \text{ in}^4$	8640 in <sup>2</sup>	fully fixed	0.4
	30'×30'×1'	100'×8"	3,000 K/in	$3.4 \times 10^8 \text{ in}^4$	8640 in <sup>2</sup>	fully fixed	-0.8
	30'×30'×1'	100'×8"	100,000 K/in	$3.4 \times 10^8 \text{ in}^4$	8640 in <sup>2</sup>	fully pinned	3.0
	30'×30'×1'	100'×8"	3,000 K/in	$3.4 \times 10^8 \text{ in}^4$	8640 in <sup>2</sup>	fully pinned	2.1
6	30'×30'×1'	100'×8"	100,000 K/in	$3.4 \times 10^8 \text{ in}^4$	8640 in <sup>2</sup>	fully fixed	0.4
	30'×30'×1'	100'×8"	3,000 K/in	$3.4 \times 10^8 \text{ in}^4$	8640 in <sup>2</sup>	fully fixed	-0.6
	30'×30'×1'	100'×8"	100,000 K/in	$3.4 \times 10^8 \text{ in}^4$	8640 in <sup>2</sup>	fully pinned	3.0
	30'×30'×1'	100'×8"	3,000 K/in	$3.4 \times 10^8 \text{ in}^4$	8640 in <sup>2</sup>	fully pinned	2.1
7	20'×20'×1'	100'×8"	100,000 K/in	$9.5 \times 10^7 \text{ in}^4$	5760 in <sup>2</sup>	fully fixed	0.4
	20'×20'×1'	100'×8"	3,000 K/in	$9.5 \times 10^7 \text{ in}^4$	5760 in <sup>2</sup>	fully fixed	0.7
	20'×20'×1'	100'×8"	100,000 K/in	$9.5 \times 10^7 \text{ in}^4$	5760 in <sup>2</sup>	fully pinned	1.1
	20'×20'×1'	100'×8"	3,000 K/in	$9.5 \times 10^7 \text{ in}^4$	5760 in <sup>2</sup>	fully pinned	0.5
8	40'×40'×1'	100'×8"	100,000 K/in	$8.2 \times 10^6 \text{ in}^4$	11520 in <sup>2</sup>	fully fixed	0.2
	40'×40'×1'	100'×8"	3,000 K/in	$8.2 \times 10^6 \text{ in}^4$	11520 in <sup>2</sup>	fully fixed	-0.9
	40'×40'×1'	100'×8"	100,000 K/in	$8.2 \times 10^6 \text{ in}^4$	11520 in <sup>2</sup>	fully pinned	5.8
	40'×40'×1'	100'×8"	3,000 K/in	$8.2 \times 10^6 \text{ in}^4$	11520 in <sup>2</sup>	fully pinned	4.4



## 2.4 Seismic shear force distribution between inter-connected walls

A second issue where nonlinear shear behaviour has a significant influence is associated with the shear force distribution between inter-connected high-rise concrete walls of different lengths. Chapter 4 of the present dissertation will investigate the shear force distribution in inter-connected walls using both a rigorous nonlinear flexural model and a rigorous nonlinear shear model.

Rutenberg (2004) studied the seismic shear force distribution between cantilever walls with different lengths used in multi-storey buildings. Figure 2.14 shows the building example that Rutenberg used in his study. The walls are attached to each other with floor slabs and therefore restrained to displace the same amount horizontally at each storey over the height. Wall 2 is twice the length of Wall 1 and the building considered was 8 stories high.

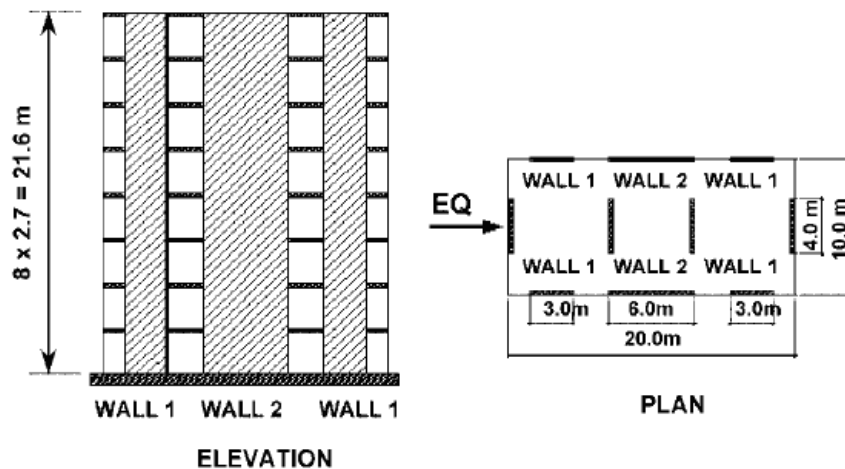


Figure 2.14 Example of building studied by Rutenberg (2004).

Ductile walls are generally designed to yield in flexure at their base and once yielding occurs in one of the walls, the initial force distribution between the walls will change. Since the curvature at yield is a function of wall lengths, walls of different length will yield at different horizontal displacements. The formation of plastic hinge in one of the walls lead to shear force transferring from the yielded wall to the un-yielded walls while transfer of bending moment is mostly carried by the coupling action of floor diaphragms. Rutenberg (2004) found that the force distribution after formation of plastic

hinge in walls is a pure nonlinear phenomenon which cannot be detected by any means of linear analysis.

Rutenberg (2004) carried out several numerical examples to study the force distribution between walls by performing pushover analysis using an inverted triangular loading pattern. Walls were modelled as column elements, and their moment-curvature relationship were assumed to be bi-linear, with initial flexural stiffness evaluated as the yield strength divided by the yield curvature and the post-yielding slope was assumed equal to 1.5% and 1.9% of the elastic stiffness in the short wall and long wall respectively. Figure 2.15 shows the bending moment and shear force distribution at the base of walls with respect to the monitored roof displacement for an example of walls shown in Fig. 2.14. Figure 2.15 shows the initial bending moment carried by the longer wall is much larger than the bending moment carried by both of shorter walls due to the relative flexural stiffness. At a roof displacement of 0.1 m, Wall 2 yielded in flexure causing the extra moment to be transferred to Wall 1. Wall 1 continued to take extra moment until it reached the yielding capacity in flexure leading to significant reduction in the flexural stiffness. Shear force distribution between walls is shown in lower plot on Fig. 2.15. By flexural yielding of Wall 2, shear force is transferred to the un-yielded shorter wall. The shear demand on shorter walls increased rapidly as Wall 2 was unable to carry the extra shear force until Wall 1 yields in flexure causing extra shear force be transferred from Wall 1 to Wall 2.

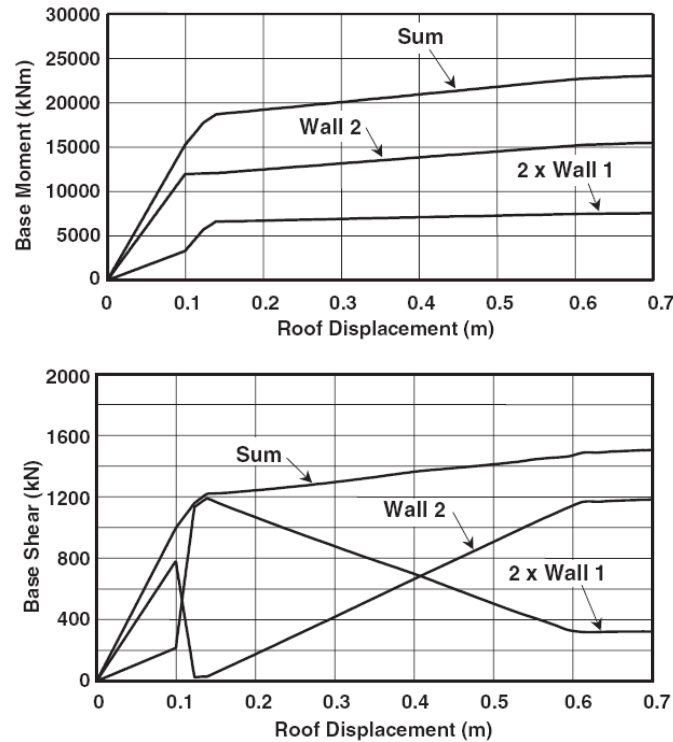


Figure 2.15 Moment and shear force distribution between structural walls in the model shown in Fig. 2.14 by Rutenberg (2004).

The maximum shear force on the shorter wall after flexural yielding of longer wall was observed to be greater than its value predicted by elastic analysis for the same peak base moment. The study showed that the shear force demand on the shorter walls can be underestimated when using a linear analysis as suggested by most design codes.

In the work done by Rutenberg (2004), nonlinear shear behaviour was neglected in the model and only nonlinear flexural response was accounted for. Studying the actual shear force distribution between connected walls in high-rise buildings requires consideration for both nonlinear flexure and nonlinear shear behaviour in structural walls. Since contribution of shear deformation is significant at the levels close to the base in inter-connected walls, it is more appropriate to include nonlinear shear behaviour in the numerical model.

In this thesis, investigation on shear force distribution between inter-connected high-rise walls is done in a more accurate method by taking into account both nonlinear flexural response and nonlinear shear response in the numerical model.

## 2.5 Dynamic shear force demand on cantilever concrete walls

The third and final topic which covers Chapter 5 of this dissertation is related to the dynamic shear demand caused by the influence of higher modes and the corresponding nonlinear action that takes place in tall cantilever walls.

Many building codes such as National Building Code of Canada (*NBCC*) suggest using a simple pseudo-static procedure to estimate seismic shear demand in low-rise to medium-rise buildings. For tall and irregular buildings, influence of higher modes of vibration is significant and therefore dynamic analysis is often required to estimate the force demand during earthquake. While linear dynamic analysis procedures are often used for design purpose, a realistic seismic behaviour which accounts for the structural damage can only be captured by performing nonlinear analysis.

Nonlinear dynamic analysis has shown that flexural yielding at the base of wall does not necessarily limit the seismic shear force. The phenomenon that shear force tends to increase as the magnitude of ground motion increases is often referred to as “dynamic shear amplification” or “dynamic shear magnification”. Dynamic shear amplification factor is defined as the ratio of shear force demand obtained from nonlinear analysis to the shear demand obtained from a linear analysis procedure such as the pseudo-static procedure. Dynamic shear amplification is mainly caused by the effect of higher modes in tall buildings and can significantly influence the distribution of bending moment and shear force over the height of structural walls.

Blakeley, Cooney and Megget (1975) were among the first who investigated the seismic shear force demand for a certain flexural capacity at the base of a cantilever wall. They observed that after yielding of wall at the base, predicted shear force demand by nonlinear analysis is greater than the predicted shear force demand using linear pseudo-static procedure. The study led to significant findings on nonlinear response of walls and as a result, dynamic amplification factor was proposed to be estimated by using Eq. 2.13:

$$\begin{aligned}\omega_v &= 0.9 + n/10 & ; & & n < 6 \\ \omega_v &= 1.3 + n/30 < 1.8 & ; & & n > 6\end{aligned}\tag{2.13}$$

$\omega_v$  is the dynamic shear amplification factor and  $n$  is the number of stories above the base level. Value of  $\omega_v$  proposed in Eq. 2.13 needs not be greater than 1.8 for building over 15 stories high.

The International Federation for Structural Concrete (CEB) suggests a similar expression to estimate the seismic shear demand on structural walls:

$$\begin{aligned}\omega_v &= 0.9 + n/10 & ; & \quad n < 5 \\ \omega_v &= 1.2 + 0.04n < 1.8 & ; & \quad n > 5\end{aligned}\tag{2.14}$$

In the study by Blakeley, Cooney and Megget (1975) nonlinear response of cantilever wall modeled to include flexural yielding at the plastic hinge near the base while shear behaviour was assumed to remain elastic. Note that the expressions given in Eq. 2.13 and Eq. 2.14 depend only on the number of stories.

Keintzel (1990) investigated the nonlinear behaviour of reinforced concrete walls subjected to ground motion and he observed that shear force amplification caused by influence of higher modes depends primarily on the  $q$  factor.  $q$  factor is expressed as  $R$  factor U.S. and Canada and accounts for the level of expected ductility in design. It was observed that during nonlinear dynamic analysis, shear force fluctuates more rapidly than overturning moment at the base of wall. Shear force continues to fluctuate after wall yields at the base. Keintzel (1990) suggested use of amplification factor given in Eq. 2.15 to modify the results obtained from linear analysis to account for nonlinear action of the wall.

$$\omega = q\gamma\sqrt{(M_y / qM_I)^2 + 0.1(\max S_{ad} / S_{ad}(T_1))^2} \leq q\tag{2.15}$$

In Eq. 2.15,  $S_{ad}(T_1)$  is the design value of the acceleration response spectrum for the fundamental period of the structure,  $M_I$  is the overturning moment at the base of wall due to design seismic load for the fundamental mode and  $q$  is known as the ratio between linear demand and provided strength.  $\gamma$  is a correction factor that is equal to 1.0 for typical buildings. In Eq. 2.15, first term under square root accounts for the fundamental period while the second term corresponds to the second mode of vibration. In this procedure, the reduction of the elastic shear force by yielding is only applied to the

fundamental mode of vibration. The expression given by Keintzel (1990) accounts for different seismic parameters associated with dynamic characteristics of the structure and is more refined compared to Eq. 2.13 and Eq. 2.14.

Ghosh (1992) studied the dynamic base shear in an isolated cantilever wall by decomposing it into two components: one associated with the effect of first mode and the other associated with the effect of higher modes. The study by Ghosh (1992) indicated that it is possible to use less number of lumped mass rather than using mass for every floor over the height of wall and yet capture the dynamic response. Four walls having 10, 20, 30 and 40 stories were analyzed using computer program DRAIN-2D (Kanaan & Powell 1973). The program uses a concentrated hinge to model the nonlinear flexural response. The moment-rotation characteristics of reinforced concrete beam-columns elements were used with a basic bi-linear relationship that develops into a hysteretic loop that follows the modified Takeda (1970) model for unloading and reloading path. It is noted that in the study by Ghosh (1992), the effect of inelastic shear was not included in the model. Based on numerical results of nonlinear dynamic analysis, the maximum shear demand at the base of isolated walls was given by Eq. 2.16 which was also addressed by Aoyama et al. (1987) .

$$V_{max}=0.25 W a_{gmax} / g + M_y / 0.67h_n \quad (2.16)$$

$W$  is the total weight of the building and  $a_{gmax}$  is the peak ground acceleration.  $M_y$  is the moment capacity at yield and  $h_n$  is the total height. Equation 2.16 suggests that the developed maximum shear force at the base of wall is equal to 25% of inertial force at peak acceleration plus required shear force acting at two third of height to form plastic hinge at the base of wall.

Eberhard and Sozen (1993) proposed Eq. 2.17 which is very similar to Eq. 2.16 by Ghosh (1992) to estimate the maximum seismic shear demand according to the results obtained from nonlinear dynamic analysis of several reinforced concrete walls.

$$V_k = V_n + D_m . W . A_e \quad (2.17)$$

$V_k$  is the estimated peak shear for the structure and  $V_n$  is the base shear capacity calculated by limit analysis assuming an inverted triangular force distribution.  $D_m$  is a coefficient that varies from 0.27 to 0.30 for a nine storey building.  $W$  is the total weight of the structure and  $A_e$  is the peak ground acceleration. In equations 2.16 and 2.17, the maximum developed shear force is solely dependent on peak ground acceleration and influence of parameters such as ductility and natural period were not included in derivation of above expressions.

Seismic shear demand on cantilever structural walls was studied from a Canadian Code prospective by Filiatrault et al. (1994). The expression given in *NBCC* to estimate base shear was based only on the first mode of vibration. Due to higher modes effect, the resultant of the seismic lateral loading would be considerably lower than two third of height associated with the first mode inverted triangular loading pattern. Five wall-type structures having 3, 6, 10, 15, and 25 stories that were designed in three different seismic zones in Canada: Montreal ( $Z_a > Z_v$ ), Vancouver ( $Z_a = Z_v$ ), and Prince Rupert ( $Z_a < Z_v$ ) were modeled to perform time history analysis. Nonlinear flexural behaviour was modeled using concentrated plastic hinges at both ends of elements while shear behaviour was assumed to remain elastic. The elastic-perfectly plastic moment-rotation behaviour was assigned to each hinge following Takeda stiffness degradation model (1970). A 5% critical Rayleigh damping based on first two modes of vibration was considered and a time-step increment of 0.0015 sec was used in all analysis cases. The analyses showed that the flexural hinge location was different for different seismic zones. In Montreal and Prince Rupert, the flexural hinge was formed at the base of wall whereas for Vancouver the flexural hinge was formed at upper levels as well as base due to the effect of higher modes. Note that the walls geometry and reinforcement changed over the wall's height. 5% dynamic amplification factor was computed from the ratio of actual shear demand to the probable shear strength at every level. The values of dynamic shear amplification factor were found to be in agreement with the proposed values by the New Zealand code. Dynamic shear amplification factor suggested by Filiatrault (1994) was equal 1.0 for  $Z_a \geq Z_v$  and equal to 1.50 for  $Z_a < Z_v$ .

Seneviratna and Krawinkler (1994) studied the same problem to investigate the shear force distribution over the height of wall. The influence of shear deformations in the wall was neglected and walls were modeled using beam-column elements with uniform stiffness over the height. Lumped mass was adjusted at every floor to result in a certain fundamental period to study walls up to forty stories. Bi-linear moment-rotation hysteretic characteristic was used for the plastic hinge at the base ignoring P-Delta effect with  $\alpha$  being the post-yielding slope. The results obtained from nonlinear time history analysis were presented in terms of normalized shear force and bending moment envelope over the height of wall.

The seismic design storey shear envelope based on *UBC-1991* is also shown by the dashed line. It was observed that in the upper quarter of the wall, the distribution of shear force follows the path given by code's provisions whereas in the lower three-quarter of the height, the pattern are significantly different from the first mode estimate of building code. For higher ductility factor in the analysis, moment in upper levels exceeded the overturning moment at the base for the tall walls due to influence of higher modes of vibration and therefore flexural hinge will likely form at upper levels as well as the base of wall. Although higher modes effect in tall walls influenced the shear force demand significantly, it had a less important effect on the global deformation demand. It was also found that the contribution of plastic hinge rotation to the total drift was relatively a stable parameter with a weak dependence on the fundamental period.

Tremblay, Leger and Tu (2001) studied the inelastic response of a 12-storey ductile RC wall under strong ground motion to investigate the P-delta effects. The effective bending stiffness for the model of wall in the analysis was considered  $EI_e=0.7EI_g$ . Two different sets of ground motions were considered according to the seismicity characteristics of Montreal and Vancouver. A bi-linear moment-rotation model was considered for the beam-column elements to represent the nonlinear behaviour of the shear walls. The shear behaviour was assumed to remain elastic similar to previous studies. It was observed that by satisfying the 2.0% inter-storey drift limit proposed by NBCC, the P-Delta contribution becomes less pronounced in the seismic response. Results obtained from nonlinear dynamic analyses also lead to important findings on dynamic shear demand in medium-rise RC walls. It was concluded that pseudo-static



procedure does not accurately capture the shear force distribution over the height of high-rise walls. The seismic shear force demand obtained from inelastic response of the wall is amplified at lower levels close to the base and also at the upper levels when compared to the prediction of pseudo-static procedure.

The average dynamic shear magnification factors obtained at the base of wall located in Montreal and Vancouver were found to be 1.54 and 1.70 respectively. Maximum dynamic amplification was observed at higher levels rather than the base of wall. This study showed that New Zealand provisions to account for dynamic shear amplification were in agreement with the obtained results from nonlinear dynamic analysis.

In a similar approach, Panneton, Legger and Tremblay (2006) investigated the seismic response of an eight-storey building located in Montreal using a 3-D nonlinear element. Interaction of axial force and bi-axial bending was considered in the model of wall. Axial and flexural failure envelopes (CSI 2003) were used together with the modified Takeda hysteretic model to represent the inelastic response of the plastic hinge zone. Dynamic response of the building was studied using synthetic earthquakes representative of credible magnitude-distance scenarios to match UHS seismic hazard of Montreal. The program *Ruaumoko-3D* (Carr 2003) was used in this study to perform three-dimensional nonlinear time history analyses. Panneton, Legger and Tremblay (2006) also observed that the inelastic shear force and bending moment is underestimated when using *NBCC* provisions for seismic design. The large shear force and bending moment in the upper levels of wall indicated the importance of higher modes effect. A mean value of dynamic shear amplification of 2.57 was calculated through the results of inelastic dynamic analysis which was greater than the value 1.57 suggested by the New Zealand code.

Priestley and Amaris (2003) used a suite of five spectrum compatible earthquake records scaled to different multiples of the design intensity from 0.5 to 2.0 in order to study the dynamic response of concrete walls. The modified Takeda hysteretic model (1970) for flexure was used to simulate the nonlinear behaviour of concrete walls with different heights. A modified superposition method based on modal analysis was proposed to obtain a better estimate of the response as was compared with the realistic nonlinear behaviour. By performing nonlinear dynamic analyses and using available capacity design methods, Priestley and Amaris (2003) found that both multi-mode analysis and conventional capacity design methods were non-conservative in estimating the seismic shear demand in high-rise concrete walls. The dynamic shear amplification in walls was found to be highly dependent on the higher modes with second mode dominating.

Rutenberg and Nsieri (2006) studied the seismic shear demand on cantilever walls. Program *Ruaumoko 2-D* (Carr 2000) was used in the analysis assuming an elastic-perfectly plastic flexural response to study the distribution of the shear force over the height of isolated walls. Shear behaviour was assumed linear and only nonlinear flexural behaviour was accounted for. Rutenberg and Nsieri (2006) proposed Eq. 2.18 to estimate the dynamic shear force obtained from nonlinear time history analysis  $V_a$  by amplification of pseudo-static shear force  $V_d$  which is taken as triangularly distributed shear force to cause flexural yielding at the base as given by Eq. 2.19 with  $n$  being the number of stories above base level.

$$V_a = [0.75 + 0.22(T + q + Tq)]V_d \quad (2.18)$$

$$V_d = \frac{M_y}{\frac{2}{3}H(1 + \frac{I}{2n})} \quad (2.19)$$

An envelope for shear force distribution over the height was also proposed by Rutenberg and Nsieri (2006) which is shown in Fig. 2.16.

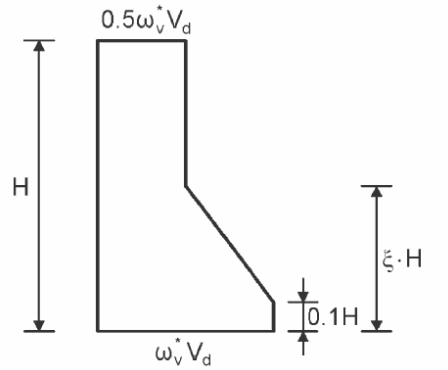


Figure 2.16 Proposed envelope for dynamic shear demand by Rutenberg and Nsieri (2006).

Parameter  $\xi$  used to define shear force envelope is given below:

$$\xi = 1.0 - 0.3T \geq 0.5 \quad (2.20)$$

For which  $T$  is the fundamental period of the wall and  $\omega_v^*$  is the dynamic shear amplification factor as expressed in Eq. 2.18.

It is noted that the dynamic shear amplification factor is mostly used to scale up the shear force demand predicted by the simplified pseudo-static analysis that corresponds to a triangular distribution of seismic forces over the height of building; however dynamic shear amplification factor can also be used to modify the shear force demand obtained through other types of linear analysis such as response spectrum analysis (RSA) or linear response history analysis.

In order to compare different methods to estimate the dynamic shear amplification, an example for several cantilever shear walls is presented here. Table 2.3 provides a summary of assumptions used in deriving the available expressions to determine the dynamic shear amplification factor. The methods described in Table 2.3 were used for the purpose of comparison in the present example. Because of the similarities in the formulas proposed by Aoyama et al. (1987), Ghosh (1992) and Eberhard et al. (1993), Eq. 2.17 suggested by Eberhard et al. (1993) was used which gives an upper-bound estimate for dynamic amplification factor.

Table 2.3 Different procedures to determine dynamic shear amplification.

	<i>NZS-3101 (1982)</i>	<i>Keintzel (1990)</i>	<i>Eberhard et al. (1993)</i>	<i>Rutenberg (2006)</i>
<i>Flexural model</i>	hinge at base	hinge at base	hinge at base	multiple hinging
<i>Shear model</i>	elastic shear	elastic shear	elastic shear	elastic shear
<i>Application</i>	pseudo-static	RSA	pseudo-static/RSA	pseudo-static
<i>Equation</i>	Eq. 2.13	Eq. 2.15	Eq. 2.17	Eq. 2.18

The height and the stiffness of walls in the example were varied, while the concentrated mass at different levels was kept constant. The total weight used to calculate the base shear is equal to the sum of concentrated masses at every story, which are 3.0 m apart, plus the self weight of the wall. The example walls had a tubular (hollow-box) section in which the length and thickness were adjusted so that the calculated natural period of the wall is equal to the number of stories divided by 10. *NBCC-2005* design spectrum for Vancouver - site class C was used to determine the parameters required to calculate the dynamic shear amplification factor using the formulas suggested by Keintzel (1990) and Eberhard et al. (1993). According to the *NBCC-2005* design spectrum for Vancouver, peak ground acceleration and peak design acceleration were

considered to be 0.46g and 0.94g respectively. Since all the proposed expressions except Eq. 2.13 depend primarily on the  $q$  factor ( $R$  factor in North America), values of  $q=2.0$  and  $q=3.5$  for moderate and ductile shear walls were used for this example. In using the formula by Eberhard et al. (2003), the response spectrum analysis (RSA) was carried out to obtain the design bending moment and shear force at the base of walls. The flexural yielding capacity for the example of walls was assumed to be the linear moment demand obtained from response spectrum analysis divided by the  $q$  factor. Similarly the linear shear force demand ( $V_l$ ) required to calculate the dynamic amplification factor by using Eq. 2.17 was assumed equal to the shear demand obtained from RSA divided by the  $q$  factor.

Figure 2.17 presents a comparison of the dynamic amplification factors obtained from the suggested methods described in Table 2.3. Both formulas given by Keintzel (1990) and the one from *NZS-3101* (1982) (originally taken from Blakeley, Cooney and Megget (1975)), maintain an upper-limit for the dynamic shear amplification factor as shown in Fig. 2.17. Dynamic amplification factor obtained by Keintzel's formula is always less than the  $q$  factor while the formula from the New Zealand code limits the amplification factor to the value of 1.8. Formulas proposed by Rutenberg (2006) and Eberhard et al. (1993) have no upper limits for the value of dynamic amplification factor.

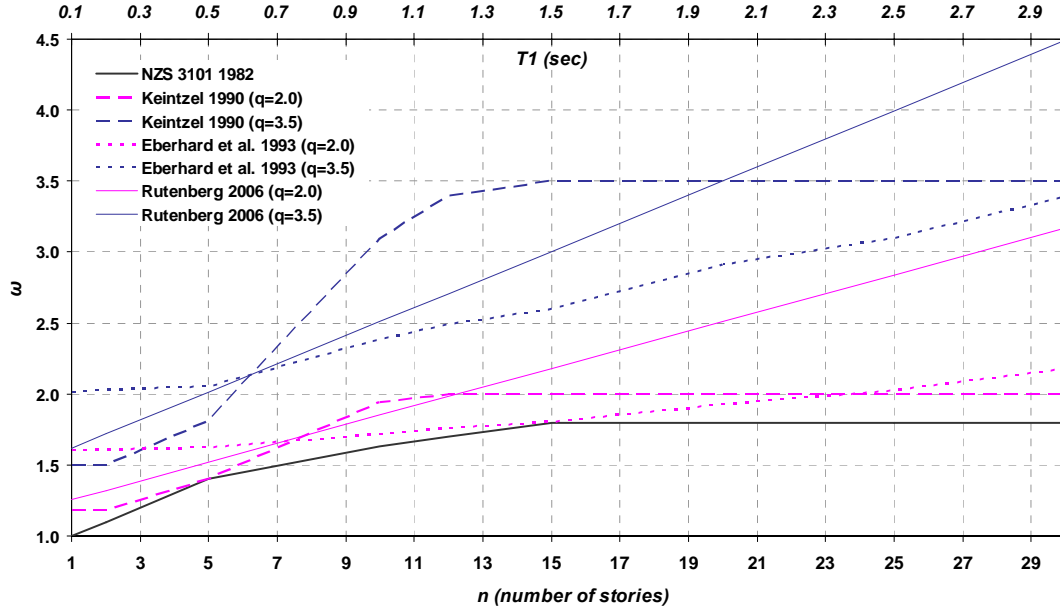


Figure 2.17 Dynamic shear amplification factor  $\omega$  for the presented example.

For  $q=2.0$ , Rutenberg's formula (Eq. 2.18) provides an upper-bound estimate of the amplification factor, while the formula from New Zealand code presents a lower-bound estimate. For low to moderately ductile concrete walls ( $q \leq 2$ ), Eq. 2.13 from the New Zealand code gives amplification values which are relatively in agreement with other formulas. It should be noted that the formula from New Zealand code has been developed for moderate ductile walls as it depends only on the number of stories and it may not be suitable for prediction of dynamic shear amplification in ductile walls. This fact is shown in Fig. 2.17 as Eq. 2.13 gives the lowest dynamic shear amplification factor when compared to other formulas.

The results for the example presented in Fig. 2.17 shows that Eq. 2.17 proposed by Eberhard et al. (1993) provides larger amplification factors for low-rise walls while Eq. 2.15 proposed by Keintzel (1990) gave more conservative values for medium-rise walls. Use of equation 2.18 proposed by Rutenberg (2006) gives the largest amplification factors for medium to high-rise walls in this example.

In general, the methods summarized here for determination of dynamic shear amplification are applicable when elastic models are used for the shear response of the concrete walls. A common shortcoming of the previous studies on the dynamic response of concrete walls was the lack of an appropriate nonlinear shear model in the numerical example. Diagonal cracking in the section of wall during earthquake shaking reduces the shear stiffness significantly which results in a reduction of dynamic shear demand. Since the nonlinear shear behaviour was not accounted for previously, the proposed expressions to determine dynamic shear amplification may not predict the seismic shear demand appropriately. Consideration for the nonlinear shear behaviour in the model of high-rise walls improves the numerical analysis and helps to achieve a better estimate of seismic shear demand during earthquake shaking. The nonlinear seismic behaviour of the wall and the shear amplification phenomenon has been addressed in Chapter 5 of the present dissertation.

## **Seismic shear demand in high-rise walls below ground**

### **3.1 Overview**

Shear walls provide an efficient lateral force resisting system in seismic design of high-rise concrete buildings. Large height to length ratio ( $H_w/L_w$ ) in a typical high-rise shear wall causes the flexural behaviour to dominate when the building is subjected to lateral excitation. In upper levels of a high-rise wall deformations are controlled mainly by flexural behaviour whereas in the lower levels the effect of shear deformations becomes very significant. The central core shear wall system in a high-rise building is known to be an efficient solution to architectural and structural demands. The core wall system with a combination of flat floor slabs has been increasingly used in Western Canada; hence it is important to understand the seismic behaviour of high-rise shear walls and their potential in order to achieve a safer and more reliable structural performance.

In most high-rise buildings, there is a large underground area surrounded by rigid perimeter retaining walls known as “foundation walls”. The purpose of underground area is to provide required space for vehicle’s parking, shopping centers or commercial facilities. The foundation walls possess high in-plane rigidity according to large dimensions along the excavated underground area.

In practice engineers often use linear analysis procedures such as response spectrum analysis for design of high-rise buildings. Presence of foundation walls and stiff



diaphragms below ground will result in development of large shear force on the core wall if response spectrum analysis is used. According to results obtained from RSA for some cases, the reverse shear force magnitude increases up to several times the magnitude of design base shear.

While use of linear methods can be time saving and easy to do, it may lead to unrealistic estimate of response since the actual structural behaviour subjected to strong ground motion, can only be captured by performing nonlinear analysis. Nonlinear response of the shear walls during earthquake may reduce the magnitude of reverse shear force while wall undergoes large shear deformation. The scope of this study is to provide solutions to help improve the seismic design of high-rise shear walls based on both linear and nonlinear analyses. A full 3-D model of a typical high-rise structure is shown in Fig. 3.1. Use of 3-D models in structural analysis can increase the accuracy of captured response; however drawback would be timeliness and complexity of analysis procedure. Since using simple structural models allows an in-depth exploration of the complex problem a 2-D model of shear wall - foundation wall system was used to study the seismic response of high-rise core walls below ground.

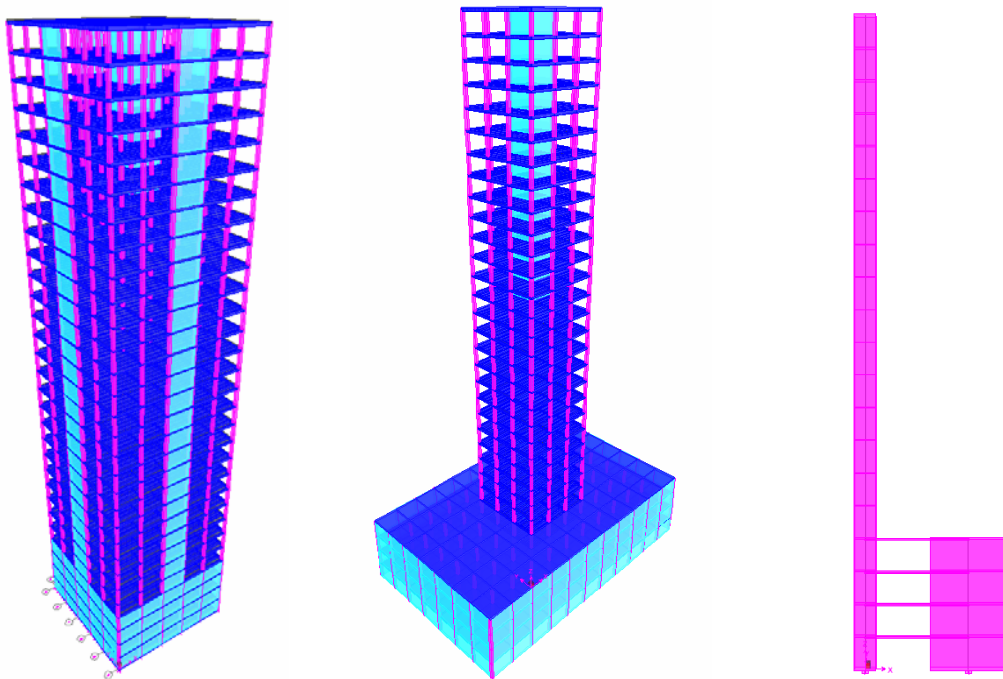


Figure 3.1 Model of two typical high-rise buildings walls and the corresponding simplified 2-D model.

### 3.2 Model definition

A simplified 2-D model of high-rise core wall which is attached to the foundation walls through below-ground diaphragms is shown in Fig. 3.2. In this model diaphragms can be modeled either using the rigid-diaphragm assumption or by considering their actual in-plane stiffness. The shear wall dimensions in this model were chosen based on real design examples in high-rise concrete buildings.

A typical bending moment and shear force distribution over the height of wall is shown in the Fig. 3.2. According to the linear analysis, the reverse shear force in the wall section below ground can be several times greater than the base shear due to action of diaphragms and foundation walls.

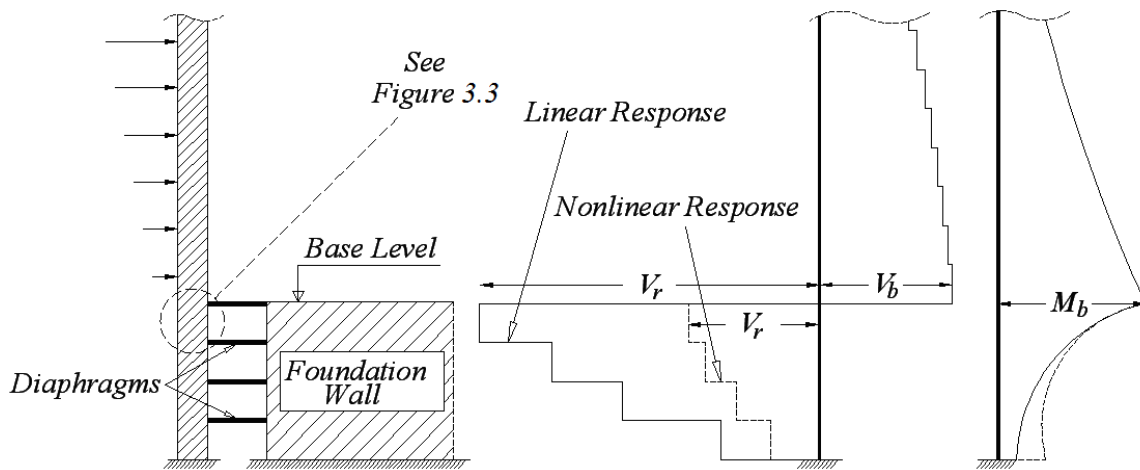


Figure 3.2 Shear reversal phenomenon in high-rise concrete walls and the corresponding moment and shear distribution.

The foundation walls are numerous in size and stiffness according to the design objectives in high-rise building. The lateral stiffness of the foundation wall is usually large compared to that of a core wall. Because of the high in-plane stiffness of foundation walls they are often considered as fully rigid in design practice. The assumption of infinite rigidity for foundation walls simplifies their behaviour as fixed supports. We will see later that this assumption would result in a small overestimation of forces in the core wall below ground.

Another influencing parameter on the magnitude of shear force below ground is the stiffness of floor slabs or “below-ground diaphragms”. One common simplification in analysis of high-rise buildings is the assumption of rigid diaphragms in modeling the behaviour of floor slabs. In a 3-D model, rigid diaphragm provides two translational and one rotational degree of freedom. In the case of a 2-D model, the number of degrees of freedom at every floor reduces to one translational component. Concrete slabs usually possess high axial rigidity; therefore many designers prefer using the rigid-diaphragm assumption to reduce computational effort. While rigid-diaphragm model is reasonable to model the floor slabs at levels above ground, it may not be suitable to represent the behaviour of diaphragms below ground during earthquake. For cases concerned with high reverse shear force in high-rise walls, the rigid-diaphragm assumption can cause significant amplification to the reverse shear force; therefore accounting for the actual diaphragm stiffness would result in a better estimate of core wall’s seismic response.

A high-rise wall shows a complicated dynamic response to seismic forces due to the effect of higher modes of vibration. For any specific deformation one can find a corresponding lateral loading pattern which is simply the product of mass and acceleration over the height at every level. Unlike low-rise buildings in which the first mode governs the total response, high-rise buildings behaviour is dependent on higher modes as well first mode of vibration. Most of present building codes are based on behaviour in the first mode of vibration with some adjustments to somehow account for the effect of higher modes. While use of simplified methods for estimating seismic demand is useful for low to medium-rise buildings, the design code suggests use of dynamic analysis for tall and irregular buildings.

Finding the actual lateral loading pattern for seismic forces is not an easy task since there are many parameters which affect the dynamic structural response. To assess the seismic response, building codes propose a lateral loading pattern over the height of structure is proposed based on the first natural mode of vibration. The code suggests a linear distribution of loads over the height of building. For high-rise buildings with a longer natural period, the seismic loading pattern is greatly dependent on the higher modes. Dynamic response analysis for a number of earthquake events has indicated that

the actual distribution of the seismic forces in high-rise buildings is not similar to the prediction by design code which depends mainly on first mode.

For a single cantilever wall, the seismic lateral loading pattern can be represented by two single parameters: Overturning moment at the base  $M_b$  and base shear  $V_b$ .

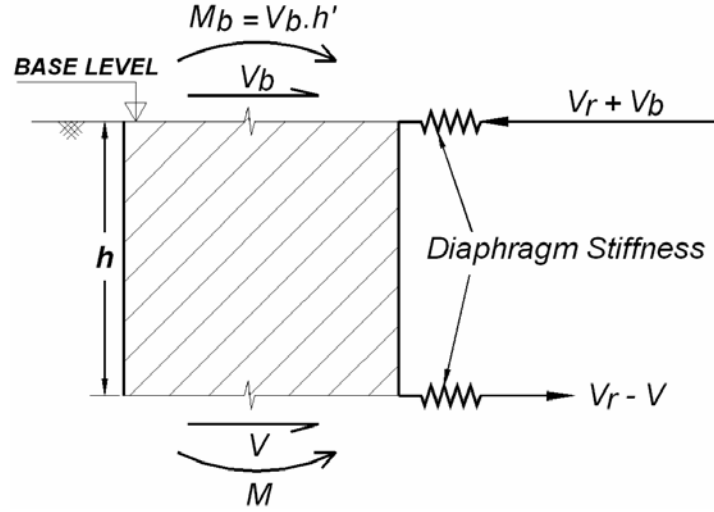


Figure 3.3 Diagram of forces at the below-ground section of wall.

Free body force diagram for a section of wall at below-ground levels is shown in Fig. 3.3. The reverse shear force is dependent on the overturning moment at the base, shear at the base and also the height of storey below ground. Diaphragms action is modeled by uniaxial springs and the foundation wall is assumed fully rigid.

Equilibrium of the internal and external forces acting on the wall results in deriving the following relationships:

$$h' = \frac{M_b}{V_b} \quad (3.1)$$

$$\frac{V_r}{V_b} = \frac{h'}{h} \left( 1 - \frac{M}{M_b} \right) \quad (3.2)$$

Where  $h$  is the height of level below ground and  $h'$  is the ratio between overturning moments and the shear force at the base of wall. Equation 3.2 shows that the reverse

shear force magnitude is in proportion to the moment to shear ratio  $h'$ . Parameter  $h'$  mainly depends on the characteristic of the ground motion as well as the wall dynamic response. Moment to shear ratio at the base of cantilever high-rise walls will be studied as thoroughly in Chapter 5 of this dissertation.

Flexural and shear strength of the wall section are important parameters to be considered in this study. More flexural capacity means more overturning moment can be transferred by the wall section below ground to the footing and higher shear strength in wall means more shear can be resisted by the wall section below ground. It is important to note that the reverse shear force and the overturning moment at the section below ground work together to balance the forces acting on the base level. The bending moment at the base can be carried by two different mechanisms: one by the bending in wall section below ground and the other one is by the coupling action of forces developed in the diaphragms above and below the specified section.

After a short introduction to the parameters which influence the reverse shear force, a complete study on influence of these parameters on the developed reverse shear force will be presented.

### 3.2.1 Diaphragm stiffness below ground

In the present study a simply supported deep beam accounting for both bending and shear deformations was considered to investigate the diaphragm rigidity below ground. The rigid foundation walls are assumed to act as lateral supports due to their high lateral stiffness. The core wall's action is modeled by applying two concentrated loads at the location of shear walls as shown on Fig. 3.4. Different thickness values of the diaphragm similar to design practice have been examined according to Table 3.1.

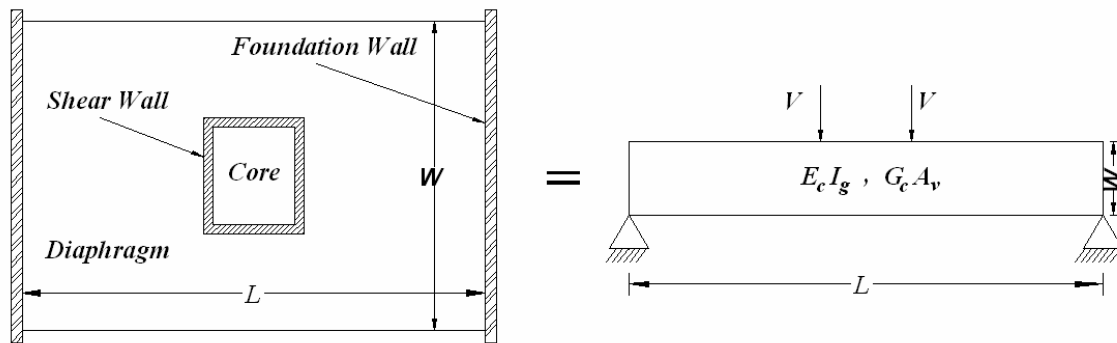


Figure 3.4 Simplified model to determine the diaphragm stiffness.

Table 3.1 Possible diaphragm stiffness used in practice (values in MN/mm).

Diaphragm $L/W$ ratio	$L/W=0.5$	$L/W=1$	$L/W=2$
8" concrete slab	12.5	5.0	1.4
16" concrete slab	25	10	2.8

The out-of-plane stiffness of the foundation walls is ignored; furthermore the foundation walls parallel to the shear forces are modeled as simple supports of the beam. Both flexure and shear deformations of the beam have been included. The stiffness of the beam depends on the span-to-depth ratio of the beam, which is equal to  $L/W$  for the diaphragm, as well as the width of the beam, which is equal to the average thickness of the floor. The stiffness of the diaphragm spring is the shear force applied per unit deflection of the beam at the location of the applied shear force. In order to examine the influence of diaphragm stiffness, three different diaphragms were used in the analyses. All diaphragms were

assumed to be uncracked, and to be constructed from 30 MPa concrete with a Modulus of Elasticity  $E_c$  of 25,000 MPa, and a Shear Modulus  $G_c$  of 10,000 MPa. Table 3.2 gives a range of possible diaphragm stiffness used concrete high-rise buildings.

Table 3.2 Diaphragm stiffnesses used for analysis cases.

Case	Diaphragm Type	Stiffness (kN/m)
<i>K30</i>	High stiffness (Rigid)	$30 \times 10^6$
<i>K10</i>	Moderate stiffness (Stiff)	$10 \times 10^6$
<i>K1</i>	Low stiffness (Soft)	$1 \times 10^6$

The most flexible diaphragm has an  $L/W$  ratio of 2 and an average thickness of 200 mm, resulting in a diaphragm (spring) stiffness of about 1.0 MN/mm. The intermediate diaphragm has an  $L/W$  ratio of 1.0, an average thickness of 400 mm, and a diaphragm stiffness of 10 MN/mm. The stiffest diaphragm has an  $L/W$  ratio of 0.5, an average thickness of 400 mm, and a diaphragm stiffness of 30 MN/mm. The three cases are referred to as *K1*, *K10* and *K30*, respectively in Fig. 3.5.

The results in Fig. 3.5 indicate that over the range considered, the diaphragm stiffness has a very significant influence on the magnitude of the reverse shear force. It is interesting to note that diagonal cracking of a diaphragm will reduce the shear stiffness of a diaphragm to about 10% of the uncracked section stiffness. Thus cracking of a diaphragm may have a very significant influence on the magnitude of the reverse shear force. The diaphragm can have a very significant effect on the distribution of shear forces. The flexibility of the diaphragms reduces the effect of shear reversal at the underground levels; therefore, it would be reasonable to consider this flexibility effect in the design to reduce the amount of shear reinforcement in the shear walls that may lead to a brittle behaviour. Figure 3.5 also shows the variation of shear reversal ratio for possible diaphragm stiffness as discussed in this section.

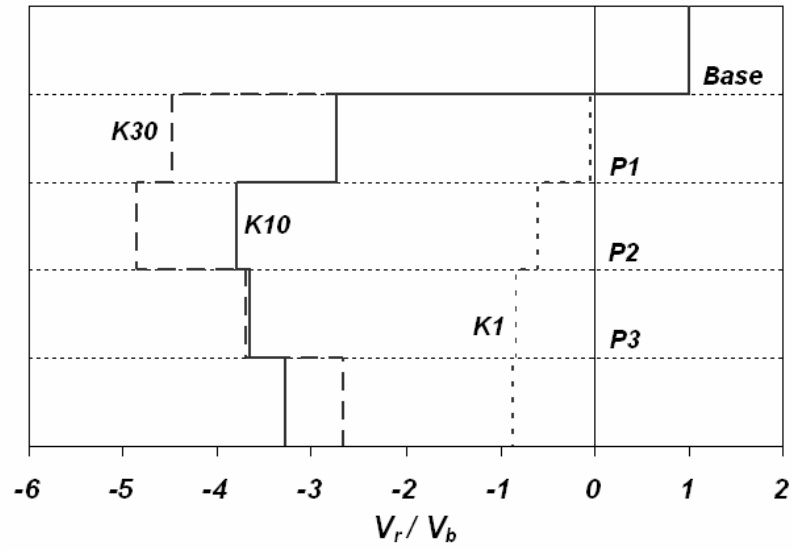


Figure 3.5 Diaphragm stiffness effect on the shear force distribution for a 30-storey wall.



### 3.2.2 Foundation wall influence

Foundation wall rigidity depends on the size and thickness of the wall. The out of plane stiffness of wall is small and therefore ignored here. Foundation walls are connected to the shear walls through diaphragms at the below-ground levels. The stiffness of the wall has a direct influence on the magnitude of the developed reverse shear force at underground area. For a specific seismic lateral force, the distribution of carried internal forces by the wall and spring elements is proportional to their relative stiffness. In Fig. 3.6 the effect of foundation wall size on the shear force distribution is illustrated. This plot is obtained for a 30-storey shear wall corresponding to a  $h'/H$  ratio of 0.67,  $H$  being the total height of wall.  $L_f$  and  $L_w$  define the foundation wall and shear wall length. The same thickness was used for both core wall and foundation wall for the entire analysis.

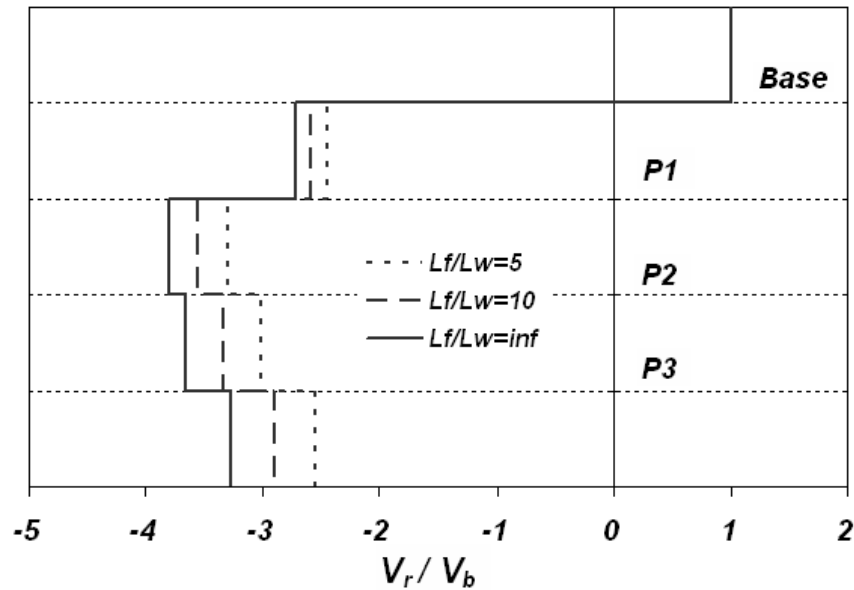


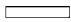


Figure 3.6 Foundation wall stiffness effect on the shear force distribution.

The analysis indicates that for the large ratios of foundation wall's length to the shear wall's length, the foundation walls may be treated as fixed supports.

### 3.2.3 Flexural and shear deformation of the wall

The core-wall shape has a significant effect on the corresponding reverse shear force at below-ground level. In order to investigate this effect, three different core-wall sections have been selected to study the influence of flexural stiffness of section on the shear force distribution below ground. The geometrical properties of the sections are given in Table 3.3. Wall *I1* is a rectangular wall having a length of 9.0 m and a thickness of 1.5 m. Wall *I2* is a flange wall in which flanges are 4.5 m long with a thickness of 0.75 m and the web is 9.0 m long with a thickness of 1.5 m. *I3* is a wall with large flanges having a length of 9.0 m equal to the web length. The thickness of flanges in *I3* is assumed 0.75 m and thickness of web equal to 1.5 m. The purpose of selecting these wall section geometries was to have a consistent shape with what exist in real buildings and also keep the effective shear area constant in all three cases.  $A_{ve}$  is the effective shear area of the section which was assumed equal to 80% of web area ignoring the flange area in flange sections.

Table 3.3 Wall sections used for analysis cases.

Wall Type	$I_g$ (m <sup>4</sup> )	$A_{ve}$ (m <sup>2</sup> )	Shape	Section
<i>I1</i>	91.125	13.5	Rectangular	
<i>I2</i>	167.90	13.5	Short Flange	
<i>I3</i>	283.07	13.5	Long Flange	

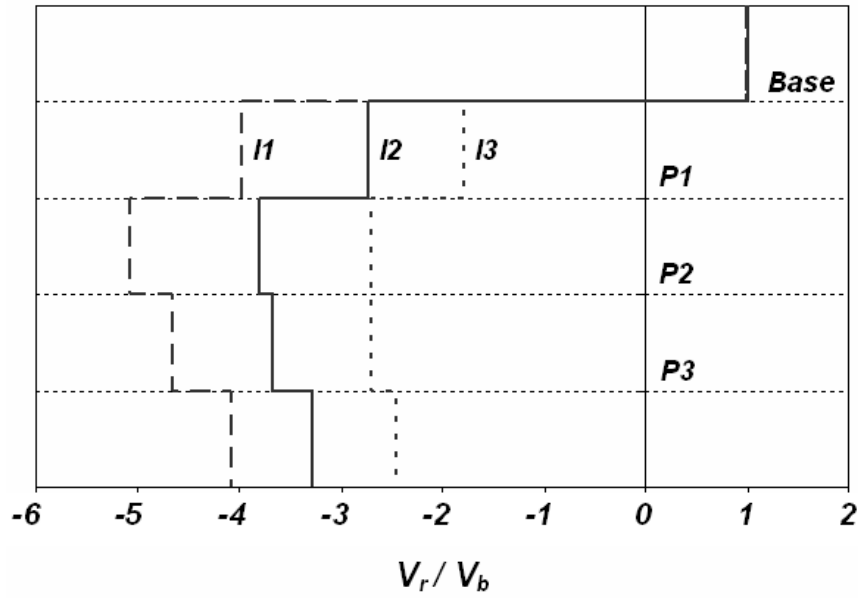


Figure 3.7 Influence of flexural rigidity of wall below ground on the reverse shear force.

The flexural rigidity however is different in each wall to examine how the flexural deformation influences the magnitude of the developed shear force at underground levels. It is expected that the wall with large flange would carry more bending moment through its section compared to two other walls having less moment of inertia about their bending axis. Where the seismic demand is the same for all walls, the reverse shear force reduces as the wall capacity in flexure increases. The results are shown for a 30-storey wall in Fig. 3.7.

Figure 3.7 shows the effect of nonlinear flexure behaviour on the wall's shear force magnitude at the first below-ground level. It is observed that development of flexural cracks due to bending action in shear walls does not have a significant influence on increasing the shear reversal in the wall (e.g  $EI_e=0.7EI_g$ ).

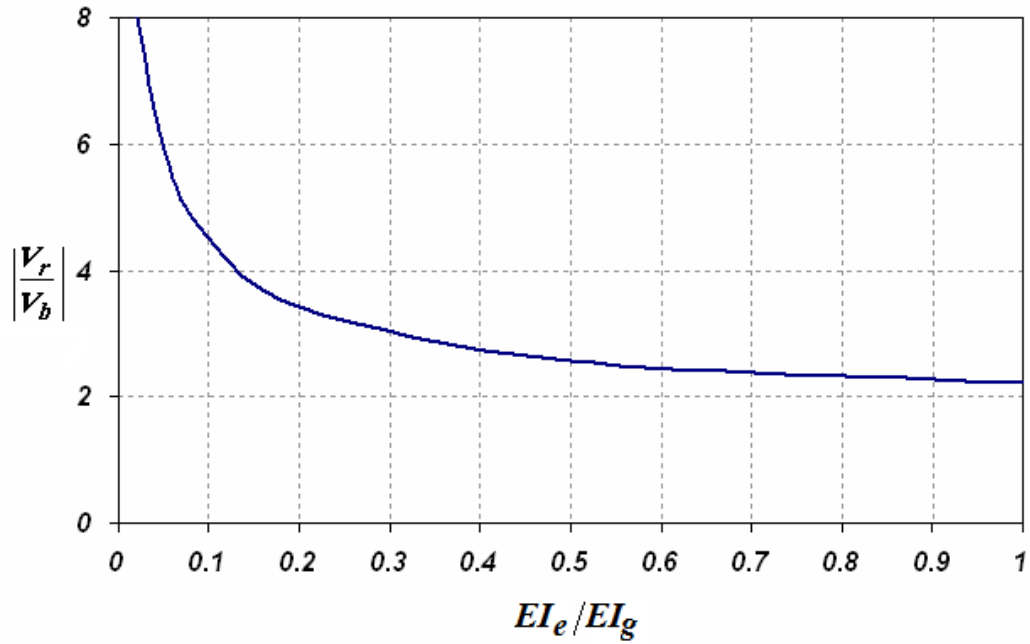


Figure 3.8 Increase in shear reversal due to reduction in effective flexural stiffness.

The influence of shear deformations is shown in Fig. 3.9. The results are shown for wall *I2* with section properties described in Table 3.3. Neglecting the shear deformation (which is significant in the behaviour of concrete walls) would lead to overestimation of response especially in levels below ground. It was also observed that reduction of shear stiffness to 10% of gross shear stiffness significantly reduced the reverse shear force at below-ground levels.

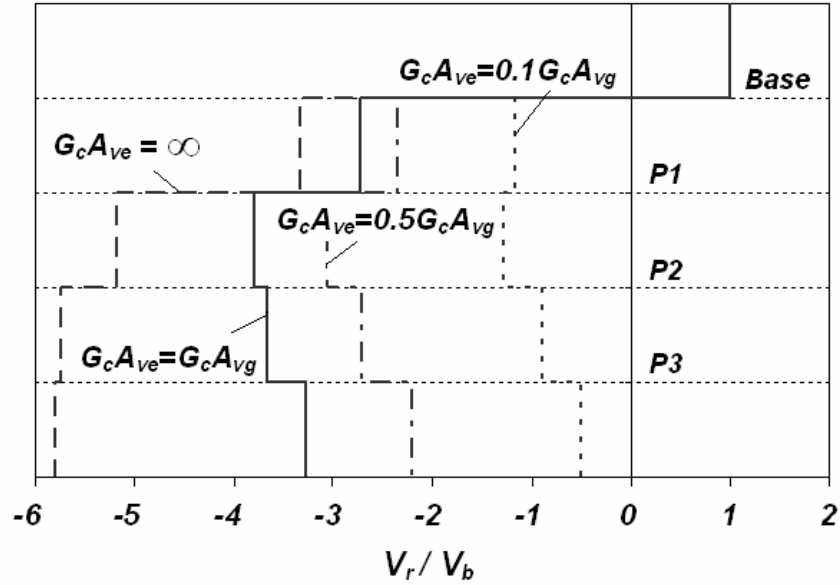


Figure 3.9 Influence of shear rigidity of wall below ground on the reverse shear force.

### 3.2.4 Effect of wall footing partial fixity

It is a common assumption in practice to model the base of wall at footing as fully fixed. This assumption basically eliminates the translational and rotational degrees of freedom at the base of wall. Since there always can be a small amount of rotational freedom at the wall base, the effect of partial fixity of the wall is important to be investigated.

In order to apply the effect of partial fixity in the simplified model, one can add a single rotational spring to the base of walls; however obtaining the actual rotational stiffness depends on geotechnical properties of underlying soil. In spite of difficulties in determining the appropriate degree of fixity at footing, lower and upper bounds for footing rotational fixity were defined by considering two cases of a fully restrained (fixed) footing and a fully free (pinned) footing.

Using a set of linear analyses, the influence of footing rotation has been studied. In the analysis, the foundation wall is assumed rigid, diaphragm stiffness “ $K30$ ” has been considered and the number of levels below ground has been varied from 1 storey to 6 stories to cover a possible range in typical high-rise buildings.

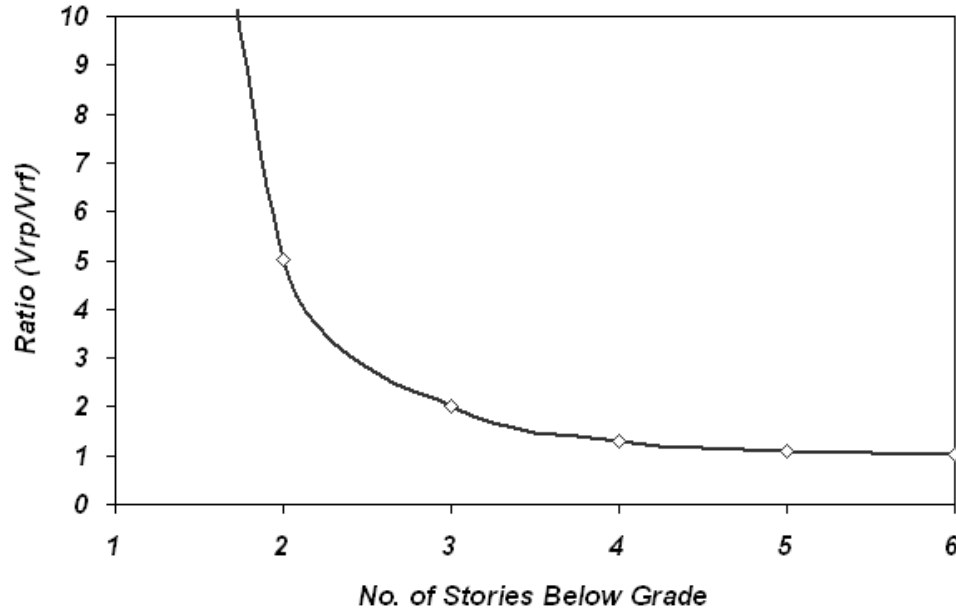


Figure 3.10 Effect of number of stories below ground and the footing fixity on reverse shear force at the first below-ground level.

Figure 3.10 shows the influence of the footing fixity on the magnitude of reverse shear force with respect to number of below-ground levels.  $V_{rp}$  is the shear force at the section below ground where the footing has no rotational constraint and  $V_{rf}$  is the shear force at the section below ground when the core wall is fixed at the footing. The rotation of the wall at the footing will result in an increase in the reverse shear force demand. This is because of the fact that more moment can be carried by flexure of the wall section below ground when it is restrained against rotation at footing and consequently less reverse shear force is developed. Another parameter which influences the magnitude of shear reversal would be the number of stories below ground. It was observed that the degree of wall fixity at footing becomes less significant where the number of below-ground stories increases.

For a typical high-rise building with more than 30 stories above ground, it is usual to consider a minimum of four stories below ground and therefore the effect of partial fixity at wall footing becomes less significant in the magnitude of developed shear reversal as shown in Fig. 3.10.

### 3.3 Dynamic response

After studying the influencing parameters in the magnitude of reverse shear force, dynamic behaviour of the wall will be investigated. Seismic analysis was performed on the model of core wall for both linear dynamic analysis and nonlinear dynamic analysis.

In order to study the dynamic response of high-rise walls, two simplified 2-D models were considered as shown in Fig. 3.11. Stiffness and mass are adjusted to represent a specific fundamental period for the wall. Where nonlinear analysis is performed, the nonlinear hinge is considered at the base of wall as shown in Fig. 3.11. The model on the left shown in Fig. 3.11 is a cantilever wall which is referred to as Model 1 and the model on the right is a combined model of high-rise wall and the below-ground diaphragms which is referred to as Model 2 in this study.

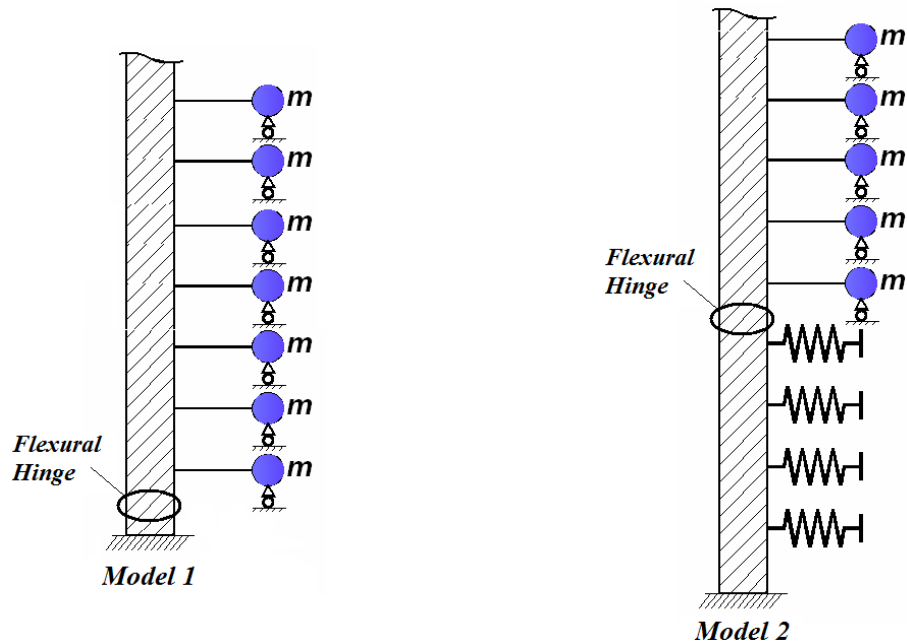


Figure 3.11 Left: Cantilever model of wall (Model 1), Right: Core wall and below-ground diaphragms (Model 2).

In order to perform dynamic analysis on the models of high-rise concrete wall, program SAP-2000 (CSI 2006) was used to perform response spectrum analysis and direct-integration time history analysis. For more information regarding implementation of dynamic analysis refer to “SAP-2000 Analysis and Theory Reference Manual 2006”.

### 3.3.1 Linear dynamic response

Linear dynamic analysis was carried out to address some important issues on the earthquake response of tall walls. In order to study the portion of buildings above ground, a cantilever shear wall with adjusted mass to simulate the building response has been considered as shown in Fig. 3.11.

Figure 3.12 shows distribution of normalized shear and moment by their peak values at the base for 2 different heights of Model 1. Figure 3.12 also shows the effect of higher modes for structures. The response spectrum considered is the 5% damped spectrum associated with horizontal component of Northridge earthquake.

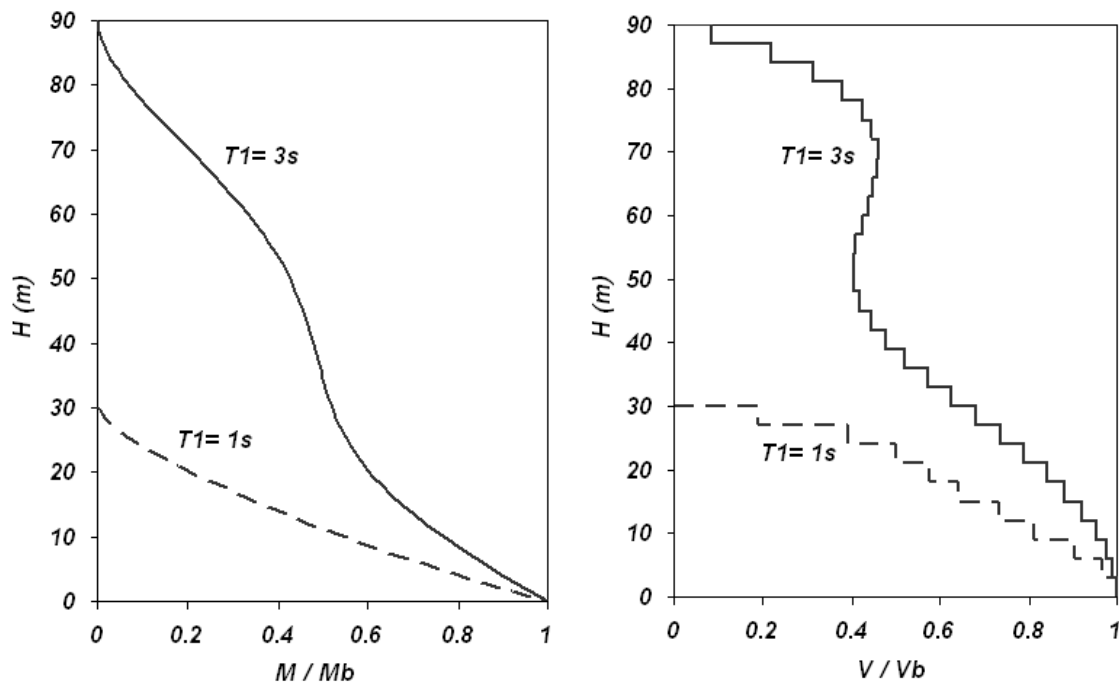


Figure 3.12 RSA results for normalized shear force and overturning moment over the height of a cantilever wall (Model 1).

It is noted that the final results of RSA are obtained by combination of peak responses in each individual modes of vibration and since the peak response of different modes are not likely to occur at the same time, the distribution of forces are not quite similar to the actual response. In addition, RSA uses the absolute values for the final combination and does not give a realistic force distribution over the height considering the direction of developed forces.



To investigate the possible values of  $h'$  through response spectrum analysis for typical buildings with fundamental periods ranging from  $T_f=1$  sec to  $T_f=5$  sec, two different design spectra of *NBCC-1995* and *IBC-2000* were chosen. The results are shown in Fig. 3.13.

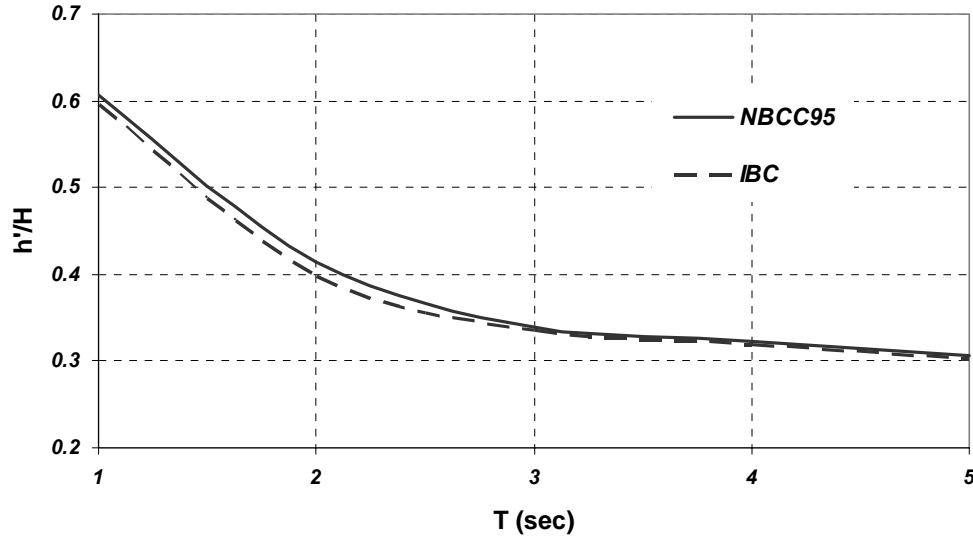


Figure 3.13 Moment to shear ratio at the base of cantilever wall having different fundamental periods obtained from RSA (Model 1).

According to RSA, the parameter  $h'$  ranges between  $0.2H$  to  $0.7H$  for the high-rise to low-rise walls. Possible values of  $h'$  obtained from linear time history analysis (LTHA) and nonlinear time history analysis (NTHA) of high-rise cantilever walls will be presented in Chapter 5 of the present document

Linear dynamic analyses in the form of RSA and time history analysis was performed on the model of wall with  $T_f=3$  sec. The Northridge earthquake acceleration record was used for LTHA. *I2* was used for wall section and the diaphragm stiffness was assumed to be  $K30$ . Figure 3.14 shows the distribution of bending moment and shear force over the height of wall for each type of linear dynamic analysis.

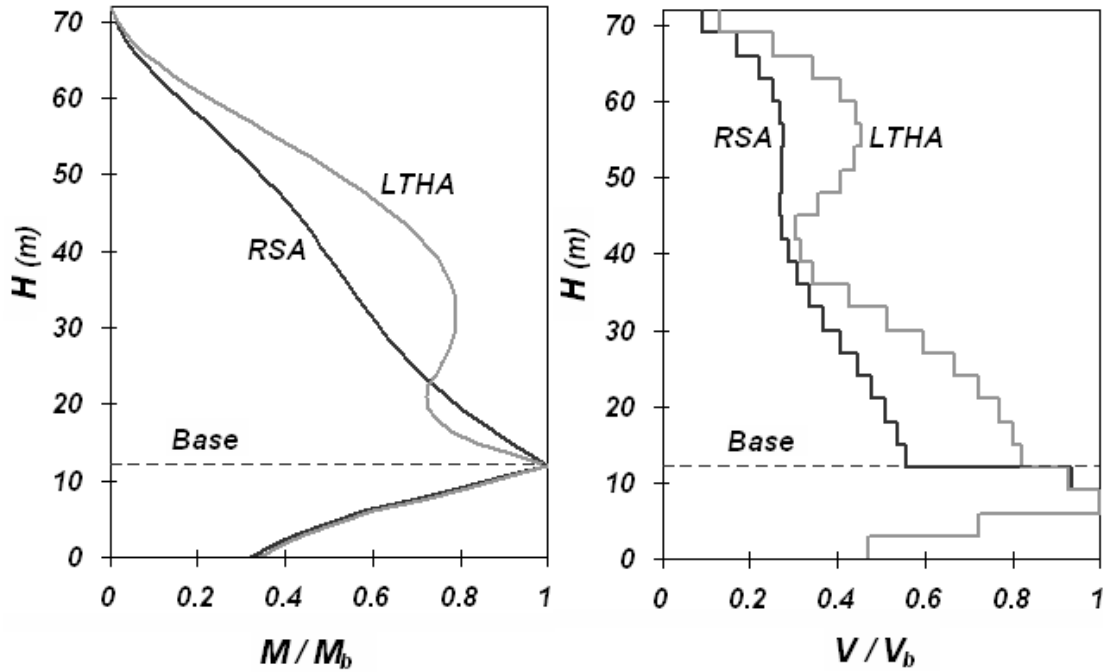


Figure 3.14 Response spectrum analysis vs. Linear Time history analysis (Model 2).

*NBCC-2005* response spectrum was considered for RSA to demonstrate the effect of response spectrum used by the design code. As shown in the Fig. 3.14, use of design spectrum results in a linearly varying bending moment diagram whereas use of LTHA for specific record pronounces the influence of higher modes. A fair estimate of forces over the height is essential to determine the location of potential hinges and other aspects of a safe seismic design.

### 3.3.2 Nonlinear dynamic response

Both the core wall and diaphragm can undergo nonlinear behaviour during earthquake. In some design procedures, the diaphragm is assumed to crack under severe ground motion. This assumption can help reduce the shear reversal at the below-ground level; however there is a question if this assumption would be applicable given the high in-plane rigidity of diaphragms below ground.

In order to investigate the actual dynamic response of high-rise walls, a series of nonlinear analyses were performed. It is reasonable to build up the model gradually to

understand the nonlinear response transparently. For this purpose, dynamic response of a cantilever wall subjected to horizontal component of El Centro ground motion was studied. The dimension of wall and the concentrated mass associated with each level were adjusted to represent a typical natural period corresponding to buildings with different heights.

To simplify the nonlinear dynamic response, a rigid plastic hinge was considered to form at the base of wall by neglecting strain hardening. The hysteretic behaviour considered for the hinge at the base was Takeda model (1970) which was consistently used in previous studies (see Fig. 3.15).

The analyses were performed for four levels of natural periods ranging from  $T_1=1$  sec to  $T_1=4$  sec. The time history values for the corresponding bending moment and shear force at the base are shown in Fig. 3.16 through Fig. 3.19. These figures show the normalized bending moment and shear force history at the base. All plots are given for the first 20 seconds of the total response. Yielding points are shown as flat lines at peak responses. The plots are magnified during periods of yielding to clearly show the variation of shear force at the base of wall.

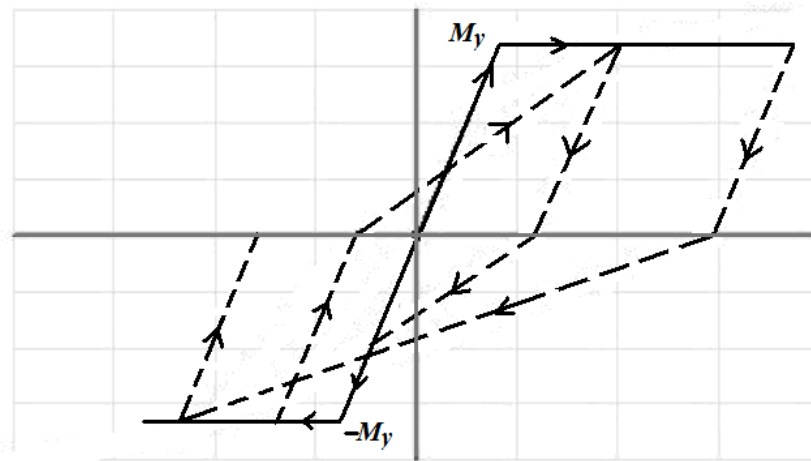


Figure 3.15 Nonlinear Takeda model (1970) for the plastic hinge at the base of wall.

Once the flexural hinge forms at the base of wall, moment demand at the base remains constant while the corresponding base shear varies with respect to time. As walls are usually detailed for flexural yielding at the base, it is useful to study the variation of moment and shear forces at the base of the wall during this event. For taller walls with a

higher fundamental period of vibration, the shear force magnitude at the base can reach zero during yielding at the base. This is due to effect of the higher modes and distribution of the lateral forces along the height of building. In other words since there are many modes of lateral force distribution over the height of wall, it is possible that at an instance of time, shear forces acting on opposite directions would balance each other effect so that the shear at the base of wall becomes very small.

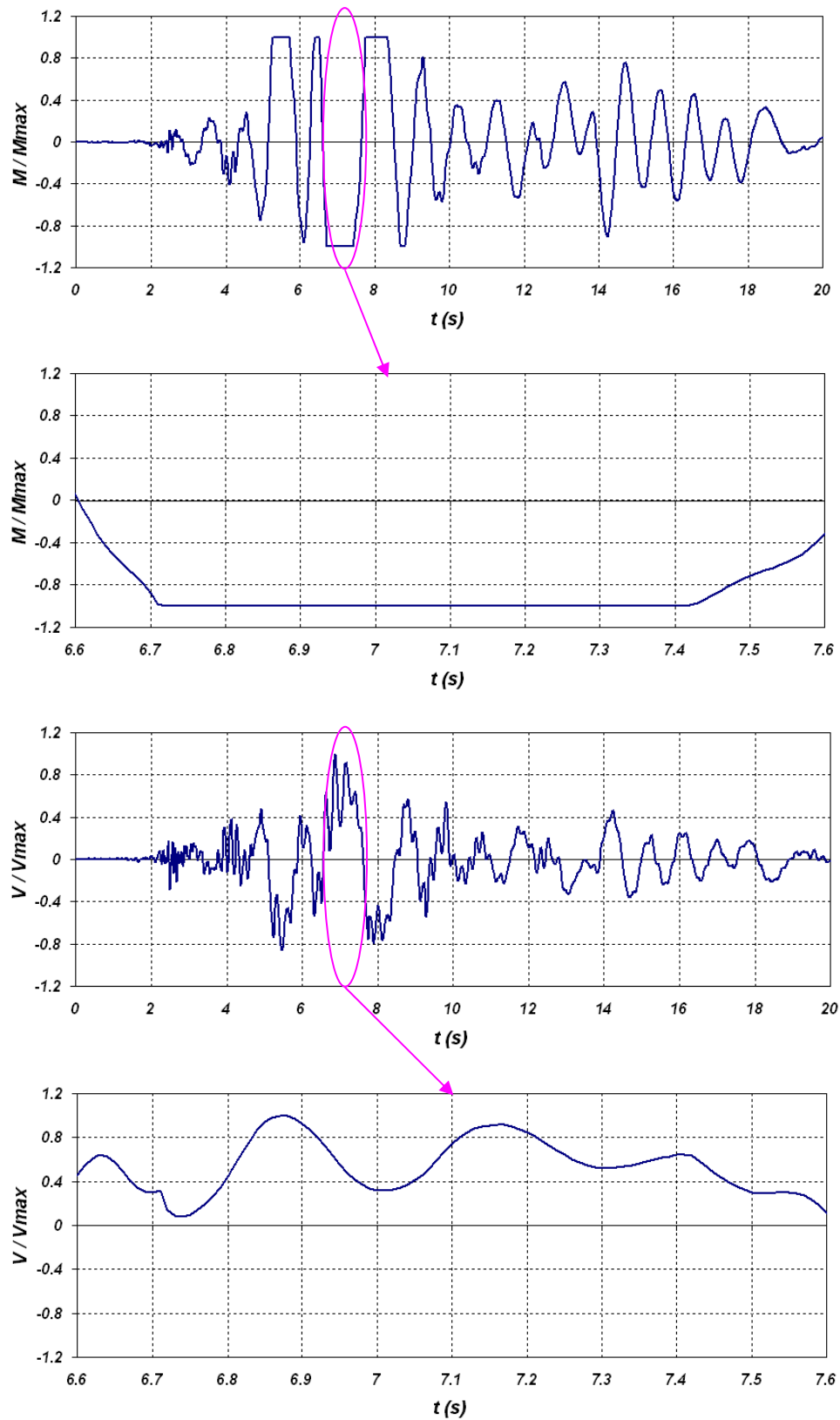


Figure 3.16 Normalized bending moment and shear force history at the base of a cantilever wall with  $T_I=1$  sec (Model 1).

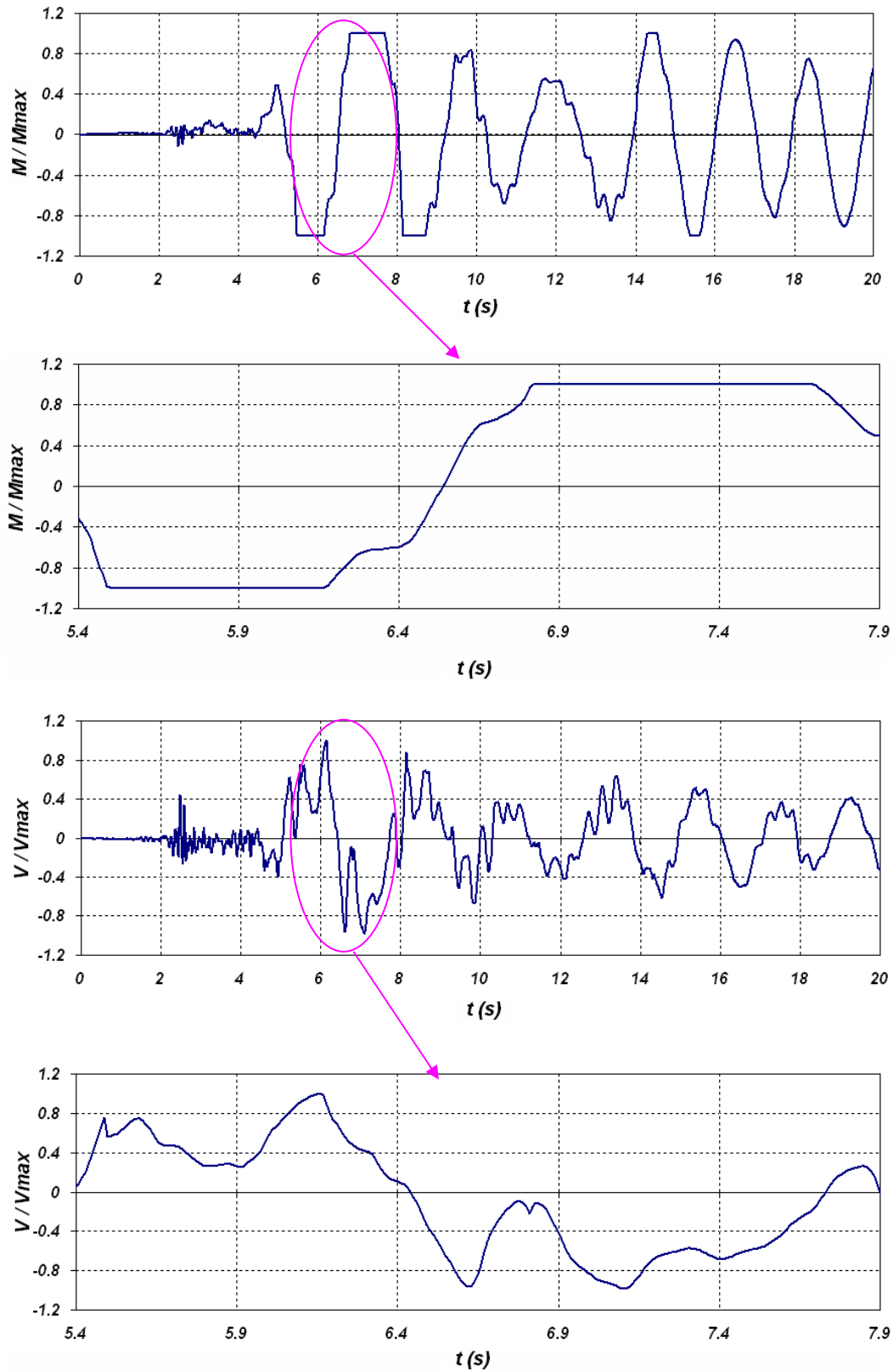


Figure 3.17 Normalized bending moment and shear force history at the base of a cantilever wall with  $T_I=2$  sec (Model 1).

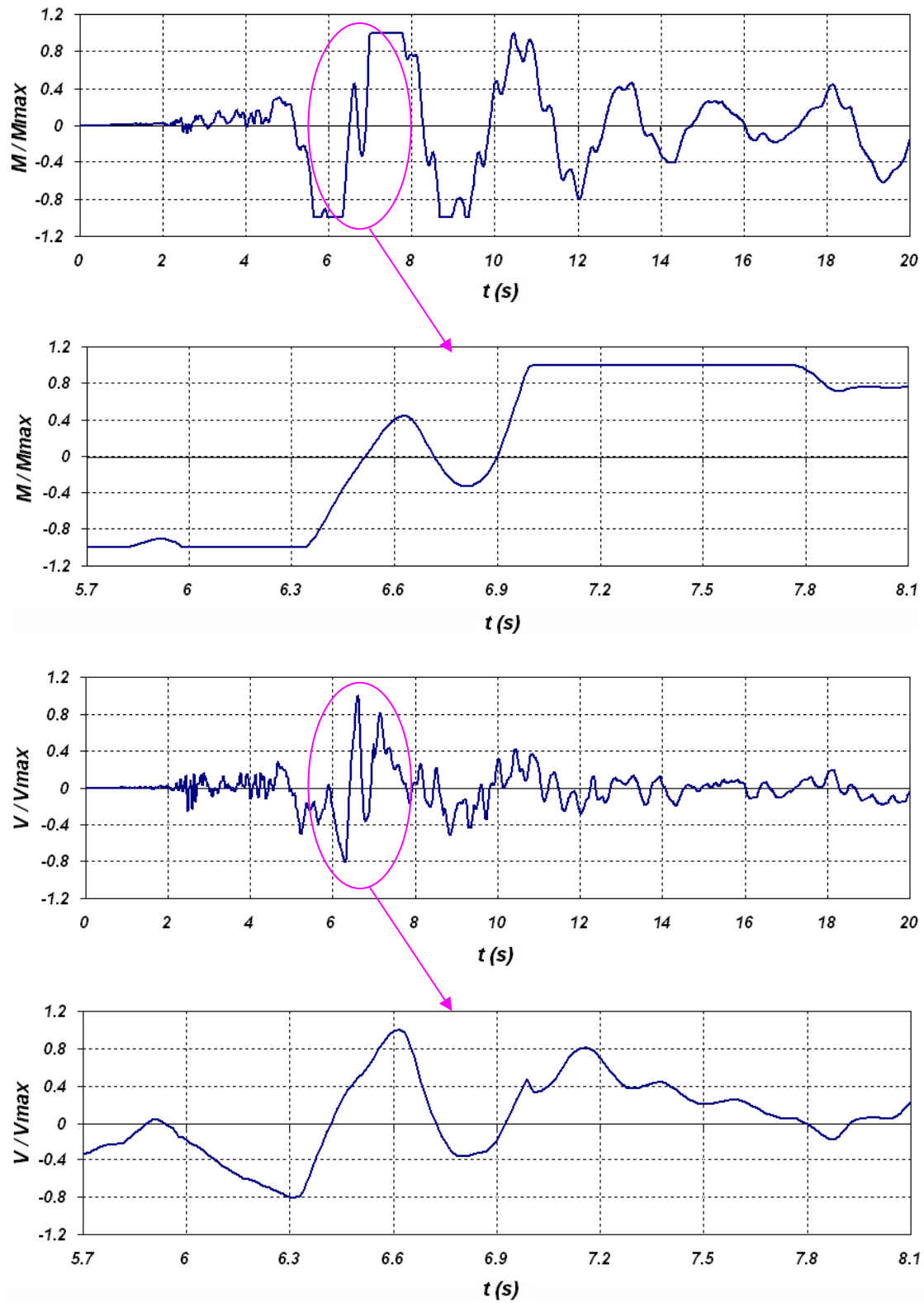


Figure 3.18 Normalized bending moment and shear force history at the base of a cantilever wall with  $T_l=3$  sec (Model 1).

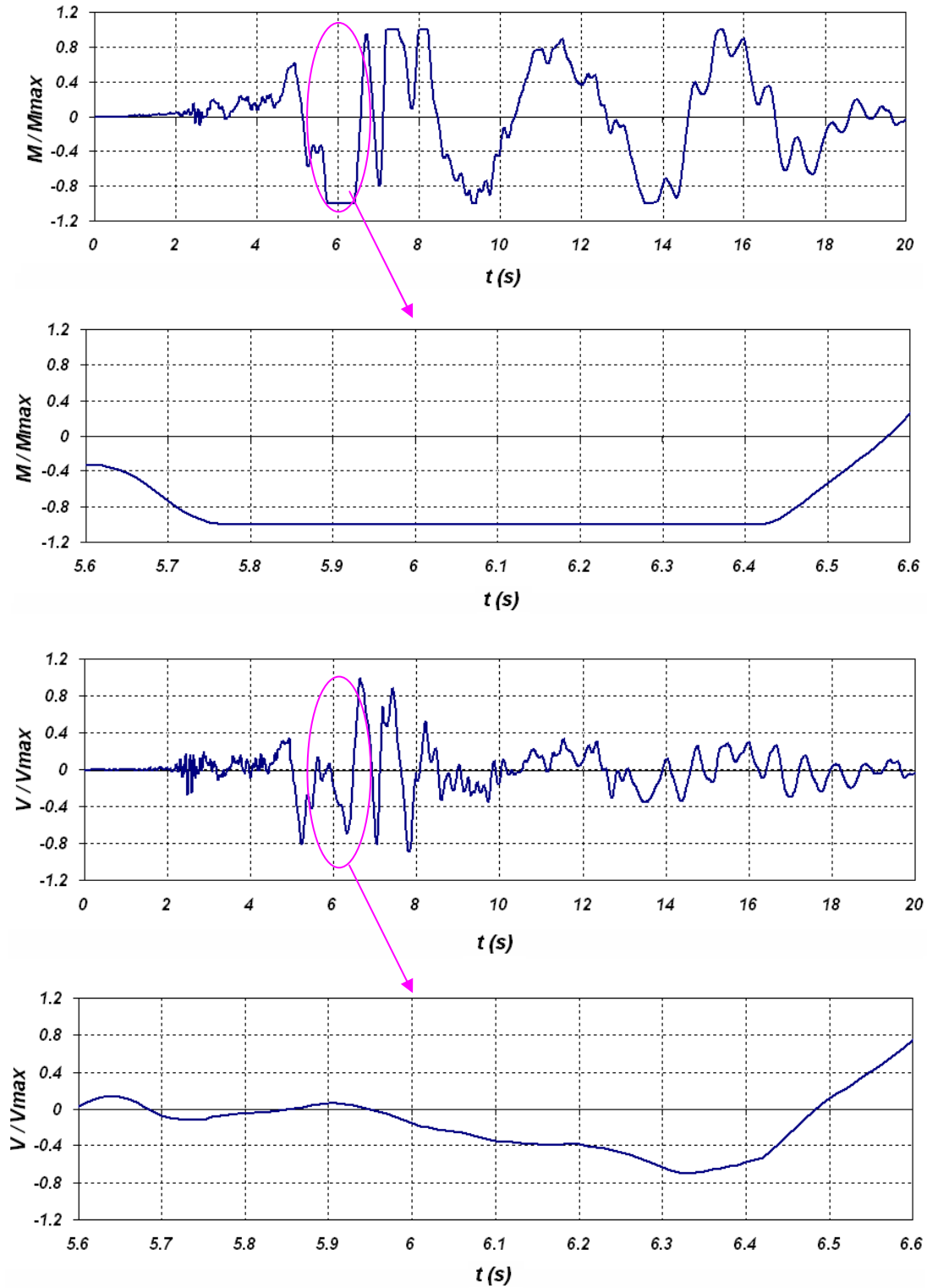


Figure 3.19 Normalized bending moment and shear force history at the base of a cantilever wall with  $T_I=4$  sec (Model 1).



After studying the behaviour of cantilever walls, a model of the concrete wall and the sub-ground structure is considered for nonlinear dynamic analysis. The model considered for nonlinear dynamic analysis is shown in Fig. 3.11 as Model 2. Nonlinear flexural behaviour is considered by providing a concentrated hinge at the base of wall similar to Model 1. The diaphragms and corresponding dead load of the floors are modeled as concentrated masses throughout the height of wall. The wall's height and corresponding concentrated floor masses were adjusted for two fundamental periods of  $T_f=4$  sec and  $T_f=1$  sec. Foundation walls were modeled as fixed supports and axial springs were added to the section of wall below ground at various levels to represent the influence of parking slabs as shown in Fig. 3.11. The  $K30$  spring was chosen to provide the extreme case corresponding to the magnitude of the developed reverse shear force.

A set of ten different ground motions was selected for performing nonlinear time history analysis. The specification of the earthquake records are indicated in Table 3.4. These records were chosen from recorded acceleration history presented in *FEMA-440* library of ground motions for site class C.

Table 3.4 Ground motions used for NTHA.

ID	Earthquake	Station	Date	Magnitude ( $M_s$ )	PGA, (cm/s <sup>2</sup> )
1	Morgan Hill	Gilroy #6, San Ysidro Microwave Site	04/24/84	6.1	280.4
2	Northridge	Castaic Old Ridge Route	01/17/94	6.8	557
3	Northridge	Lake Hughes #1, Fire station #78	01/17/94	6.8	84.9
4	Loma Prieta	Santa Cruz, UCSC	10/17/89	7.1	433.1
5	Loma Prieta	Anderson Dam (downstream)	10/17/89	7.1	239.4
6	Loma Prieta	Gilroy #6, San Ysidro Microwave site	10/17/89	7.1	166.9
7	Loma Prieta	Gilroy, Gavilon college Phys Bldg	10/17/89	7.1	349.1
8	Loma Prieta	APEEL 7, Pulgas	10/17/89	7.1	153
9	Landers	Yermo, Fire Station	06/28/92	7.5	240.3
10	Loma Prieta	Saratoga, Aloha Ave.	10/17/89	7.1	494.5

Variation of parameters  $V_b$  and  $V_r$  have been studied throughout the nonlinear analysis. It was observed that shear reversal magnitude at the below-ground level is mainly influenced by the bending moment at the base. The magnitude of  $V_b$  was found to have less pronounced influence on the developed reverse shear force. The amount of bending moment that is transferred to the below-ground section of wall is the controlling parameter on the magnitude of reverse shear force  $V_r$ . Higher base shear force ( $V_b$ ) would push back the diaphragm at the base level so that more deformation is carried by the wall and hence more bending moment is transmitted to the sections below ground which, in turn, results in reduction of balancing reverse shear force. Figures 3.20 and 3.21, show the developed reverse shear force at below-ground section of wall ( $V_r$ ), shear force developed at the base of wall ( $V_b$ ) and the shear force developed in the diaphragm at ground level ( $V_d$ ). The vertical axis in the plots corresponds to the normalized shear force as a ratio of  $(Vh / M_{yb})$  where  $h$  is the height of first level below ground and  $M_{yb}$  is the yielding moment at the base. The horizontal axis is the duration of earthquake in seconds. The critical case was observed for the developed maximum bending moment with combination of minimum shear force at the base.

Note that the all the data in Fig. 3.20 and Fig. 3.21 correspond to the case where a flexural hinge has been formed at the base of wall and therefore the overturning moment at the base has reached its maximum value. The shear force carried by the diaphragm at this point is simply the summation of  $V_r$  and  $V_b$ . Since diaphragm shear force is dependent on both shear forces developed in the section of wall at the base and one level below, and  $V_r$  is mainly dependent on  $M_b$  not  $V_b$ , it can be concluded that the influence of  $V_b$  is more important on the total shear force developed in the diaphragm at the ground level.

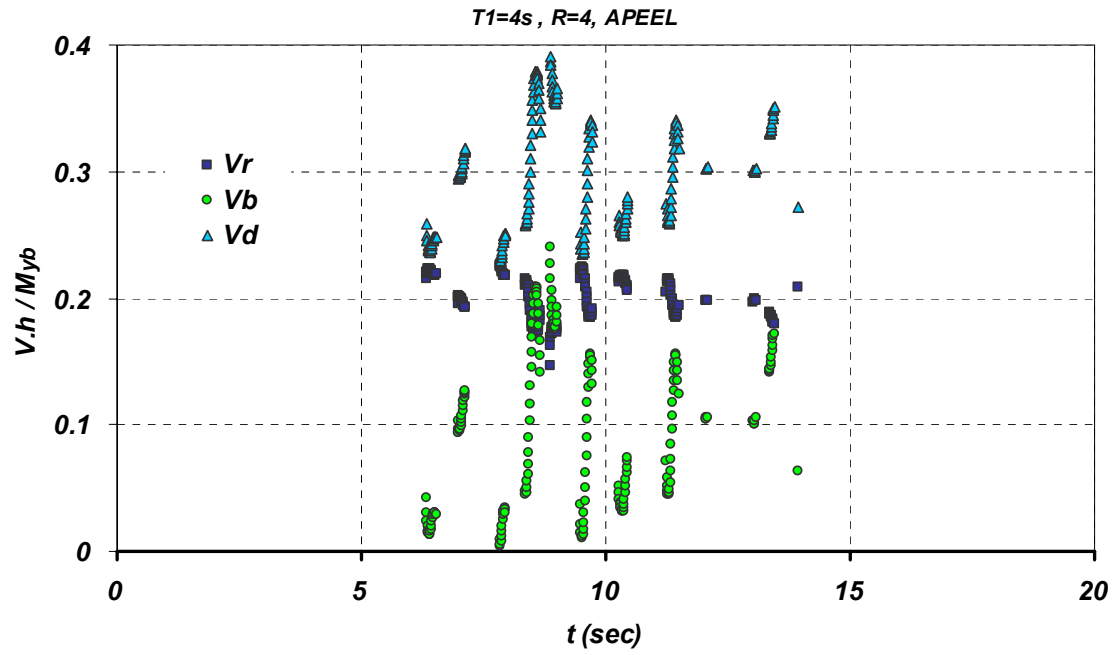


Figure 3.20 Normalized shear force in the wall section and the diaphragm at yielding for  $T_1=4$  sec (Model 2).

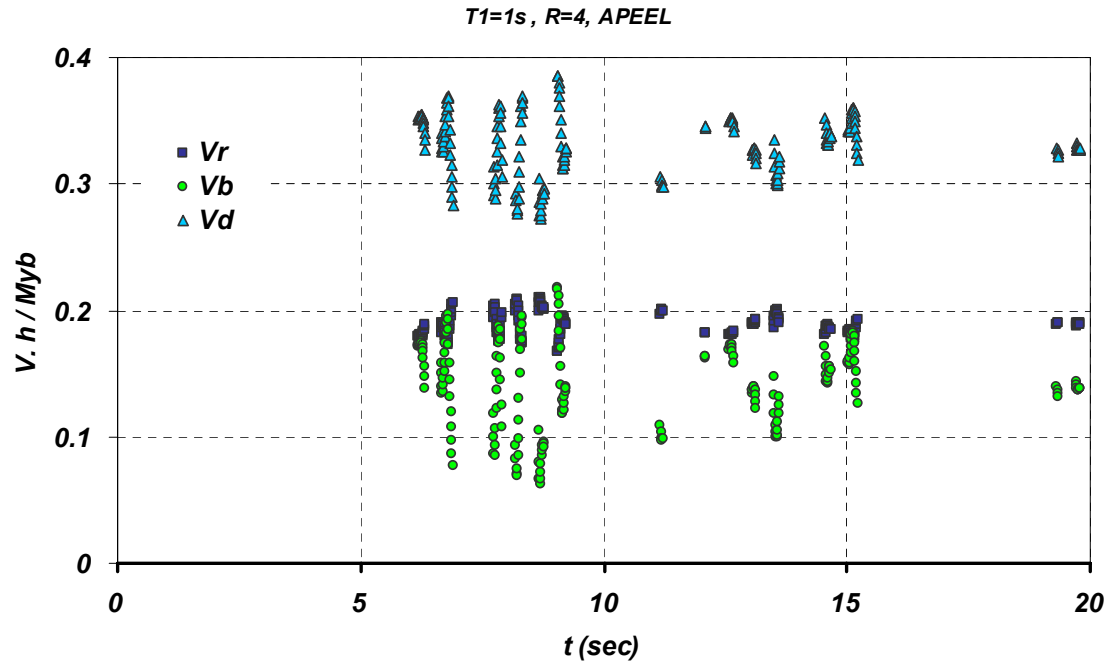


Figure 3.21 Normalized shear force in the wall section and the diaphragm at yielding for  $T_1=1$  sec (Model 2).

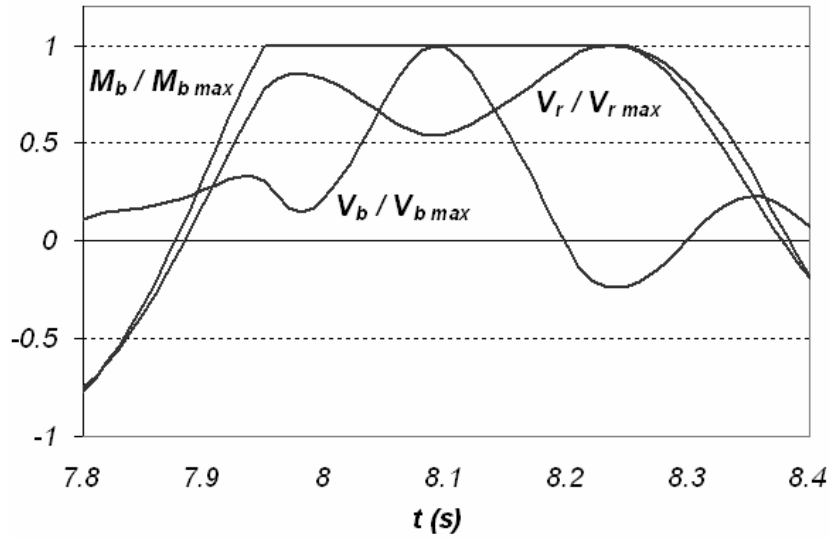


Figure 3.22 Normalized shear force and bending moment in the wall section during Northridge event for  $T_l=4$  sec (Model 2).

Figure 3.22 shows the phenomenon in a similar way at the instant of yielding during the Northridge earthquake. This figure shows three different curves; one defines the ratio of overturning moment at the base to the maximum yielding moment while other curves show the ratio of shear at the base and the shear at the first level below ground normalized by their maximum envelope values.

Because of insignificant strain hardening, overturning moment at the base does not change during the instant of yielding from  $t=7.95$  sec to about  $t=8.25$  sec. During this time the base shear forces in the wall fluctuates and it can be seen that  $V_r$  reaches its minimum value when  $V_b$  is at its peak and it reaches its minimum value when  $V_b$  value is a maximum.

Figure 3.23 and Fig. 3.24 are presented to provide the information obtained from nonlinear dynamic analysis of walls and substructure with fundamental periods of  $T_l=4$  sec and  $T_l=1$  sec respectively. From left to right each bar gives the results corresponding to a specific earthquake in the order which it appears in Table 3.4 which are sorted in the order of descending base shear for case of  $R=4$  (See Fig. 3.23-b).  $R$  factor was assumed equal to the linear peak overturning moment to the yielding overturning moment at the base. Each vertical bar gives four statistical parameters. The middle horizontal bar shows the mean value (averaged over the time of yielding) obtained during the nonlinear time

history analysis. The top and bottom vertical lines give maximum and minimum values observed during analysis and finally the standard deviation is also shown by half the length of middle vertical bar.

In Fig. 3.23-a, normalized reverse shear force has been illustrated. The mean value for  $V_r h / M_{yb}$  is 0.2 and is inversely proportional to the base shear. Figure 3.23-b shows the shear force at the base at instance of flexural yielding. The mean value for  $V_b h / M_{yb}$  ranges from 0.22 to 0.08 and correspondingly moment to shear ratio at the base ranges from  $0.12H$  to  $0.35H$  for  $T_I=4$  sec.

Figure 3.23-c shows the result for shear force carried by the diaphragm at the base level. The shear force in the diaphragm at the base is the sum of reverse shear force and the base shear. Figure 3.24 shows the similar results for  $T_I=1$  sec. The variation of shear forces are very small compared to the case of  $T_I=4$  sec. The observed mean value of normalized reverse shear force ( $V_r h / M_{yb}$ ) is equal to 0.19 where as mean value for normalized base shear ( $V_b h / M_{yb}$ ) varies from 0.13 to 0.20 stating that moment to shear ratio at the base ranges from ranges from  $0.5H$  to  $0.75H$  for  $T_I=1$  sec.

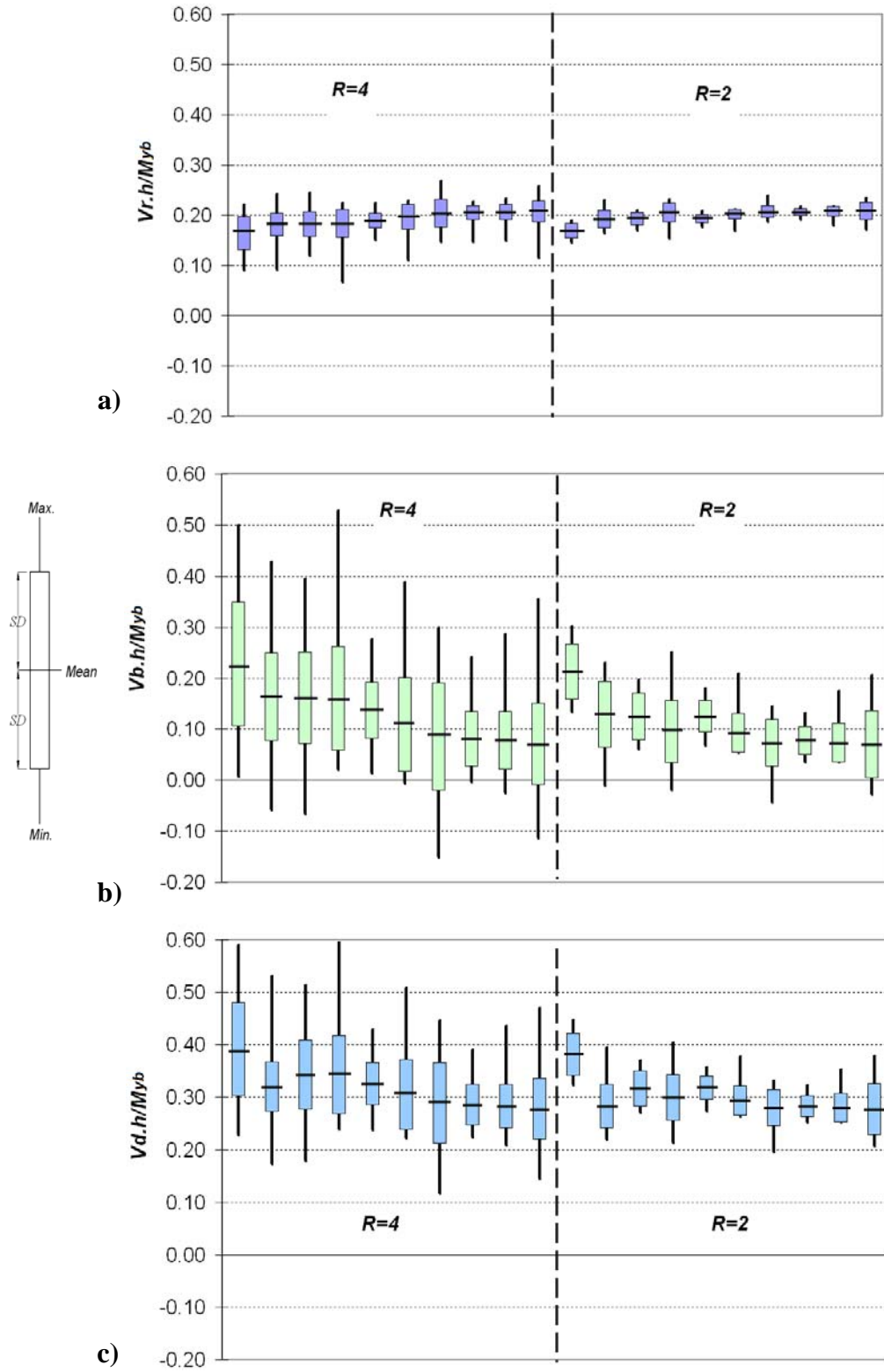


Figure 3.23 Normalized shear force: a) wall section below-ground (top), b) base of wall (middle), c) diaphragm at ground level (bottom) for  $T_I=4$  sec (Model 2).

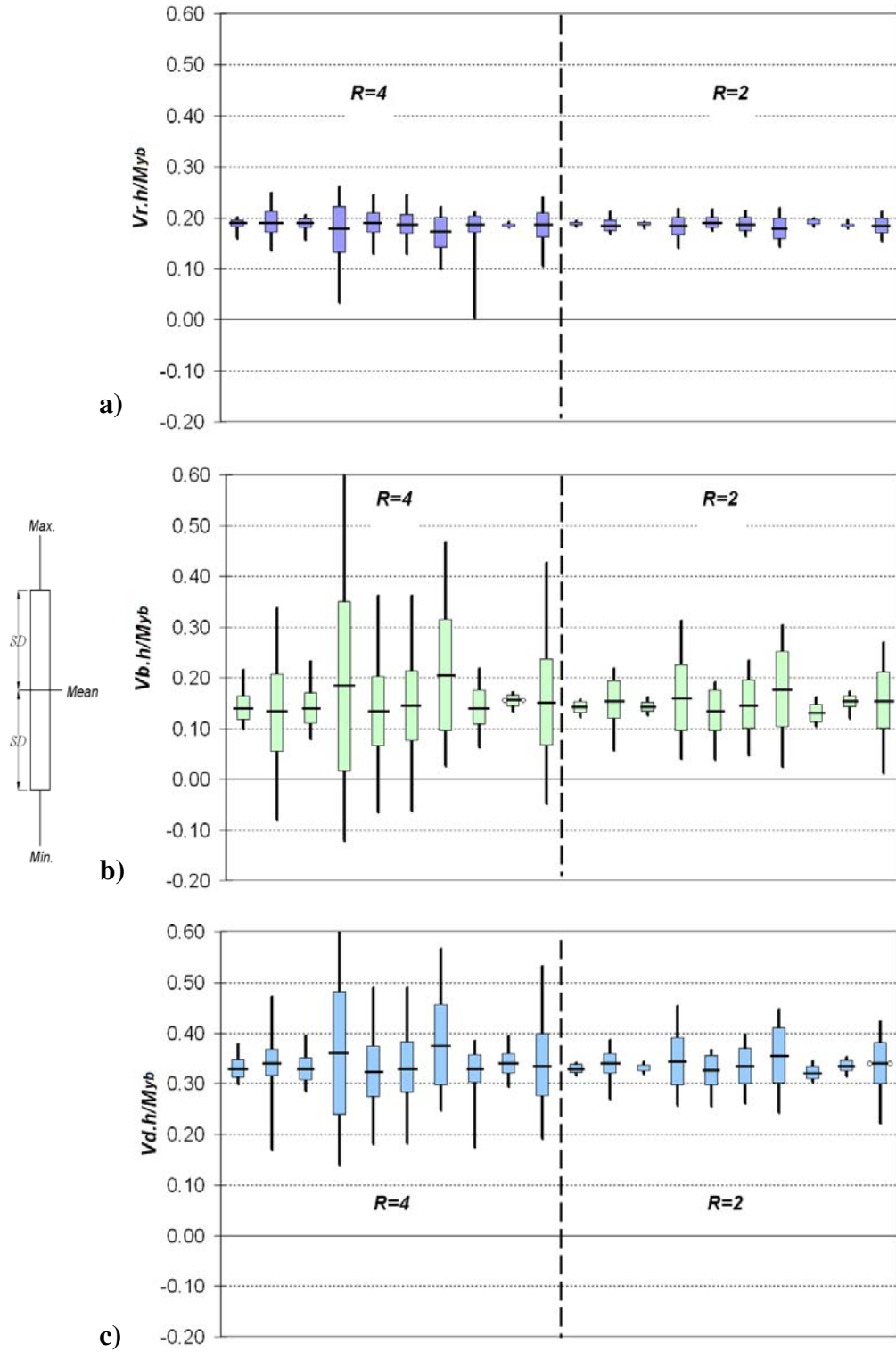


Figure 3.24 Normalized shear force: a) wall section below-ground (top), b) base of wall (middle), c) diaphragm at ground level (bottom) for  $T_I=1$  sec (Model 2).

Figure 3.25 shows the ratio of  $h'/H$  for a 40-storey building with  $T_I=4$  sec (Top) and a 10-storey building with  $T_I=1$  sec (bottom) at the time of hinge formation at the base. It is interesting to see how the higher modes lower the point of application of seismic lateral forces in high-rise shear walls.

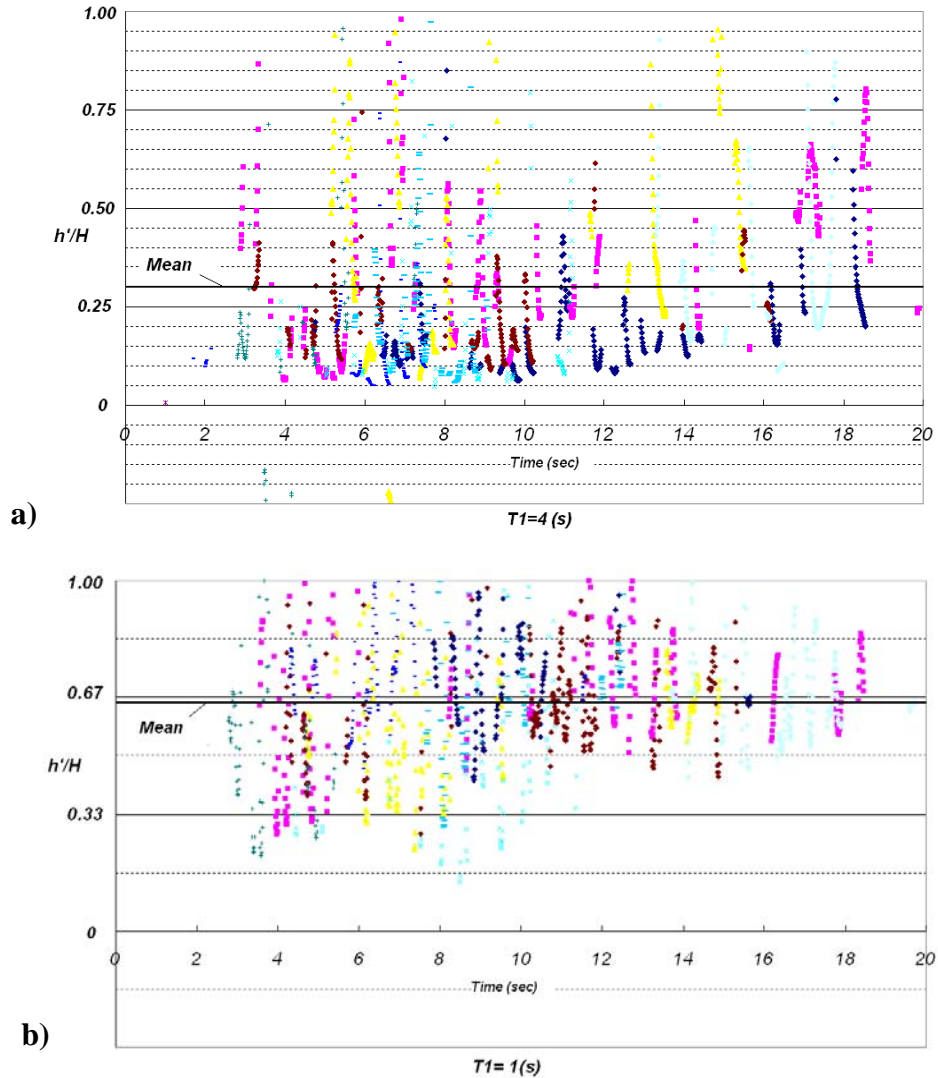


Figure 3.25 Normalized overturning moment to shear force ratio at the base of wall during flexural yielding (Model 2).

Based on findings from NTHA for the model of high-rise wall, the critical case was identified as when the shear force at the base is minimum at instance of flexural yielding at the base.



### 3.3.3 Shear-flexure interaction

The research on finding the suitable models for shear-flexure interaction in reinforced concrete walls is still in progress and a verified reliable shear-flexure interaction model has not been identified or used in previous studies. Furthermore, none of the available programs to perform nonlinear time history analysis has been developed to consider the simultaneous nonlinear action in concrete walls due to bending and shear.

Program Response-2000 (Bentz 2000) was used to determine a simplified shear-flexure interaction diagram as shown in Fig. 3.26. The plot is shown for the section of the model of the flange-wall described in Section 2.1. The wall has vertical reinforcement ratios equal to 2.5% at flange and 1% at the web. Horizontal reinforcement ratio in the web of the core wall is equal to 1%. This section is also used for nonlinear time history analyses performed in Chapter 5 of this dissertation (See section 5.6). The wall section is subjected to a constant axial compression of  $0.1f_c'$  consistent with the level of stress expected to develop at the base of a typical high-rise core wall.

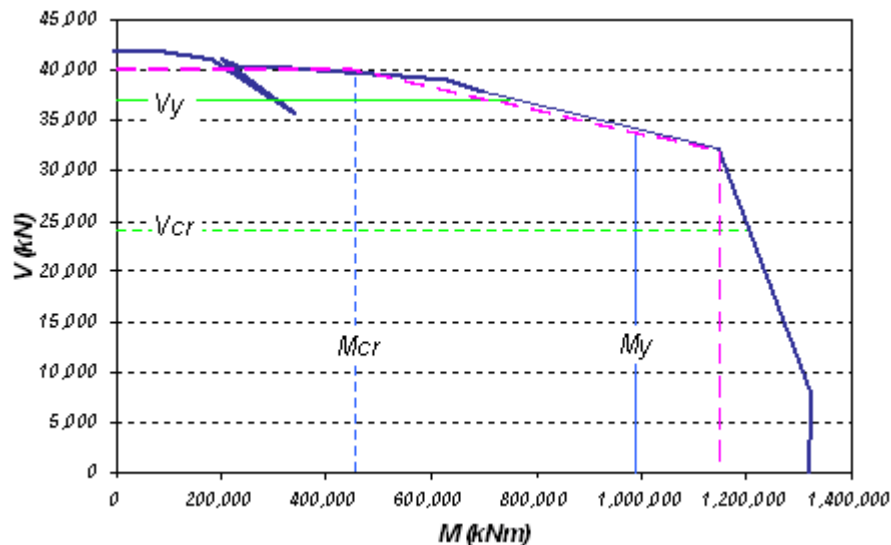


Figure 3.26 Shear-flexure interaction diagram for the example of core wall (Response-2000).

In Fig. 3.26 Horizontal axis shows the bending moment capacity of the wall while the vertical axis shows the corresponding shear force strength. The thick solid line corresponds to the actual interaction curve using Response-2000 and the thick dashed line

corresponds to a simplified approximation of the actual interaction curve. Thin vertical dashed line shows the limits for cracking of concrete due to bending and vertical thin solid line shows the limit for yielding of vertical reinforcement. Similarly the horizontal dashed line and solid line show the limits for cracking of concrete and yielding of horizontal reinforcement under application of pure shear respectively. The specified limits shown in Fig. 3.26 were used to build the nonlinear models for flexure and shear in the present study. According to the shear-flexure interaction diagram, a strong interaction between flexure and shear does not exist for the example of the core wall prior to yielding of vertical reinforcement. Shear-flexure interaction causes a reduction of less than 20% in the shear strength for the regions beyond flexural cracking (thin dashed line) up to flexural ultimate capacity (thick dashed line). The interaction was noticeable when flexure action starts as the vertical reinforcement yields and that this gives away considerable strength reserve.

A simple shear-flexure interaction model that is suitable for implementation into a dynamic analysis is not readily available. In fact, a rational model to predict the shear response in a wall associated with yielding of vertical reinforcement has not been developed. Since the focus of the present work is to investigate nonlinear seismic performance of large core walls in which the shear-flexure interaction is less pronounced and also in order to simplify the complicated nonlinear response, independent flexural and shear models were used to study the seismic demand on the example of high-rise shear walls in the present work.

### **3.4 Nonlinear static analysis**

Nonlinear static analysis provides useful information regarding nonlinear performance of the wall and it is fairly easy to use in design practice. In the next stage of this study, the nonlinear behaviour of a high-rise shear wall attached to a rigid foundation wall at the underground levels will be investigated.

Gérin and Adebar (2004) studied the experimental results on shear response of concrete walls and showed that a tri-linear calibrated shear stress–shear strain model can

properly capture the nonlinear shear behaviour. This model presents the nonlinear shear response while accounting for cracking of concrete and yielding of horizontal reinforcement due to extensive shear deformations.

#### 3.4.1 Nonlinear shear behaviour in concrete walls

Expressions used to present the nonlinear behaviour of concrete walls in shear will be explained in this section.

*ACI318* recommends the upper limit for the nominal shear strength of the wall as:

$$V_n = A_{cv}(\alpha_c \sqrt{f'_c} + \rho_n f_y) \quad (3.3)$$

Where,  $A_{cv}$  is the effective shear area and  $\rho_n$  is the horizontal steel ratio in the wall section. Coefficient  $\alpha_c$  is taken as 1/4 for  $h_w/l_w \leq 1.5$  and is taken as 1/6 for  $h_w/l_w \geq 2.0$ .

In addition to the above formula, the shear strength at yield point cannot exceed the capacity of concrete in diagonal compression which is defined below.

$$V_n = 0.83 \sqrt{f'_c} b h \quad (ACI-318) \quad (3.4)$$

$$V_n = 0.15 f'_c b d \quad (CSA-23.3) \quad (3.5)$$

The width and height of section are shown by  $b$  and  $h$  in the above expression.

The shear strain of concrete member at yielding of horizontal reinforcement can be estimated by following expression (Gérin and Adebar, 2004):

$$\gamma_y = \frac{f_y}{E_s} + \frac{v_y - n}{\rho_v E_s} + \frac{4v_y}{E_c} \quad (3.6.a)$$

With the following condition:

$$0 < \frac{v_y - n}{\rho_v E_s} < \frac{f_y}{E_s} \quad (3.6.b)$$

$f_y$  is the stress at yielding and  $E_s$  the modulus of elasticity for reinforcement steel. Shear stress in concrete at yielding is shown by  $v_y$  and axial compression stress by  $n$ . The horizontal steel ratio is  $\rho_v$  and the concrete modulus of elasticity is shown with  $E_c$  (units in MPa).

The corresponding shear strain at yielding is a function of tensile strain of the horizontal and vertical reinforcement as well as the compressive strain of concrete (Gérin and Adebar 2004). According to this model, the shear strain varies between a range of 0.0021 and 0.0047 for typical shear wall sections. The shear strain ductility of concrete walls in terms of shear strain can be estimated using following equation where  $\gamma_u$  is the shear strain at shear failure. According to this, significant reserve ductility in shear is expected in reinforced concrete walls unlike commonly assumed brittle behaviour in shear for concrete columns.

$$\mu_\gamma = \frac{\gamma_u}{\gamma_y} = 4 - 12v_y / f'_c \quad (3.7)$$

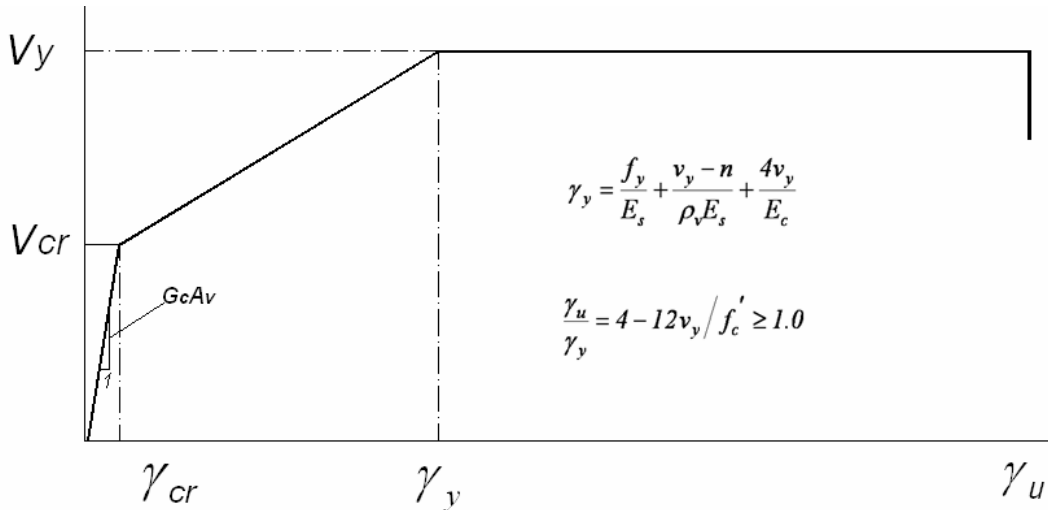


Figure 3.27 Proposed tri-linear model for shear in shear walls (Gérin and Adebar 2004).

Figure 3.28 presents five levels of nonlinear shear behaviour for the model of wall used in nonlinear static analysis.

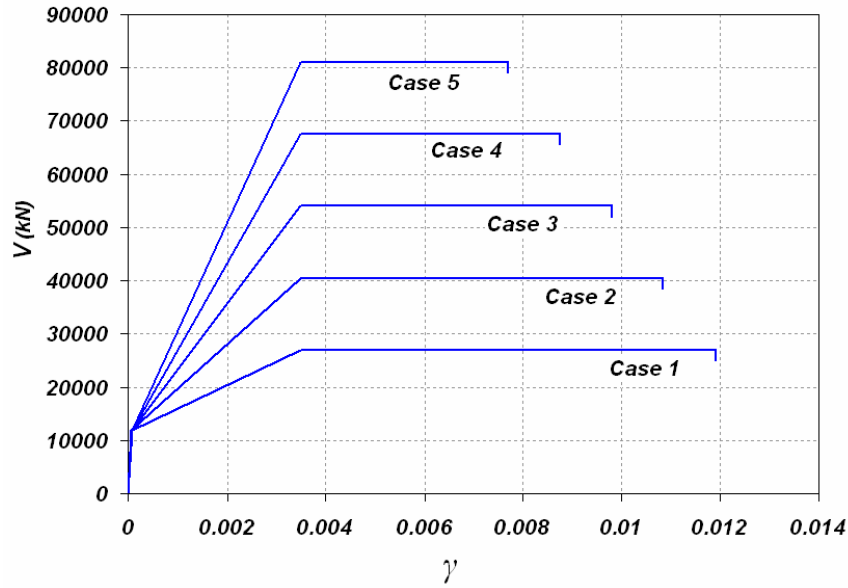


Figure 3.28 Tri-linear shear force- shear strain ( $V$ - $\gamma$ ) Curves in present study.

For the purpose of nonlinear analysis, a computer code has been developed (Rad, 2005) to perform pushover analysis on the model of high-rise shear walls. This code uses Visual basic programming language to perform the nonlinear static analysis similar to pushover analysis procedure. The nonlinear shear model in terms of tri-linear shear force-shear strain has been used to analyze the response of the wall below ground. Both flexural and shear hinges can be defined for the frame elements by the user. The advantage of this program compared to available commercial programs (at the time that this study was conducted) is the capability of considering tri-linear shear backbone developed by Gérin (2003) for the reinforced concrete walls.

In order to perform the nonlinear static analysis, a rectangular 9.0 m×0.75 m section for shear wall model having a concrete compressive strength of  $f'_c=50$  MPa has been considered. The foundation wall is assumed to be rigid in all analysis cases. Four levels of below-ground slabs were considered with a storey height of  $h=3$  m. Figure 3.29 shows the model used to perform nonlinear static analysis where nonlinear shear behaviour was considered in the core wall below ground.

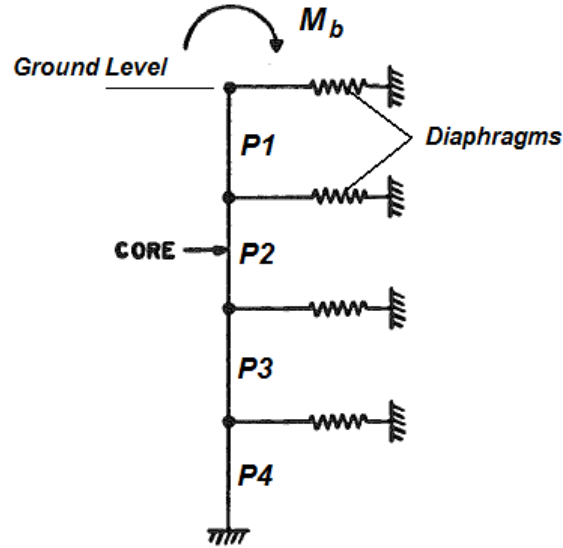


Figure 3.29 Model of wall below ground to perform nonlinear static analysis.

A procedure to run the nonlinear static analysis is provided in accordance with information obtained from nonlinear dynamic analysis which was discussed in the previous section. The “target overturning moment at the base” is defined as the yielding moment demand at the base of wall. Analysis runs until the overturning moment at the base reaches its specified target value. The target moment at the base corresponding to the level of shear strength at the base of wall was determined by considering  $h^*/h$  ratio in which  $h^*$  is defined as the ratio of flexural to shear strength ( $h^*=M_n/V_n$ ) for the section of wall at the base.

The shear strain developed in the below-ground section of is representative of the level of damage due to nonlinear shear behaviour. When the shear strain reaches the ultimate shear strain capacity of the wall, failure may be experienced. “Shear strain ratio” is defined as the ratio of shear strain demand in the wall to the ultimate shear strain capacity of the wall ( $\gamma / \gamma_{ult}$ ). In a similar way, “Shear strength ratio” is defined as the level of shear stress at the wall’s section to the compressive strength of concrete ( $v_c/f_c$ ).

Table 3.5 Target overturning moment ( $M_n$ ) in kN.m at the base of wall for different cases of nonlinear static analysis in this study.

	Case 1	Case 2	Case 3	Case 4	Case 5
$v_n$	$0.050f_c'$	$0.075f_c'$	$0.100f_c'$	$0.125f_c'$	$0.150f_c'$
$V_n$ (kN)	27,000	40,500	54,000	67,500	81,000
$h^*/h=10$	810,000	1,215,000	1,620,000	2,025,000	2,430,000
$h^*/h=15$	1,215,000	1,822,500	2,430,000	3,037,500	3,645,000
$h^*/h=20$	1,620,000	2,430,000	3,240,000	4,050,000	4,860,000
$h^*/h=25$	2,025,000	3,037,500	4,050,000	5,062,500	6,075,000
$h^*/h=30$	2,430,000	3,645,000	4,860,000	6,075,000	7,290,000

In Table 3.5, the target overturning moment at the base are obtained according to the level of shear strength at the base of wall. Figures 3.30 through 3.32 show the results for the nonlinear analysis in terms of shear strain ratio vs. shear strength ratio explained above for three different diaphragm stiffnesses. Data points in each figure include five different cases of shear stress level and five  $h^*/h$  ratios. Each case of the analysis represents a set of different wall capacities in shear. For example in the first case , the shear strength of the shear wall at the base is assumed 27,000 kN, which corresponds to a ductile wall with a low percentage of shear reinforcement whereas the fifth case shows a heavily reinforced wall with a shear strength of 81,000 kN which is the maximum shear strength allowed by *CSA 23.3*. The wall section is categorized as *I3* and the diaphragm type is chosen as *K30*. The results are shown for the ratio of developed shear strain to ultimate shear strain ( $\gamma/\gamma_u$ ) and also the ratio of developed shear strain to the yielding shear strain ( $\gamma/\gamma_y$ ) in the wall section below ground level. According to obtained results, for higher diaphragm stiffness and  $h^*/h$  ratios, it is possible to encounter shear failure at below-ground levels. In these cases the shear reversal problem becomes an important issue and special provisions should be considered to achieve a safer seismic design for the core wall below ground levels.

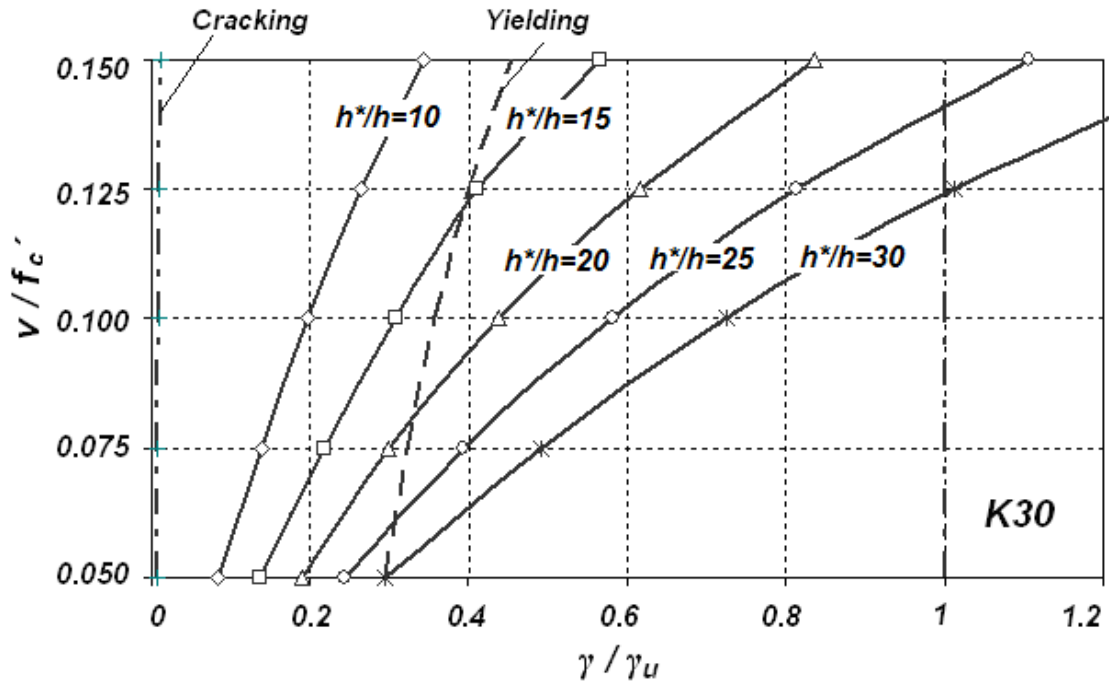


Figure 3.30 Shear strain vs. shear strength of wall below ground at target moment for different  $h^*/h$  ratio and for diaphragm stiffness  $K30$ .

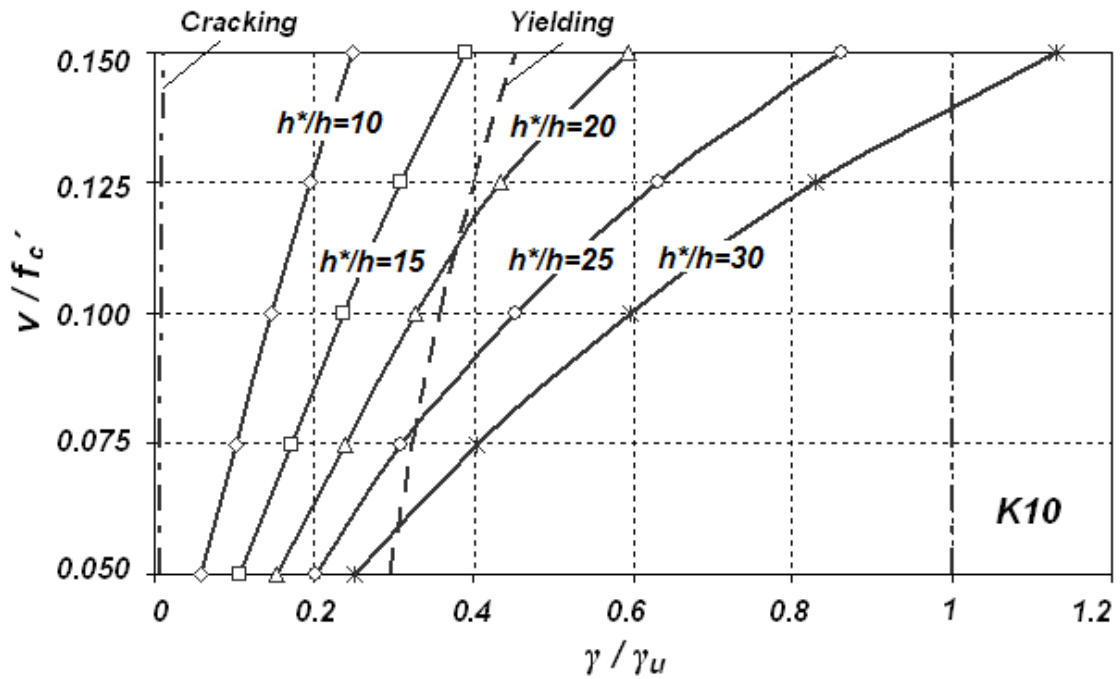


Figure 3.31 Shear strain vs. shear strength of wall below ground at target moment for different  $h^*/h$  ratio and for diaphragm stiffness  $K10$ .



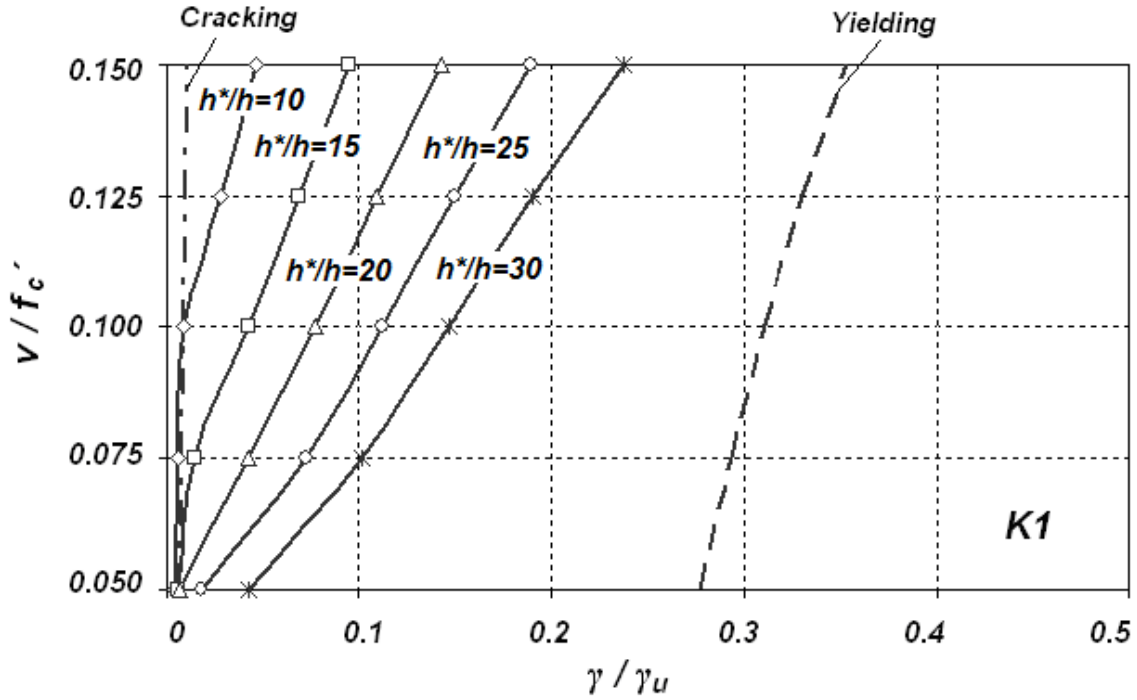


Figure 3.32 Shear strain vs. shear strength of wall below ground at target moment for different  $h^*/h$  ratio and for diaphragm stiffness  $K1$ .

Figure 3.30 shows the results of nonlinear analysis for diaphragm  $K30$ . Cracking, yielding and ultimate capacity in shear are plotted by separate dashed lines. Each curve shows a specific  $h^*/h$  ratio and each dot on the curve corresponds to a specific level of shear strength at the base of wall (See table 3.5). In total, 25 different cases were analyzed for each figure (Figures 3.29-3.31). In Fig. 3.30 in two of the cases ( $h^*/h = 25$  and  $h^*/h = 30$ ) section strain has exceeded the ultimate shear strain capacity and wall section below ground has yielded in shear for  $h^*/h = 15$  and  $h^*/h = 20$ . In all 25 cases, wall's section has suffered diagonal cracking at levels below ground. Figure 3.31 shows the analysis results for the case where diaphragm used was  $K10$ . Only one case of shear failure was identified for this case ( $h^*/h = 30$  and  $v/f'_c = 0.15$ ). For the case of diaphragm  $K1$  which has the lowest stiffness, wall did not reach shear yielding limit and the magnitude of reverse shear force remained well below the specified shear capacity in all cases as shown in Fig. 3.32.

According to the analysis results, for the cases where the diaphragm stiffness below ground is large and the wall shear demand at the base is high, extra provision should be made in order to make sure the wall below ground performs safe during earthquake.

Having a well designed diaphragm with smallest possible in-plane stiffness may be a suitable solution to large shear reversal problem.

Heavily reinforced wall sections possess a less ductile behaviour in shear which in some cases can result in a poor shear performance. This study showed that among parameters that influence the shear reversal magnitude in high-rise walls, the effect of diaphragm stiffness is the most important. The results for the nonlinear analysis imply that for tall buildings with relatively stiff diaphragms at underground levels, the shear reversal effect is significant. In such cases an appropriate ductile shear design allows the wall to deform beyond its yielding limit before reaching its ultimate shear capacity.

It was also found that any damage to the below-ground section of wall caused by flexural cracking or yielding of longitudinal reinforcement would lead to a reduction in flexural strength to carry the developed bending moment. In such cases an increase in shear demand on wall below ground would lead to larger shear deformations that can cause result in catastrophic shear failure.

### 3.4.2 Shear reversal solution through a design example

By looking at a design example, alternative solutions for the shear reversal problem will be discussed here.

The flanged walls shown in Fig. 3.33 are two realistic examples for geometry of core walls used in high-rise buildings. Sections bend about their strong axis in this example.

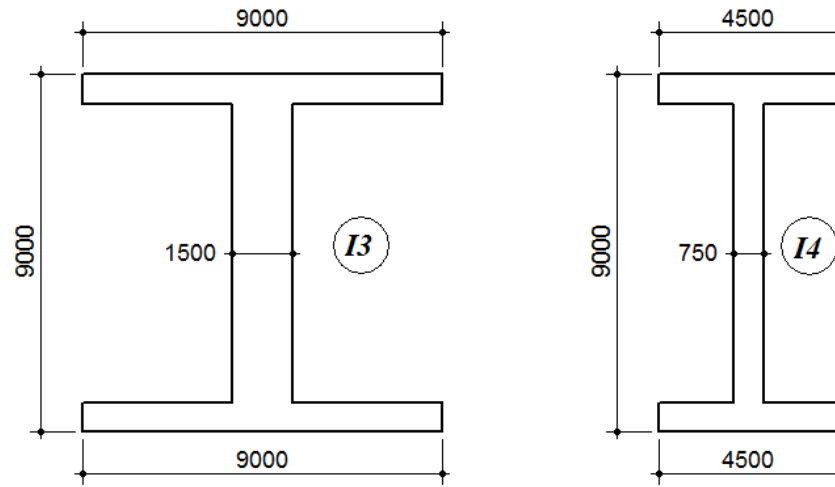


Figure 3.33 Flanged section core walls considered in the present example (Left: Section *I3*, Right: Section *I4*).

Similar to what was explained earlier in this chapter, nonlinear static analysis will be performed to reach a target moment at the base ( $M_b = M_n$ ) with an  $h^*/h$  ratio equal to 15 and a shear strength level of  $0.1f'_c$  which is associated with a horizontal web reinforcement ratio of 0.65%. The model used for performing nonlinear static analysis is the same model as shown in Fig. 3.29. Diaphragm *K10* was used to model the floor slabs at ground level and below.

According to practical design procedures, following design options provide alternate solutions to the shear reversal problem:

Alternative I: Increasing the horizontal shear reinforcement without further increase in the wall dimensions (Wall dimension is unchanged).

In this case strengthening the wall below ground in shear is done by adding horizontal shear reinforcement while initial wall dimension is unchanged. By doing this, the initial effective flexural and shear stiffnesses of the wall's section remain constant and the only change is made to the level of shear strength by adding horizontal steel to the wall section below ground.

The level of axial compressive stress was assumed equal to  $0.1f_c'$ . The concrete compressive strength is assumed 50 MPa. Since the wall dimension is unchanged, the cracking shear strength level in the section below ground is constant while the yielding stress level increases by adding horizontal reinforcement. Figure 3.34 shows how this design option influences the response of wall below ground. The dashed line shows the result for initial wall at level P1 having a shear strength of  $V_n=27,000$  kN and the solid lines show the results for shear strengthened section of wall to a shear strength of  $V_n=54,000$  kN which was achieved only by adding horizontal reinforcement to the web of wall at levels below ground.

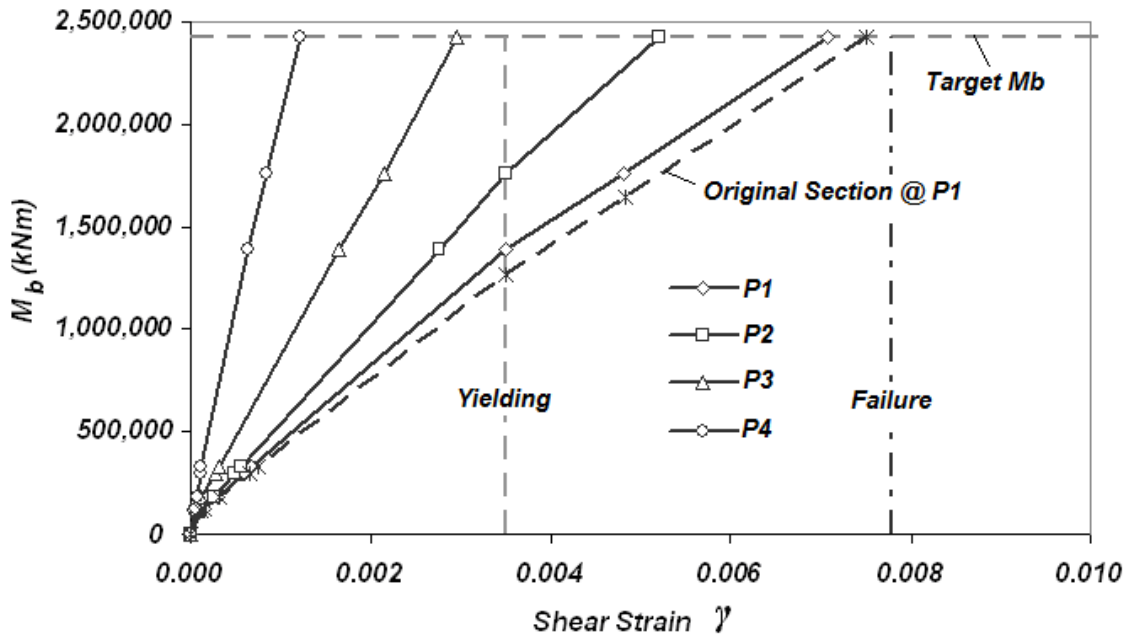


Figure 3.34 Bending moment at the base vs. shear strain for section I4 (Alternative I).

As it is shown in Fig. 3.35, for an increase of about two times the initial shear strength of wall by just adding horizontal steel, the reduction in the shear strain demand was insignificant (less than 10%). However the increase in amount of reinforcement

reduced the shear ductility significantly (more than 40%) as shown in Fig. 3.34 which may ultimately lead to an undesirable shear failure in the section below ground. According to results, this design alternative has the disadvantage of reducing shear ductility in the section of wall.

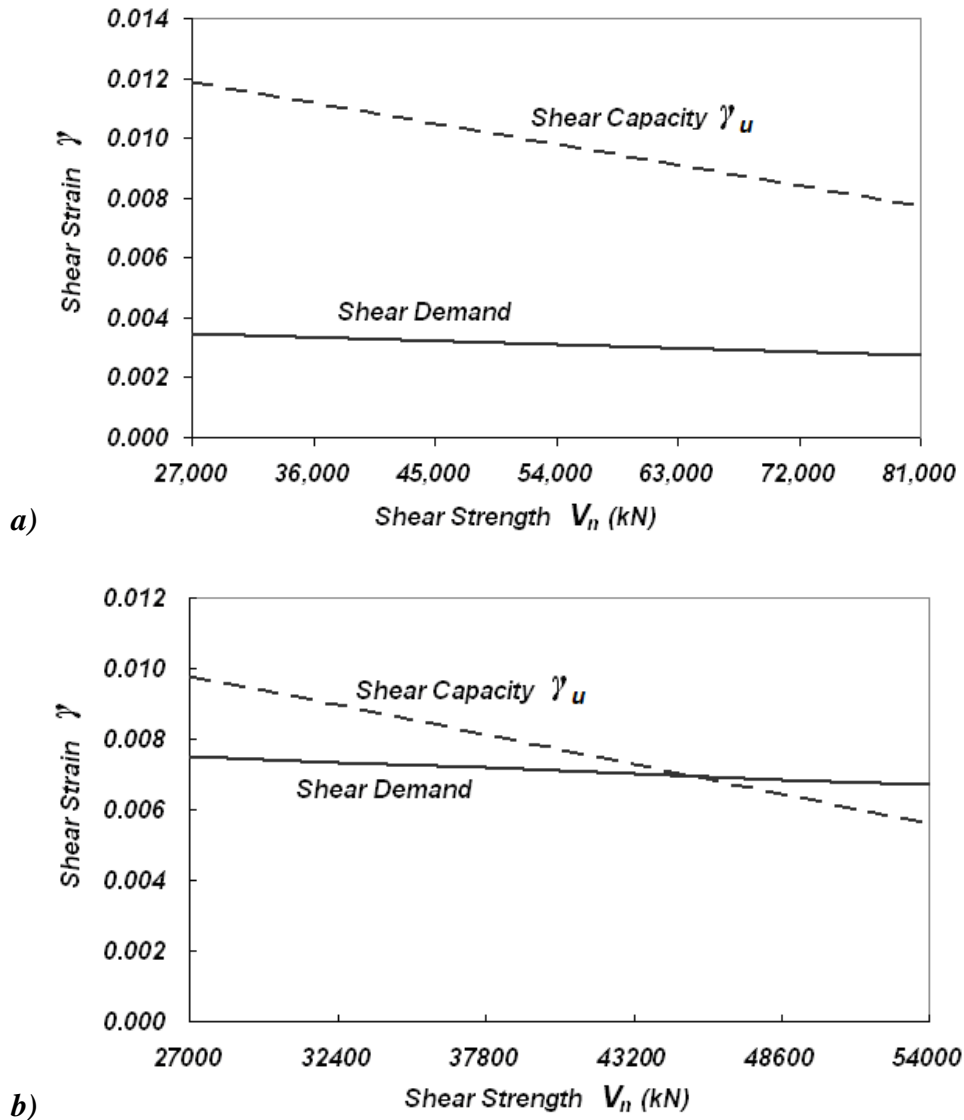


Figure 3.35 Shear strain vs. shear strength of wall section below ground (Alternative I)  
a): Section I3, b): Section I4.

Alternative II: Increasing the wall dimension and adding horizontal steel so that the level of shear stress and ductility remain unchanged.

Fig. 3.36 shows the relationship between bending moment at the base vs. shear strain at below ground levels for Alternative II. The dashed line represents initial section of wall below ground having a shear strength equal to  $V_n=27000$  kN. The solid lines show the results for a section of wall which is strengthened in shear by increasing the thickness as well as providing required horizontal reinforcement so that the level of shear stress in the wall's section remains constant to reach a shear strength of  $V_n=54,000$  kN.

The level of shear strain in the section of wall below ground reduced as the wall was strengthened in shear by increasing the wall web thickness and adding horizontal steel. All assumptions for this example were similar to Alternative I. The basic difference was the change in wall dimension that influenced both cracking and yielding shear stress levels.

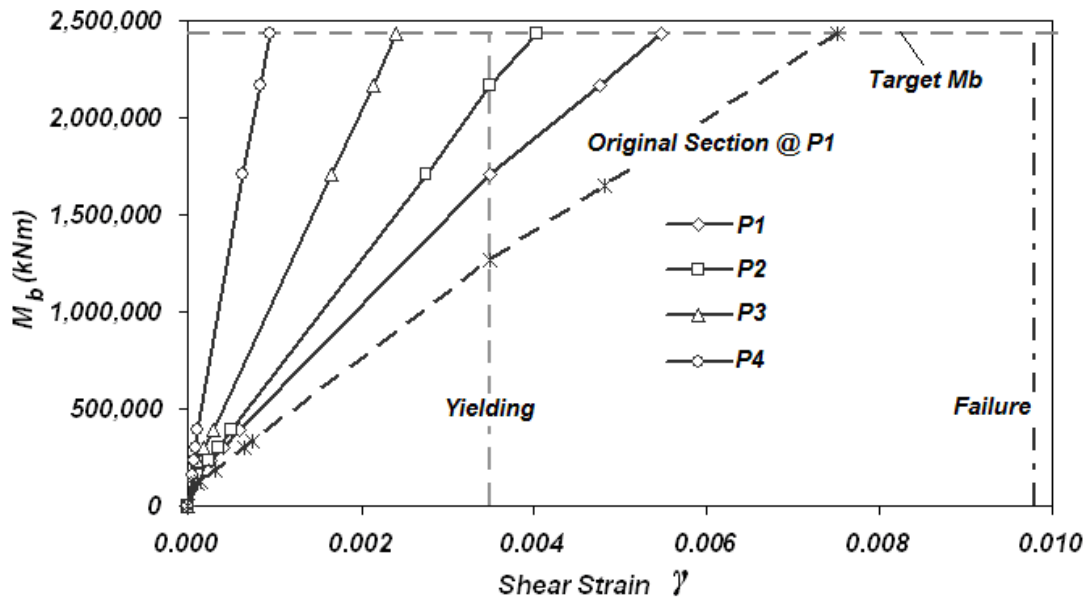


Figure 3.36 Bending moment at the base vs. shear strain for section I4 (Alternative II).

As it is shown in Fig. 3.37 the amount of reduction in shear strain demand in the section of wall compared to its initial condition was about 28% while the wall initial level of strain ductility was maintained by keeping the level of shear stress constant.

By comparing the results from two different solutions, it can be found that Alternative II gives a better overall shear response for the section of wall below ground compared to Alternative I.

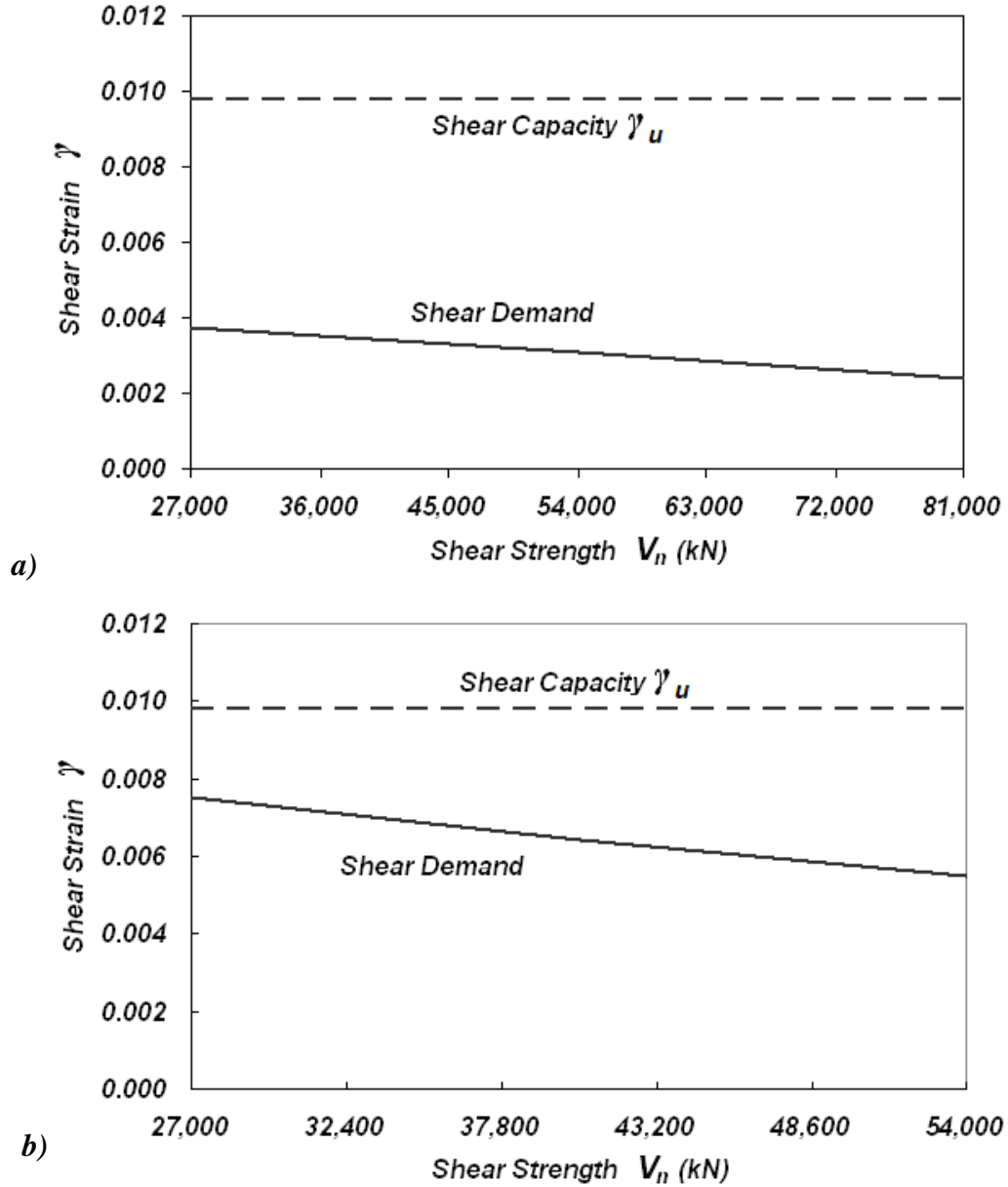


Figure 3.37 Shear strain vs. shear strength of wall section below ground (Alternative II):  
a) Section I3, b) Section I4.

In order to have a measure for amount of damage caused by shear deformation beyond yielding of horizontal reinforcement, coefficient  $k$  was introduced as follows:

$$k = \frac{\gamma - \gamma_y}{\gamma_u - \gamma_y} \quad (3.8)$$

Where  $\gamma$  is the strain demand in the wall section below ground and  $\gamma_y$  and  $\gamma_u$  are the shear strain at yielding and shear strain at failure respectively.  $k$  ranges between 0 and 1.0 with 0 as an indication of yielding and 1.0 as an indication of shear failure. Figure 3.37 shows how considering different effective shear stiffness for the wall's section below ground resulted in various levels of shear demand. The results were compared to the tri-linear shear response of the wall. In order compare the nonlinear analysis solution to results obtained from simplified linear analysis considering the effective shear stiffness of wall section below-ground, three dashed lines are plotted on Fig. 3.38.

The upper dashed line presents the case where all the below ground sections of wall have cracked with effective shear stiffness is equal to  $GA_{ve} = V_n / \gamma_y$ . The shear force demand in the wall section below ground in this case is 54,000 kN which is about 35% greater than the actual shear demand. The middle dashed line represents the case in which the first level below ground has yielded and has reached 50% of reserved ductility in shear beyond yielding point ( $k=0.5$ ). This solution achieved the closest result to the actual tri-linear behaviour and finally the lower dashed line represented a case where all the sections reached their 50% reserve shear ductility ( $k=0.5$ ).



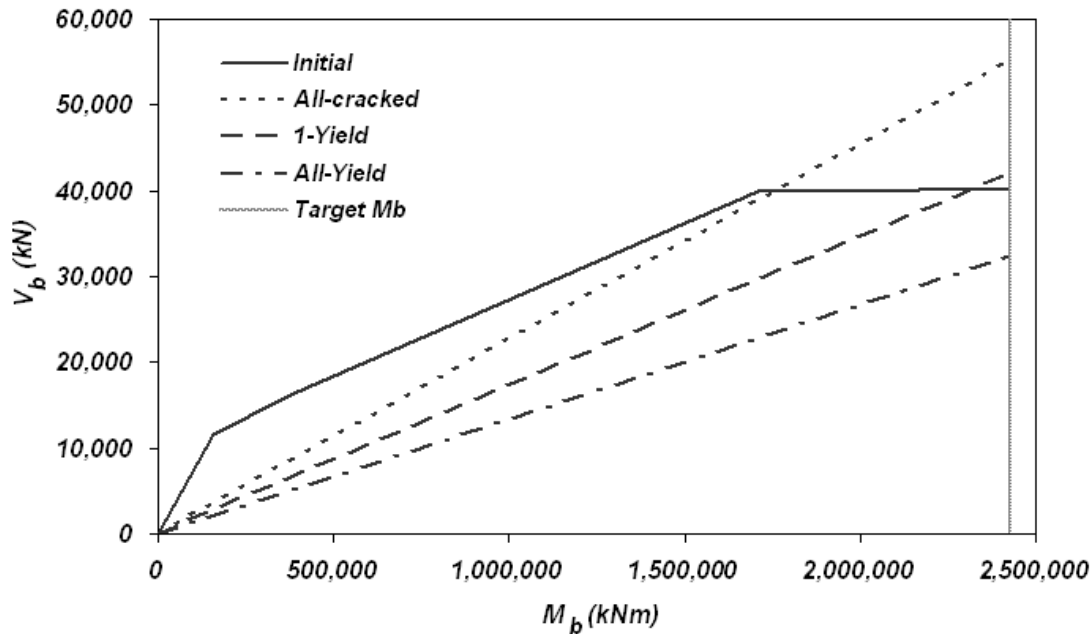


Figure 3.38 Shear force in the below-ground section vs. overturning moment at the base of wall (Alternative II).

Although design Alternative II provided a promising solution to the shear reversal problem, there is still very small change in shear strain demand for a relatively large increase in shear strength. Alternative I provided a poor solution to reduce the shear strain demand in the wall section.

Alternative III: Reduction in the shear force demand by allowing the diaphragms below ground to crack in shear.

Another solution to the shear reversal problem could be carried out by allowance in cracking of the diaphragms prior to the core wall. As discussed earlier, the diaphragm stiffness below ground has a great influence on the shear force demand of the core wall. Figure 3.39 shows how the diaphragm stiffness can influence the shear demand in the wall below ground for the previous example.

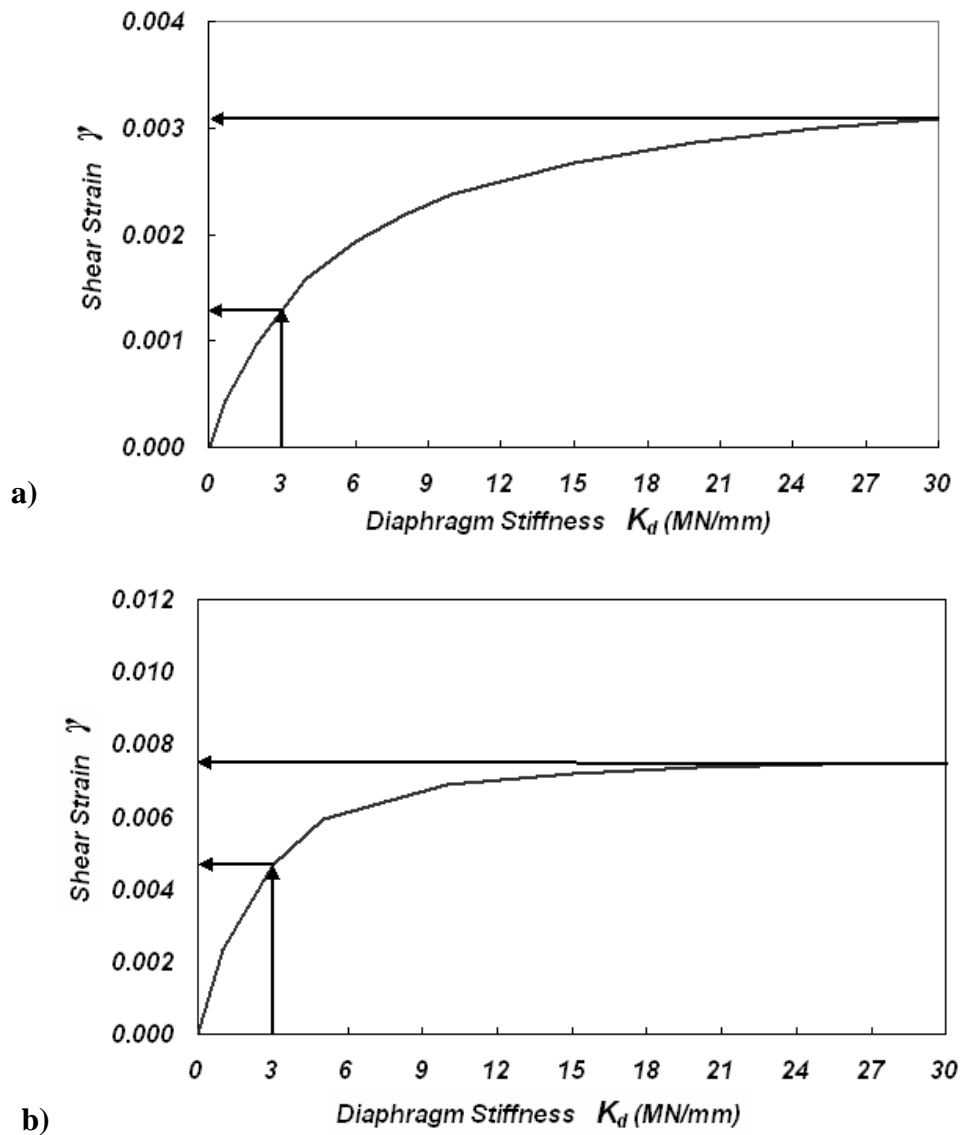


Figure 3.39 Shear stain in the wall section below ground vs. diaphragm stiffness at the base level: a) Section I4, b) Section I3.

As shown in Fig. 3.39 in a case where the diaphragm has an initial uncracked in-plane stiffness of about 30 MN/mm, shear cracking in diaphragm would reduce the stiffness to about 10% of the initially un-cracked stiffness value which is 3 MN/mm. The amount of reduction in the shear strain demand was found to be 40% in this case.

Alternative III provided an efficient solution to the shear reversal problem since no further change in the core wall was required. However special detailing of diaphragms

below ground to crack in shear while maintaining their stability should be considered carefully to ensure a safer seismic design in high-rise buildings.

In order to achieve an appropriate design in accordance with Alternative III two methods are suggested here:

- Provide special weak links in the diaphragm to control the cracking mechanism as desired.
- Design the diaphragms below ground as optimized as possible so that cracking in diaphragm reduces the seismic shear demand on high-rise core wall below ground.

Figure 3.40 shows the results of four example nonlinear static analyses on Model shown in Fig. 3.29 where the diaphragm stiffness is  $K30$ . The vertical axis is the ratio of reverse shear force couple  $V_r \times h$  to total applied bending moment at the base  $M_b$ , while the horizontal axis is the corresponding shear strain of the tower wall at the below-ground level. Two levels of flexural capacity  $h^*/h = 15$  (solid lines) and  $h^*/h = 30$  (dashed lines), and two different percentages of horizontal reinforcement in the core wall corresponding to shear stress ratios  $v/f_c' = 0.15$  (upper line) and  $v/f_c' = 0.10$  (lower line) are shown in Fig. 3.40. Prior to diagonal cracking of walls, the reverse shear force times storey height  $V_r \times h$  resists about 18% of the total applied bending moment  $M_b$  in all four walls. After diagonal cracking, the reverse shear force reduces depending on the amount of horizontal shear reinforcement. There is a larger reduction in the walls with less horizontal reinforcement (lower  $v/f_c'$ ) because the cracked-section shear rigidity is lower in these wall. At the shear strain corresponding to horizontal reinforcement yielding (0.0035), the reverse shear force resists 8% of the applied bending moment in the wall with  $v/f_c' = 0.15$  and about 6% of the bending moment in the wall with  $v/f_c' = 0.10$ . In only one of the walls ( $h^*/h = 15$  and  $v/f_c' = 0.10$ ) is the shear strain less than yielding (0.0035) when the flexural capacity of the wall is reached. In the other three cases, the shear strain is pushed beyond yielding.

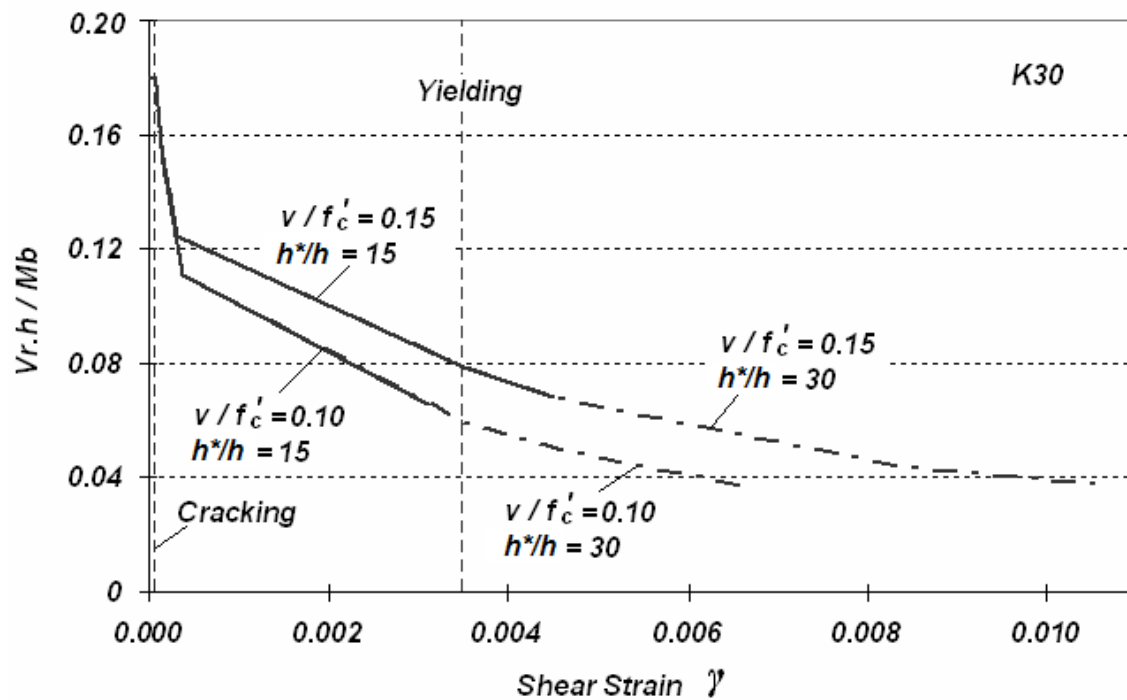


Figure 3.40 Results from four nonlinear static analyses showing reduction in reverse shear force demand due to shear strain from diagonal cracking of wall, and yielding of horizontal wall reinforcement.

### 3.5 Nonlinear shear response of concrete floor diaphragms

Cracking will reduce the stiffness of floor diaphragms, which will reduce the reverse shear force. Unfortunately, the shear behaviour of floor diaphragms is very complex making it difficult to use a simple model for the nonlinear shear behaviour of diaphragms. Normally, it is conservative to use a simple model of force transfer in complex concrete structures; but in this case, a simpler model will predict a lower stiffness of floor diaphragms, which will result in an unsafe prediction of reverse shear force. A simple model of the floor diaphragm is that it acts as a beam transmitting the force entirely to the foundation walls that are parallel to the shear force in the walls, and this was the model used earlier to estimate the stiffness of the uncracked diaphragms.

Depending on the relative dimensions (length-to-width) of the floor diaphragm, the shear force in the walls may be transmitted primarily by compression stresses in the diaphragm, which will result in less cracking and a stiffer response overall. If the foundation walls are cast directly against the ground, the deformation of the diaphragm

will be reduced by the out-of-plane walls bearing against the ground. Once diagonal cracking does occur in the diaphragm, it is not clear how much reduction in shear stiffness there will be as a significant reduction requires numerous closely spaced cracks. The small percentage of reinforcement in floor slabs and the arrangement of this reinforcement may result in poor crack control when the slab cracks due to in-plane shear stresses. Floor beams further complicate the issue.

If it is reasonable to assume that the reverse shear force is transmitted primarily to the in-plane foundation walls (parallel to shear force) by compression and tension stresses that are relatively uniform over the diaphragm, and that there will be good crack control in the diaphragm, the nonlinear shear model for shear walls can also be used for concrete floor diaphragms. The shear force to cause cracking of diaphragms can be estimated from Eq. 2.8 through Eq. 2.11 by substituting  $P/A_g = 0$ , and by substituting the average diaphragm thickness for  $b_w$  and length of diaphragm in the direction of shear force (overall depth of equivalent beam representing diaphragm) for  $l_w$ .

### **3.6 Procedure for design of the shear wall below ground**

**Step (1):** Determine design forces at the base level (immediately above base structure) using, for example, response spectrum analysis (RSA). As shear force reverses below base level (this procedure is to deal with such cases), maximum bending moment in tower wall occurs at the base level.

**Step (2):** Design tower walls for design bending moment at the base level. Provide reinforcement over height of plastic hinge region of wall above base level, and all the way down to the foundation. Refined analyses with appropriate stiffness assumptions as per later steps could be used to avoid extending all wall reinforcement to the foundation.

**Step (3):** As increased flexural deformations of tower wall below base level will reduce flexural stiffness of tower wall, which will increase reverse shear force, provide additional vertical reinforcement in tower wall below base level to ensure yielding will not occur below base level and to increase flexural rigidity of wall below base level.

**Step (4):** Determine probable flexural strength of wall  $M_{pr}$  at the base level taking into consideration applied axial compression in wall at the base level and actual reinforcement provided in wall. To ensure an upper-bound estimate, assume yield strength of reinforcement is equal to 1.25 times specified yield strength.

**Step (5):** Design tower walls for shear force above base level (maximum base shear). If RSA is used to determine the shear force, account for flexural overstrength plus dynamic amplification of shear. Provide adequate wall thickness so that shear stress level does not exceed  $\phi_c 0.15f'_c$ , where  $\phi_c$  is the appropriate strength reduction factor for shear (e.g., 0.75 in *ACI 318*, 0.65 in *CSA A23.3*). Use this as the initial shear design of tower wall below base level.

**Step (6):** Analyze interaction between tower walls and base structure using linear static analysis. The applied forces at the base level are  $M_{pr}$  determined in Step 4 and  $V_b = 0$ . Use uncracked shear rigidity  $G_c A_{vg}$  of tower wall, and an appropriate model to determine stiffness of uncracked floor diaphragms. To account for flexural cracking of tower wall below base level, use an effective flexural rigidity equal to  $M_n \times l_w / 0.0025$ , where  $M_n$  is the nominal flexural capacity of the tower wall at the particular level and  $0.0025/l_w$  is the curvature of the wall at initial yielding of vertical reinforcement (Adebar and Ibrahim 2002). If maximum shear within tower wall below base level is less than base shear  $V_b$ , the initial design from Step 5 is adequate, otherwise continue to next step.

**Step (7):** Determine if significant diagonal cracking of tower wall will sufficiently reduce reverse shear force in tower wall below base. Repeat linear static analysis of tower wall – base structure interaction as specified in Step (6) except use an effective shear rigidity of tower wall equal to  $G_c A_{ve} = V_n / 0.003$ , where  $V_n$  is the nominal shear strength of tower wall using initial design determined in Step 5 and 0.003 is a simple estimate of yield shear strain. A larger value of yield shear strain, which results in less shear stiffness, can be determined from Eq. 3.6. If maximum shear force within tower wall below base level is less than  $V_n$ , the initial design from Step 5 is adequate, otherwise continue to next step.

**Step (8):** Determine if cracking of floor diaphragms will sufficiently reduce reverse shear force in tower wall. Caution is needed regarding an overly simplified model that gives too low of an effective stiffness of the diaphragm. A nonlinear finite element

model that correctly accounts for tension stiffening of cracked reinforced concrete is the best approach for estimating the stiffness of cracked diaphragms. Repeat linear static analysis of tower wall – base structure interaction as specified in Step (7) except use the reduced stiffness of the diaphragms. If maximum shear force within tower wall below base level is less than  $V_n$ , the initial design from Step 5 is adequate, otherwise continue to next step.

**Step (9):** Increase shear strength of tower wall below base, providing adequate wall thickness so that shear stress level does not exceed  $\phi_c 0.15f'_c$ , where  $\phi_c$  is the appropriate strength reduction factor for shear. Repeat linear static analysis as in Step (8) except using an effective shear rigidity of tower wall equal to  $G_c A_{ve} = V_n/\gamma_y$ , where  $V_n$  is the increased shear strength of tower wall and  $\gamma_y$  is the yield shear strain taken as 0.003 or determined from Eq. 3.6. If maximum shear force within tower wall below base level is less than  $V_n$ , the revised design is adequate, otherwise modify design and repeat Step (9). Note that increasing the shear strength of the tower wall also increases the effective shear stiffness of the tower wall which results in a larger reverse shear force. If a reasonable solution cannot be found by increasing the shear strength of the tower wall, continue to next step.

**Step (10):** Either use refined analysis procedures to reduce calculated reverse shear force or jump to next step and modify design of structure. Possible refinements in analysis include: (i) NTHA to justify a lower design bending moment at the base level in Step 1, (ii) NTHA to determine a larger minimum base shear ( $V_b$ ) in Step 6, (iii) use of a higher effective flexural rigidity of tower wall below base in Step 6, (iv) use of more sophisticated model that gives a lower stiffness of diaphragms, or (v) NTHA with appropriate concrete models – particularly for the shear response of diaphragms and tower walls – to determine the reverse shear force directly.

**Step (11):** Modify design of structure to reduce reverse shear force. Possible solutions include: (i) reduce stiffness of floor diaphragms by modifying design of floor, (ii) provide a gap in floor slabs around tower walls and support floor slabs on corbels projecting from tower walls, (iii) increase height of critical stories in base structure, (iv) modify design of tower walls to increase flexural stiffness of tower walls.

### 3.7 Summary and Conclusions

The shear reversal problem and its corresponding design solution were studied in this chapter. The magnitude of the wall reverse shear force below ground in tall buildings is dependent on parameters such as foundation wall size, diaphragm stiffness below ground, the developed maximum moment and shear at the base and the degree of fixity at footing. The recently calibrated nonlinear model for shear proposed by Gérin and Adebar (2004) was used to study the shear reversal problem in this chapter. As the performed analyses indicated, among the parameters influencing the shear reversal, the effect of overturning moment at the base had the most significant influence. The dynamic analysis of the simplified model of wall showed that the maximum developed base moment with a combination of minimum shear at the base will result in the largest reverse shear force at the levels below ground. This fact was verified by the fact that more moment transmitted to the section of wall below ground, the less shear force is developed to satisfy the equilibrium of forces at the section of wall.

Although considering nonlinear shear behaviour can reduce the reverse shear force demand, it may not be practical to design the walls for such high shear demand. The study showed that a large increase in wall dimension is required in order to reach the acceptable level of shear strain in the wall. A more convenient solution to this problem would be allowing the diaphragm below ground to crack during strong earthquakes. Cracking of the diaphragms below ground would reduce the reverse shear force demand significantly. An appropriate design to allow cracking of diaphragm requires ductile detailing of diaphragm at weak joints and avoiding using oversized below-ground slabs in design of high-rise concrete buildings. In practice, when encountering huge shear reversal demand in the high-rises, one needs to keep the diaphragm's thickness below ground as thin as possible to satisfy design requirements. Any flexural damage to the below ground section of wall which would result in a reduction of wall effective stiffness would cause an increase in the shear force demand.

A complete design procedure for design of the core wall's section below the ground level was proposed that can be used in design practice.



## **Seismic shear demand in inter-connected high-rise walls**

### **4.1 Overview**

In Chapter 3, the seismic shear demand was investigated at below-ground sections of a core wall which is used as the main seismic force resisting system for typical high-rise concrete buildings. It was observed that the nonlinear shear response significantly influences the magnitude of the developed reverse shear force at the below-ground levels.

As the largest seismic shear force develops at below-ground levels of the core wall for which the wall has to be designed, the seismic shear force at the base is the most important parameter to design the wall above the ground level. Like the below-ground sections of a high-rise core wall, shear deformation shares a significant part of the lateral displacement in the above-ground sections of the wall near the base; therefore accounting for the nonlinear shear response at the lower above-ground levels is equally important in determination of seismic shear demand in concrete walls.

In high-rise buildings, concrete walls are tied together over the height by rigid floor slabs at every floor level. The thickness of slabs is usually too small to prevent flexural cracking of slabs at the face of concrete shear walls and columns due to high rotational demand during an earthquake; however in-plane stiffness of floor slabs is large enough to carry the load between the vertical members and would cause significant redistribution between forces developed in different levels of the building.

At the upper levels of a high-rise building, shear force distribution between walls depends primarily on the relative flexural rigidity of the walls. In the lower levels of the building however the shear force distribution depends more on the relative shear rigidity of the walls. Due to cracking of concrete and yielding of reinforcement, the shear and flexural rigidities of concrete walls will change as the wall is subjected to increasing shear and bending moment demands.

In the design of high-rise concrete buildings, linear dynamic (response spectrum) analysis is normally used to determine the displacement demands on the overall structure, and the force demands on the individual components of the structure. During ground motion the structural members which contribute to the stiffness of the lateral resisting system would suffer some damage which would result in reduction of their initial uncracked section stiffness. The stiffness properties used in the analysis model must account for the presence of cracked regions of the concrete members.

The reduction factors to account for cracking of concrete members are proposed by codes for columns, beams and shear walls. For simplicity, one reduction factor (e.g., 70%) is normally used for all elements in the structure. The effective shear rigidity of concrete walls is usually assumed to equal the gross section shear rigidity  $G_c A_{ve}$  which means the effect of shear cracking is usually not accounted for. The reason is the complicated unknown behaviour of reinforced concrete members in shear. Since the shear failure is the most dramatic mode of failure in a structure, engineers often try to be conservative in their design especially when it comes to the shear design of critical elements to resist earthquake lateral motion such as shear walls.

While these simple assumptions about effective member rigidities lead to reasonable estimates of overall structural displacement, such as the displacement at the top of concrete walls, they may result in poor estimates of shear force distribution between concrete walls. In this study, nonlinear analysis is used to make an accurate estimate of the shear force distribution in high-rise concrete walls. Experimentally calibrated models accounting for uncracked, cracked and post-yielding response of reinforced concrete were used to determine both flexure and shear rigidities of concrete walls.

## 4.2 Model of two walls

To investigate the issue of shear force distribution in high-rise concrete walls, a simple two-wall example as shown in Fig. 4.1 was used. Walls are inter-connected through diaphragms at levels above ground. The connections between walls and floor slabs are not capable of resisting the existing overturning moments as they crack due to large rotations during ground motion and hence are considered as pinned connections. Connection of walls through rigid diaphragms would cause the lateral displacement at each level to be identical for both walls. Lateral seismic resisting system of a typical high-rise may be provided by a number of shear walls having different shapes and dimensions. If two walls are identical in geometry, the distribution of forces between them is almost identical since the walls possess the same lateral stiffness. This case is of less interest in this study. On the other hand this uniform distribution between walls is highly disturbed when walls have different geometry and size. Compressive strength of concrete was assumed  $f'_c=50$  MPa and a modulus of elasticity equal to  $E_c=32000$  MPa was considered for the concrete walls.

In order to maximize the variation in shear force distribution, two walls were purposely chosen to be very different. Wall *W1* is a 9.0 m long wall with large transverse walls attached to the ends, i.e., a large flanged wall, while wall *W2* is a rectangular wall that is 4.5 m long (half as long). Both walls have a “web” thickness of 0.75 m. Wall *W1* represents a typical cantilever wall that is part of a building core. Same geometry for wall *W1* is used to study the dynamic response of a 30-story cantilever wall which will be discussed in the next chapter of the present dissertation. As both walls have the same overall height (81 m), wall *W1* has half the height-to-length ratio of wall *W2*.

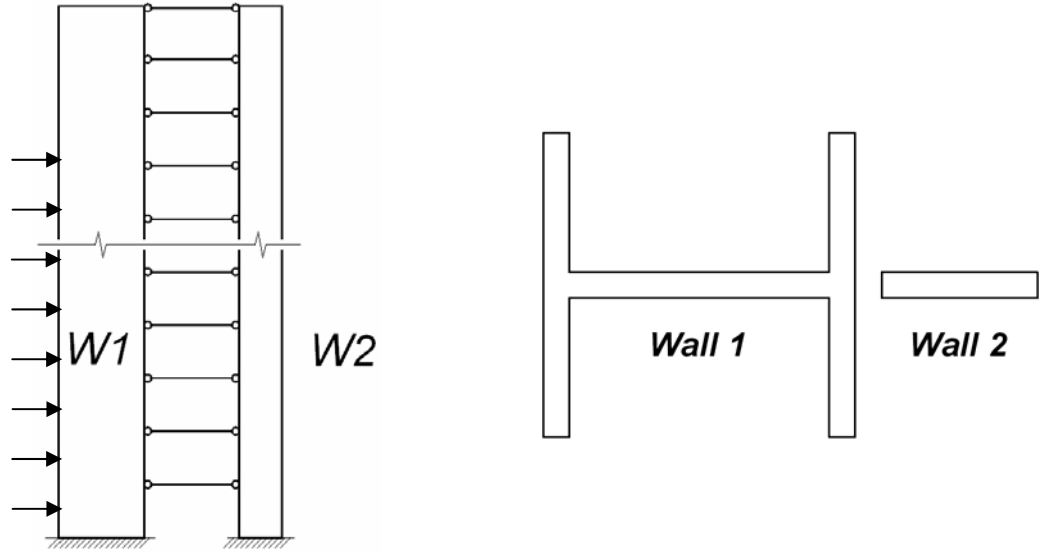


Figure 4.1 Example of two-wall model used in the present study.

Table 4.1 Geometrical properties of the walls shown in Fig. 4.1.

Walls	$I_g$ (m <sup>4</sup> )	$A_g$ (m <sup>2</sup> )	$A_{ve}$ (m <sup>2</sup> )
<i>W1</i>	222.32	19.125	6.75
<i>W2</i>	5.69	3.375	2.7

In order to make it a realistic example, the strengths of the walls were determined the way it is done in practice, so the strengths are greater than or equal to the forces determined from a linear analysis.

Response spectrum analysis (RSA) is the most common analysis method used in Canadian design practice to estimate the seismic demand on high-rise buildings. Thus this method was used to establish the relative strengths of the walls at the base of the building. The RSA was conducted for the simple two-wall model by adjusting the uniform mass over the height of the 30-storey building so that the fundamental period of the two-wall model was 3 sec., which is the typical value for a complete 30-storey concrete building. In other words, only the appropriate portion of the total mass of a complete 30-storey building was applied to the two-wall model. The design spectrum that was used for the RSA was Vancouver site class C. To account for the effect of

flexural cracking in the concrete walls, the effective flexural rigidity  $E_c I_e$  was taken as 70% of the uncracked flexural rigidity  $E_c I_g$  as is normally done in practice.

The shear forces and bending moment near the base of the walls determined from the RSA are as follows. The factored bending moments in walls  $W1$  and wall  $W2$  are  $M_{f1} = 1,125,500$  kNm and  $M_{f2} = 49,000$  kNm respectively. The factored shear force in wall  $W1$  at Level 1  $V_{f1} = 34,000$  kN, while the factored shear force in wall  $W2$  at Level 1  $V_{f2} = 7,100$  kN. Note that the ratio of  $M_{f1}$  to  $M_{f2}$  is 23.0, while the ratio of  $V_{f1}$  to  $V_{f2}$  at Level 1 is 4.78. The ratio of  $(M_{f1} + M_{f2})$  to  $(V_{f1} + V_{f2})$  at the base is 28.5 m, note that the ratio of developed forces in walls are controlled more by flexural action at the upper levels while the shear deformations in walls become important in lower levels.

Two structural walls in the example were designed so that the resistances of the walls were about equal to the forces determined in the RSA. Both walls were assumed to be subjected to an axial compression equal to  $0.1 f'_c A_g$  at the base of the walls, which for wall  $W1$  is 114,750 kN, and  $W2$  is 20,250 kN. This value is a vertical load that a wall in a high-rise building is subjected to. The reinforcement in the chosen walls in this study is designed according to the wall force demand obtained from RSA and is similar to a real case of wall detailing in practice. In order to have the required flexural capacity at the base, wall  $W1$  required about 2.5% vertical reinforcement in the transverse walls (flanges), and about 0.5% vertical reinforcement in the web. Wall  $W2$  required 1% vertical reinforcement over 15% of the wall length at each end of the wall. To have adequate shear resistance, wall  $W1$  required about 1% horizontal reinforcement at Level 2, while wall  $W2$  required about 0.3% horizontal reinforcement at Level 1. The applied shear forces cause shear stress ratios  $v/f'_c = 0.1$  in wall  $W1$  at Level 2, and  $v/f'_c = 0.045$  in wall  $W2$  at Level 1.

### **4.3 Nonlinear analysis**

Nonlinear time history analysis is the most accurate procedure to assess the seismic performance of a concrete building; however this type of analysis is not widely accepted to be used in practice because of a number of disadvantages such as selection and scaling of input ground motions, complex hysteretic models, timeliness of analysis procedure and interpretation of output results. In order to study shear force distribution between walls one does not require such a complex analysis. Other aspects of nonlinear shear behaviour of concrete walls, such as the influence of higher modes on total shear demand on concrete walls in a building must be investigated using nonlinear dynamic analysis. The relative shear force distribution between walls depends only on the nonlinear material behaviour of the concrete walls, and this can be investigated using nonlinear static analysis. The advantage of nonlinear static analysis is the simplicity and transparency of the analysis results which allows a complete understanding of the behaviour of the structure.

#### **4.3.1 Model assumptions**

A uniformly distributed lateral load over a height of 62 m from the base (resultant lateral load at 31 m from the base) was used for the static analysis. The resulting distribution of bending moments and shear forces over lower stories of the building from the RSA and the static analysis are compared in Fig. 4.2.

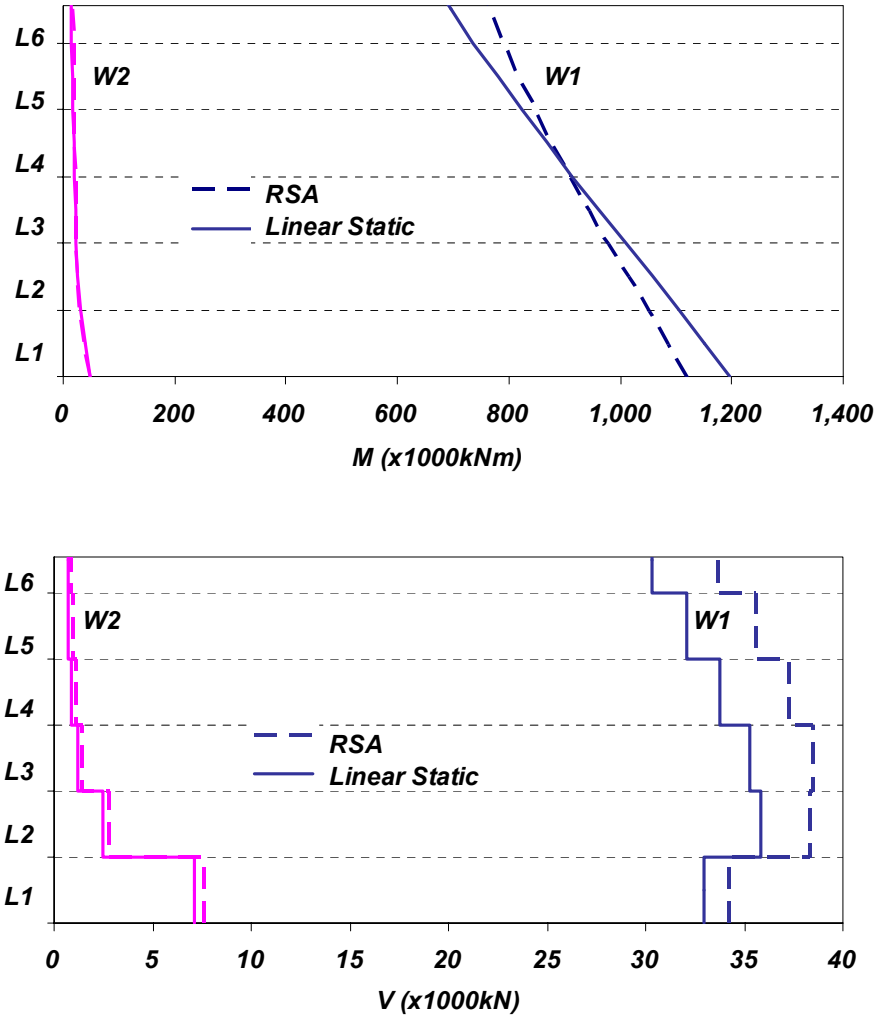


Figure 4.2. Comparison of bending moment and shear force distributions over lower floors from RSA (dashed lines) and linear static analysis (solid lines).

The shear forces and bending moments determined at the base of walls from linear static analysis are summarized in Table 4.2. These are referred to as the factored forces, analogous to factored forces in design, and are used to normalize the plots in the results section. Note that the ratio of  $M_{f1}$  to  $M_{f2}$  is 24.4 while the ratio of  $V_{f1}$  to  $V_{f2}$  at Level 1 and 2 are 4.64 and 14.5. The ratio of  $(M_{f1} + M_{f2})$  to  $(V_{f1} + V_{f2})$  at the base is 31 m. Note that seismic response of inter-connected walls is greatly dependent on the lateral loading pattern that is used in the pushover analysis. An appropriate loading pattern which is controlled by parameter  $h' = M_b/V_b$  can be estimated using nonlinear time history analysis which will be investigated in Chapter 5 of this dissertation.

Table 4.2 Summary of forces determined at the base of walls from linear static analysis.

Factored Forces	Wall 1 ( <i>W1</i> )	Wall 2 ( <i>W2</i> )
$V_f$ Level 2 (kN)	35,820	2,470
$V_f$ Level 1 (kN)	33,000	7,100
$M_f$ base (kNm)	1,195,500	49,000

The nonlinear static analyses were done using the tri-linear models for flexure and shear described above. A summary of the nonlinear model parameters are given in Table 4.3 and Table 4.4. The pushover analyses were performed using SAP-2000 (CSI 2006). The flexural hinge length for walls was taken as the full storey height; in addition, sensitivity analysis was conducted to determine parameters such as event tolerance and the total number of analysis steps for the accuracy of results (See SAP-2000 Analysis and Theory Reference Manual (2006) for more details). The walls were assumed to be fixed at the base, and the structure below ground was not included in the current study.

Table 4.3 Nonlinear flexural model parameters used for analysis.

Tri-linear Flexural Model		
Wall	<i>W1</i>	<i>W2</i>
$M_l$ (1000 kNm)	424.9	22.47
$\phi_l$ (rad/km)	0.047	0.113
$M_n$ (1000 kNm)	1,195	49.00
$\phi_y$ (rad/km)	0.393	1.200
$M_u$ (1000 kNm)	1,198	49.13
$\phi_u$ (rad/km)	3.889	7.778

Table 4.4 Nonlinear shear model parameters used for analysis.

Tri-linear Shear Model				
	<i>W1</i>		<i>W2</i>	
Level	1	2	1	2
$V_{cr}$ (1000 kN)	23.75	23.75	6.39	2.22
$\gamma_{cr} \times 1000$	0.315	0.315	0.170	0.059
$V_n$ (1000 kN)	33.00	35.80	7.10	2.47
$\gamma_y \times 1000$	2.705	2.765	2.305	2.105
$V_u$ (1000 kN)	33.03	35.82	7.12	2.49
$\gamma_u \times 1000$	7.505	7.385	8.005	8.035



#### 4.3.2 Moment to shear ratio at the base

The seismic base moment to shear ratio ( $h'=M_b/V_b$ ) is one important parameter which determines the height at which the base shear  $V_b$  generates the bending moment  $M_b$  at the base. Determination of this parameter, which refers to the point of application of the base shear along the height of wall, depends mainly on the assumptions used for modelling and the type of analysis. For example if a response spectrum analysis (RSA) is used for design of low-rise walls, where moment to shear ratio at the base is influenced mainly by the first mode response, it is reasonable to consider  $h'$  values close to 70% of the total height. For high-rise buildings where the higher modes significantly contribute to the seismic response, the point of application of base shear becomes lower along the height compared to low-rise walls. As an example, the point of base shear resultant of for the described model of a 30-storey wall was approximately at 40% of the total height based on RSA..

It should be noted that since the force distribution between walls is the main point of interest, only one base moment to shear ratio ( $h'$ ) associated with RSA (consistent with design practice) was used to define the seismic loading pattern for pushover analysis of the model of two walls in this Chapter.

The value of moment to shear ratio at the base also depend on the level of nonlinear action in the section of wall. Nonlinear time history analysis (NTHA) that was performed as a part of present work in Chapter 5 showed that formation of plastic hinge at the base of wall further reduces the base moment to shear ratio as compared to linear analysis.

Chapter 5 will investigate the variation of the base moment to shear ratio for a model of high-rise wall subjected to different earthquake accelerations while taking into account a variety of nonlinear models associated with the provided flexural and shear strengths at different sections of wall over the height.

### 4.3.3 Analysis parameters and results

In order to understand how the nonlinear model influences the shear force distribution, nonlinear static analyses were performed on the two-wall example using different nonlinear models. Figure 4.3 summarizes these different models. For flexure, either bi-linear or tri-linear models were used, while for shear, linear, bi-linear and tri-linear models were used. In the case of the linear and bi-linear shear models, unlimited strength was assumed as shown in Fig. 4.3. Combination of different flexural model and shear models shown on Fig 4.3 are also summarized in Table 4.5.

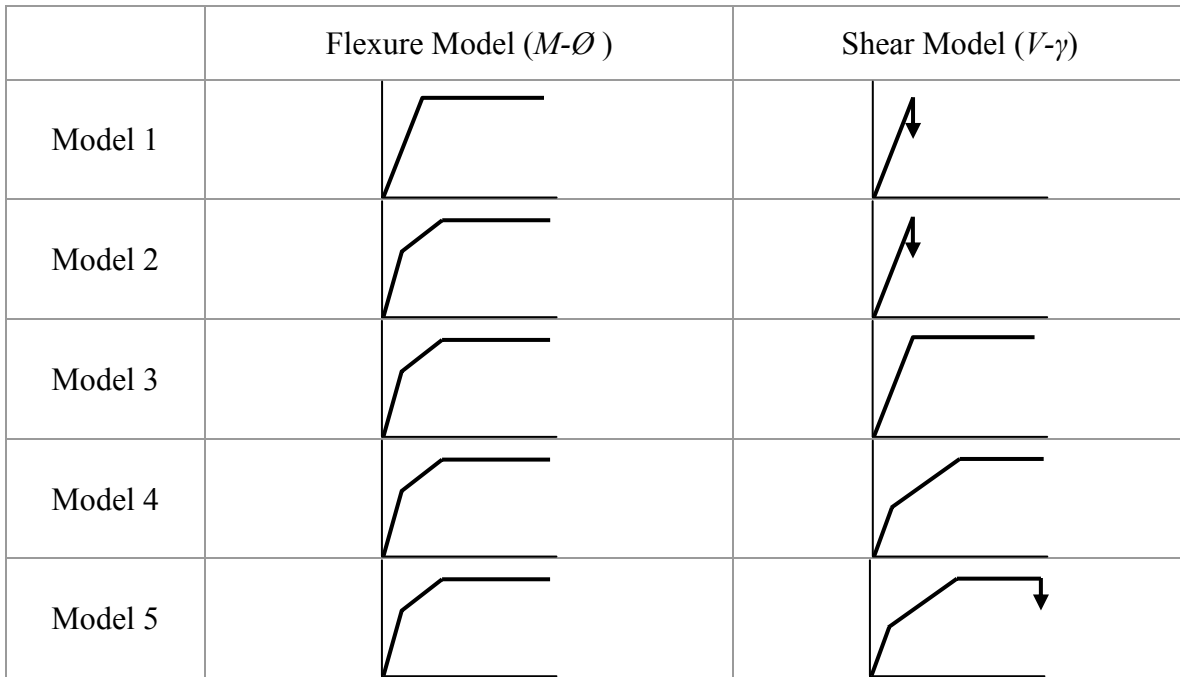


Figure 4.3 Flexural and Shear models used in the present study.

Table 4.5 Nonlinear flexure and shear models used for analysis.

Model	Flexure	Shear	Description
1	Bi-linear	Linear	Infinite shear strength
2	Tri-linear	Linear	Infinite shear strength
3	Tri-linear	Bi-linear	Infinite shear strength
4	Tri-linear	Tri-linear	Infinite shear strength
5	Tri-linear	Tri-linear	Limited shear strength

A standard format is used in the figures to summarize the results. The dark blue (darker color) lines in the plots shows the results for the longer wall ( $W1$ ), while the magenta lines (lighter color) indicate the results for the smaller wall ( $W2$ ). Solid and dashed lines represent the results for the first and second storey, respectively. Two separate plots are given to present the flexure and shear demands on walls. The shear and bending moment demands, shown on the vertical axes, have been normalized by the forces determined in the linear static analysis and summarized in Table 4.2. In all cases, the horizontal axis is the displacement at the top of walls. A summary of the important points in the response is given in the tables corresponding to each figure.

The abbreviation used to indicate the nonlinear state of walls during analysis is described as (A-B-#), in which “A” indicates either Flexure (F) or Shear (S) nonlinearity, “B” indicates three possible states of Cracking (C) , Yielding (Y) or Failure (F) and “#” indicates the level in which the nonlinearity has been monitored.

Figure 4.4 summarizes the results from Model 1 (see Fig. 4.3) in which the walls are assumed to respond linearly in shear and bi-linearly (elastic-perfectly plastic) in flexure. The analysis was performed using  $0.7E_cI_g$  for effective flexural rigidity of the walls as was done to determine the factored forces given in Table 4.2. Since the stiffnesses are proportional to the strengths, the walls yield at the base at exactly the same time. This simple response is what most engineers assume is happening in concrete walls. Note that while the shear strengths of the walls are assumed to be unlimited, the shear demand is limited by flexural yielding at the base. The shear force demand is limited exactly to the shear force determined in the linear analysis. As the figure shows yielding in both walls occur at a monitored top displacement of 0.38 m and beyond this point the walls reach their flexural and shear capacity at the same time.

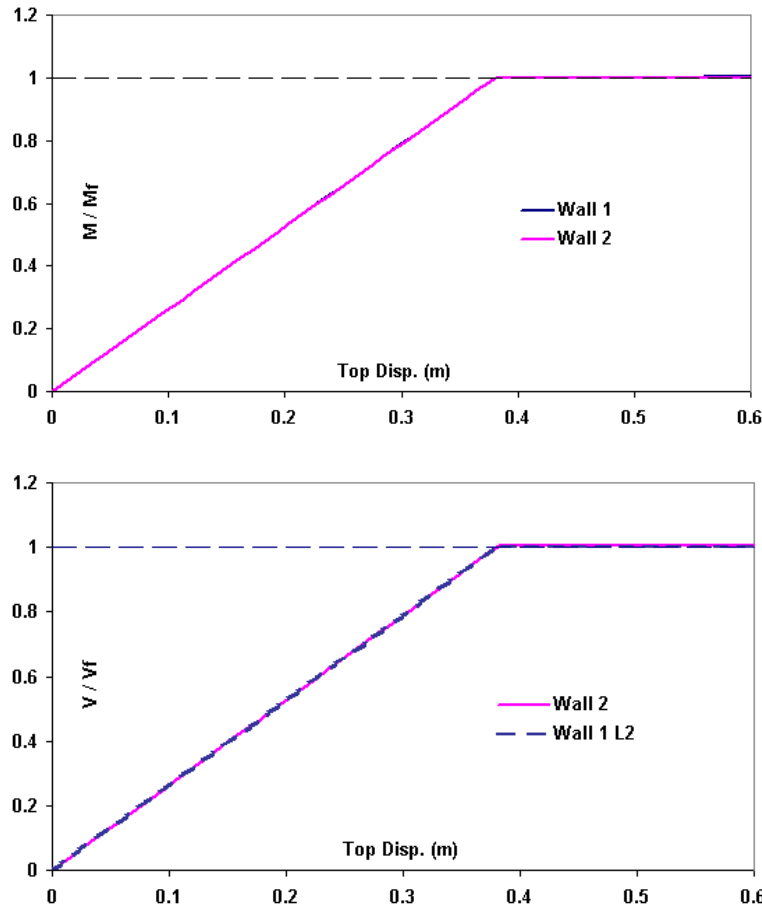


Figure 4.4 Normalized shear and flexure demand predicted by Model 1.

Table 4.6 Nonlinear states captured by Model 1.

Top Displacement (m)	State*	Level
0.380	F-Y-1	1
0.380	F-Y-2	1

\* (A-B-#) A: (Flexure, Shear), B: (Cracking, Yielding, Failure), #: (Wall 1, Wall 2).

The results from Model 2 are shown in Fig. 4.5. The shear model is unchanged (linear with unlimited strength), while the flexural model is now tri-linear. The initial flexural rigidity is increased to the uncracked section rigidity  $E_c I_g$  of the wall, but a significant reduction in flexural rigidity occurs after cracking (see Fig. 4.3). The reduction in flexural rigidity occurs at a curvature  $\phi_l$  in wall W1 that is less than half the  $\phi_l$  of wall W2 (0.047 versus 0.113; see Table 4.3).

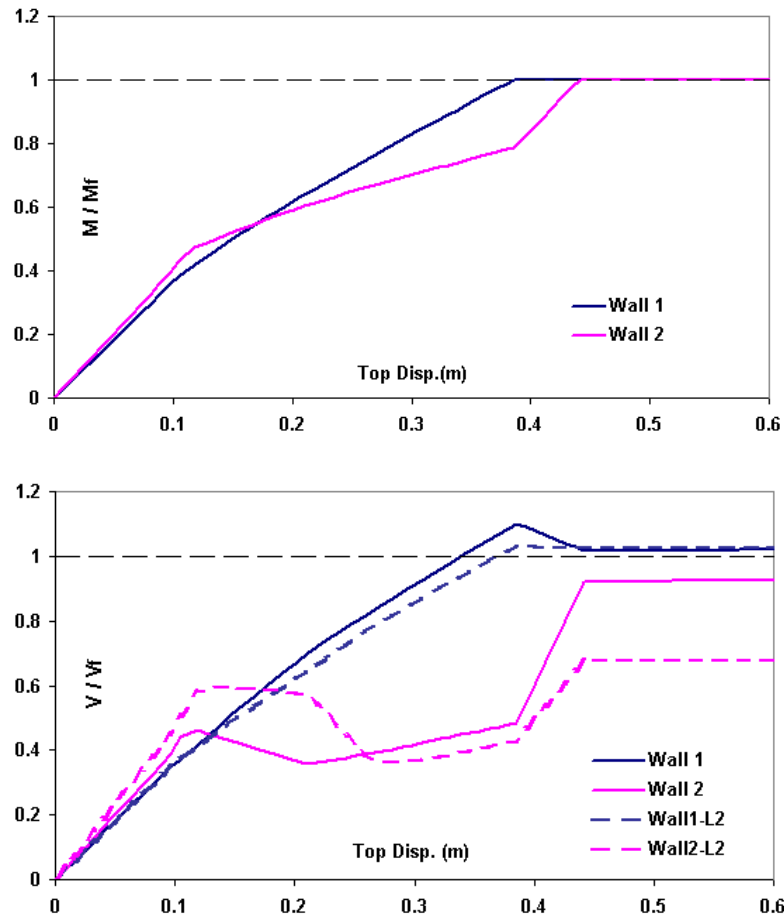


Figure 4.5 Normalized shear and flexure demand predicted by Model 2.

Table 4.7 Nonlinear states captured by Model 2.

Top Displacement (m)	State*	Level
0.097	F-C-1	1
0.118	F-C-2	1
0.118	F-C-1	2
0.219	F-C-2	2
0.385	F-Y-1	1
0.441	F-Y-2	1

\* (A-B-#) A: (Flexure, Shear), B: (Cracking, Yielding, Failure), #: (Wall 1, Wall 2).

As a result, flexural cracking occurs at the base of wall *W1* first at a top wall displacement of 0.1 (0.097) m. At that point, the shear begins to redistribute so that wall *W2* picks up an increasing amount of the total shear. Flexural cracking at the base of wall *W2* occurs at a top displacement of 0.12 m, and at that point the shear force in wall *W2* at Level 1 (solid magenta line) begins to drop. Flexural cracking also occurs at that point in

wall *W1*, Level 2, so the drop in shear in wall *W2* at Level 2 is delayed until a top displacement of 0.22 m when wall *W2* cracks at that level. At a displacement of 0.27 m, wall *W2* cracks at level 3 causing the shear in wall *W2* Level 2 to start increasing again. Yielding of wall *W1* occurs at a top displacement of 0.39 m, while yielding of wall *W2* does not occur until a top displacement of 0.44 m. Note that according to the tri-linear bending moment – curvature models that were assumed, yielding of wall *W2* occurs at a curvature  $\phi_y$  that is about three times the yield curvature  $\phi_y$  of wall *W1* (1.20 versus 0.39; see Table 4.3). Due to the large reduction in flexural rigidity at cracking in wall *W2*, wall *W1* is subjected to a shear force that is about 10% larger than what is estimated by a linear analysis. As the wall *W1* yields in flexure, the moment capacity is limited and therefore the extra demand moment should be resisted by either wall *W2* or the action of floor slabs that would result in an excessive tensile force for the lower slabs. This tensile force would increase the shear demand on the longer wall by 10% as illustrated in the figure. Figure 4.6 presents the results from Model 3, which is the same as Model 2 (Fig. 4.5) except that the reduction in shear rigidity that occurs at shear cracking is now included. The initial response in Fig. 4.6 is the same as the response in Fig. 4.5. At a top displacement of 0.22 m, shear cracking occurs in wall *W1* at both Level 1 and Level 2 where the shear is largest in that wall. Shortly after this event, *W2* cracks in shear at Level 2 causing the curve to get flat due to its low shear slope after cracking. *W2* at Level 1 cracks in shear afterwards at a top displacement of 0.32 m and also suffers a flexural yielding after this at top displacement of 0.34 m. The distribution of forces does not change until *W1* yields in flexure at Level 1 at a top displacement of 0.43 m. At this instance of time, the curves go flat since the flexural mechanism has formed at the base of walls due to yielding. Due to the shear deformations of wall *W1* and the resulting shear force redistribution, wall *W2* yields at a top displacement of 0.34 m, while wall *W1* yields at a top displacement of 0.43 m. That is, the wall with a yield curvature that is three times larger actually yields first. This is a very significant result.

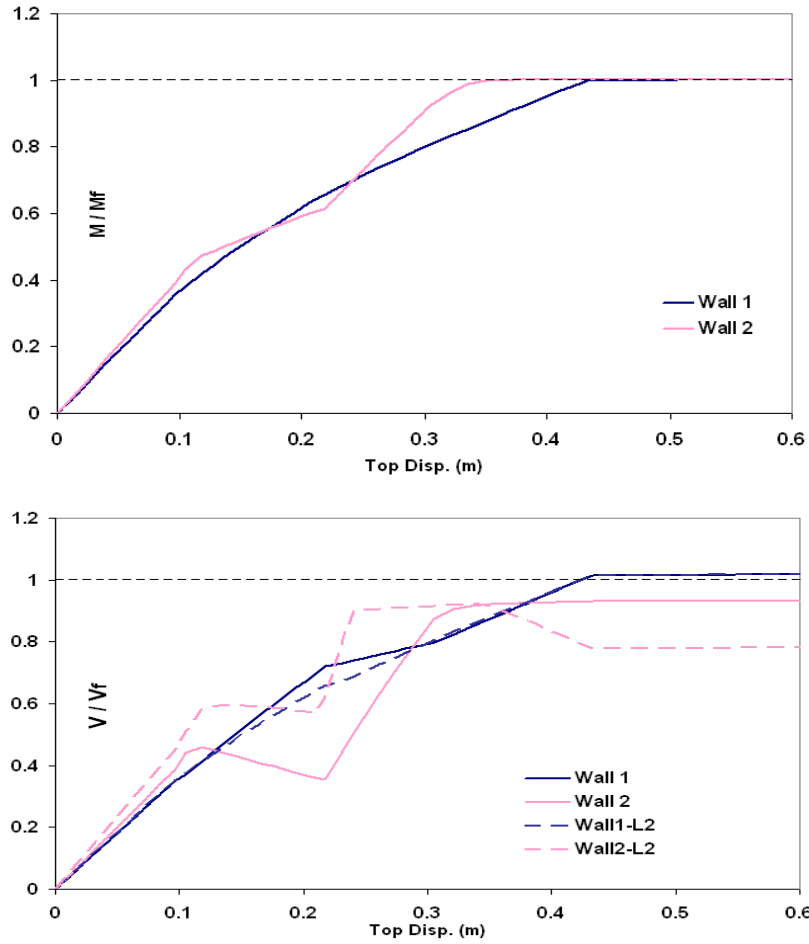


Figure 4.6 Normalized shear and flexure demand predicted by Model 3.

Table 4.8 Nonlinear states captured by Model 3.

Top Displacement (m)	State*	Level
0.097	F-C-1	1
0.118	F-C-2	1
0.118	F-C-1	2
0.218	S-C-1	1
0.218	S-C-1	2
0.218	F-C-2	2
0.241	S-C-2	2
0.321	S-C-2	1
0.350	F-Y-2	1
0.433	F-Y-1	1
0.715	F-F-1	1

\* (A-B-#) A: (Flexure, Shear), B: (Cracking, Yielding, Failure), #: (Wall 1, Wall 2).

Figure 4.7 presents the results from Model 4 in which shear yielding is included. The shear strengths of the walls were set equal to the shear demands determined from a linear analysis and summarized in Table 4.3. Yielding of the horizontal reinforcement in the wall, i.e., shear yielding of the wall, occurs in wall *W1* at both Level 1 and Level 2 at a top displacement of 0.42 m (see Table 4.9).

The distribution of forces in Model 4 is similar to Model 3 until walls reach a top displacement of 0.42 m. At this stage *W1* yields in both Level 1 and Level 2. *W2* yields in shear at Level 2 shortly after at a top displacement of 0.43 m has been reached and at the same time *W1* yields in flexure at Level 1. The flexural mechanism forms at the base of walls at this point.

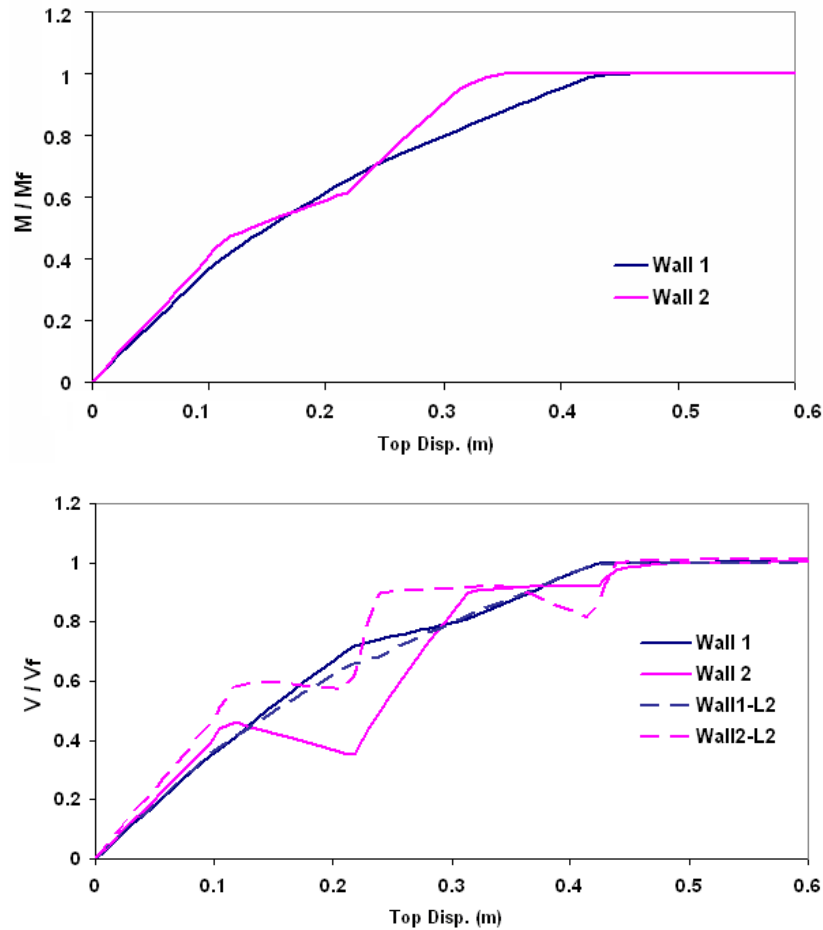


Figure 4.7 Normalized shear and flexure demand predicted by Model 4.



Table 4.9 Nonlinear states captured by Model 4.

Top Displacement (m)	State*	Level
0.097	F-C-1	1
0.118	F-C-2	1
0.118	F-C-1	2
0.218	S-C-1	1
0.218	S-C-1	2
0.218	F-C-2	2
0.241	S-C-2	2
0.313	S-C-2	1
0.350	F-Y-2	1
0.423	S-Y-1	1
0.423	S-Y-1	2
0.439	S-Y-2	2
0.439	F-Y-1	1
0.504	S-Y-2	1

\* (A-B-#) A: (Flexure, Shear), B: (Cracking, Yielding, Failure), #: (Wall 1, Wall 2).

The behaviour of walls in Model 5 is similar to Model 4 except that the walls have a limited shear capacity rather than an infinite shear capacity assumed in Model 4. Walls reached their ultimate capacity in shear at Level 2 at a corresponding top displacement of 0.50 m according to Model 5. This model shows that unlike the most common taught about shear failure at the base of wall, it is possible to encounter shear failure even in upper levels; therefore it is vital to estimate a realistic shear demand when using linear dynamic analysis. The shear failure at Level 2 rather than first level which most anticipated to fail is a quite significant finding in this case of analysis.

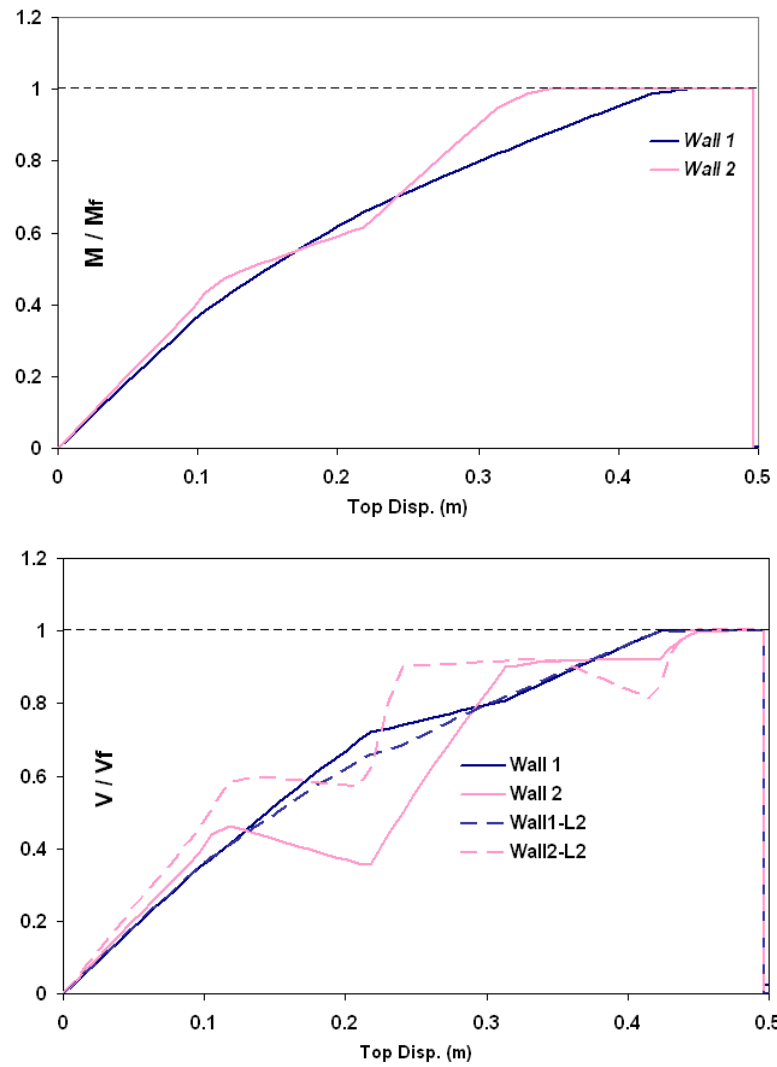


Figure 4.8 Normalized shear and flexure demand predicted by Model 5.

Table 4.10 Nonlinear states captured by Model 5.

Top Displacement (m)	State*	Level
0.105	F-C-1	1
0.123	F-C-2	1
0.123	F-C-1	2
0.221	S-C-1	1
0.221	S-C-1	2
0.221	F-C-2	2
0.242	S-C-2	2
0.314	S-C-2	1
0.357	F-Y-2	1
0.426	S-Y-1	1
0.426	S-Y-1	2
0.442	S-Y-2	2
0.457	F-Y-1	1
0.475	S-Y-2	1
0.502	S-F-2	2
0.502	S-F-1	2

\* (A-B-#) A: (Flexure, Shear), B: (Cracking, Yielding, Failure), #: (Wall 1, Wall 2).

The influence of a 10% increase in the flexural capacity of wall *W2* over the linear flexural demand is investigated in Fig. 4.9 and Fig. 4.10. Figure 4.9 presents the results from Model 1 (bi-linear flexure and linear shear), and thus should be compared with the results in Fig. 4.4. Model 1 predicts about a 20% increase in shear demand at the first level and about a 15% increase in shear demand at the second level due to the 10% increase in flexural capacity.

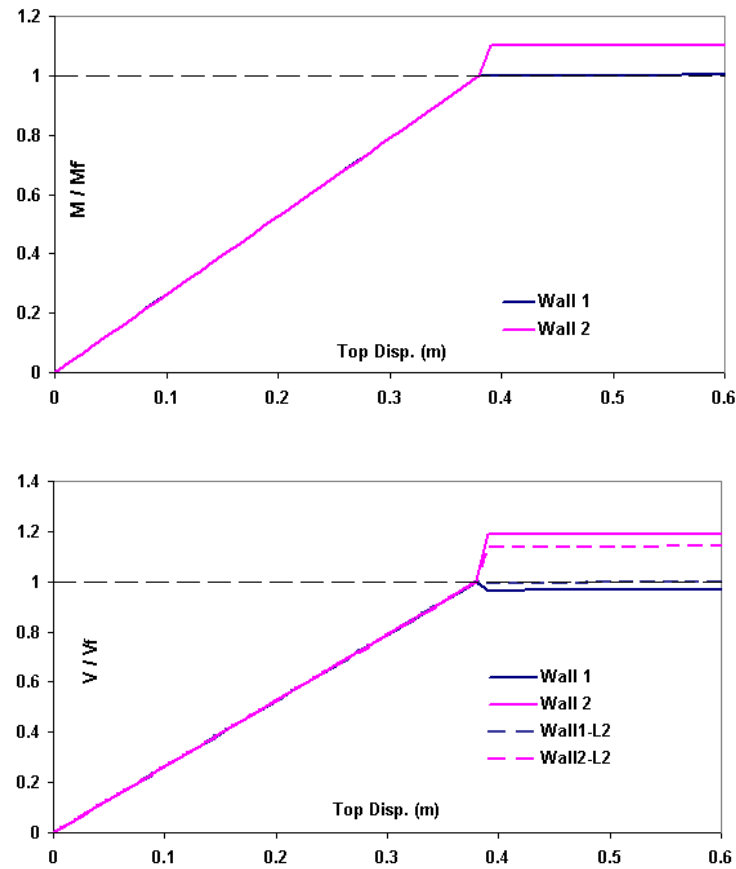


Figure 4.9 Influence of 10% flexural overstrength of  $W2$  according to Model 1.

Table 4.11 Nonlinear states captured according to Fig. 4.9.

Top Displacement	State*	Level
0.380	F-C-1	1
0.391	F-C-2	1

\* (A-B-#) A: (Flexure, Shear), B: (Cracking, Yielding, Failure), #: (Wall 1, Wall 2).

Figure 4.10 presents the results from Model 3 (tri-linear flexure and bi-linear shear), and should be compared with the results in Fig. 4.6. The figure shows that when the cracking effects in shear are considered in the behaviour of walls, a significant change in shear force demand was not observed. The behaviour in this model is similar to the behaviour observed in Model 3 without any increase in flexural strength of walls (Fig. 4.6).

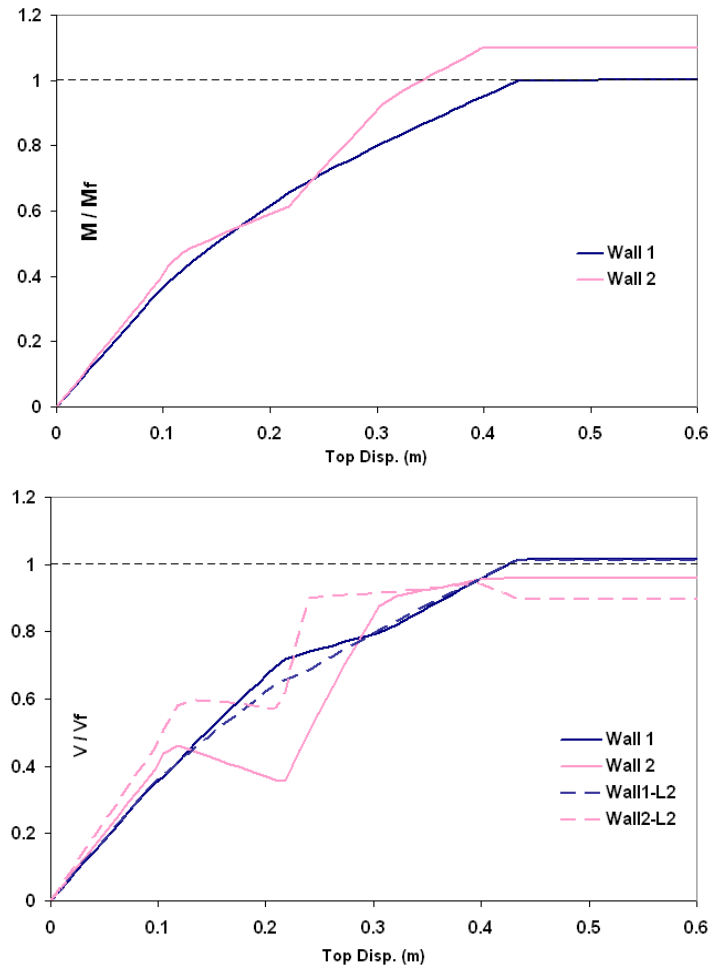


Figure 4.10 Influence of 10% flexural overstrength of *W2* according to Model 3.

Table 4.12 Nonlinear states captured according to Fig. 4.10.

Top Displacement (m)	State*	Level
0.097	F-C-1	1
0.118	F-C-2	1
0.118	F-C-1	2
0.218	S-C-1	1
0.218	S-C-1	2
0.218	F-C-2	2
0.241	S-C-2	2
0.321	S-C-2	1
0.413	S-Y-1	1
0.413	F-Y-2	1
0.432	S-Y-1	2
0.434	F-Y-1	1

\* (A-B-#) A: (Flexure, Shear), B: (Cracking, Yielding, Failure), #: (Wall 1, Wall 2).

To summarize the findings from this set of analysis two important results are recalled:

- In a case where two walls having different lengths are connected together through diaphragm slabs, it is possible for the shorter wall to yield in flexure prior to the longer wall. This phenomenon is caused by the fact that longer wall takes more of its total lateral deformation in the form of shear displacement whereas the shorter wall deformation is mainly caused by bending behaviour.
- Two connected walls can reach their ultimate shear capacity in upper levels earlier than the base. This is caused by the redistribution of forces due to changes in the relative stiffness of walls when undergoing nonlinear deformation.

The best behaviour was observed in the case in which both walls yielded in flexure at the base leading to a ductile flexural mechanism.

#### 4.4 Simplified effective stiffness approach

The next set of analyses investigates the problem using a simple linear approach. In this part the initial tri-linear flexural and shear response curves are used to determine the effective stiffnesses corresponding to a fully cracked section and then these values are used to get a first trial estimate of shear forces and bending moments for the walls. For the example of two walls, three symmetrical cross sections were considered as shown in Fig. 4.11.

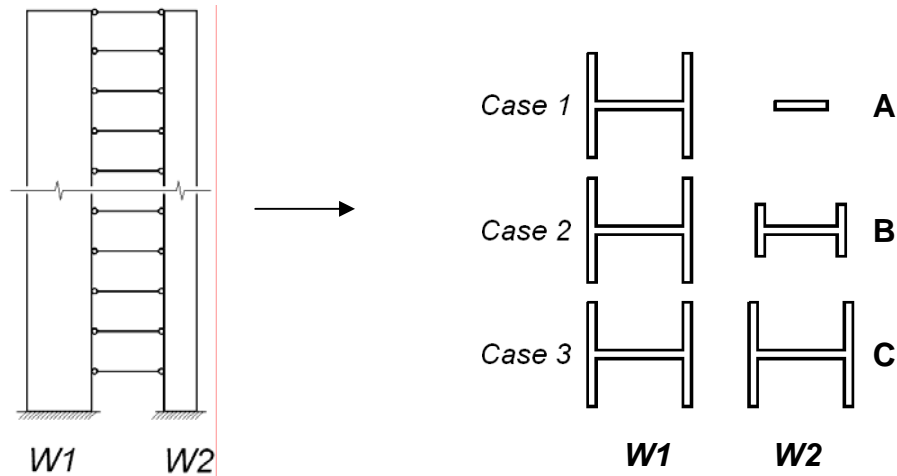


Figure 4.11 Sections of walls considered in the present example.

Section A corresponds to a rectangular section with a length of 4.5 m and a thickness of 0.75 m. Section B is an *I*-section with a flange length of 4.5 m and a web length of 7.0 m and a uniform thickness of 0.75 m. Section C is also an *I*-section with larger dimensions compared to section B. The length of web and flange is 9.0 m each and the thickness is 0.75 m everywhere. Section C is the same section that was considered for *W1* in the previous example. More information about section properties of walls are given in Table 4.13.

Table 4.13 Section properties for walls shown in Fig. 4.12.

Cross Section A			Cross Section B			Cross Section C		
$f'_c$	50	MPa	$f'_c$	50	MPa	$f'_c$	50	MPa
$E_c$	31820	MPa	$E_c$	31820	MPa	$E_c$	31820	MPa
$L_w$	4.5	m	$L_w$	7.0	m	$L_w$	9.0	m
$A_g$	3.375	m <sup>2</sup>	$A_g$	10.875	m <sup>2</sup>	$A_g$	19.125	m <sup>2</sup>
$I_g$	5.69	m <sup>4</sup>	$I_g$	76.63	m <sup>4</sup>	$I_g$	256.71	m <sup>4</sup>
$A_{vg}$	2.81	m <sup>2</sup>	$A_{vg}$	5.25	m <sup>2</sup>	$A_{vg}$	6.75	m <sup>2</sup>
$EI_g$	181,054	MNm <sup>2</sup>	$EI_g$	2,438,351	MNm <sup>2</sup>	$EI_g$	8,168,462	MNm <sup>2</sup>
$GA_{vg}$	35,765	MN	$GA_{vg}$	66,821	MN	$GA_{vg}$	85,913	MN

In order to study the redistribution of forces between walls three different cases were examined with different arrangement of wall sections as below:

Case 1:  $W1$ : Section C,  $W2$ : Section A.

Case 2:  $W1$ : Section C,  $W2$ : Section B.

Case 3:  $W1$ : Section C,  $W2$ : Section C.

Same material properties for the previous example have been considered for the walls. Nonlinear behaviour for the walls is assumed to be a realistic tri-linear behaviour for both flexure and shear. The values required to construct the tri-linear curve were given in Table 4.3. In order to get an initial estimate of the moment and shear demand on two walls, the cracked section stiffnesses were used in terms of  $EI_e$  and  $GA_{ve}$  which correspond to the slope between origin and the yielding point. The same lateral loading pattern was used as described in Fig. 4.2 to run a simple linear analysis while using the cracked section stiffnesses (referred to as “Stage 2”).

Table 4.14 through Table 4.17 present the results for bending moment and shear force values obtained according to use of both uncracked section stiffnesses (Stage 1) and cracked section stiffnesses (Stage 2) in the linear analysis. Once the updated values of bending moment and shear force were obtained using cracked section properties, the walls' strength were redesigned for new values and pushover analyses were performed using the same lateral loading pattern described in Section 4.2. Figure 4.12 shows the results for pushover analysis in Case 1.



## Case 1

Table 4.14 Resulting moments and shear forces for  $W1$  in Case 1.

	$W1$	$M(kNm)$	$V(kN)$	$EI_e/EI_g$	$GA_e/GA_g$
Stage 1	Level 1	1,194,855	32,506	1	1
	Level 2	1,194,855	32,506	1	1
Stage 2	Level 1	1,196,000	33,514	0.33	0.12
	Level 2	1,196,000	36,231	0.33	0.13

Table 4.15 Tri-linear flexural and shear models used for  $W1$  in Case 1.

$W1$ Tri-linear $M$			$W1$ Tri-linear $V$			
	$M(MNm)$	$\varnothing$ (rad/km)	$V_{L1}(MN)$	$\gamma_{L1} \times 1000$	$V_{L2}(MN)$	$\gamma_{L2} \times 1000$
$Cr$	424.9	0.047	23.75	0.315	23.75	0.315
$Y$	1,196	0.393	33.5	2.765	36.20	2.765
$U$	1,200	3.890	33.85	7.385	36.55	7.385

Table 4.16 Resulting moments and shear forces for  $W2$  in Case 1.

	$W2$	$M$	$V$	$EI_e/EI_g$	$GA_e/GA_g$
Stage 1	Level 1	53,725	7,738	1	1
	Level 2	53,725	3,133	1	1
Stage 2	Level 1	52,582	6,730	0.33	0.07
	Level 2	52,582	2,182	0.33	0.03

Table 4.17 Tri-linear flexural and shear models used for  $W2$  in Case 1.

$W2$ Tri-linear $M$			$W2$ Tri-linear $V$			
	$M(MNm)$	$\varnothing$ (rad/km)	$V_{L1}(MN)$	$\gamma_{L1} \times 1000$	$V_{L2}(MN)$	$\gamma_{L2} \times 1000$
$Cr$	22.47	0.113	6.390	0.170	1.962	0.059
$Y$	52.58	1.200	6.730	2.305	2.180	2.105
$U$	53.00	7.778	6.797	8.005	2.202	8.035

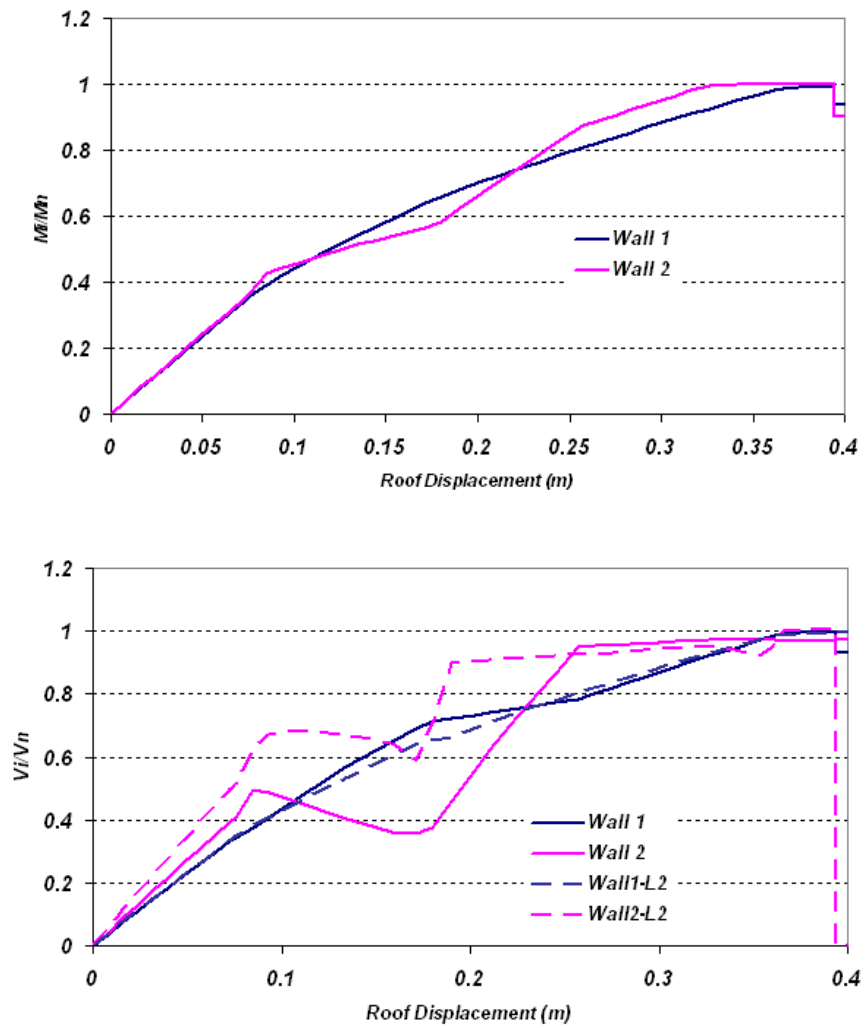


Figure 4.12 Moment and shear force demand according to Case 1.

Table 4.18 Nonlinear states captured by Case 1 according to Fig. 4.12.

Top Displacement (m)	State*	Level
0.075	F-C-1	1
0.085	F-C-2	1
0.085	F-C-1	2
0.172	F-C-2	2
0.180	S-C-1	1
0.180	S-C-1	2
0.190	S-C-2	2
0.258	S-C-2	1
0.340	F-Y-2	1
0.361	S-Y-1	2
0.366	S-Y-2	2
0.379	S-F-1	2
0.392	S-F-2	2

\* (A-B-#) A: (Flexure, Shear), B: (Cracking, Yielding, Failure), #: (Wall 1, Wall 2).

Shear failure was observed in the second storey due to redistribution of forces in Case 1 at a small top displacement of 0.37 m. Flexural cracking in *W1* and *W2* in first level is followed by flexural cracking in second level as walls reach a top displacement of 0.17 m. Shear cracking occurs in *W1* at Level 1 and Level 2 which is followed by cracking in *W2* at the second level and at the base. *W2* suffers flexural yielding at first level at a top displacement of 0.34 m. Shear yielding in both walls occur at about the same top displacement at Level 2, leading to a shear failure at this level.

It is important to note that flexural yielding in *W1* was not observed in this case which is not quite the way commonly expected about behaviour of two wall system. It is also important to note when cracked section stiffnesses were used, the longer wall (*W1*) takes more of the forces due to redistribution compared to the initial uncracked case. The ratios for section shear stiffnesses are 12% in *W1* vs. 7% in *W2* at the base and 13% in *W1* vs. 3% in Level 2. This comparison shows the significant influence of shear force redistribution at second level for the shorter wall (*W2* with Section A). These numbers show that after the walls crack, a larger portion of the shear force demand at each level is carried by the stronger wall (*W1* in this example).

Use of updated section stiffness values in Case 1 lead to an undesired shear failure of walls in second level. A practical solution to improve the walls' performance is proposed here which is referred to as Case 1-2.

Case 1-2 is similar to the Case 1 except that the shear strength in  $W2$  was maintained over the height for the first four lower stories. The results for this case are shown in Fig. 4.13. Shear demand in  $W2$  associated with Case 1-2 remained well below the ultimate shear capacity compared to Case 1.

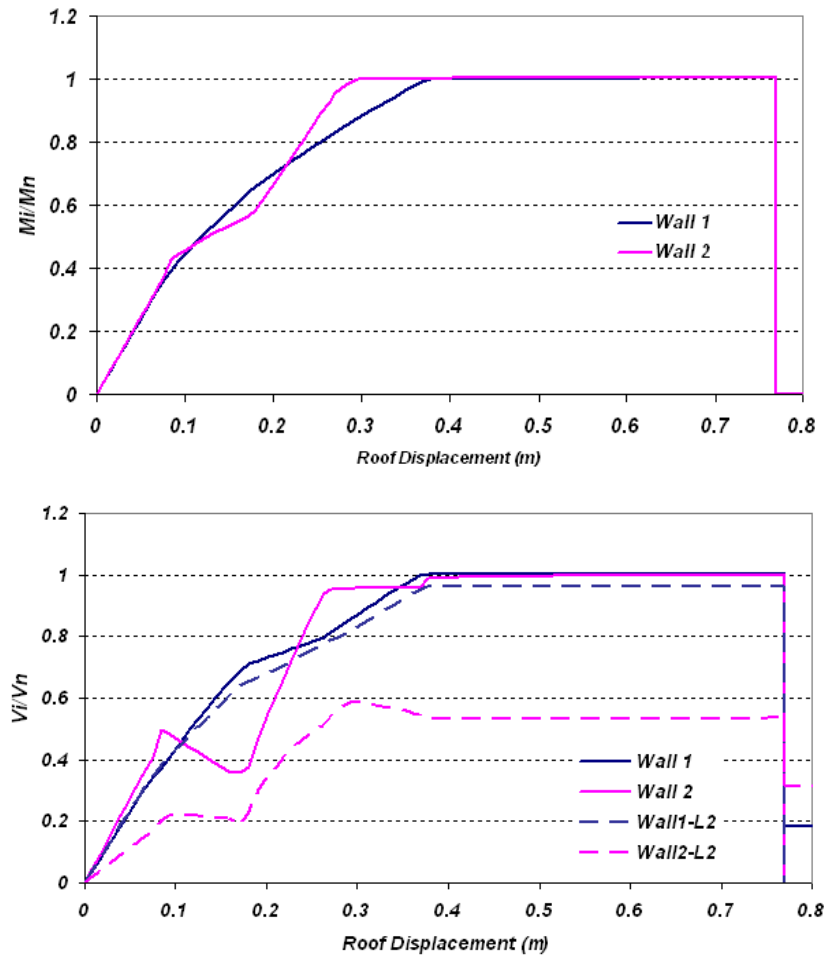


Figure 4.13 Reduction of moment and shear force demand according to Case 1-2.

Table 4.19 Nonlinear states captured by Case 1-2 according to Fig. 4.13.

Top Displacement (m)	State*	Level
0.075	F-C-1	1
0.085	F-C-2	1
0.085	F-C-1	2
0.172	F-C-2	2
0.180	S-C-1	1
0.180	S-C-1	2
0.272	S-C-2	1
0.296	F-Y-2	1
0.369	S-Y-1	1
0.377	F-Y-1	1
0.533	S-Y-2	1
0.662	F-F-1	1
0.770	F-F-2	1

\* (A-B-#) A: (Flexure, Shear), B: (Cracking, Yielding, Failure), #: (Wall 1, Wall 2).

No critical failure mode in shear was observed for Case 1-2 during pushover analysis until the anticipated flexural hinging mechanism occurred in the base level. All walls' sections in first and second storey suffered cracking due to flexure and shear response while yielding in *W2* happened prior to *W1* at the base level. A more ductile behaviour can be achieved once the flexural mechanism forms compared to shear failure observed in Case 1.

## Case 2

Table 4.20 Resulting moments and shear forces for  $W1$  in Case 2.

	$W1$	$M(kNm)$	$V(kN)$	$EI_e/EI_g$	$GA_e/GA_g$
Stage 1	Level 1	1,194,855	31,420	1	1
	Level 2	1,194,855	32,580	1	1
Stage 2	Level 1	1,192,200	32750	0.33	0.12
	Level 2	1,192,200	33540	0.33	0.13

Table 4.21 Tri-linear flexural and shear models used for  $W1$  in Case 2.

$W1$ Tri-linear M			$W1$ Tri-linear V			
	$M(MNm)$	$\emptyset$ (rad/km)	$V_{L1}(MN)$	$\gamma_{L1} \times 1000$	$V_{L2}(MN)$	$\gamma_{L2} \times 1000$
Cr	424.9	0.047	23.75	0.315	23.75	0.315
Y	1192.2	0.393	32.75	2.760	33.54	2.765
U	1200	3.890	33.07	7.380	33.87	7.385

Table 4.22 Resulting moments and shear forces for  $W2$  in Case 2.

	$W2$	$M(kNm)$	$V(kN)$	$EI_e/EI_g$	$GA_e/GA_g$
Stage 1	Level 1	445,400	21,440	1	1
	Level 2	445,400	17,870	1	1
Stage 2	Level 1	447,820	20,100	0.32	0.11
	Level 2	447,820	16,920	0.32	0.09

Table 4.23 Tri-linear flexural and shear models used for  $W2$  in Case 2.

$W2$ Tri-linear M			$W2$ Tri-linear V			
	$M(MNm)$	$\emptyset$ (rad/km)	$V_{L1}(MN)$	$\gamma_{L1} \times 1000$	$V_{L2}(MN)$	$\gamma_{L2} \times 1000$
Cr	140.0	0.057	16.32	0.270	15.23	0.243
Y	447.8	0.571	20.10	2.305	16.92	2.105
U	450.0	7.778	20.30	8.005	17.08	8.035

In Case 2 (See Fig. 4.14)  $W2$  has a larger cross section compared to Case 1 as shown in Fig. 4.12. Flexural cracking in  $W2$  is followed by flexural cracking in  $W1$  at first level and also flexural cracking in both walls at second level at a top displacement of 0.09 m. From a top displacement of 0.2 m to a top displacement of 0.25 m,  $W1$  and  $W2$  undergo shear cracking in both first and second levels. Shear yielding in  $W2$  happens at both first and second level followed by the shear yielding in  $W1$  at the base and flexural yielding in  $W2$ . Shear yielding in  $W1$  at second level happens at a top displacement of 0.38 m while  $W2$  at this level has already suffered shear yielding. A shear failure mechanism at second level was observed in this case which was similar to Case 1.

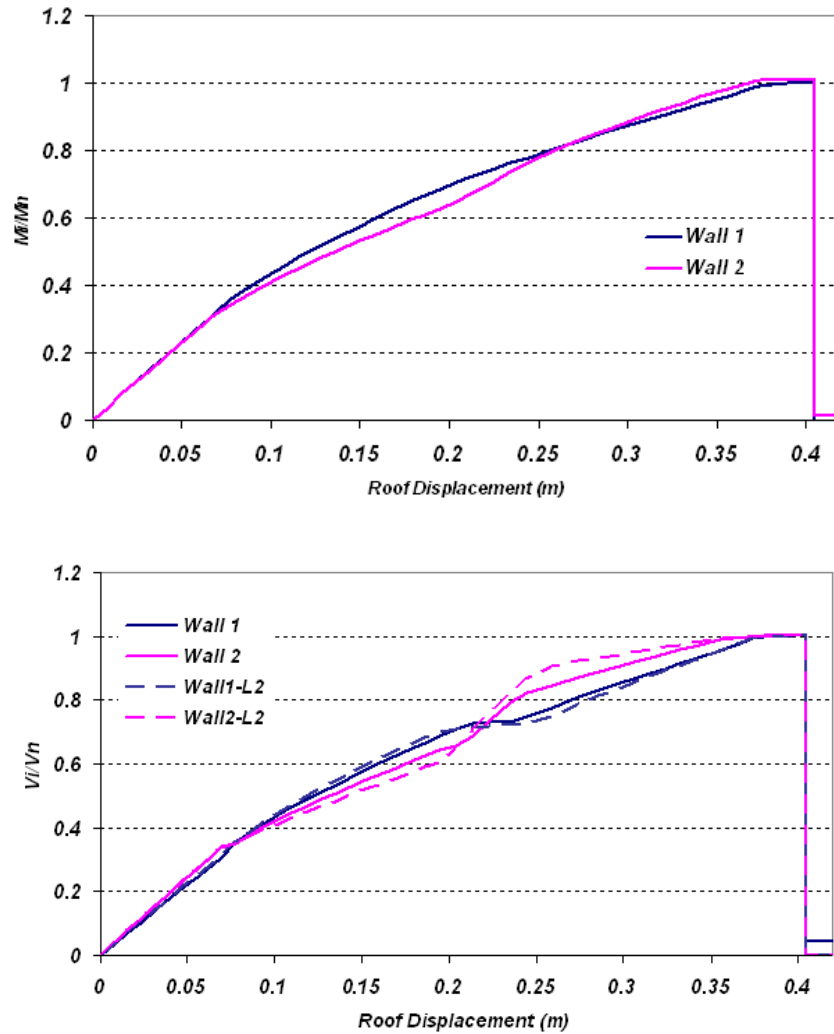


Figure 4.14 Moment and shear force demand according to Case 2.

Table 4.24 Nonlinear states captured by Case 2 according to Fig. 4.14.

Top Displacement (m)	State*	Level
0.069	F-C-2	1
0.093	F-C-1	1
0.093	F-C-1	2
0.093	F-C-2	2
0.204	S-C-1	2
0.213	S-C-1	1
0.244	S-C-2	1
0.259	S-C-2	2
0.370	S-Y-2	1
0.370	S-Y-2	2
0.374	S-Y-1	1
0.374	F-Y-2	1
0.380	S-Y-1	2
0.405	S-F-1	2
0.405	S-F-2	2

\* (A-B-#) A: (Flexure, Shear), B: (Cracking, Yielding, Failure), #: (Wall 1, Wall 2).

The shear force redistribution observed in Case 2 was not as significant as shown for Case 1 due to the changes in walls' geometrical properties. Wall B bending stiffness is about one third of Wall C whereas Wall A bending stiffness is 45 times less than bending stiffness in Wall C. The redistribution of forces after using the cracked section stiffnesses would be dependent on the relative stiffness properties of walls which was observed to be 0.12 in *W1* vs. 0.11 in *W2* at the base and 0.13 in *W1* vs. 0.09 in *W2* at second level.

Figure 4.15 shows the pushover analysis results for the case when walls possess similar section geometries.



### Case 3

Table 4.25 Tri-linear flexural and shear model for  $W1$  and  $W2$  in Case 3.

$W1$ & $W2$ Tri-linear M			$W1$ & $W2$ Tri-linear V	
	M	$\phi$	V1	$\gamma_1$
Cr	424.9	0.047	23.75	0.315
Y	1195	0.393	38.5	2.76
U	1200	3.89	38.885	7.38

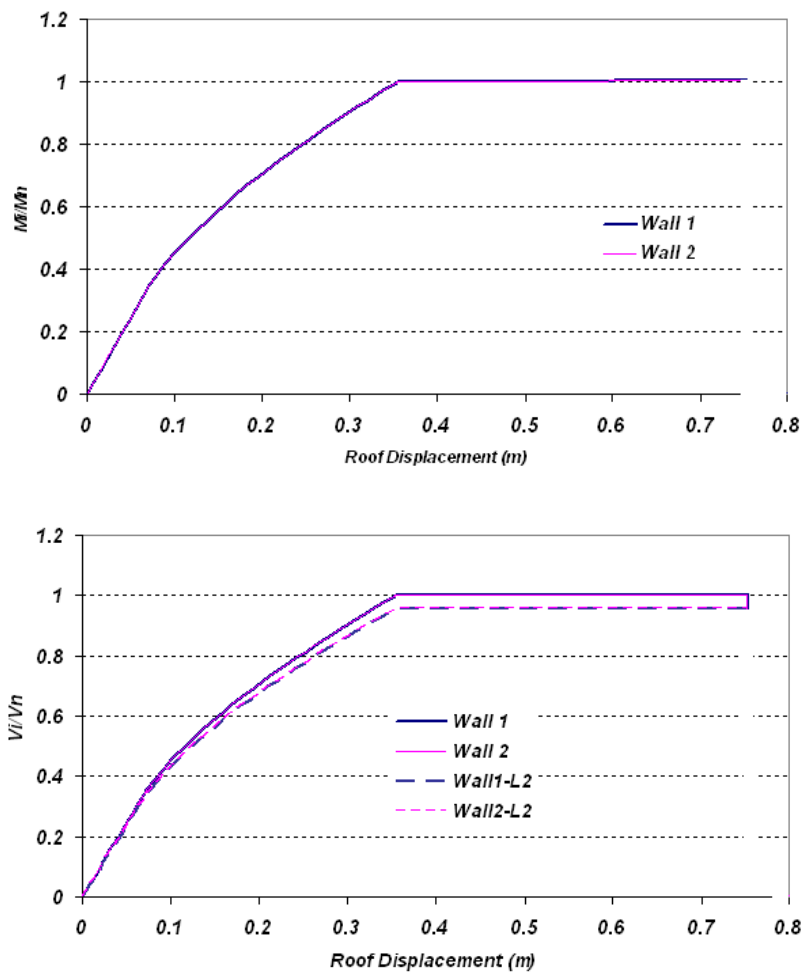


Figure 4.15 Moment and shear force demand according to Case 3.

Table 4.26 Nonlinear states captured by Case 2 according to Fig. 4.15.

Top Displacement (m)	State*	Level
0.074	F-C-1	1
0.074	F-C-2	1
0.092	F-C-1	2
0.092	F-C-2	2
0.169	S-C-1	1
0.169	S-C-2	1
0.181	S-C-1	2
0.181	S-C-2	2
0.354	S-Y-1	1
0.354	S-Y-2	1
0.358	F-Y-1	1
0.358	F-Y-2	1
0.645	F-F-1	1
0.645	F-F-2	1

\* (A-B-#) A: (Flexure, Shear), B: (Cracking, Yielding, Failure), #: (Wall 1, Wall 2).

No significant shear force distribution was observed for Case 3 in which both walls have the same geometry. All the nonlinear stages happened simultaneously in both walls leading to an ultimate yielding in flexure at the base of walls at a top displacement of 0.36 m.

In all cases changes in bending moment redistribution after using the cracked section stiffness was not noticeable whereas this change for shear force redistribution was significant especially for the case in which walls were different in size and shape. The redistribution of forces in walls after using cracked section properties tends to increase the shear force demand on the larger wall (*W1* in this study). The amount of increase in shear force on *W1* after considering effective shear stiffness is given in Table 4.27 for different analysis cases.

Table 4.27 Amount of increase in shear force demand in *W1* relative to uncracked state.

Case	Wall 1 at 1st level	Wall 1 at 2nd level
1	13%	31%
2	2%	9%
3	0%	0%

## 4.5 Conclusions

The simple model that is normally used for concrete shear walls is bi-linear (elastic–plastic) in bending and linear until brittle failure in shear. If the strengths of the walls are proportional to the stiffness, i.e., proportional to the results from a linear analysis, this model predicts a simple response where the shear forces in all walls increase proportionally until all walls yield at the same displacement. The actual bending moment – curvature response of a concrete shear wall is close to tri-linear (Adebar and Ibrahim 2002), due to the significant reduction in flexural rigidity that occurs after flexural cracking. When this is accounted for, the shear distribution in concrete shear walls becomes much more complicated (see Fig. 4.5).

The shear force distribution changes significantly as the walls crack at various levels. As a result of this redistribution, the shear force will be higher in some walls and lower in other walls than predicted by a linear analysis. This higher demand requires higher shear strength to avoid a shear failure. When diagonal cracks form in concrete shear walls, the shear rigidity reduces significantly. Gérin and Adebar (2004) have presented a simple tri-linear model to account for diagonal cracking in concrete shear walls. When this is accounted for, very significant changes occur to the shear force distribution.

The other very significant consequence of accounting for diagonal cracking is the change in the displacement at which the walls yield in flexure. This can best be seen by comparing the flexural results (right-hand side) of Figures 4.5 and 4.6. When the shear deformations due to diagonal cracking are ignored, the predicted yield displacements of wall *W1* and *W2* are 0.39 m and 0.44 m, respectively. When the additional shear deformations are included, the yield displacement of wall *W1* (longer wall) increases to 0.43 m, while the yield displacement of wall *W2* actually reduces to 0.35 m. The reason is the longer wall (*W1*) has much more shear deformation than wall *W2* near the base of the structure, and therefore significant shear is transferred to wall *W2* locally at the base of the wall. These high shear forces near the base (as opposed to shear applied near the top of the wall) cause the wall to yield at a smaller displacement.

The important observation that accounting for shear deformations from diagonal cracking results in a shorter length wall yielding prior to a longer wall (both walls have the same height) was subsequently confirmed by Bohl and Adebar (2007) using nonlinear finite element analysis of cantilever concrete shear walls.

The fact that a shorter length wall yields prior to a longer wall is very significant as it has been suggested by others (e.g., Paulay 2001) that cantilever shear walls can be designed by assuming the yield displacement is proportional to wall length. Adebar et al. (2005) have demonstrated that when high-rise cantilever walls are tied together by rigid floor slabs at numerous levels, all walls yield at the same displacement (the system yield displacement) regardless of wall length. The results presented in this study demonstrate that when diagonal cracking is included in the analysis, all walls do not necessarily yield at the same displacement due to the differing shear deformations; however the results do reaffirm that the yield displacement of the walls is a system phenomenon and is not proportional to wall length.

It is common practice to increase the shear demand proportional to any flexural over-strength using the results from linear analysis. See for example Mitchell and Paultre (2006). The results from the nonlinear analysis summarized in Figures 4.9 and 4.10 suggest that this may be unconservative as the increase in shear demand can be larger than the increase in flexural capacity. According to the results obtained in this study more care and attention should be made to the walls having a shorter length used as a part of core shear wall systems.

Studying the simplified model of inter-connected walls through pushover analysis showed that the shear failure can occur at the second level rather than the commonly expected base level. This fact is caused by the redistribution of the shear forces when diagonal cracking effects are included in the wall's behaviour.

Based on the findings from the presented pilot study on the model of inter-connected high-rise walls, if RSA is used for seismic design of the walls, it is recommended that the horizontal reinforcement arranged for the base of the shorter walls be extended over the height (i.e. 25% of the lower height should be designed for the shear force demand at the base) so that the weaker wall at the lower levels above the base

maintains the required shear capacity to withstand extra shear demand caused by nonlinear interaction between the inter-connected walls of different lengths.

## **Dynamic shear demand in high-rise cantilever walls**

### **5.1 Overview**

In the previous chapters, a nonlinear shear model was used to investigate two important issues in the seismic design of high-rise walls. Chapter 3 investigated the nonlinear shear response of the core wall at below-ground levels of a high-rise building, whereas Chapter 4 investigated the nonlinear force distribution between inter-connected shear walls above the base level. In both of the previous chapters the simplified nonlinear model was used in terms of tri-linear shear stress-shear strain envelope to study the seismic response of concrete walls. In the present chapter a more sophisticated hysteretic shear model is used to study the seismic shear demand in high-rise cantilever walls.

Dynamic shear demand in a high-rise shear wall building during earthquake is greatly dependent on the nonlinear behaviour of the core wall. Previous studies indicated that while yielding of longitudinal reinforcement at the plastic hinge zone limits the flexural demand it does not limit the seismic shear demand at the base of wall. The amount of increase in shear force at the plastic hinge is a nonlinear phenomenon which can not be predicted by any of the linear analysis procedures. In order to account for this in design practice, designers often use amplification factors to estimate the seismic shear demand when linear analysis is used. Some building codes (i.e., *NZS3101* 1982-1995)

suggest using certain amplification factors to account for the increase in the seismic shear demand obtained from simplified pseudo-static procedures.

In order to study the seismic behaviour of a reinforced concrete wall, both nonlinear flexural response and nonlinear shear response must be considered in the analytical model. An appropriate nonlinear shear model for the concrete walls however has not been available for many years and hence previous studies on nonlinear behaviour of concrete walls were limited to nonlinear flexural behaviour neglecting any nonlinearity due to shear cracking in concrete and yielding of horizontal reinforcement.

The focus of this Chapter is to use nonlinear shear behaviour proposed by Gérin and Adebar (2004) to investigate the seismic shear demand in high-rise concrete walls.

## 5.2 Model of high-rise wall in this study

A cantilever model of a 30-storey core wall similar to the flanged wall example described in Chapter 4 was used for analyses. Parameters used for the modeling were chosen according to realistic examples of core walls built in high-rise buildings. Figure 5.1 shows the cross section of the wall which is uniform over a total height of 81.0 m. The wall has an I-shape section with a web length of 9.0 m, a flange length of 9.0 m and a uniform thickness of 0.75 m. The concrete compressive strength is assumed  $f'_c = 60$  MPa. A linearly varying axial compression is acting on the wall over its height with an axial compression increasing from zero at the top section to a typical level of compression at the base of high-rise core walls equal to  $n = 0.1 f'_c$ .

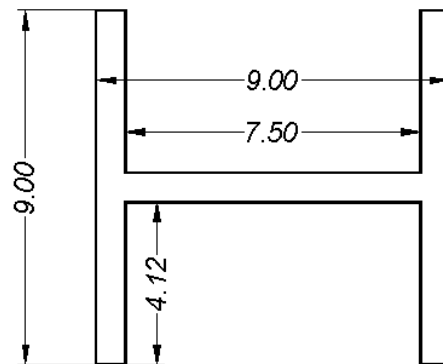


Figure 5.1 Section of the core wall used in dynamic analysis.

Flexural strength of the wall is controlled by arrangement and quantity of longitudinal reinforcement at the web and flange area. To represent wall's behaviour, beam-column frame elements were used in the finite element to include deformations associated with bending and shear at every section of the core wall. Nonlinear models for flexural and shear behaviour used in the NTHA of the high-rise cantilever wall will be discussed later in this chapter. P-Delta effects were also considered in all the dynamic analysis cases in this study to account for geometrical nonlinearity.

### **5.3 Ground motions used for dynamic analysis**

In order to perform nonlinear time history analysis a set of ten recorded acceleration history were chosen as the final selection of records from two likely seismic sources at West Coast known as Crustal and Subduction earthquakes. The crustal records suite consists of 20 ground motions recorded on National Earthquake Hazard Reduction Program (NEHRP) for site class C. Information regarding characteristics of these records is presented in Table 5.1. From the complete suite of 20 records, 7 earthquake events recorded in California with magnitudes ranging from 6.0 to 7.5 were considered for analysis. The procedure for selection of 7 crustal records will be discussed next in the ground motion scaling section.



Table 5.1 Set of recorded earthquakes used in *FEMA-440 (ATC-2005)* for site class C.

EQ.	year	Earthquake Name	Ms	Station Name	Distance (km)	PGA (cm/s <sup>2</sup> )	PGV (cm/s)	PGD (cm)
1	1979	Imperial Valley	6.8	El Centro, Parachute Test Facility	14.2	200.2	20	7.8
2	1971	San Fernando	6.5	Pasadena, CIT Athenaeum	31.7	107.9	14.7	6.6
3	1971	San Fernando	6.5	Pearblossom Pump	38.9	133.4	4.8	1.4
4	1992	Landers	7.5	Yermo, Fire Station	23.2	240.3	57.5	37.5
5	1989	Loma Prieta	7.1	APEEL 7, Pulgas	47.7	153	18.9	6.9
6	1989	Loma Prieta	7.1	Gilroy #6, San Ysidro Microwave site	19.4	166.9	14.9	2.9
7	1989	Loma Prieta	7.1	Saratoga, Aloha Ave.	13	494.5	50.3	14.9
8	1989	Loma Prieta	7.1	Gilroy, Gavilon college Phys Sch Bldg	11.6	349.1	21	5.5
9	1989	Loma Prieta	7.1	Santa Cruz, UCSC	17.9	433.1	20.6	6.7
10	1989	Loma Prieta	7.1	San Francisco, Dimond Heights	77	110.8	11.6	3.8
11	1989	Loma Prieta	7.1	Freemont Mission San Jose	43	121.6	12.1	4.8
12	1989	Loma Prieta	7.1	Monterey, City Hall	44.8	71.4	3.7	1.1
13	1989	Loma Prieta	7.1	Yerba Buena Island	80.6	66.5	8.5	2.8
14	1989	Loma Prieta	7.1	Anderson Dam (downstream)	21.4	239.4	20.4	6.8
15	1984	Morgan Hill	6.1	Gilroy Gavilon college Phys Scl Bldg	16.2	95	2.7	0.6
16	1984	Morgan Hill	6.1	Gilroy #6, San Ysidro Microwave Site	11.8	280.4	33.4	5.1
17	1986	Palm Springs	6	Fun Valley	15.8	126.5	7.9	1
18	1994	Northridge	6.8	Little Rock, Brainard Canyon	46.9	70.6	6.7	1.3
19	1994	Northridge	6.8	Castaic Old Ridge Route	22.6	557.2	43.1	8
20	1994	Northridge	6.8	Lake Hughes #1, Fire station #78	36.3	84.9	10.3	3.3

The peak ground acceleration for the complete set of crustal records range from 84.9 cm/s<sup>2</sup> to 557 cm/s<sup>2</sup>. These ground motions are the same records used in the calibration of the displacement modification procedure included within *FEMA-440 (ATC-2005)* for the site class C. The seismic hazard associated with the Cascadia subduction zone has been addressed by Geological Survey of Canada. Therefore it is essential to include the effect of Subduction zone in studying the dynamic behaviour of high-rise shear walls. Since records from previous seismic activities in Canadian West Coast are not available, recorded data from the 2003 Tokachi-Oki earthquake event was used in this study. The Tokachi-Oki earthquake occurred near the island of Hokkaido in Northern Japan having a moment magnitude of 8.0. This earthquake is very close in magnitude to what is expected from the Cascadia subduction zone. There were 48 records available

within 150 km of the epicenter from the Kyoshin Network (K-Net) and the Kiban-Kyoshin Network (Kik-Net) from which a suite of ten records for subduction earthquake on site class C were selected. Information regarding these records is given in Table 5.2.

Table 5.2 Selected subduction records from Tokachi-Oki earthquake.

Number	Station Name	Component	Station Code	Distance (km)	PGA (cm/s <sup>2</sup> )	PGV (cm/s)	PGD (cm)	NEHRP Site Class
1	OBIHIRO, K-Net	E-W	HKD095	146.00	190.60	36.10	19.40	C
2	OBIHIRO, K-Net	N-S	HKD096	146.00	148.40	37.10	27.20	C
3	NAKASATSUNAI, K-Net	E-W	HKD096	128.00	199.00	33.90	16.00	C
4	NAKASATSUNAI, K-Net	N-S	HKD097	128.00	176.90	24.20	10.50	C
5	SAMANI, Kik-Net	E-W	HDKH07	104.00	197.00	39.70	20.30	C
6	SAMANI, Kik-Net	N-S	HDKH08	104.00	169.50	27.20	15.10	C
7	TAIKI, K-Net	E-W	HKD098	103.00	345.50	91.40	31.50	C
8	TAIKI, K-Net	N-S	HKD099	104.00	365.30	75.30	38.70	C
9	MEGURO, K-Net	E-W	HKD113	74.00	205.10	16.10	5.80	C
10	MEGURO, K-Net	N-S	HKD114	75.00	156.20	13.50	7.70	C

The epicentral distance of these events ranges from 74 km to 146 km. Major urban areas including Victoria, Vancouver, Seattle, and Portland fall within or just outside this distance range from the Cascadia subduction zone. Significant damage has been observed within or beyond this distance range for previous subduction earthquakes (2004 Sumatra, 1985 Mexico, 1964 Alaska, and 1960 Chile). While epicentral distance is not the ideal parameter for determining the distance from subduction sources, it provides a reasonable distance parameter which is easily obtained

### 5.3.1 Ground motion scaling

Since the selected ground motions maintain different levels of acceleration magnitude, scaling is done to bring the acceleration magnitudes to a target scaling level. Scaling is usually done by comparison between the spectrum corresponding to the unscaled ground motion and the target spectrum. Two different methods of spectrum scaling are widely used in practice: Spectrum Matching and the Single Scale Factor methods.

In the Spectrum Matching procedure, the initial recorded ground accelerations are modified so that their corresponding response spectrum for a SDOF matches perfectly with the specified target spectrum. In this procedure the frequency contents are changed as sine and cosine waves are added to the initial unscaled record. In other word the only way to have a perfectly matched spectrum is to modify the original properties of the earthquake record. Since by use of spectrum matching procedure the original characteristics of record are disturbed, there is a debate if this method is the appropriate way of scaling the earthquake records (Naeim and Lew 1994).

Scaling in the single scale factor method is done by a single scale factor applied on the whole record to scale it up or down to the desired level of target spectrum. The advantage of this method is that it does not influence the seismic characteristics of motion compared to Spectrum Matching procedure. The single scale factor method is often used to match a specific range of interest over the spectrum. The basis for this procedure is to scale the original spectrum so that it produces equal area under the range of interest compared with the area under the target design spectrum curve.

For the structures with dominating first mode of vibration, considering a shorter range of periods close to the fundamental period of vibration may be adequate for scaling. In the case of high-rise buildings, the influence of higher modes of vibration is very significant and therefore a wider range should be considered for scaling. Since a two-dimensional model of high-rise wall is considered in the present study, the effect of second mode is highly important in the seismic response. The range under consideration for scaling must include the first and second mode of vibration in the model, therefore a period range between  $0.2T_1$  and  $1.5T_1$  in which  $T_1$  is the fundamental period of vibration has been considered for scaling of records in this study. This range corresponds to a period range between 0.5 sec and 4.5 sec for the 30-storey model of wall with a fundamental period of  $T_1=3.0$  sec and the second mode period of  $T_2=0.57$  sec. It is desired to have a total number of 10 earthquake records for performing time history analysis. Among ten records seven are selected from crustal records and three are picked from the subduction category.

In order to select seven earthquakes from the complete set of records by *ATC* measured on site class C, all the spectra for 20 records given in Table 5.1 were scaled to

match the *NBCC-2005* Site class C design spectrum for Vancouver city within the specified period range mentioned above. Figure 5.2 shows the scaled spectra with thin solid lines, the *NBCC-2005* design spectrum with a thick solid line and the average scaled spectrum by a thick dashed line.

To choose the best three records from the subduction earthquakes all 10 records presented in Table 5.2 are scaled to match the *NBCC-2005* design spectrum for site class C. The scaled spectra for Subduction earthquakes and the corresponding *NBCC-2005* site class C design spectrum for Vancouver are shown in Fig. 5.3. It should be noted that the subduction records need also be scaled corresponding to a design spectrum which is specifically developed for these types of ground motions; such a design spectrum was not readily available at the time of this work and therefore same *NBCC-2005* design spectrum was also used for scaling of the subduction records.

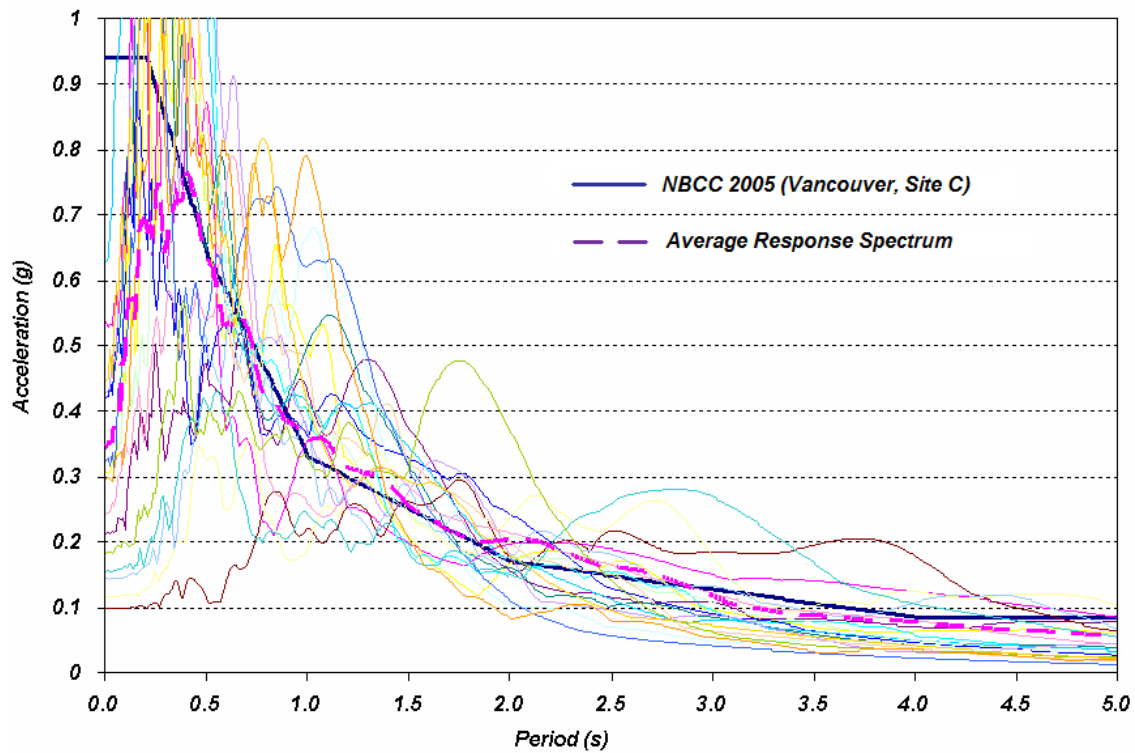


Figure 5.2 Scaled spectra within period range of 0.5 sec and 4.5 sec corresponding to crustal earthquakes given in Table 5.1.

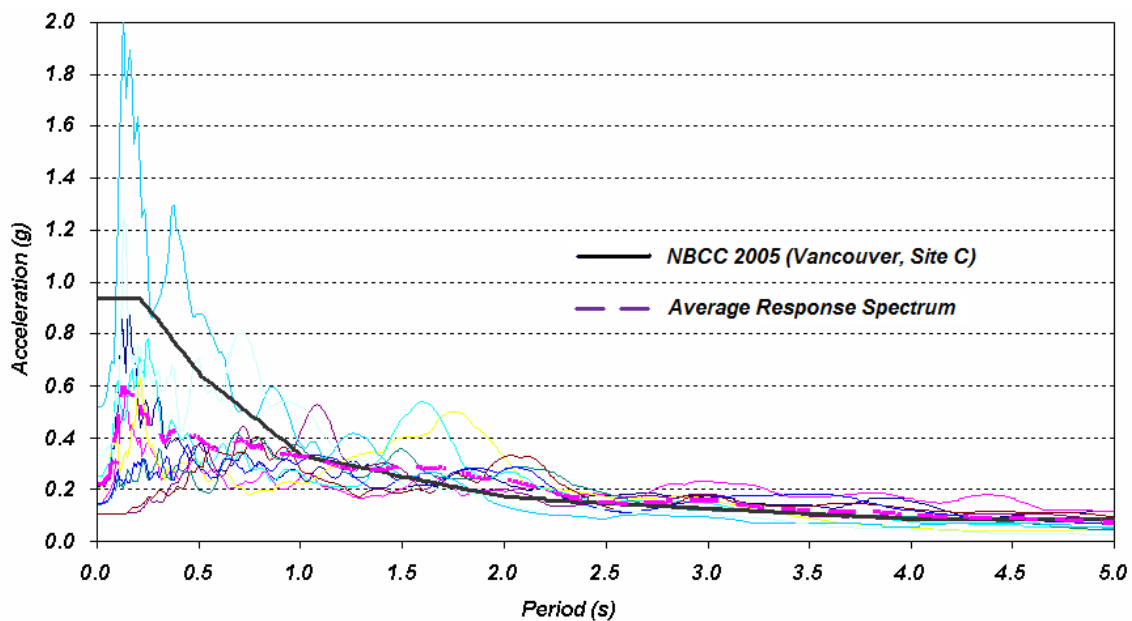


Figure 5.3 Scaled spectra within period range of 0.5 sec and 4.5 sec corresponding to subduction earthquakes given in Table 5.2.

### 5.3.2 Acceleration records used for analysis

Once all the spectra corresponding to each acceleration record were scaled to match the design spectrum, the best set of seven records from the crustal earthquakes and the best set of three records from subduction earthquakes were selected. The set for each category is selected based on the best fit obtained from the corresponding average scaled spectrum. The spectra for final selection of crustal and subduction motions are shown in Fig. 5.4.

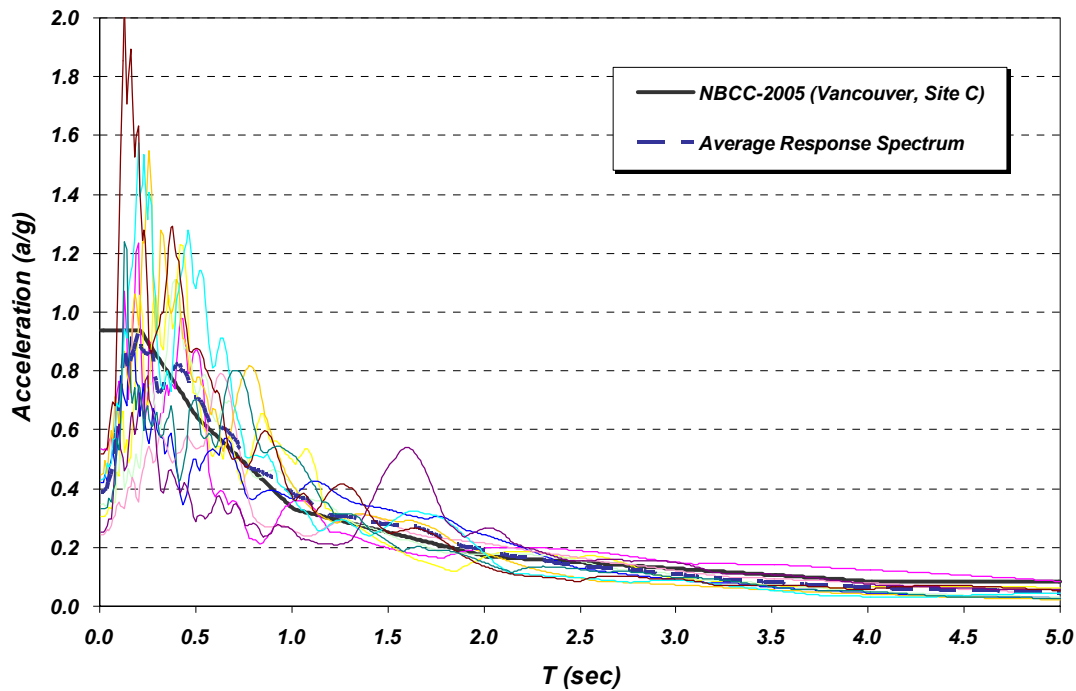


Figure 5.4 Scaled spectra within period range of 0.5 sec and 4.5 sec corresponding to selected earthquakes and their corresponding average spectrum.

The original set of ten selected records and the corresponding information is presented in Table 5.3. These records are scaled to match the target *NBCC-2005* for site class C design spectrum for Vancouver city over the range of 0.5 sec to 4.5 sec with the scaling values presented in Table 5.4.

Table 5.3 Final selection of records used for analysis.

<b>EQ ID</b>	<b>Earthquake Name</b>	<b>Category</b>	<b>(Ms)</b>	<b>Station Name</b>	<b>Comp. (deg)</b>	<b>Distance (km)</b>	<b>PGA (cm/s<sup>2</sup>)</b>	<b>PGV (cm/s)</b>	<b>PGD (cm)</b>
C-1	Imperial Valley	Crustal	6.8	El Centro, Parachute Test Facility	315	14.2	200.2	20	7.8
C-2	San Fernando	Crustal	6.5	Pasadena, CIT Athenaeum	90	31.7	107.9	14.7	6.6
C-3	Loma Prieta	Crustal	7.1	Saratoga, Aloha Ave.	0	13	494.5	50.3	14.9
C-4	Loma Prieta	Crustal	7.1	San Francisco, Dimond Heights	90	77	110.8	11.6	3.8
C-5	Loma Prieta	Crustal	7.1	Anderson Dam (downstream)	270	21.4	239.4	20.4	6.8
C-6	Loma Prieta	Crustal	7.1	Yerba Buena Island	90	80.6	66.5	8.5	2.8
C-7	Northridge	Crustal	6.8	Castaic Old Ridge Route	360	22.6	557.2	43.1	8
S-1	Tokachi-Okii	Subduction	8	NAKASATSUNAI, K-Net	NS	128	176.9	24.2	10.5
S-2	Tokachi-Okii	Subduction	8	MEGURO, K-Net	EW	74	205.1	16.1	5.8
S-3	Tokachi-Okii	Subduction	8	MEGURO, K-Net	NS	74	156.2	13.5	7.7

Table 5.4 Scaling factors used for final selection of records.

<b>C-1</b>	<b>C-2</b>	<b>C-3</b>	<b>C-4</b>	<b>C-5</b>	<b>C-6</b>	<b>C-7</b>	<b>S-1</b>	<b>S-2</b>	<b>S-3</b>
2.60	2.76	0.82	3.03	1.75	3.58	0.78	1.38	2.45	2.06

#### 5.4 Linear time history analysis (LTHA) vs. response spectrum analysis (RSA)

Results obtained from two different linear dynamic analyses are compared here. The 30-storey model of the wall as explained in Section 5.2 was used for performing linear response history and response spectrum analysis. 5% viscous damping was also included in the model of wall for linear time history analysis using Rayleigh damping for first and second mode of vibration. The scaled records described in Section 5.3 were used to perform linear dynamic analysis. Results from analyses were compared in terms of bending moment and shear force demand over the height of wall.

Figure 5.5 shows the results for bending moment demand over the wall's height. The thick solid line illustrates the moment distribution associated with the response spectrum analysis and the thick dashed line presents the envelope for the average bending

moment obtained from LTHA. The envelopes for each of individual ground motions are also shown by thin lines. Similar plots for shear force diagram over the height are shown on Fig. 5.6. According to bending moment and shear force obtained from LTHA, the averaged envelopes of both sets of ground motions are in good agreement with the results obtained from RSA.

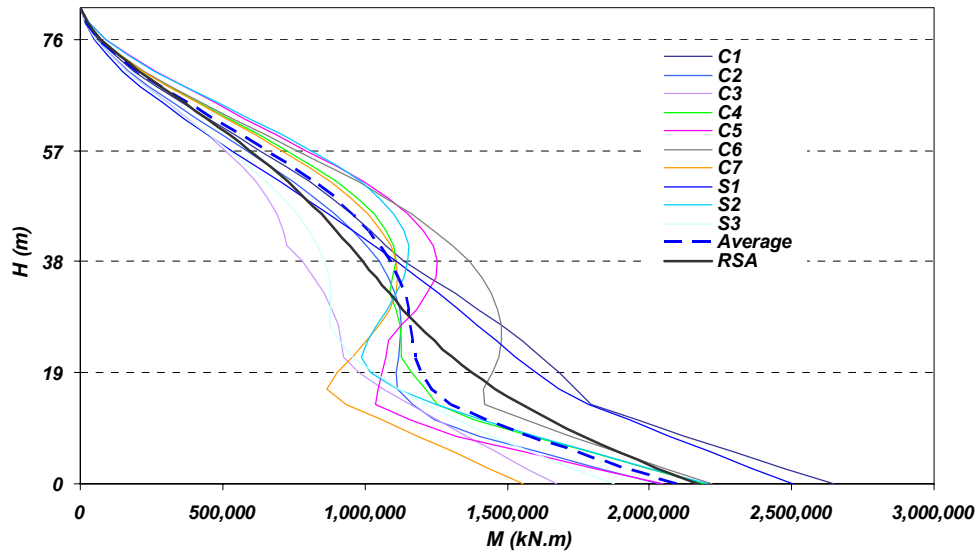


Figure 5.5 Bending moment envelopes obtained from LTHA and RSA.

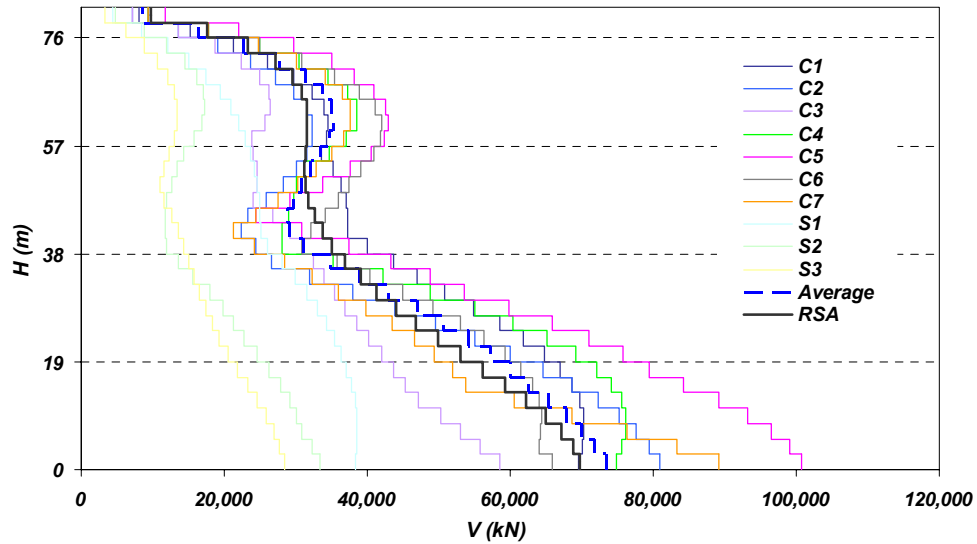


Figure 5.6 Shear force envelopes obtained from LTHA and RSA.



## 5.5 Nonlinear time history analysis

In order to perform nonlinear dynamic analysis on the model of high-rise concrete wall, program SAP-2000 (CSI 2006) was used to perform direct-integration time history analysis. A variety of common methods are available for performing direct-integration time history analysis. Hilber-Hughes-Taylor alpha (HHT) method was used to perform direct-integration time history analysis in this study. The HHT method uses a single parameter called alpha. This parameter may take values between 0 and  $-1/3$ . For  $\alpha = 0$ , the method is equivalent to the Newmark method (1959) with  $\gamma = 0.5$  and  $\beta = 0.25$ , which is the same as the average acceleration method (also called the trapezoidal rule.) Using  $\alpha = 0$  offers the highest accuracy but may permit excessive vibrations in the higher frequency modes, i.e., those modes with periods of the same order as or less than the time-step size. For negative values of alpha, the higher frequency modes are more severely damped. Different values of alpha and time-step size were examined in this study to ensure that the solution is not too dependent upon these parameters. Similar to any nonlinear analysis, iteration was used to make sure that equilibrium is achieved at each step of the analysis. A relative convergence tolerance that was used in the analysis controls the accuracy of analysis results by comparing the magnitude of force error with the magnitude of the force acting on the structure. For time history analyses, the relative convergence tolerance was set small enough so that the accuracy of output results is no longer influenced by this parameter.

Viscous damping was used for all time history analysis cases which was also referred to as effective damping. Rayleigh damping was used based on 5% critical damping ratio for the first and the second mode of vibration for the 2-D model of wall. Nonlinear elements that were used in the time-history analysis account for energy dissipation in the elements directly and correctly take into account the effects of modal cross-coupling.

Since direct integration results are extremely sensitive to time-step, this value was decreased for the same analysis until the step size was small enough that the results were no longer affected by it. The maximum value of the time-step that was used for nonlinear time history analysis was  $t=0.001$  sec for all analysis cases in the present study.

### 5.5.1 Model definition

Nonlinear “Link” element was used to model the nonlinearities associated with flexural and shear behaviour for the model of high-rise wall. This nonlinear element is fully described in SAP-2000 Reference Manual (2006).

A 3-D Link element is assumed to be composed of six separate “springs” one for each of six deformational degrees of freedom (axial, shear, torsion, and pure bending). Six independent internal deformations are defined for the 3-D Link element and are calculated from the relative displacements of joint  $j$  with respect to joint  $i$ .

A 2-D Link is composed of three internal “springs” or “hinges” one for each of three internal deformations. Figure 5.7 shows the 2-D Link element that was used in this study. Deformation of the shear spring can be caused by rotations as well as translations at the joints. The force in this spring will produce a linearly varying moment along the length. This moment is taken to be zero at the shear spring, which acts as a moment hinge. The moment due to shear is independent of and additive to the constant moment in the element due to the pure bending spring.

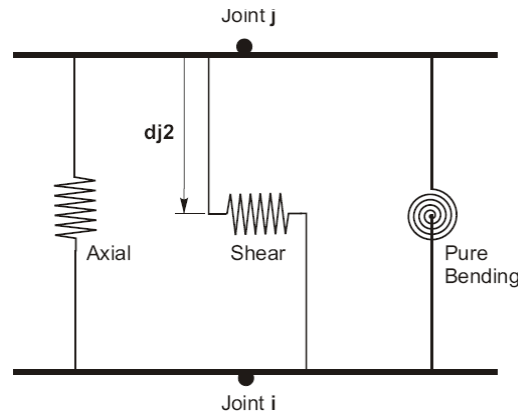


Figure 5.7 2-D Link element used in SAP-2000 (CSI 2006).

In dynamic analysis, the mass of the structure is used to compute inertial forces. The mass contributed by the Link element is lumped at the joints  $i$  and  $j$ . Nonlinear force-deformation relationships were assigned to all the link elements to simulate the nonlinear

behaviour corresponding to flexure and shear. The linear effective stiffness was used for the members that remain elastic during analysis.

### **5.5.2 Hysteretic models**

In order to simulate the hysteretic response in the Link element, two different models were used: one to model the hysteretic flexural response and one to model the hysteretic shear response.

The hysteretic behaviour considered for the flexural hinge in this study was the Multi-Linear Takeda model (1970) which was described in Section 3.3.2. In order to simulate hysteretic shear response in the model of concrete wall in the present work, the Multi-Linear Pivot model was used. The Multi-Linear Pivot hysteretic model is similar to the Multi-Linear Takeda model, but has additional parameters to control the degrading hysteretic loop. It is particularly well suited for reinforced concrete members, and is based on the observation that unloading and reverse loading tend to be directed toward specific points, called pivot points, in the force-deformation (or moment-rotation) plane. This model is fully described in Dowell, Seible and Wilson (1998).

## **5.6 Influence of flexural strength distribution over the height**

Section response analysis was used to determine nonlinear stress-strain relationship for flexure of reinforced concrete section. Program “Response-2000” was used to determine the nonlinear flexural behaviour in terms of moment-curvature response. Shear response for the wall was assumed to be elastic for this case.

A typical example of core wall section provided in high-rise buildings was considered for performing NTHA. Vertical reinforcement amount changes linearly at different height intervals. Wall section is kept uniform over the height and the amount of vertical reinforcement controls the flexural strength of wall in various heights. Wall section has a 2.5% vertical reinforcement ratio in flange area and a 0.5% vertical reinforcement ratio at the web area at its base. The vertical reinforcement amount was reduced linearly every seven stories over the height reaching the minimum reinforcement

amount allowed by the code (CSA 23.3) equal to 0.5% at the top section. Four different sections with different reinforcement ratios were considered for the model of core wall in this study as shown in Fig. 5.9. For modeling the nonlinear flexural behaviour of wall, the tri-linear moment-curvature backbone was used as shown in Fig. 5.8 which includes the cracking of concrete and yielding of vertical reinforcement for the reinforced concrete section. These limits are also shown over different heights of wall in Fig. 5.9.

It should be noted that the model for flexural strength of the wall shown on Fig. 5.9 corresponds to an example of vertical reinforcement that is typically used in some of existing core wall buildings in Vancouver, Canada but does not cover a complete range of designed walls in practice.

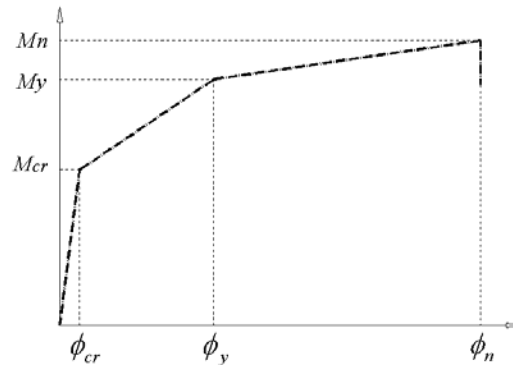


Figure 5.8 Moment-curvature backbone used for hysteretic flexural response.

Table 5.5 Parameters used to define tri-linear moment-curvature response.

	State	$M$ (kNm)	$\phi$ (rad/km)
Section 4 (Levels 22-30)	Cracking	178,880	0.022
	Yielding	250,310	0.044
	Ultimate	325,740	5.720
Section 3 (Levels 15-21)	Cracking	288,500	0.044
	Yielding	499,400	0.109
	Ultimate	635,860	5.630
Section 2 (Levels 8-14)	Cracking	367,700	0.044
	Yielding	742,480	0.127
	Ultimate	940,630	5.610
Section 1 (Levels 1-7)	Cracking	456,240	0.056
	Yielding	986,080	0.173
	Ultimate	1,236,120	5.560

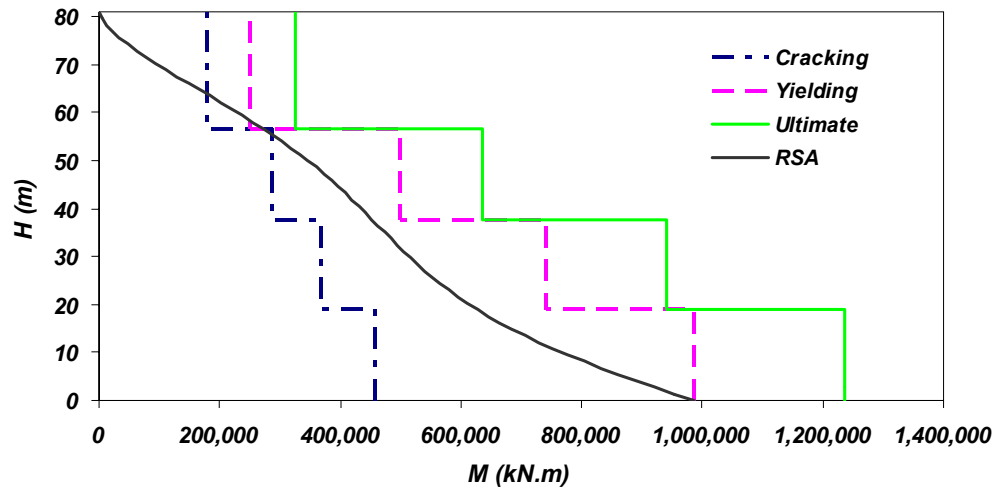


Figure 5.9 Flexural limits over the height in the high-rise wall model.

In reality the flexural strength envelope is sloped between different sections. In order to simplify the model of wall, the flexural strength is assumed to be constant over each section as shown in Fig. 5.9. In order to improve the analysis and prevent problems such as instability due to local failure, the moment-curvature response maintained its strength beyond ultimate flexural failure point following the post-yielding strain hardening slope. The ultimate curvature capacity increases with elevation and for the model of wall ranged between 5.6 (Rad/km) for lower sections to 6.0 (Rad/km) in upper sections.

In studying the nonlinear behaviour of concrete walls, it is generally assumed that the nonlinear behaviour caused by yielding of longitudinal reinforcement occurs at the plastic hinge zone near the base of wall. In low-rise buildings where seismic response is significantly affected by the first mode response, bending moment diagram increases consistently over the height from top level to its peak at the base of wall. In this case it is not unrealistic to limit the nonlinear flexural behaviour to the base of wall.

In high-rise concrete walls, the influence of higher modes of vibration becomes very significant. Large bending moment is developed at mid-height of the wall caused by the effect of higher modes. This shows that in high-rise walls, the nonlinear flexural behaviour takes place in various heights and one cannot assume that the nonlinear action occurs only at the base of wall.

Another important issue which must be accounted for in studying the nonlinear response of concrete walls is the quantity and distribution of reinforcement over the wall's height. Most of high-rise concrete walls are designed by using the response spectrum analysis (RSA). Use of a smooth design spectrum suggested by the codes would lead to a linearly increasing bending moment diagram over the wall's height. According to the flexural demand obtained through use of response spectrum analysis, the flexural strength provided by the reinforcement should change linearly from top to the base of wall. In practice the reduction in strength takes place not for every single storey but rather for a number of stories over the wall's height. In order to compare the results obtained from different analysis assumptions, nonlinear dynamic analysis was performed for two different cases.

First case which is referred to as "Case SH" is the case where wall is allowed to yield due to bending at the plastic hinge zone defined at the base as explained in Section 3.3.2. This model presents the commonly assumed nonlinear model for high-rise walls. The length of hinge zone is controlled by the number of nonlinear Link elements considered over a specific height of wall. The flexural hinge length can be extended up to 150% of the wall's length. The rest of wall above plastic hinge was modeled elastic and therefore no nonlinear behaviour was captured by the wall sections above the plastic hinge zone. Nonlinear elements used in the model of wall were spread over a length equal to 18.9 m (7 stories) above the base to ensure sufficient length for plastic hinge has been considered. The nonlinear flexural model in the plastic hinge zone is described as "Section 1" in Table 5.5.

The second case for nonlinear dynamic analysis referred to as "Case MH" considers a more appropriate flexural behaviour compared to Case SH. In this case nonlinear elements are considered over the wall's height according to the specified flexural strength of wall sections at different levels. The flexural strength increases from top of the wall reaching its maximum at the base. Four different sections are defined according to the information given in Table 5.5 for Sections 1-4 which is also shown on Fig. 5.9. Unlike Case SH, wall is not restricted to undergo nonlinear behaviour only at its base in the Case MH. In this case there is no restriction on the length and location at which the nonlinear flexural action occurs over the wall's entire height. Due to the effect

of higher modes and specially the second mode in the simplified 2-D model, the wall is expected to develop large bending moment demand at the regions close to mid-height.

Time history analysis was done for a 30-storey wall having a fundamental period of  $T_f=3.0$  sec. Time step used in the analysis was 0.001 sec and Takeda model (1970) was used to simulate the hysteretic flexural behaviour.

Nonlinear time history analyses were performed for  $R=2.0$ ,  $R=3.5$  and  $R=5.0$ . Figure 5.9 through Fig. 5.16 show the envelope results for bending moment and shear force demand over the wall's height for two cases of  $R=2.0$  and  $R=5.0$  to consider a lower and upper bound for this factor. As examples, the recommended  $R$  factors by Canadian code (*NBCC-2005*) for moderate ductile and ductile shear walls are  $R=2.0$  and  $R=3.5$  (i.e.  $R_d$ ).

As explained, the results were compared for two different cases of nonlinear flexural behaviour in the wall which are called "Case SH" and "Case MH". SH stands for single hinge at the base of wall and MH stands for multiple hinges over the wall's height. Figure 5.10 and Fig. 5.11 show the bending moment envelopes for seven crustal earthquakes ( $R=2.0$ ) for Case SH and Case MH respectively. The length of plastic hinge zone for Case SH covers a height between base and 18.9 m shown on these plots. In Fig. 5.10, the bending moment is limited to the flexural yielding limit at the base only and therefore the flexural demand has increased above the plastic hinge significantly. Figure 5.11 shows the similar moment envelope results for Case MH where the nonlinear flexural response is not limited to a specific zone at the base of wall. Wall yielded in flexure at four different zones according to specified flexural strength over the height.

To observe how the shear force demand was influenced by different flexural responses in Case SH and Case MH, see Fig. 5.12 and Fig. 5.13 respectively. As illustrated in these figures, the shear force demand is generally larger in Case SH when compared with values obtained for Case MH. The amount of increase in shear demand for Case SH is specially noticeable at the base and also upper quarter length of wall close to the top. As shown in Fig. 5.13, the shear force demand at upper levels is limited by influence of flexural yielding over the wall's height. This is a very significant result. A moderate increase in seismic shear force demand was observed for  $R=2.0$  as shown in the first set of figures from Fig. 5.10 through Fig. 5.13. The second set of figures show the

result for a more severe case of  $R=5.0$ . Figure 5.14 through Fig. 5.17 present results of NTHA for  $R=5.0$ .

Figure 5.14 shows the envelope of bending moment results for Case SH. As shown, seismic bending moment demand at mid-height of the wall is larger than the demand at the base of wall. The large value at mid-height is an effect of assuming an elastic behaviour for the high-rise wall above the plastic hinge at the base. A more appropriate flexural behaviour captured by Case MH is shown in Fig. 5.15 where wall yields at four different regions over its height. Corresponding shear force diagrams are shown in Fig. 5.16 and Fig. 5.17. Again the shear force demand obtained at the base and upper levels close to top of wall are significantly larger for Case SH shown in Fig. 5.16 compared with Case MH shown in Fig. 5.17.



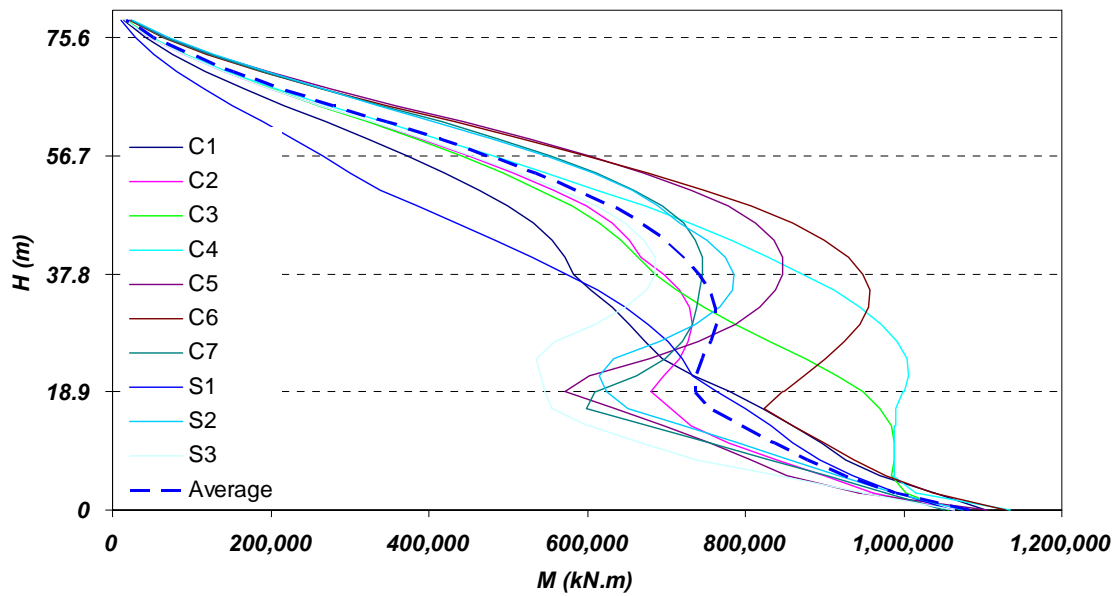


Figure 5.10 Envelopes for bending moment over the height (Case SH-R=2.0).

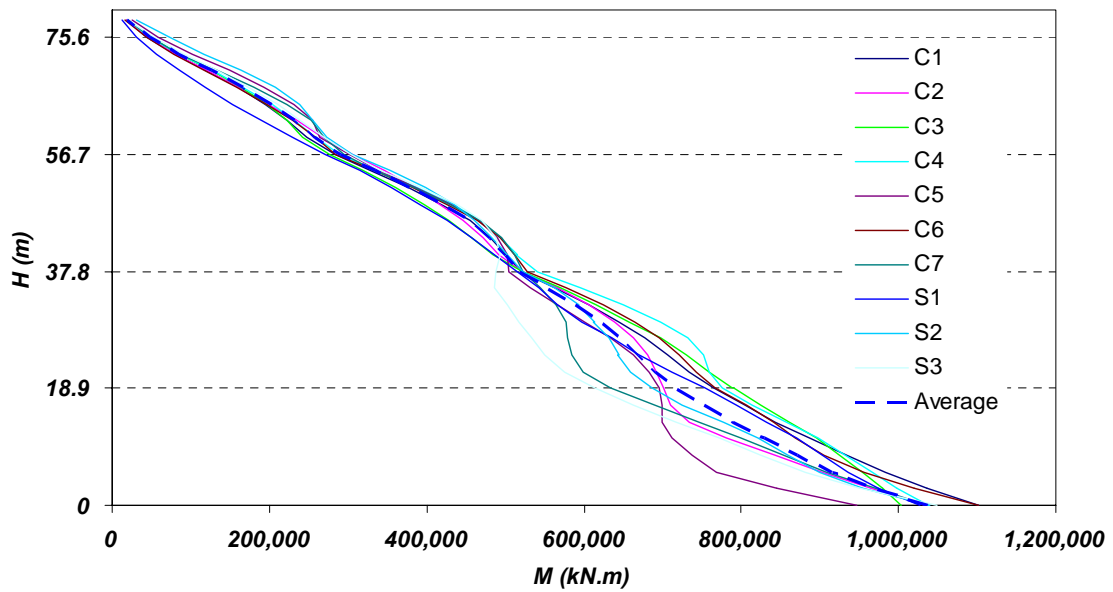


Figure 5.11 Envelopes for bending moment over the height (Case MH-R=2.0).

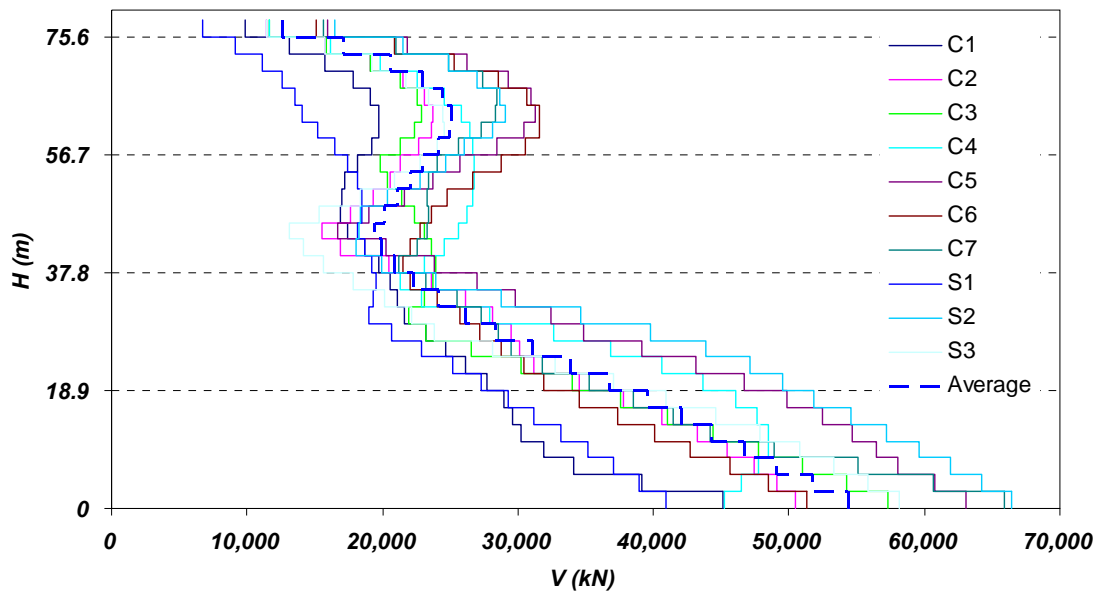


Figure 5.12 Envelopes for shear force over the height (Case SH-R=2.0).

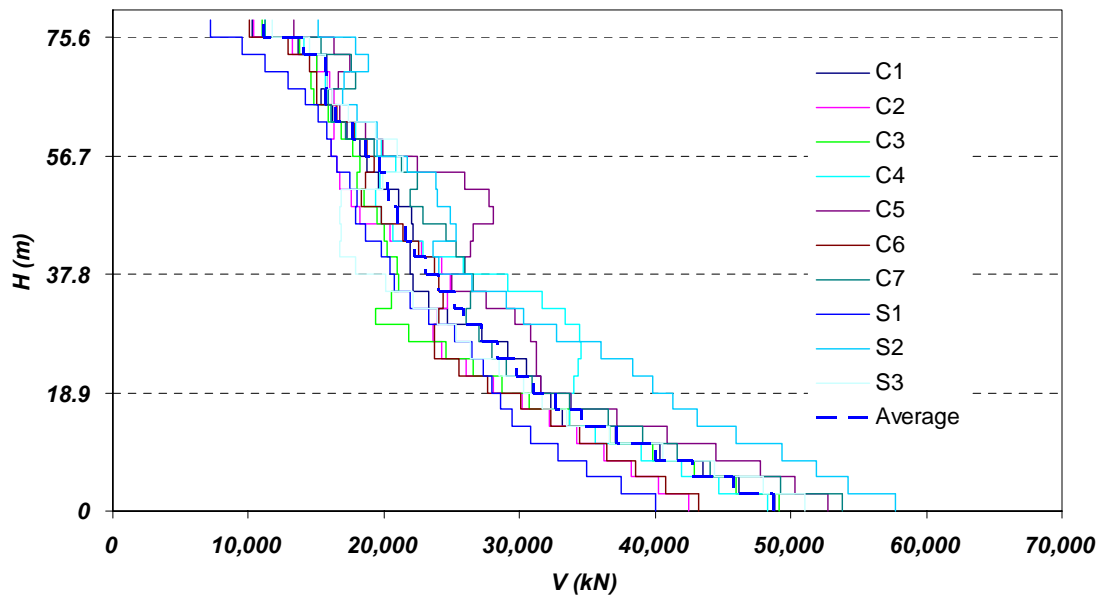


Figure 5.13 Envelopes for shear force over the height (Case MH-R=2.0).

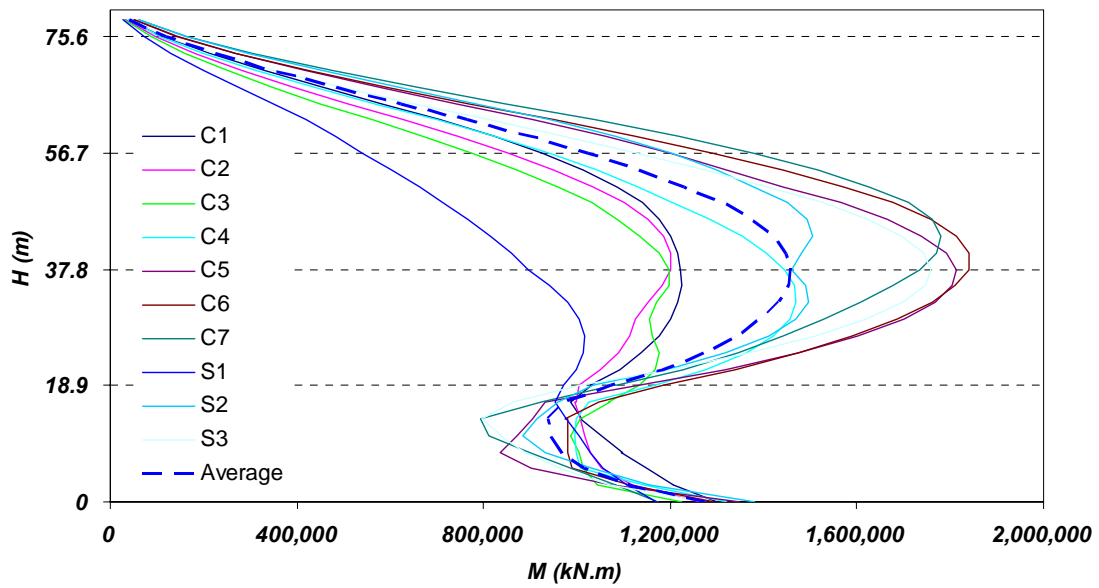


Figure 5.14 Envelopes for bending moment over the height (Case SH- $R=5.0$ ).

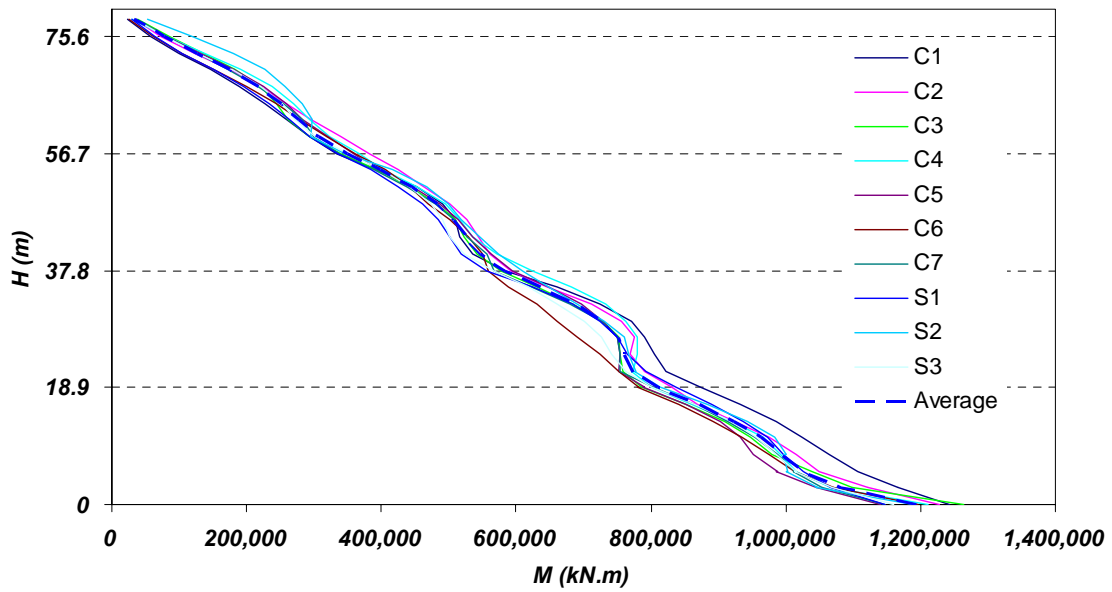


Figure 5.15 Envelopes for bending moment over the height (Case MH- $R=5.0$ ).

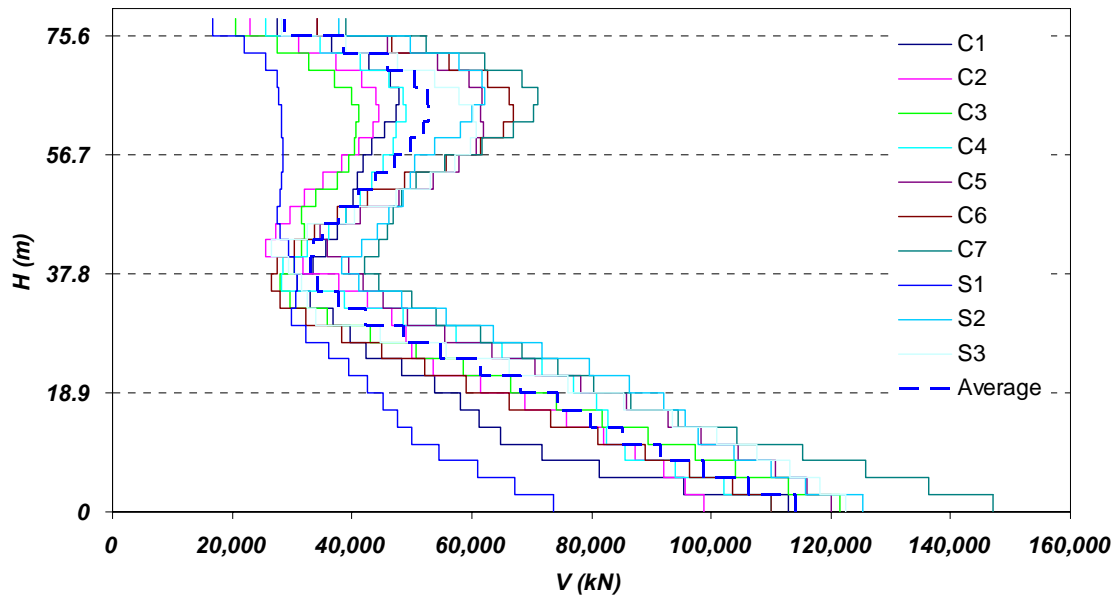


Figure 5.16 Envelopes for shear force over the height (Case SH-R=5.0).

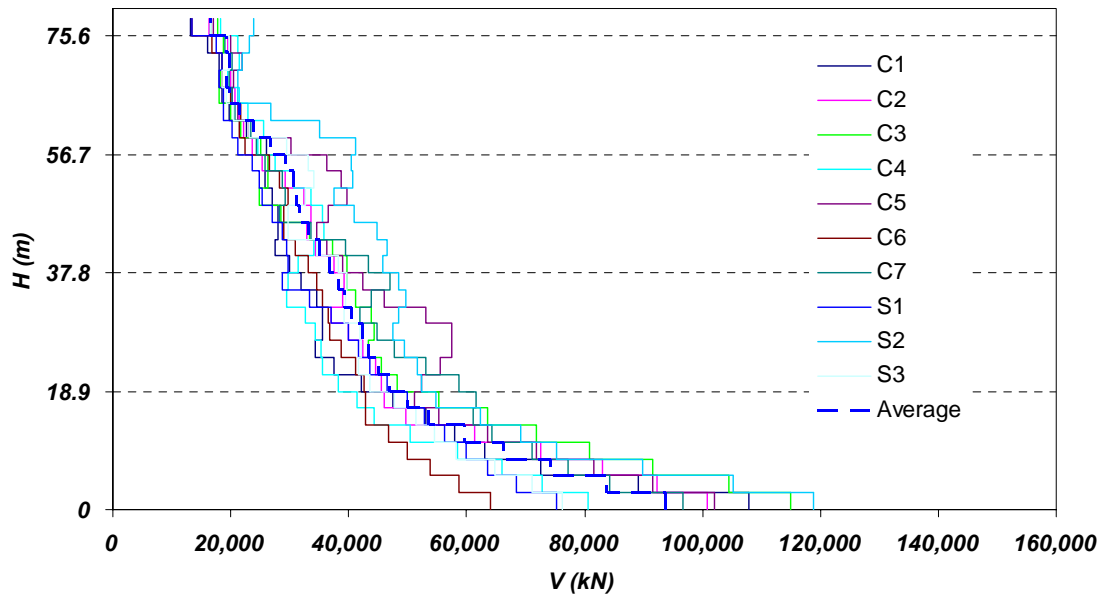


Figure 5.17 Envelopes for shear force over the height (Case MH-R=5.0).

Yielding in flexure which limits the bending moment demand at the plastic hinge zone increases the curvature demand correspondingly. The amount of increase in the curvature demand is proportional to the slope of the post yielding line in the moment-curvature response. Since curvature demand is a very important parameter, the plots for curvature over the wall height are given in Fig. 5.18 and Fig. 5.19. The curvature demand is largest at the section close to the top which is caused by definition of flexural yielding limit as shown in Fig. 5.9.

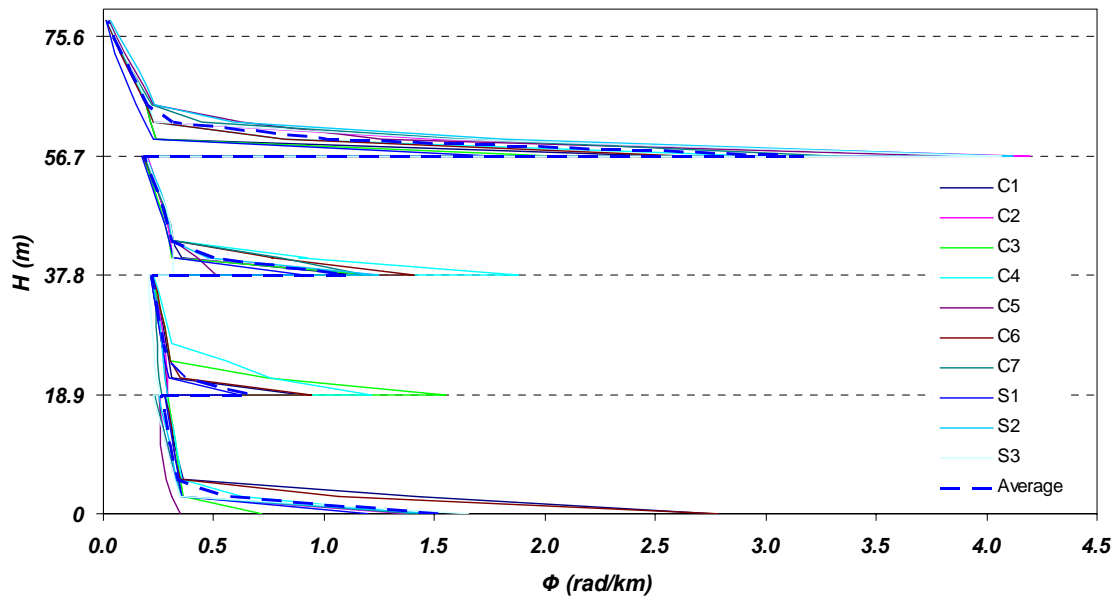


Figure 5.18 Envelopes for curvature demand over the height (Case MH-R=2.0).

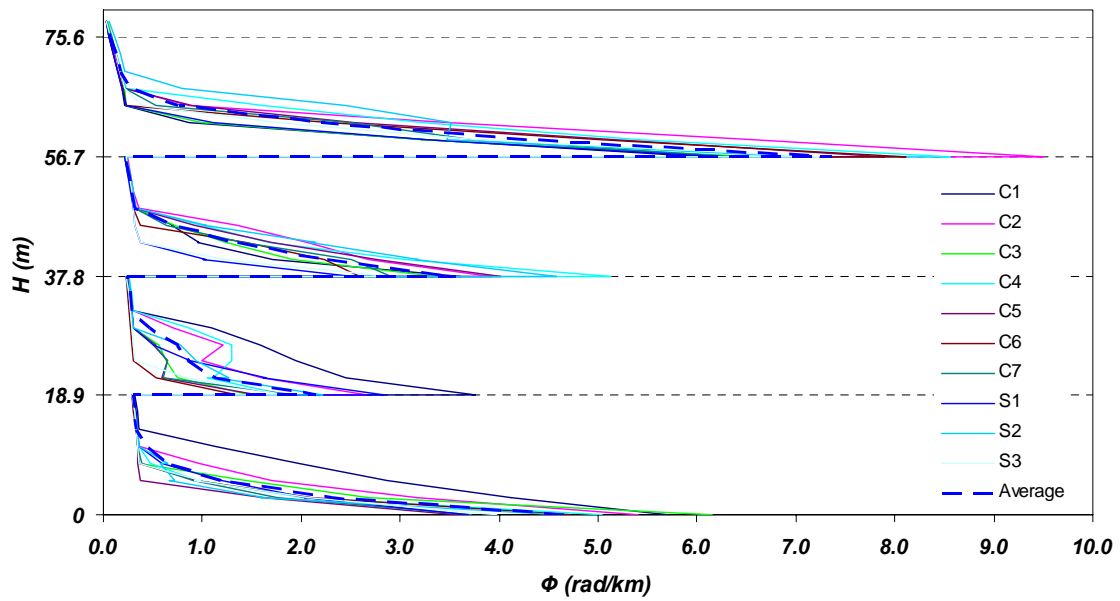


Figure 5.19 Envelopes for curvature demand over the height (Case MH-R=5.0).

Summary of shear force envelopes for two cases of analysis and three different values of  $R$  factor are given in Table 5.6. Maximum shear force demands are presented at two critical locations over the wall's height. "Base" in this table corresponds to the region of plastic hinge at the base of wall and "Top" in the table corresponds to region between El. 56.7 m and El. 75.6 m (Section 4) as described in Section 5.6. By comparison of values in Table 5.6, it was observed that shear force values for Case SH is generally larger than the corresponding values obtained for Case MH.

Table 5.7 provides a summary of the results in terms of the amount of increase in shear force demand in Case SH with respect to the results obtained from Case MH. According to the table, the amount of increase in shear force at the base for different  $R$  factors ranged between 12% and 25% while this amount at upper levels ranged between 36% and 102%.

Table 5.6 Shear demand obtained from nonlinear dynamic analysis (values in kN).

$R$	Case	Loc.	C-1	C-2	C-3	C-4	C-5	C-6	C-7	S-1	S-2	S-3
2.0	1 (SH)	Top	19,727	23,742	22,867	26,683	31,304	31,613	28,447	16,444	29,044	24,600
		Base	45,115	50,499	57,344	48,492	63,083	51,282	65,954	40,967	66,448	58,165
	2 (MH)	Top	18,221	16,429	17,705	19,759	19,933	18,748	19,269	16,073	19,526	20,938
		Base	48,809	42,467	49,134	48,297	52,711	43,155	53,820	40,016	57,767	51,002
3.5	1 (SH)	Top	34,191	33,050	32,012	36,721	45,431	52,926	50,521	23,262	45,511	42,451
		Base	81,683	74,808	89,632	82,882	92,348	81,646	110,401	58,247	101,521	92,163
	2 (MH)	Top	24,359	20,359	20,649	23,330	22,696	20,776	27,104	18,648	26,255	22,742
		Base	84,568	79,713	79,033	66,635	72,483	56,198	71,348	66,090	85,100	73,641
5.0	1 (SH)	Top	47,919	44,464	41,044	48,927	62,062	67,081	70,948	28,489	62,219	60,817
		Base	112,929	98,861	121,567	110,012	119,970	109,968	147,177	73,593	125,246	122,341
	2 (MH)	Top	26,062	23,645	25,060	25,462	30,312	22,385	24,244	21,217	41,048	29,363
		Base	107,937	100,905	114,938	80,613	102,004	64,051	96,780	75,234	118,747	76,276

Table 5.7 Amount of shear demand increase in Case SH with respect to Case MH.

<i>R</i>	<i>Location</i>	<i>C-1</i>	<i>C-2</i>	<i>C-3</i>	<i>C-4</i>	<i>C-5</i>	<i>C-6</i>	<i>C-7</i>	<i>S-1</i>	<i>S-2</i>	<i>S-3</i>	<i>Mean</i>
2.0	Top	1.08	1.45	1.29	1.35	1.57	1.69	1.48	1.02	1.49	1.17	1.36
	Base	0.92	1.19	1.17	1.00	1.20	1.19	1.23	1.02	1.15	1.14	1.12
3.5	Top	1.40	1.62	1.55	1.57	2.00	2.55	1.86	1.25	1.73	1.87	1.74
	Base	0.97	0.94	1.13	1.24	1.27	1.45	1.55	0.88	1.19	1.25	1.19
5.0	Top	1.84	1.88	1.64	1.92	2.05	3.00	2.93	1.34	1.52	2.07	2.02
	Base	1.05	0.98	1.06	1.36	1.18	1.72	1.52	0.98	1.05	1.60	1.25

The dynamic shear amplification factors obtained from NTHA are given in the Table 5.8. The results for two cases of different flexural strength over the wall height are compared at two different critical locations over the wall's height. Amplification factors provided in the Table present the ratio between shear forces obtained from NTHA to shear forces obtained from RSA using *NBCC-2005* design spectrum for Vancouver, site class C. Dynamic amplification factor was larger in Case SH compared with Case MH. Case SH indicates dynamic shear amplification factors ranging from 1.48 to 3.09 for the base section and amplification factors ranging from 1.53 to 3.21 for the top section. The corresponding amplification factors for Case MH were observed to range from 1.32 to 2.53 at the base and from 1.12 to 1.61 at top section.

Table 5.8 Dynamic shear amplification for nonlinear response history analysis vs. RSA.

<i>R</i>	Case	At base section	At top section
2.0	1 (SH)	1.48	1.53
	2 (MH)	1.32	1.12
3.5	1 (SH)	2.34	2.38
	2 (MH)	1.99	1.36
5.0	1 (SH)	3.09	3.21
	2 (MH)	2.53	1.61



This study showed that including the effect of flexural yielding over the entire height of wall would result in reduction of seismic shear force demand. Based on findings of this section, use of FE models of high-rise wall where the plastic hinge is only considered at the base can lead to overestimation of shear force demand at the base and the top levels of the wall.

### 5.7 Influence of effective shear stiffness due to diagonal cracking

One simple approach to consider the influence of nonlinear shear behaviour associated with cracking of reinforced concrete section is to use the effective shear stiffness. Effective shear stiffness is often defined as a fraction of gross shear stiffness ( $G_c A_{vg}$ ) in the concrete walls. Depending on the amount of diagonal cracking caused by shear deformation of wall, values of cracked shear stiffness varies. Fully cracked shear stiffness is often considered as the slope of line from origin to the yielding of first horizontal reinforcement in shear.

By considering equal area approach, the tri-linear shear stress-strain relationship can be simplified to a bi-linear curve in which the effective shear stiffness is defined as the slope of the line between origin and the point of yielding as shown in Fig. 5.20. An appropriate estimate of effective shear stiffness can account for influence of diagonal cracking in reinforced concrete walls in a simple way. Results obtained from testing of RC panels were used to determine the effective shear stiffness of walls which possess different sectional geometry and horizontal reinforcement.

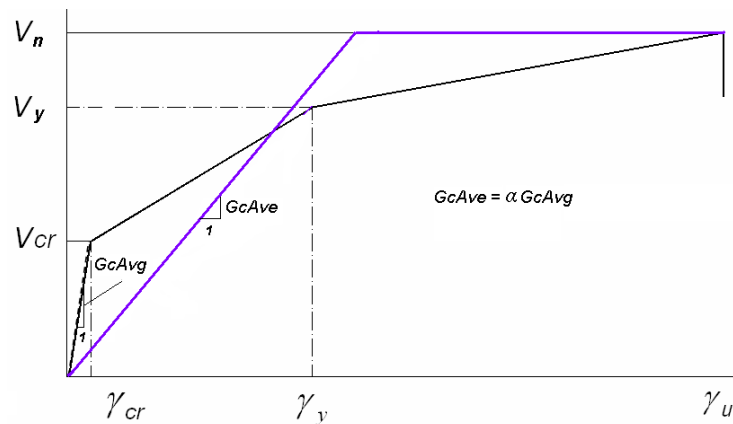


Figure 5.20 Use of equivalent area approach to estimate the effective shear stiffness.

Villani (1995) observed that the shear stress at the point of yielding ranges between 5 MPa and 6 MPa with the corresponding shear strain ranging between 0.003 and 0.004. The ratio of cracked section shear stiffness to the uncracked gross shear stiffness ( $G_c A_{ve}/G_c A_{vg}$ ) ranged between 0.067 and 0.011 for the above values. Considering the realistic stress–strain relationship for concrete walls in a case where wall has suffered significant diagonal cracking, a value of effective shear stiffness equal to 10% of initial gross shear stiffness ( $G_c A_{ve} = 0.1 G_c A_{vg}$ ) may be used to get a rough estimate of effective shear stiffness for the wall.

A wide range of effective shear stiffnesses was considered to investigate the nonlinear response of the model of high-rise wall. Dynamic nonlinear analyses were performed for different  $R$  factors equal to 2.0, 3.5 and 5.0 from a moderately ductile behaviour to a highly ductile behaviour.  $R$  factor in this study was assumed to be the ratio between the peak bending moment at the base of wall from linear time history analysis (LTHA) to the yielding bending moment at the base obtained from nonlinear time history analysis (NTHA). Since the wall geometry and strength properties were unchanged during all cases of analysis, the acceleration records were scaled according to the desired level of  $R$  factor. In order to study the effect of nonlinear shear behaviour in a simple way, four levels of effective shear stiffness was used over the entire wall's height. These four levels of effective shear stiffness ( $G_c A_{ve}$ ) were defined as 5%, 10%, 20% and 100% of gross shear stiffness ( $G_c A_{vg}$ ). A time step of  $t=0.001$  sec was used for nonlinear time history analysis. Results are shown in terms of envelopes for bending moment diagram, shear force and curvature diagram over the height of wall in Figures 5.21 through 5.24.

Flexural model of wall for analysis was similar to the model used in Section 5.6 where the wall possesses four different steps in flexural strength over the entire height. Figure 5.21 and Fig. 5.22 show the distribution of shear force demand over the height of wall for  $R=2.0$  and  $R=5.0$  respectively. The plots shown are the average of envelope values for the 10 selected earthquakes described in Section 5.3. According to the analyses results, reduction of shear stiffness over the wall height would result in a lower estimate of shear demand at the base of wall.

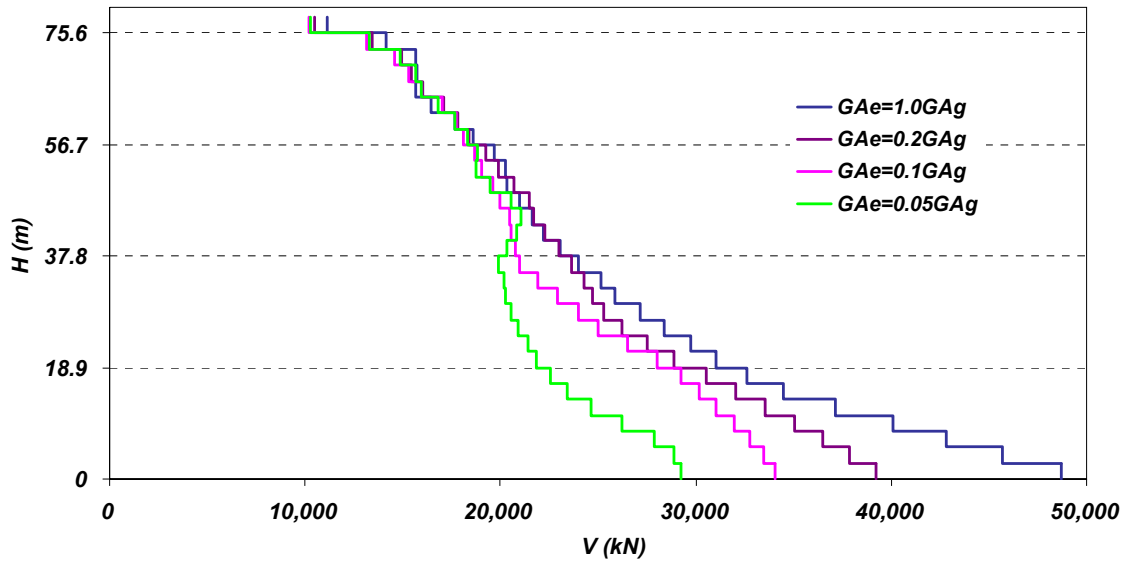


Figure 5.21 Influence of effective shear stiffness on shear force demand (Average for all earthquakes,  $R=2.0$ ).

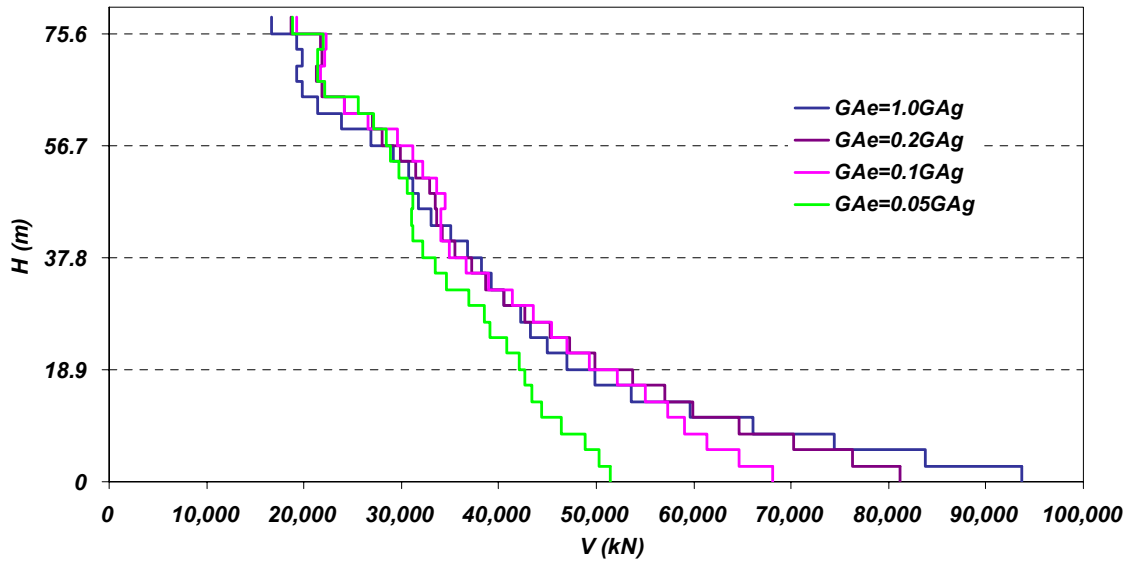


Figure 5.22 Influence of effective shear stiffness on shear force demand (Average for all earthquakes,  $R=5.0$ ).

Curvature demand tends to increase over the height and was observed to be largest at three fourth of total height. This is mainly caused by justification of yielding limits shown on Fig. 5.9. It is noted that variation of flexural strength over the height shown in Fig. 5.9 is very similar to design example of existing core walls in high-rise buildings in Western Canada. Due to the reduction in axial compression over the height, the curvature ductility was greater in the upper levels of the wall compared to the lower levels. The results for curvature demand are shown in Fig. 5.23 and Fig. 5.24 for  $R=2.0$  and for  $R=5.0$  respectively. Curvature demand was significant at the base and also the upper levels of wall.

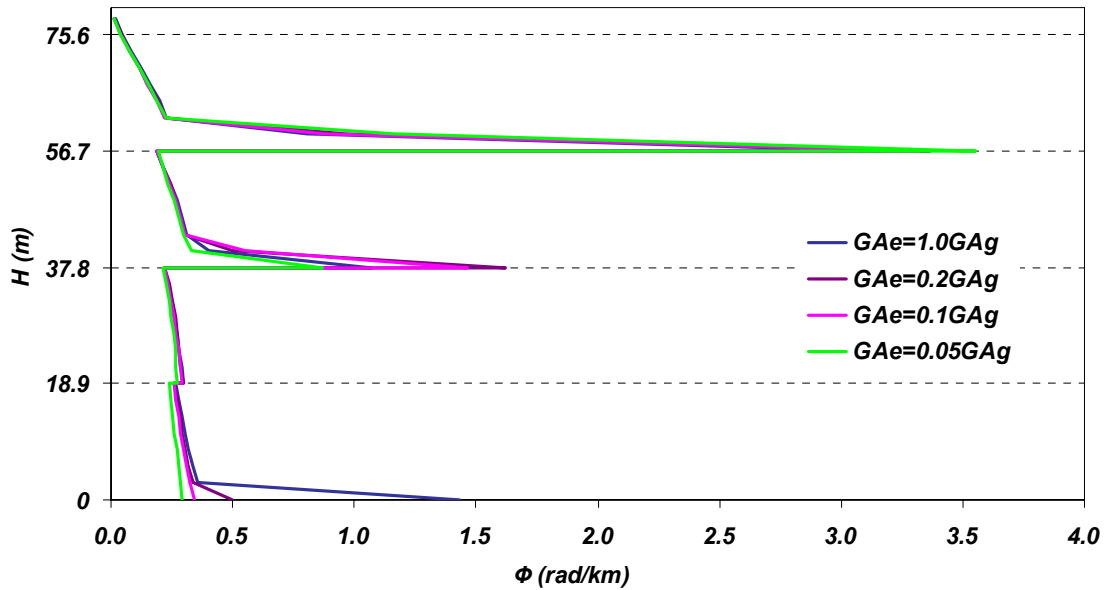


Figure 5.23 Influence of effective shear stiffness on curvature demand (Average for all earthquakes,  $R=2.0$ ).

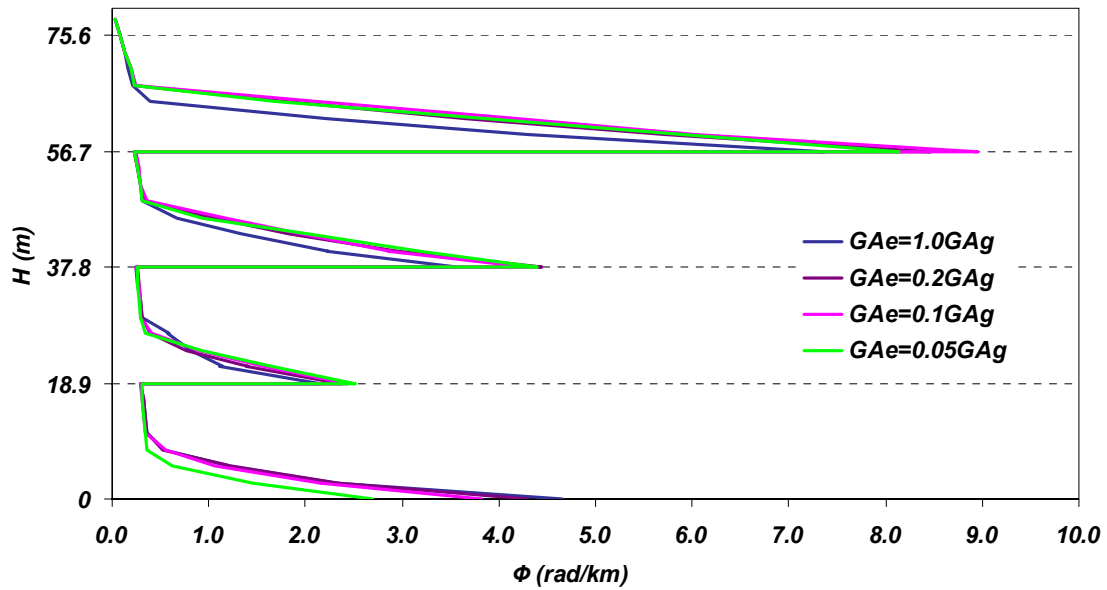


Figure 5.24 Influence of effective shear stiffness on curvature demand (Average for all earthquakes,  $R=5.0$ ).

Influence of effective shear stiffness on the shear force demand is shown in Fig. 5.25 and Fig. 5.26. In these plots the reduction of shear force at the base obtained from nonlinear response history analysis are shown with respect to the effective shear strength over the wall's height. The thin lines present the envelope values for 10 selected ground motions and the thick dashed line presents the corresponding averaged envelope values.

The reduction in shear force demand caused by influence of diagonal cracking was found to be insignificant for the lower levels of cracking where  $G_c A_{ve} \geq 0.2 G_c A_{vg}$ . For higher levels of diagonal cracking where  $G_c A_{ve} \leq 0.1 G_c A_{vg}$  the shear force reduction was noticeable. Shear force demand in some cases reduced to values lower than prediction of linear response spectrum analysis (i.e.  $G_c A_{ve} = 0.05 G_c A_{vg}$ ). Any reduction in shear force demand due to nonlinear behaviour is compensated by an increase in localized deformations. According to results, a reduction of uncracked shear stiffness to an cracked shear stiffness of  $G_c A_{ve} = 0.1 G_c A_{vg}$  caused a 30% reduction on shear force demand at the base of the modeled high-rise wall compared to the case where shear behaviour is assumed to remain elastic.

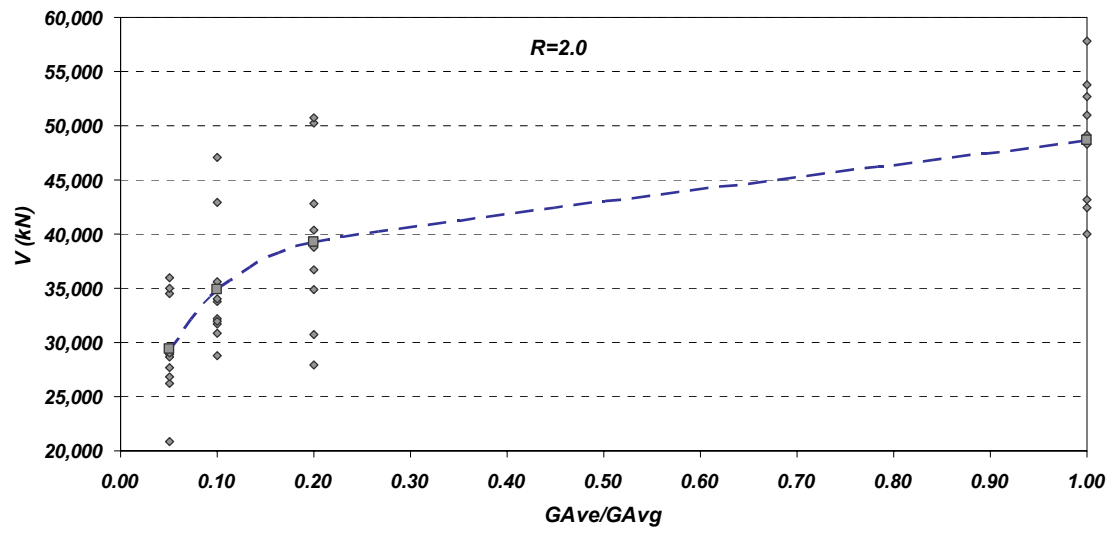


Figure 5.25 Dynamic shear demand at the base for nonlinear response history analysis,  $R=2.0$ .

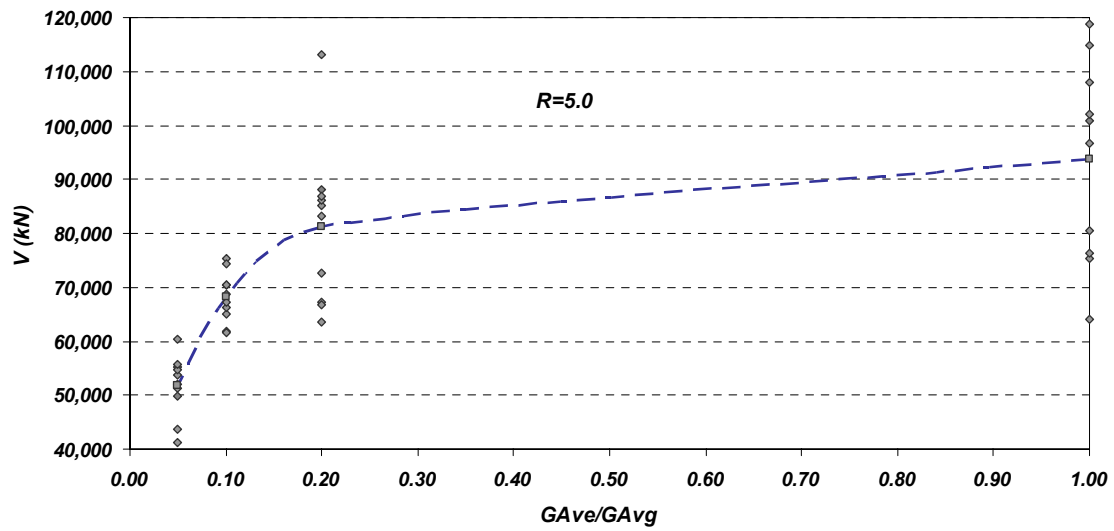


Figure 5.26 Dynamic shear demand at the base for nonlinear response history analysis,  $R=5.0$ .

A summary of the obtained results for the shear force demand at the base is presented in Tables 5.9 through Table 5.11. Table 5.9 summarizes the shear force demand at the base of wall obtained from nonlinear dynamic analysis with respect to different effective shear stiffness and different  $R$  factors. The results presented in Table 5.9 and Table 5.10 correspond to the crustal and subduction earthquakes respectively. Table 5.11 presents the mean values obtained from different earthquake events. Note that term “C” in Tables corresponds to crustal and term “S” corresponds to subduction earthquakes.

Table 5.9 Dynamic shear force demand at the base obtained from crustal events for different effective shear stiffness (values in kN).

$R$	$GA_{ve}/GA_{vg}$	$C-1$	$C-2$	$C-3$	$C-4$	$C-5$	$C-6$	$C-7$
2.0	1.00	48,809	42,467	49,134	48,297	52,711	43,155	53,820
	0.20	38,810	50,198	36,733	30,683	40,347	27,916	50,684
	0.10	47,117	31,671	33,749	32,225	35,647	28,743	30,833
	0.05	28,933	34,469	28,621	26,195	26,772	27,701	35,054
3.5	1.00	84,568	79,713	79,033	66,635	72,483	56,198	71,348
	0.20	62,624	65,387	71,287	58,234	67,855	44,561	64,339
	0.10	44,758	43,200	55,017	55,687	54,737	50,967	44,505
	0.05	41,124	42,142	38,502	46,498	44,249	44,093	37,022
5.0	1.00	107,937	100,905	114,938	80,613	102,004	64,051	96,780
	0.20	85,256	88,023	86,082	72,531	83,155	63,458	86,750
	0.10	61,953	68,700	64,985	66,175	70,452	67,238	75,288
	0.05	51,973	49,916	43,759	60,444	55,306	53,755	54,810

Table 5.10 Dynamic shear force demand at the base obtained from subduction events for different effective shear stiffness (values in kN).

$R$	$GA_{ve}/GA_{vg}$	$S-1$	$S-2$	$S-3$
2.0	1.00	40,016	57,767	51,002
	0.20	42,830	34,914	39,319
	0.10	31,999	42,916	34,003
	0.05	36,003	29,053	20,839
3.5	1.00	66,090	85,100	73,641
	0.20	51,022	72,317	57,559
	0.10	51,466	57,546	46,902
	0.05	42,934	42,771	33,770
5.0	1.00	75,234	118,747	76,276
	0.20	67,213	113,043	66,832
	0.10	74,318	70,444	61,503
	0.05	51,410	55,646	41,316

Table 5.11 Mean dynamic shear force demand at the base obtained from different earthquake events for different effective shear stiffness (values in kN).

$R$	$GA_{ve}/GA_{vg}$	$Mean-C$	$Mean-S$	$Mean\ all$
2.0	1.00	48,342	49,595	48,718
	0.20	39,339	38,979	39,243
	0.10	33,134	36,306	34,890
	0.05	29,489	28,632	29,364
3.5	1.00	72,854	74,944	73,481
	0.20	62,041	60,299	61,518
	0.10	49,769	51,971	50,479
	0.05	41,214	39,812	41,310
5.0	1.00	95,318	90,086	93,748
	0.20	80,751	82,362	81,234
	0.10	67,802	68,755	68,106
	0.05	52,230	49,458	51,834



Dynamic shear magnification factor is often expressed as the ratio between the shear demand obtained from dynamic analysis considering only flexural nonlinearity to the seismic shear demand obtained from simplified pseudo-static procedures. Dynamic shear amplification is defined with respect to results obtained from response spectrum analysis (RSA) in the present study. Dynamic shear amplification values are presented for the shear force at the base of wall in Table 5.12. Values are given as mean values obtained from influence of crustal and subduction earthquakes separately and also for all earthquake records. Dynamic amplification factor for  $R=2.0$  ranged between 1.48 and 0.79 for different effective shear stiffnesses. Results of NTHA for  $R=3.5$  suggested values for dynamic amplification which ranged from 2.34 to 1.12. Case  $R=5.0$  resulted in the greatest shear amplification factors which ranged from 3.09 to 1.40 for different effective shear stiffnesses.

Table 5.12 Mean dynamic shear force amplification at the base with respect to shear force demand obtained from RSA.

$R$	$GA_{ve}/GA_{vg}$	<i>Mean-C</i>	<i>Mean-S</i>	<i>Mean all</i>
2.0	1.0-Case SH	1.47	1.49	1.48
	1.0	1.31	1.34	1.32
	0.2	1.06	1.05	1.06
	0.1	0.90	0.98	0.94
	0.05	0.80	0.77	0.79
3.5	1.0-Case SH	2.37	2.27	2.34
	1.0	1.97	2.03	1.99
	0.2	1.68	1.63	1.66
	0.1	1.35	1.40	1.36
	0.05	1.11	1.08	1.12
5.0	1.0-Case SH	3.17	2.89	3.09
	1.0	2.58	2.43	2.53
	0.2	2.18	2.23	2.20
	0.1	1.83	1.86	1.84
	0.05	1.41	1.34	1.40

## 5.8 Influence of degrading hysteretic shear response

The final sets of analysis are performed using state-of-the-art nonlinear shear model in reinforced concrete walls through hysteretic response proposed by Gérin (2003). Program Response-2000 may also be used to predict nonlinear shear backbone for the section of wall; however because of uncertainties in using many required parameters to construct nonlinear shear response using Response-2000 and some of its shortcomings such as modeling the appropriate strut action, a more transparent simplified tri-linear shear model (Gérin 2003) was used in the present study.

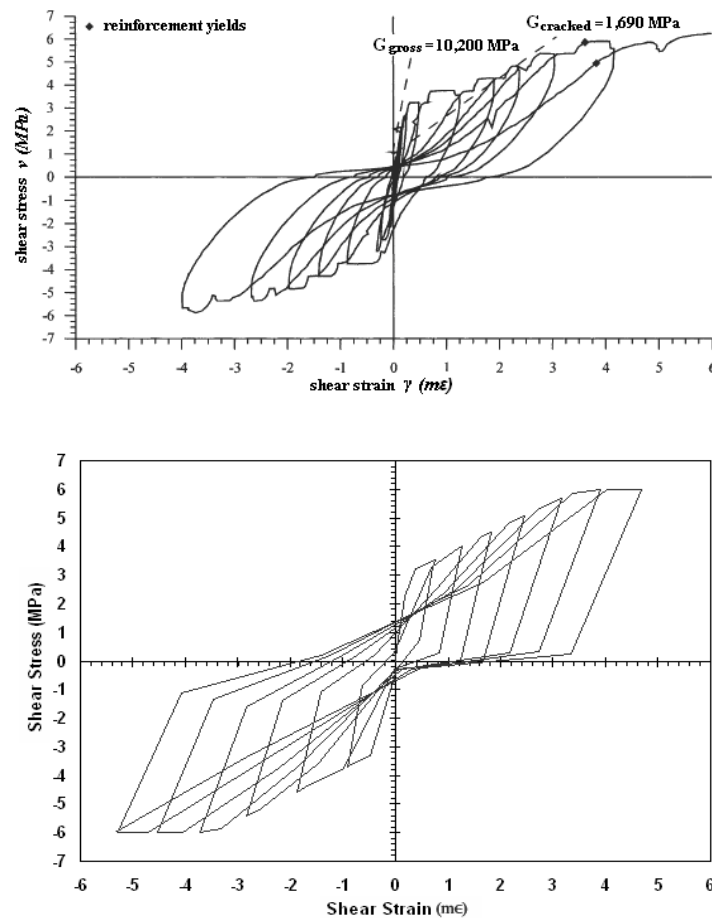


Figure 5.27 Hysteretic shear models in walls a) Experimental data (from Gérin, 2003) b) Simplified Model used in this study using NLINK element (SAP-2000, CSI 2006).

The hysteretic model for reverse cyclic shear that was used in this work is based on experimental testing conducted at the University of Toronto. The considered test element reinforcement ratio was similar to a section of high-rise wall at its base and therefore was used for verification of numerical model in this study.

In order to construct the appropriate hysteretic shear model the NLINK nonlinear element (SAP-2000, CSI 2006) was used and the actual hysteretic behaviour was simulated using Pivot Model (Dowell, Seible and Wilson 1998). Figure 5.27 and Fig. 5.28 present comparisons between experimental test data and the simplified hysteretic shear model used in this study. The backbone curve for hysteretic shear model was constructed based on tri-linear shear model proposed by G  rin (2003) which defines diagonal cracking of concrete and yielding limit for horizontal reinforcement for a given reinforced concrete section.

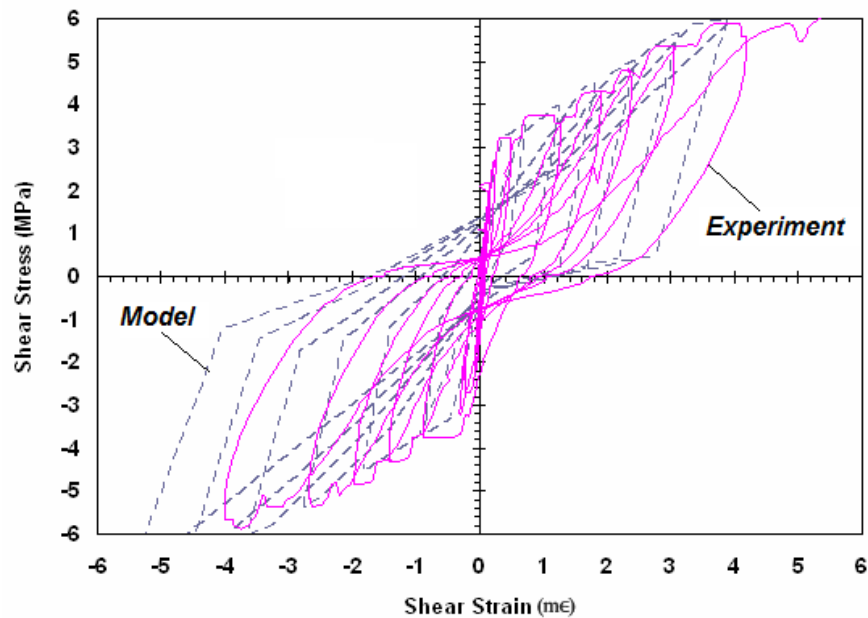


Figure 5.28 Hysteretic shear comparisons between experimental data and simplified model used in this study.

The nonlinear shear behaviour for the high-rise concrete wall was simulated in two different ways: one by using effective shear stiffness as a simplified method of accounting for diagonal cracking and the other by using a complete hysteretic shear model. Reliability of hysteretic shear model was also verified and validated by comparing

the results obtained from using hysteretic shear model and the results of NTHA obtained from using simplified shear stiffness properties for the model of high-rise wall.

### 5.8.1 Estimate of shear strength at cracking

In order to develop the tri-linear shear envelope used as the backbone of hysteretic behaviour, a proper estimate of cracking and yielding point is required. Comparison between values obtained from each of equations used to estimate  $V_c$  is shown in Fig. 5.29. Equation 11-12 taken from *ACI-318-05* was used for a lower-bound estimate of shear strength at cracking of concrete.

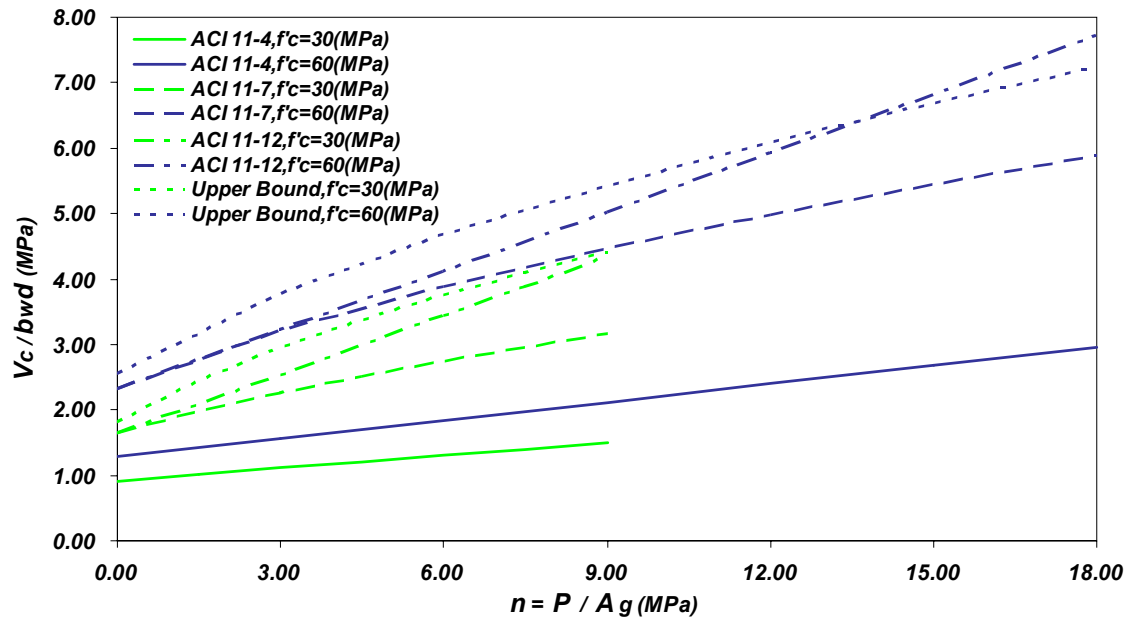


Figure 5.29 Shear at cracking for concrete walls predicted by ACI 318-05.

### 5.8.2 Estimate of shear strength at yielding

As designers typically use the RSA prediction for design of high-rise concrete walls, similar procedure was used here to estimate the initial shear strength for the wall. Figure 5.30 shows the different design spectra used to perform RSA. Three different design spectra was used which include *NBCC-2005* design spectrum for Vancouver (site class C), *IBC-2006* spectrum for Site Class B with  $F_a=F_v=1.0$  and *UBC-97* spectrum with  $C_a=C_v=0.4$ .

The design spectra were scaled to result in the same overturning moment equal to flexural strength at the base of the 30-storey model of wall with  $T_f=3.0$  sec. The scaled spectrum ended up having equal acceleration magnitude in a range between  $T=2.5$  sec and  $T=3.5$  sec as shown in Fig. 5.30.

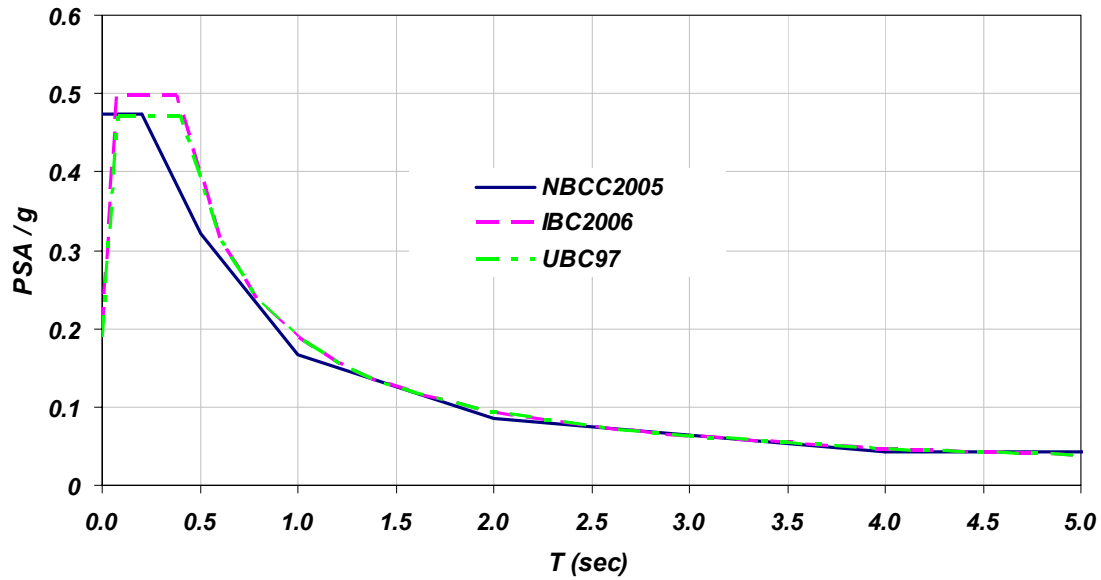


Figure 5.30 Scaled design response spectra used for RSA.

The ratio between overturning moment and shear force at the base of wall was also determined according to the results obtained from RSA. The normalized values of  $h'/H = (M_b/V_b)/H$  are given in Table 5.13, also shown on Fig. 5.31.  $h'/H$  ratio was obtained for linear time history analysis (*LTHA*) considering 10 different ground motions used for this study. Table 5.14 presents the  $h'/H$  values obtained from *LTHA*.

Table 5.13 Ratios of  $h'/H$  for walls according to RSA of different design spectra.

$T_1$	0.5 s	1.0 s	2.0 s	3.0 s	5.0 s
<i>IBC-2006</i>	0.72	0.63	0.44	0.37	0.26
<i>NBCC-2005</i>	0.71	0.59	0.42	0.38	0.29
<i>UBC-97</i>	0.72	0.60	0.40	0.36	0.25

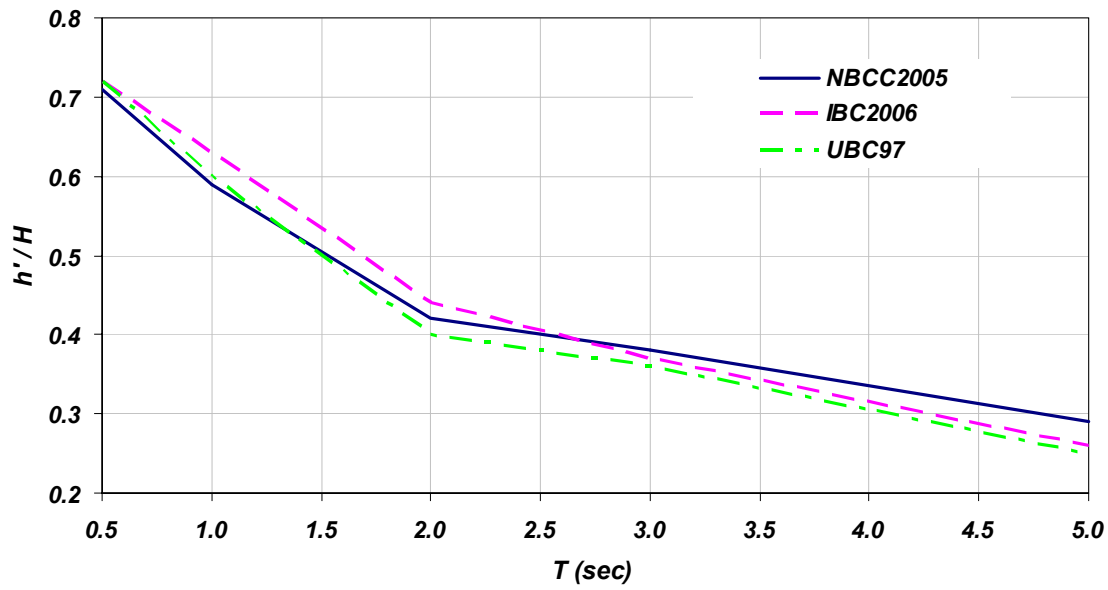


Figure 5.31 Ratios of  $h'/H$  for walls according to RSA of different design spectra.

Table 5.14 Ratios of  $h'/H$  for walls according to LTHA for different earthquakes.

<i>Earthquake</i>	<i>M<sub>b</sub>/V<sub>b</sub></i>	<i>h'/H</i>
C-1	38.15	0.47
C-2	25.19	0.31
C-3	28.60	0.35
C-4	29.31	0.36
C-5	20.32	0.25
C-6	33.65	0.42
C-7	17.45	0.22
S-1	47.32	0.58
S-2	26.90	0.33
S-3	31.94	0.39
Mean Value	29.88	0.37

The previous example of 30-storey wall had a flexural strength of  $M_b=1,050,000$  kNm.  $h'/H$  ratio was assumed to be 0.37 corresponding to a 30-storey wall with  $T_l=3.0$  sec. This value is associated with a design shear strength value of  $V_b=35,000$  kN at the base of wall.

The distribution of seismic shear force demand over the height of wall is also determined using RSA in practice. Distribution of bending moment and shear force over the height of the 30-storey wall for the three different design spectra (see also Fig. 5.30) is shown in Fig. 5.32.

Wall's shear strength at every 7 storey reduces based on force distribution obtained from RSA. The shear strength is controlled by providing horizontal steel at each section. In total four different sections were considered over the wall's height. The shear strength changes every seven stories similar to the model used for flexural strength. The shear strength for section 1 from the base to the 7<sup>th</sup> storey (El. 19.0) is equal to  $V_{s1}=V_b$ , shear strength for section 2 from the 8<sup>th</sup> storey to the 14<sup>th</sup> storey (El. 38.0) is  $V_{s2}=0.85V_b$ , shear strength for section 3 from the 15<sup>th</sup> storey to the 21<sup>st</sup> storey (El. 57.0) is  $V_{s3}=0.60V_b$  and the strength for section 4 from the 22<sup>nd</sup> storey to top of wall (El. 81.0) is  $V_{s3}=0.45V_b$ . The shear strength envelope for the example of wall is shown in Fig. 5.33.

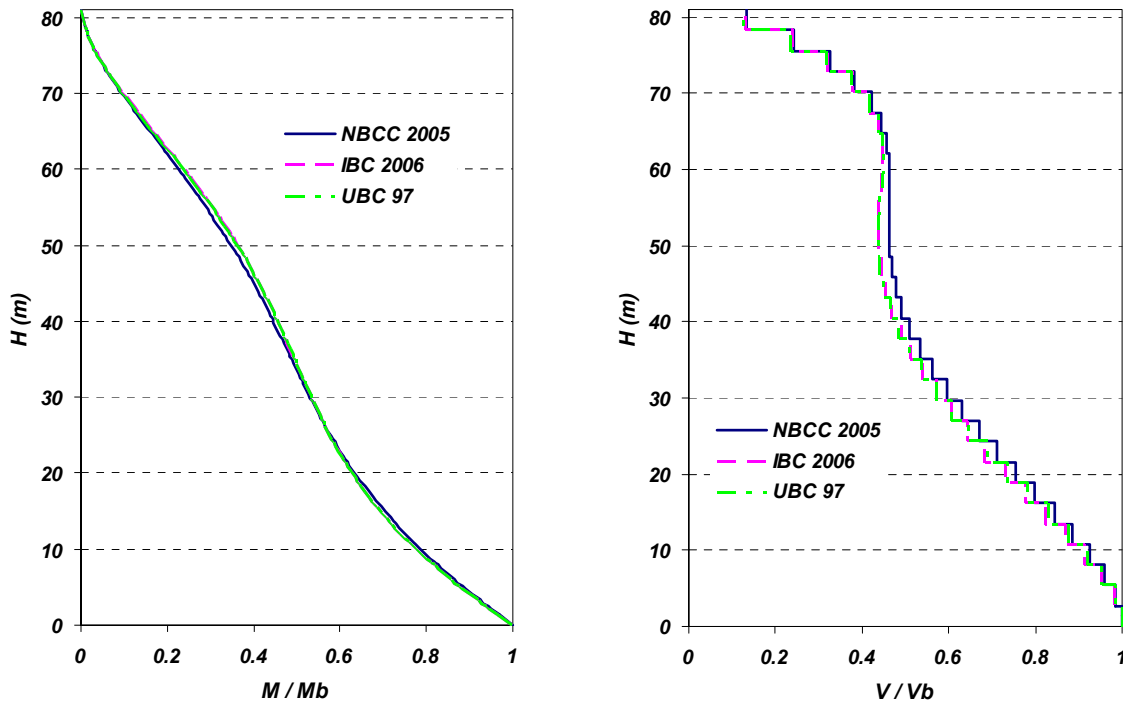


Figure 5.32 RSA prediction of bending moment and shear force over the height for  $T_f=3.0$  sec.

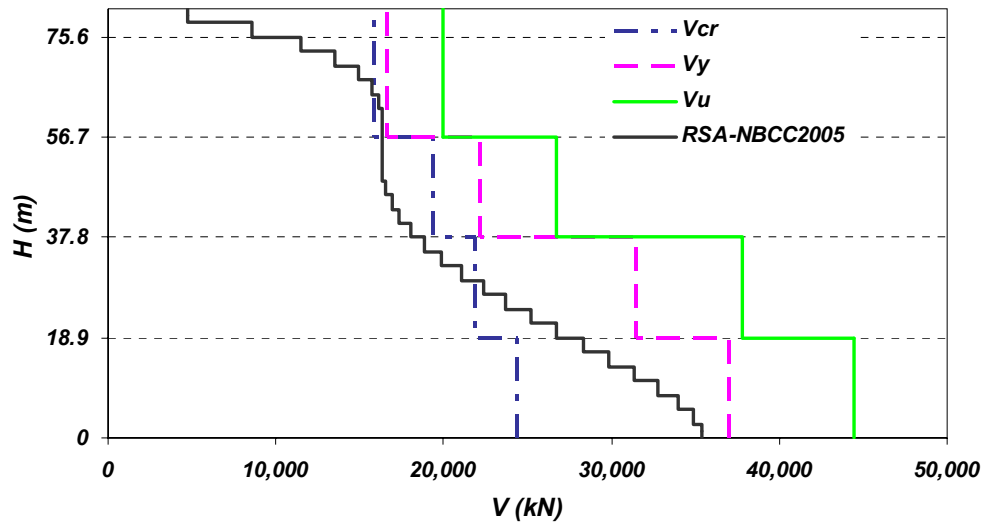


Figure 5.33 Shear strength envelopes over the height of the 30-storey wall model.

Tri-linear shear force-shear strain relationship was used for four different section of the wall over its height. The tri-linear model for shear force-shear strain was used to model the wall nonlinear behaviour in shear. The envelope of nonlinear shear force-shear strain model for section of wall is shown in Fig. 5.34. Table 5.15 presents the parameters used in defining the tri-linear shear force-shear strain backbone for hysteretic shear model.

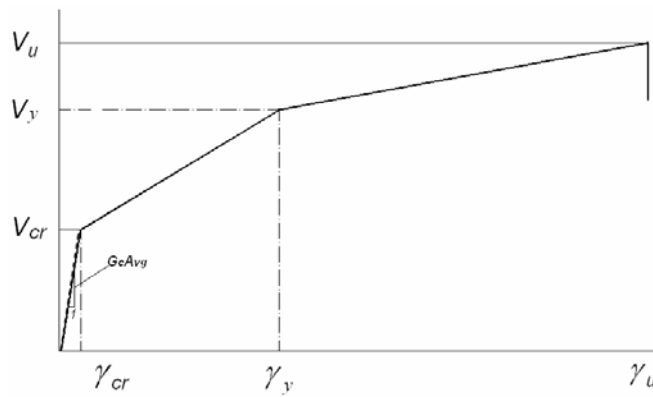


Figure 5.34 Shear force-shear strain envelope used for hysteretic shear response.



Table 5.15 Nonlinear shear model used in the example of wall.

	$V_{cr} \text{ (kN)}$	$\gamma_{cr}$	$V_y \text{ (kN)}$	$\gamma_y$
Section 1	24,444	0.00028	37,037	0.00293
Section 2	21,913	0.00026	31,481	0.00312
Section 3	19,381	0.00023	22,222	0.00307
Section 4	15,833	0.00020	16,667	0.00366

The ultimate shear strength ( $V_u$ ) was considered equal to  $1.2V_y$  in all cases (see Fig. 5.33). The ultimate shear strain capacity was determined using expression proposed by Gérin (2003). The nonlinear elements were considered over the entire height of wall with strength changing at every seven stories. To model the nonlinear behaviour over the height of wall two nonlinear spring elements to simulate the hysteretic flexural and shear behaviour were used as shown in Fig. 5.35. The nonlinear spring elements are referred to as *NLINK* in the program SAP-2000 (CSI 2006) that was used in this study. Tri-linear envelope using Takeda model was used to incorporate moment-curvature response at the section of wall. In order to simulate the nonlinear hysteretic shear response, the tri-linear shear force–shear strain backbone was used with a combination of modified pivot model accounting for pinching. The results from using this model were compared to the experimental results shown in Fig. 5.28 earlier in this chapter.

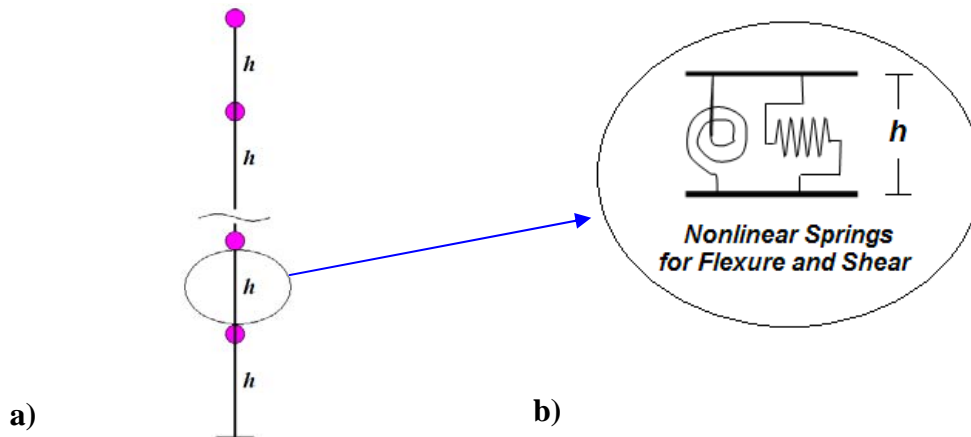


Figure 5.35 a): Model of the 30-storey wall and b): the nonlinear springs used to simulate nonlinear flexure and shear model (NLINK, SAP-2000).

## 5.9 Discussion of dynamic response due to hysteretic shear model

Nonlinear time history analysis was performed for the selected ground motions using program SAP-2000 (CSI 2006). Nonlinear flexural and shear models for the model of 30-storey cantilever core wall were considered for analyses.

Nonlinear response history analysis was performed for ten earthquake records all scaled to fit *NBCC-2005* design spectrum as explained in Section 5.3. Three different  $R$  factors were used as  $R=2.0$ , 3.5 and 5.0. The magnitude of the earthquakes are proportional to the level of  $R$  factor and as the  $R$  factor increases, more damage is expected in terms of deformations at the critical section of the reinforced concrete wall. The wall's shear strength over the height was defined according to values given in Table 5.15. In tables,  $SF$  stands for shear strength factor applied on the values given in Table 5.15, for example  $SF=1.5$  means the shear strength values in Table 5.15 are multiplied by a factor of 1.5 to set the shear strength of high-rise wall model in different sections.

The results for  $R=2.0$  are shown in Fig. 5.36 through Fig. 5.39. Envelopes for bending moment diagram are shown on Fig. 5.36. Thick dashed line shows the average envelope for bending moment from all earthquake records. Flexural yielding limit at different sections of wall over the height is also illustrated by thin dashed line. It was observed that due to yielding of wall sections at different heights, bending moment diagram over the height follows the flexural strength pattern.

Corresponding curvature demands are shown in Fig. 5.37. At the zones where reinforced concrete wall yields, elongation of longitudinal reinforcement caused significant rotation which can be expressed in terms of curvature demand at the plastic hinge. The curvature demand was significant at the base and upper sections of wall. Envelopes for shear force and shear strain demand are shown in Fig. 5.38 and Fig. 5.39 respectively.

Once wall reached the yielding capacity, the shear strain demand increased significantly. Localization of shear strain for regions where there is a sudden change in strength was noticeable. This also signifies the importance of considering the nonlinear shear model for studying the seismic response of high-rise concrete walls.

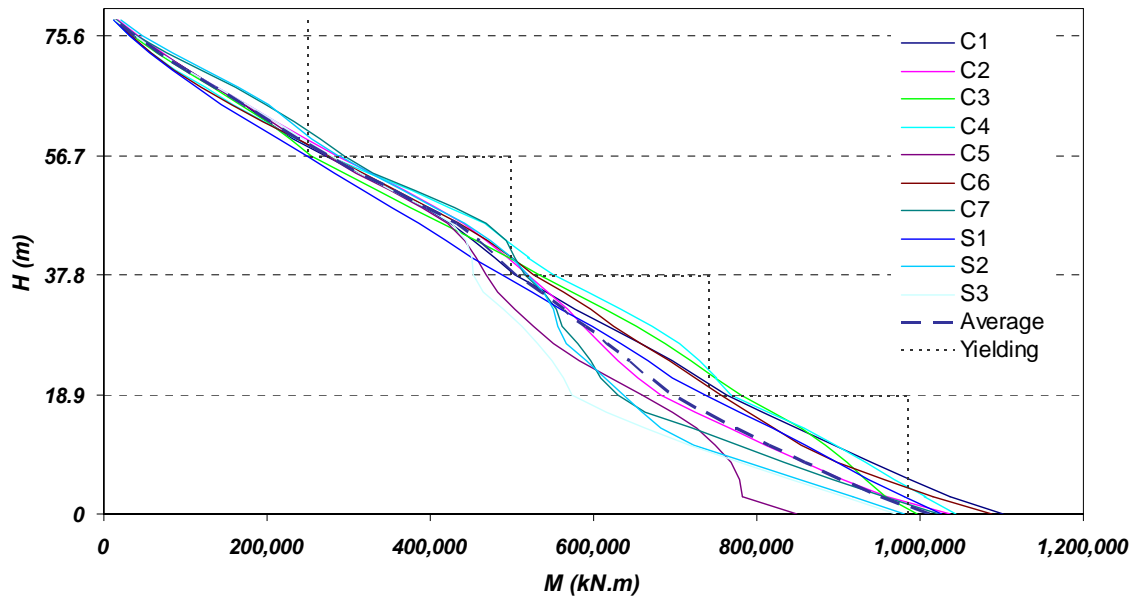


Figure 5.36 Envelope of bending moment for NTHA ( $R=2.0$ ,  $SF=1.0$ ).

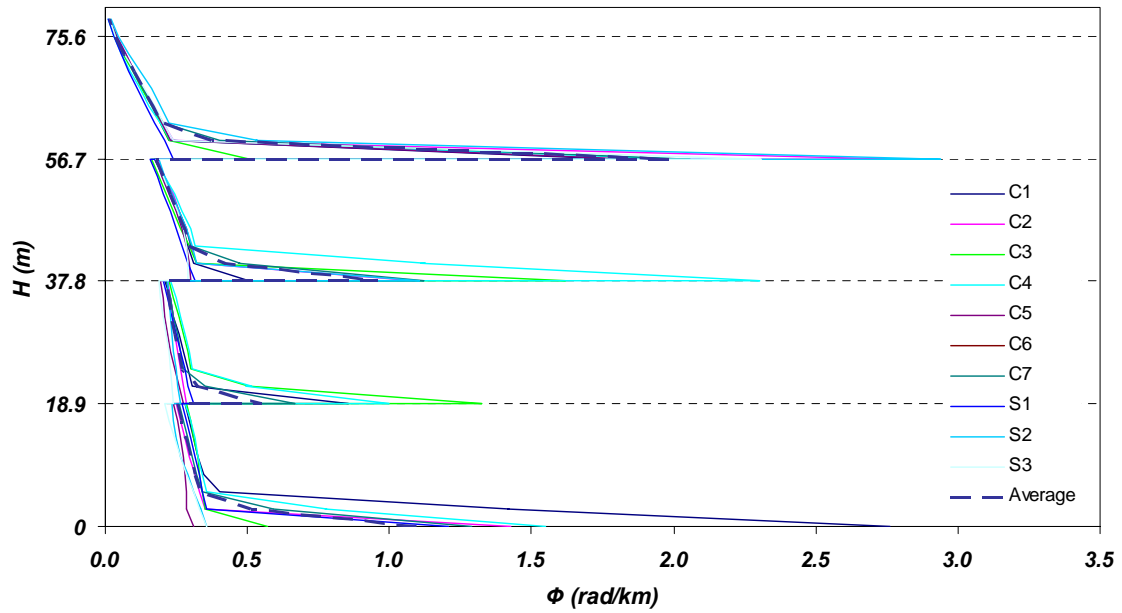


Figure 5.37 Envelope of curvature for NTHA ( $R=2.0$ ,  $SF=1.0$ ).

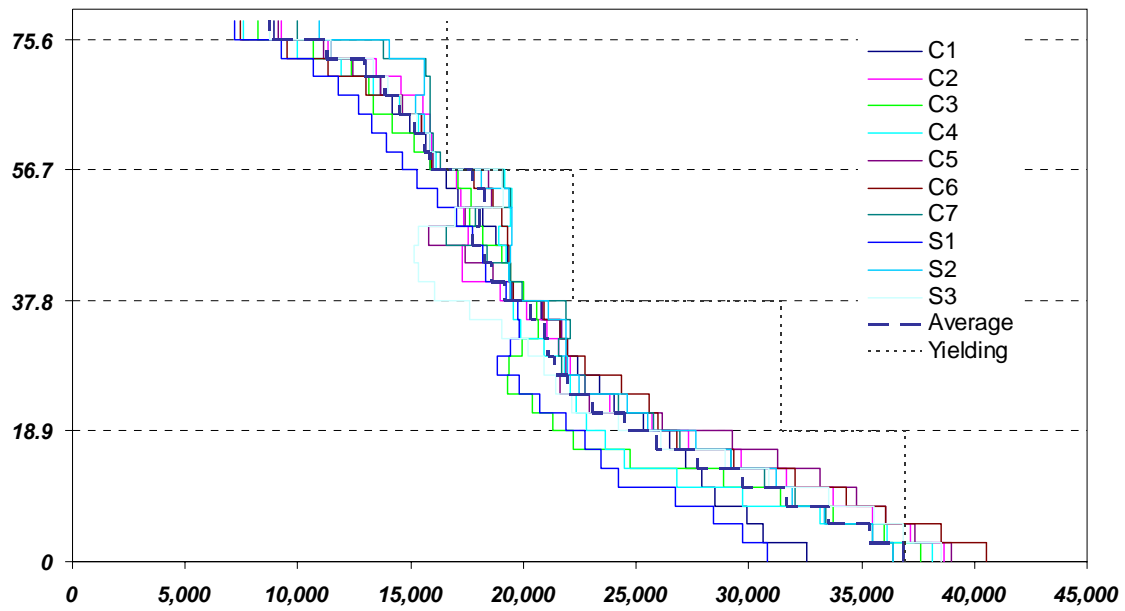


Figure 5.38 Envelope of shear force for NTHA ( $R=2.0$ ,  $SF=1.0$ ).

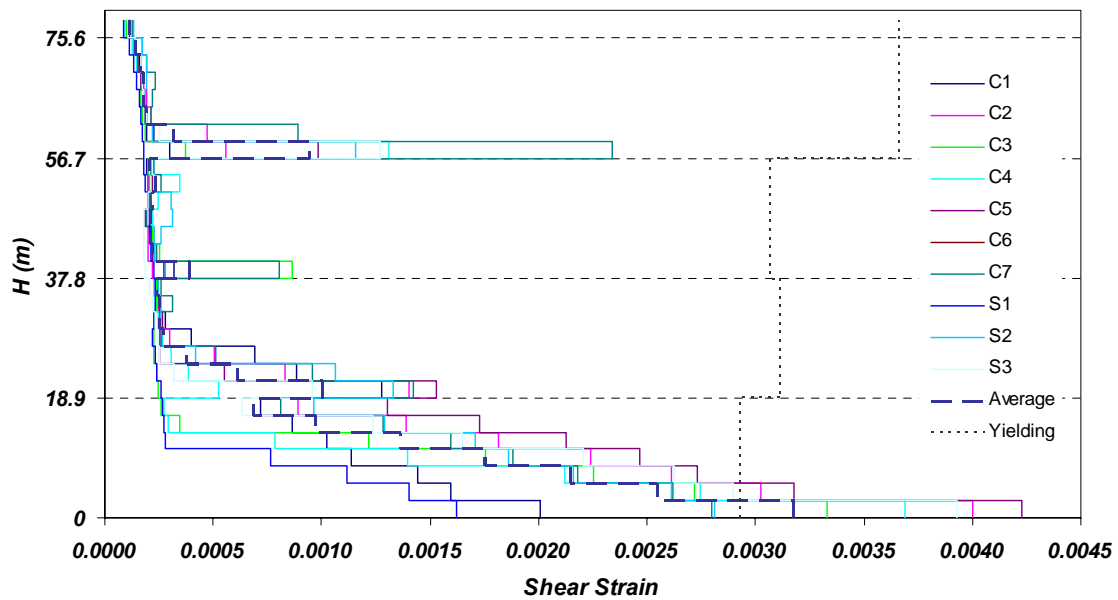


Figure 5.39 Envelope of shear strain for NTHA ( $R=2.0$ ,  $SF=1.0$ ).

Table 5.16 provides summary information on the obtained shear force demand from NTHA. This table corresponds to the values shown on Fig. 5.36 through 5.39. Table 5.16 presents the results for  $R=2.0$  and a shear strength factor of  $SF=1.0$ . The shear force capacities of wall in different states are given on top rows of the table. In the Table “C” stands for shear cracking, “Y” stands for shear yielding and “F” stands for shear failure. Term “E” refers to elastic state at the wall section.

Shear force demands were obtained from NTHA for the selected crustal and subduction earthquakes. By looking at the mean values, it was observed that the wall at the base has just exceeded its yielding capacity in shear whereas upper sections of wall have only passed their cracking limit in shear. Considering the significant reserve ductility in shear beyond yielding point, the wall seismic performance in shear was at an acceptable level and no significant shear damage was noticed for the case of  $R=2.0$ .

Table 5.17 provides results for  $R=3.5$  similar to Table 5.16. Wall reached its ultimate shear capacity at the base and yielded in shear at the upper section (Section 4). This was a critical case for shear and the provided shear strength was found to be inadequate for  $R=3.5$ . The result for the case of  $R=5.0$  is shown in Fig. 5.40 through Fig. 5.43. The shear force demand was significantly large in this case and wall exceeded its yielding shear capacity at various heights. The core wall reached its ultimate capacity at the base. Table 5.18 provides information summary of the obtained results for the case of  $R=5.0$  with  $SF=1.0$  at which the shear demand at the base was very large. A poor seismic performance was observed in this case resulting in a shear failure at the base of wall.

Table 5.16 Shear force demand and at different sections of wall for  $R=2.0$  and  $SF=1.0$ .

<i>Shear Strength Factor = 1.0 R=2.0</i>				
	<i>Section S1</i>	<i>Section S2</i>	<i>Section S3</i>	<i>Section S4</i>
<i>Cracking (C) (kN)</i>	24,444	21,913	19,381	15,833
<i>Yielding (Y) (kN)</i>	37,037	31,481	22,222	16,667
<i>Failure (F) (kN)</i>	44,444	37,778	26,667	20,000
<i>C-1</i>	32,595	25,305	19,476	15,857
	C	C	C	C
<i>C-2</i>	38,639	25,724	18,944	15,919
	Y	C	E	C
<i>C-3</i>	37,607	21,330	20,014	15,874
	Y	E	C	C
<i>C-4</i>	38,164	22,807	19,500	16,098
	Y	C	C	C
<i>C-5</i>	38,988	26,149	19,426	16,020
	Y	C	C	C
<i>C-6</i>	40,564	25,992	19,552	15,944
	Y	C	C	C
<i>C-7</i>	56,130	38,720	23,650	17,241
	F	F	Y	Y
<i>S-1</i>	30,796	21,902	19,251	14,645
	C	E	E	E
<i>S-2</i>	36,410	25,495	19,464	16,062
	C	C	C	C
<i>S-3</i>	38,527	24,246	19,110	16,088
	Y	C	E	C
<i>Mean</i>	36,866	24,474	19,154	15,885
	C	C	E	C

Table 5.17 Shear force demand at different sections of wall for  $R=3.5$  and  $SF=1.0$ .

<i>Shear Strength Factor = 1.0 R=3.5</i>				
	<i>Section S1</i>	<i>Section S2</i>	<i>Section S3</i>	<i>Section S4</i>
<i>Cracking (C) (kN)</i>	24,444	21,913	19,381	15,833
<i>Yielding (Y) (kN)</i>	37,037	31,481	22,222	16,667
<i>Failure (F) (kN)</i>	44,444	37,778	26,667	20,000
<i>C-1</i>	40,645	30,277	20,671	16,297
	Y	C	C	C
<i>C-2</i>	44,117	32,262	20,486	17,073
	Y	Y	C	Y
<i>C-3</i>	48,544	33,088	19,508	17,771
	F	Y	C	Y
<i>C-4</i>	50,965	29,066	20,163	17,265
	F	C	C	Y
<i>C-5</i>	40,378	31,755	19,966	17,079
	Y	Y	C	Y
<i>C-6</i>	41,875	28,186	20,274	17,051
	Y	C	C	Y
<i>C-7</i>	46,049	30,556	19,589	16,529
	F	C	C	C
<i>S-1</i>	40,799	25,882	20,157	15,848
	Y	C	C	C
<i>S-2</i>	45,567	30,781	21,324	18,044
	F	C	C	Y
<i>S-3</i>	44,789	29,459	19,295	16,539
	F	C	E	C
<i>Mean</i>	44,296	30,131	20,080	16,948
	Y	C	C	Y

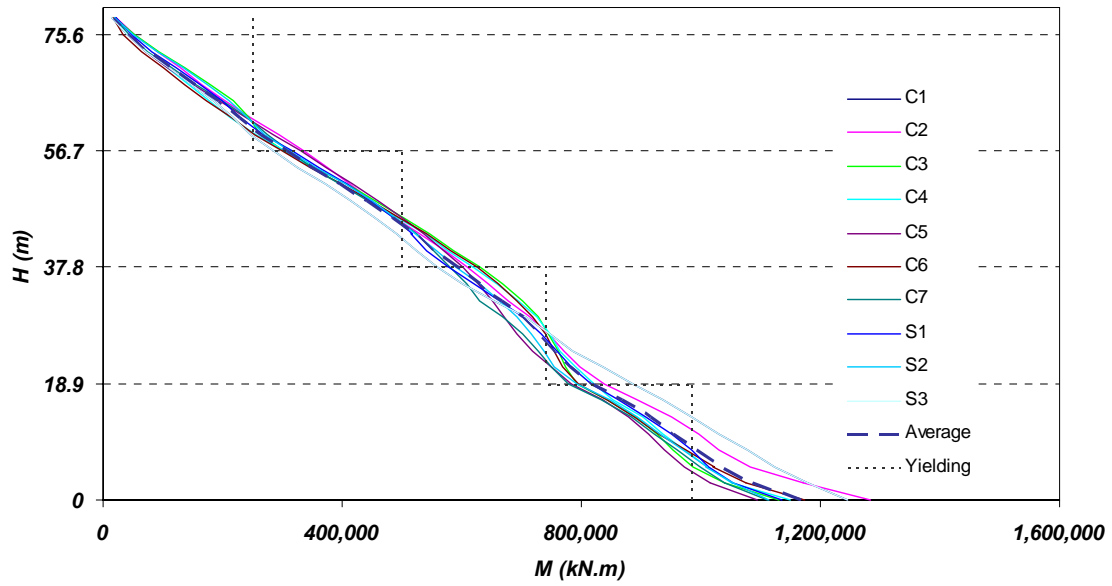


Figure 5.40 Envelope of bending moment for NTHA ( $R=5.0$ ,  $SF=1.0$ ).

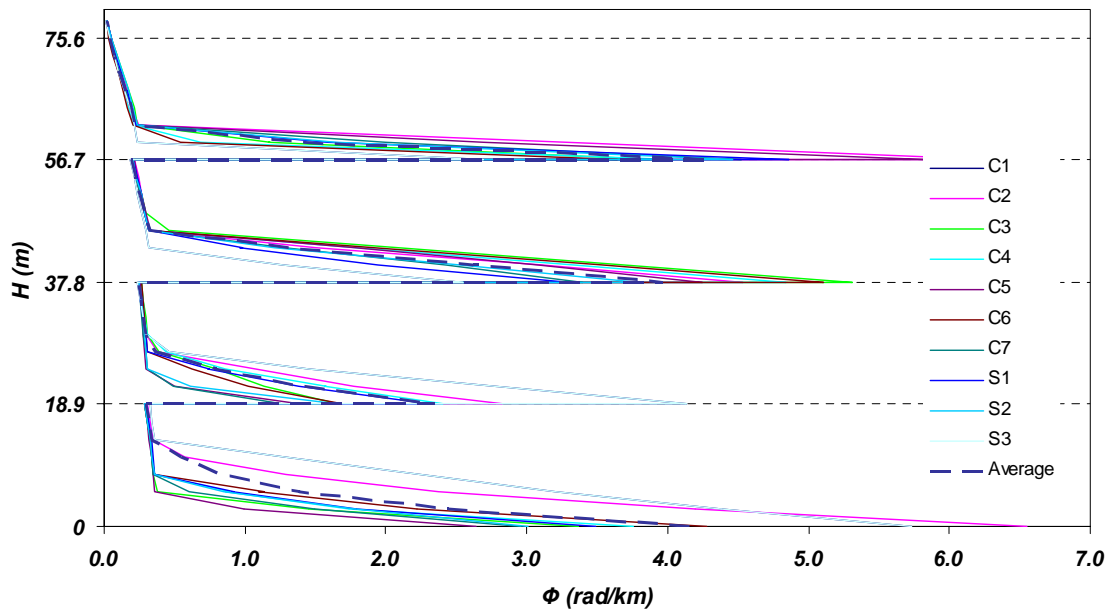


Figure 5.41 Envelope of curvature for NTHA ( $R=5.0$ ,  $SF=1.0$ ).



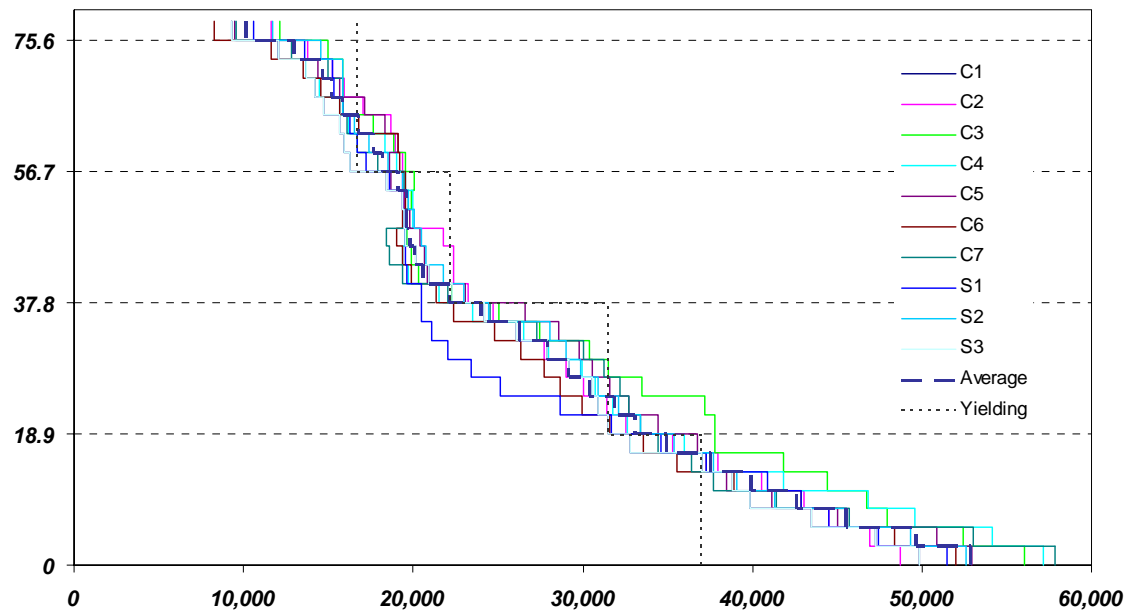


Figure 5.42 Envelope of shear force for NTHA ( $R=5.0$ ,  $SF=1.0$ ).

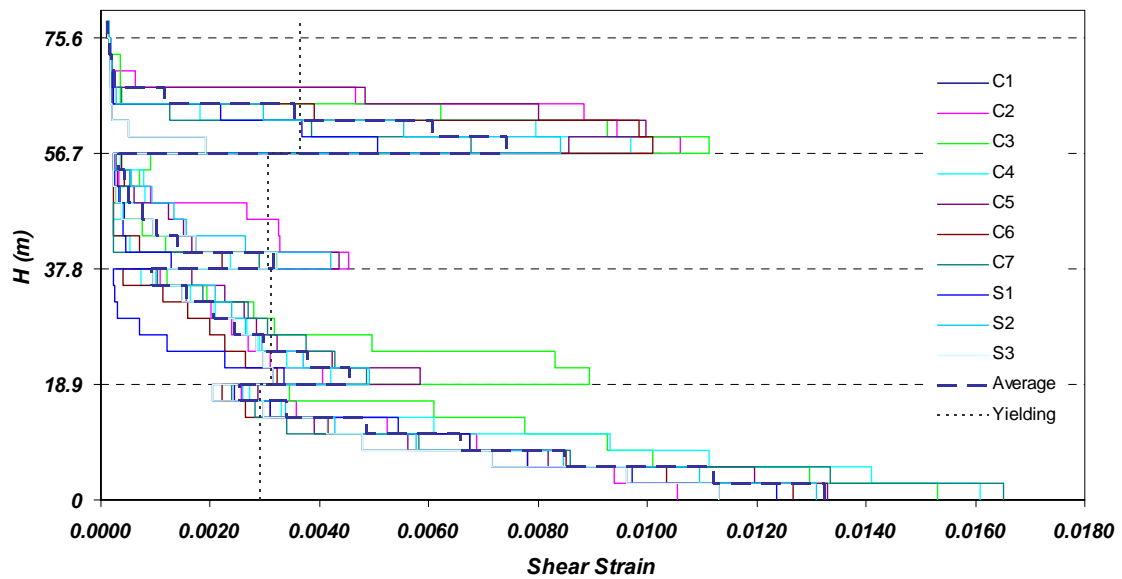


Figure 5.43 Envelope of shear strain for NTHA ( $R=5.0$ ,  $SF=1.0$ ).

Table 5.18 Shear force demand at different sections of wall for  $R=5.0$  and  $SF=1.0$ .

<i>Shear Strength Factor = 1.0 R=5.0</i>				
	<i>Section S1</i>	<i>Section S2</i>	<i>Section S3</i>	<i>Section S4</i>
<i>Cracking (C) (kN)</i>	24,444	21,913	19,381	15,833
<i>Yielding (Y) (kN)</i>	37,037	31,481	22,222	16,667
<i>Failure (F) (kN)</i>	44,444	37,778	26,667	20,000
<i>C-1</i>	49,856	31,500	22,321	16,239
	F	Y	Y	C
<i>C-2</i>	48,689	32,503	23,217	19,367
	F	Y	Y	Y
<i>C-3</i>	56,030	37,833	22,324	19,576
	F	F	Y	Y
<i>C-4</i>	57,202	32,668	21,521	19,009
	F	Y	C	Y
<i>C-5</i>	52,931	34,454	23,086	19,123
	F	Y	Y	Y
<i>C-6</i>	51,951	31,580	21,377	19,168
	F	Y	C	Y
<i>C-7</i>	57,869	33,369	22,041	17,872
	F	Y	C	Y
<i>S-1</i>	51,493	31,716	20,447	17,193
	F	Y	C	Y
<i>S-2</i>	52,603	33,441	22,996	18,509
	F	Y	Y	Y
<i>S-3</i>	49,856	31,500	22,321	16,239
	F	Y	Y	C
<i>Mean</i>	52,847	33,056	22,165	18,174
	F	Y	C	Y

In order to increase the shear strength, horizontal steel was added to the section of wall. Shear strength of the section was increased by 50% corresponding to a shear strength factor of  $SF=1.5$ .

Summary of results for  $R=3.5$  and  $SF=1.5$  is provided in Table 5.19. In order to see the changes corresponding to a 50% increase in shear strength of wall, results given for  $R=3.5$  and  $SF=1.0$  in Table 5.17 should be compared with values given in Table 5.19. By comparing the mean values for crustal and subduction events from the tables, it was observed that the wall performance has been improved from a undesirable shear failure at the base to a safer yielding state with considerable amount of reserved ductility. Yielding in upper sections of the wall for the case of  $SF=1.0$  improved to a safer cracking state in shear for the case of  $SF=1.5$ . Table 5.20 provides the results for the case of  $R=5.0$  and  $SF=1.5$ . Results in this table need to be compared with Table 5.18 for the case  $SF=1.0$ .

The shear performance was improved by moving from the shear failure state to a post-yielding state very close to the ultimate shear capacity. Although the shear performance of the wall has been improved by increasing the amount of horizontal reinforcement in the section, a safe shear behaviour was not achieved. In order to increase the wall shear strength in the case of  $R=5.0$ , the shear strength was increased by a factor of two compared to the initial horizontal reinforcement provided at the section. The results for this case is referred to as  $R=5.0$  and  $SF=2$  which are presented in Fig. 5.44 through Fig. 5.47. Table 5.21 provides a summary of obtained maximum shear demand at different sections of wall over the height.

As it is shown in figures, by adding horizontal reinforcement, the wall shear performance for  $SF=2.0$  was further improved compared to the case of  $SF=1.5$ . An acceptable seismic shear behaviour was achieved by increasing the wall shear strength according to Table 5.21. The results show that increasing the amount of reinforcement for large values of  $R$  factor is an effective solution to improve the wall's shear performance during earthquake.

Table 5.19 Shear force demand at different sections of wall for  $R=3.5$  and  $SF=1.5$ .

<i>Shear Strength Factor = 1.5 – R=3.5</i>				
	<i>Section S1</i>	<i>Section S2</i>	<i>Section S3</i>	<i>Section S4</i>
<i>Cracking (C) (kN)</i>	24,444	21,913	19,381	16,850
<i>Yielding (Y) (kN)</i>	55,556	47,222	33,333	25,000
<i>Failure (F) (kN)</i>	66,667	56,667	40,000	30,000
<i>C-1</i>	55,656	32,696	22,636	18,595
	Y	C	C	C
<i>C-2</i>	58,324	39,480	29,686	18,725
	Y	C	C	C
<i>C-3</i>	61,709	42,299	25,814	18,013
	Y	C	C	C
<i>C-4</i>	58,709	28,952	23,434	19,936
	Y	C	C	C
<i>C-5</i>	54,153	39,841	27,680	19,387
	C	C	C	C
<i>C-6</i>	50,509	32,399	23,497	19,290
	C	C	C	C
<i>C-7</i>	56,848	36,722	26,884	19,214
	Y	C	C	C
<i>S-1</i>	51,443	33,308	21,485	16,743
	C	C	C	E
<i>S-2</i>	56,712	34,532	26,203	19,390
	Y	C	C	C
<i>S-3</i>	57,787	41,641	25,441	20,252
	Y	C	C	C
<i>Mean</i>	56,184	36,172	25,276	18,948
	Y	C	C	C

Table 5.20 Shear force demand at different sections of wall for  $R=5.0$  and  $SF=1.5$ .

<i>Shear Strength Factor = 1.5 – R=5.0</i>				
	<i>Section S1</i>	<i>Section S2</i>	<i>Section S3</i>	<i>Section S4</i>
<i>Cracking (C) (kN)</i>	24,444	21,913	19,381	16,850
<i>Yielding (Y) (kN)</i>	55,556	47,222	33,333	25,000
<i>Failure (F) (kN)</i>	66,667	56,667	40,000	30,000
<i>C-1</i>	63,310	40,058	25,481	20,344
	Y	C	C	C
<i>C-2</i>	68,906	42,598	32,810	20,338
	F	C	C	C
<i>C-3</i>	71,637	45,811	34,524	20,856
	F	C	Y	C
<i>C-4</i>	64,958	34,929	31,885	23,236
	Y	C	C	C
<i>C-5</i>	68,013	42,218	34,447	22,493
	F	C	Y	C
<i>C-6</i>	58,131	39,372	29,002	19,593
	Y	C	C	C
<i>C-7</i>	69,187	42,370	33,502	20,515
	F	C	Y	C
<i>S-1</i>	59,902	40,679	21,345	18,385
	Y	C	C	C
<i>S-2</i>	68,038	42,432	32,467	21,291
	F	C	C	C
<i>S-3</i>	61,225	45,888	33,368	19,101
	Y	C	Y	C
<i>Mean</i>	65,330	41,289	30,866	20,609
	Y	C	C	C

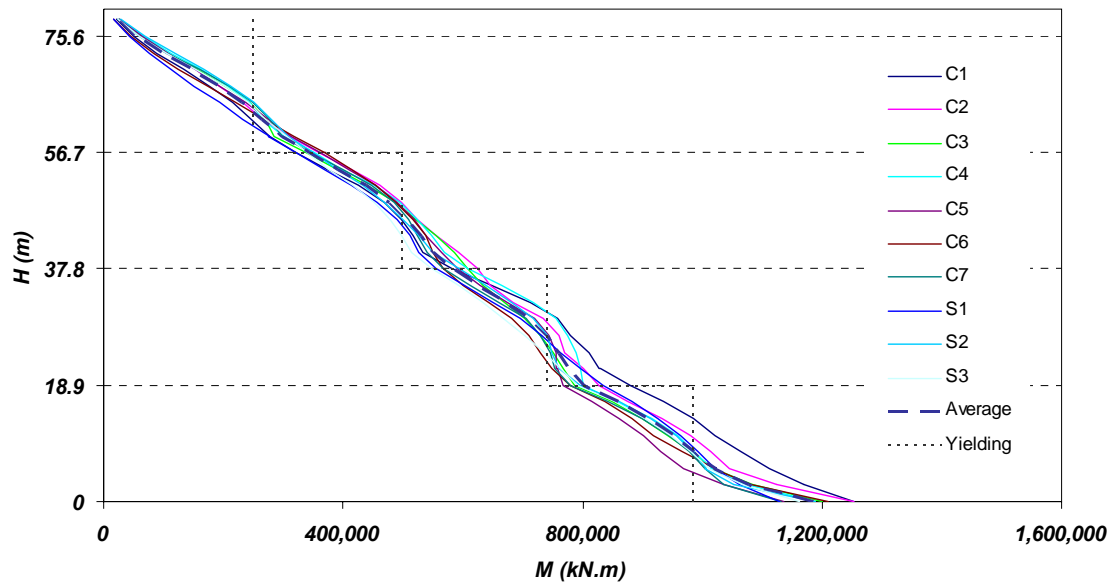


Figure 5.44 Envelope of bending moment for NTHA ( $R=5.0$ ,  $SF=2.0$ ).

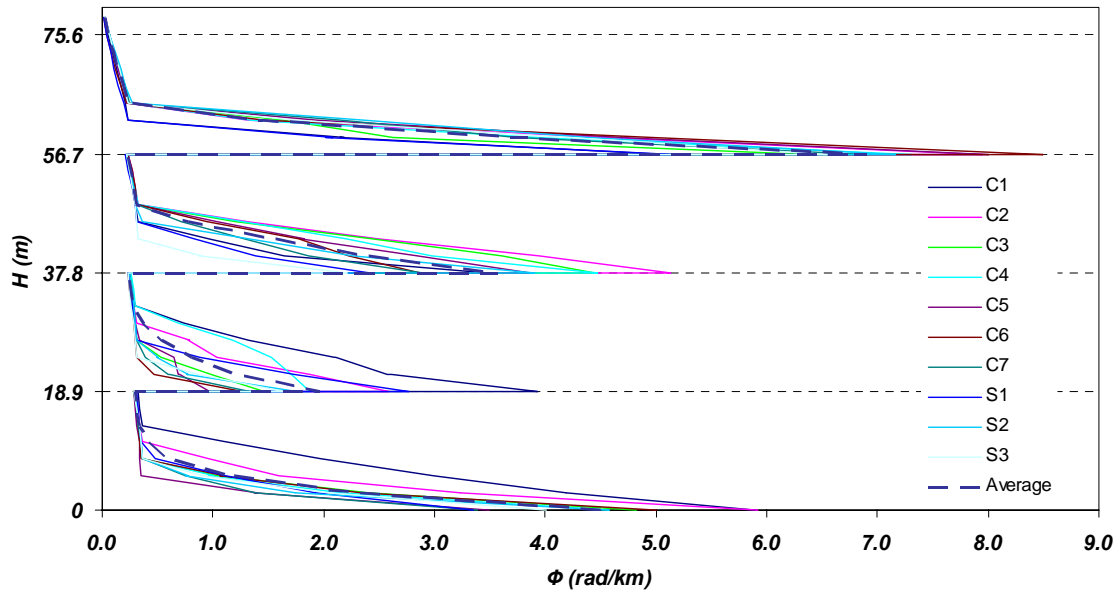


Figure 5.45 Envelope of curvature for NTHA ( $R=5.0$ ,  $SF=2.0$ ).

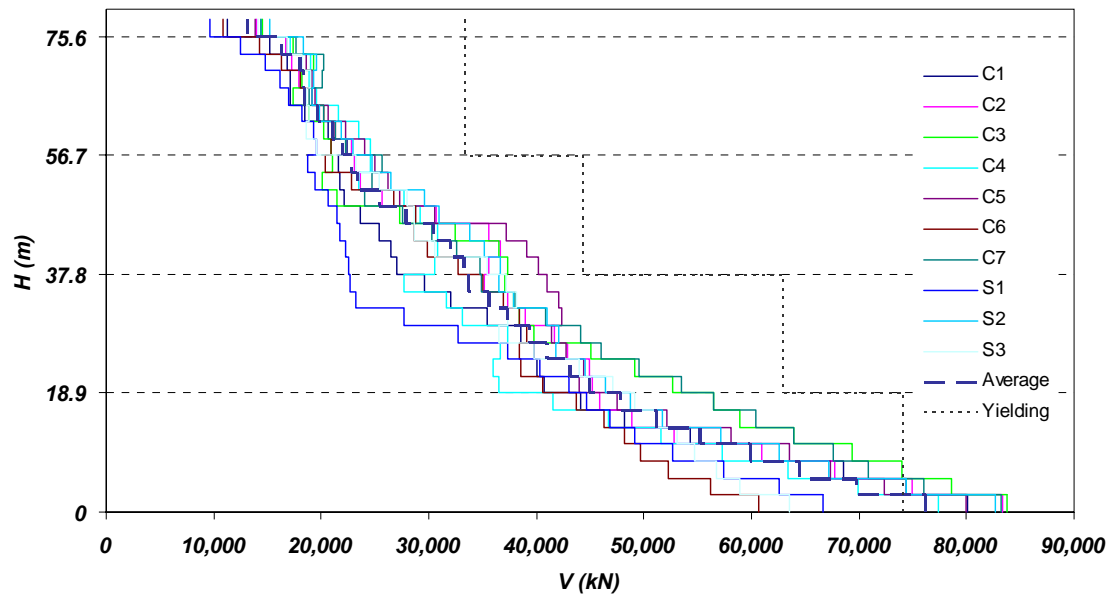


Figure 5.46 Envelope of shear force for NTHA ( $R=5.0$ ,  $SF=2.0$ ).

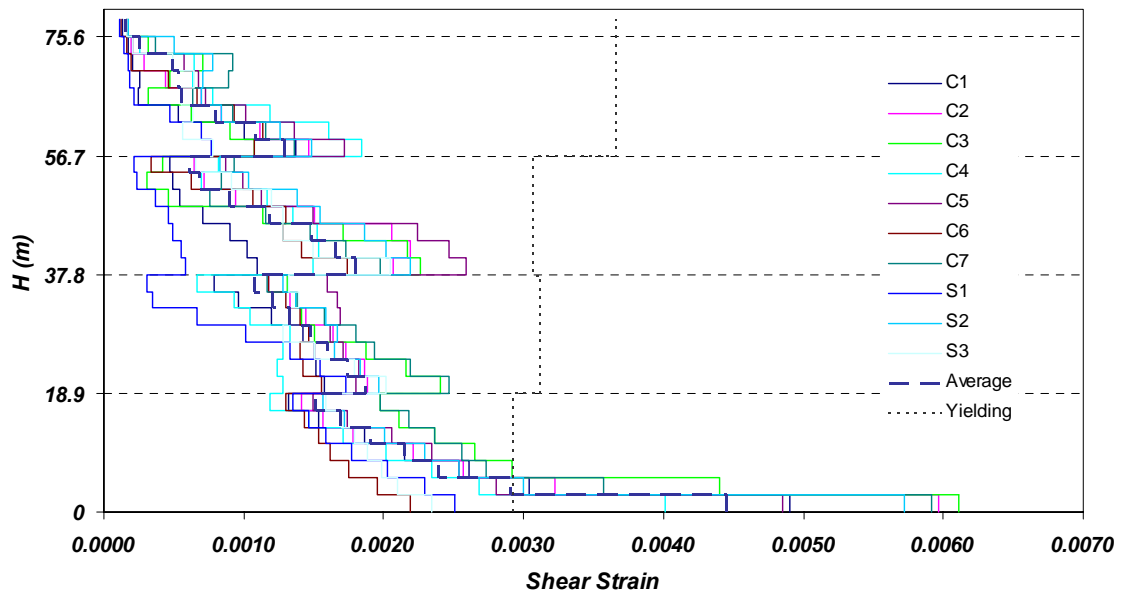


Figure 5.47 Envelope of shear strain for NTHA ( $R=5.0$ ,  $SF=2.0$ ).

Table 5.21 Shear force demand at different sections of wall for  $R=5.0$  and  $SF=2.0$ .

<i>Shear Strength Factor = 2.0 R=5.0</i>				
	<i>Section S1</i>	<i>Section S2</i>	<i>Section S3</i>	<i>Section S4</i>
<i>Cracking (C) (kN)</i>	24,444	21,913	19,381	16,850
<i>Yielding (Y) (kN)</i>	74,074	62,963	44,444	33,333
<i>Failure (F) (kN)</i>	88,889	75,556	53,333	40,000
<i>C-1</i>	80,104	40,771	27,060	22,383
	Y	C	C	C
<i>C-2</i>	83,352	45,221	36,645	22,798
	Y	C	C	C
<i>C-3</i>	83,806	52,662	37,324	20,962
	Y	C	C	C
<i>C-4</i>	77,401	37,274	30,867	24,564
	Y	C	C	C
<i>C-5</i>	79,968	44,343	40,188	23,988
	Y	C	C	C
<i>C-6</i>	60,683	40,575	32,689	21,246
	C	C	C	C
<i>C-7</i>	83,209	53,532	34,758	22,316
	Y	C	C	C
<i>S-1</i>	66,705	43,053	22,534	19,543
	C	C	C	C
<i>S-2</i>	82,620	46,408	36,695	22,898
	Y	C	C	C
<i>S-3</i>	63,592	47,138	35,399	19,582
	C	C	C	C
<i>Mean</i>	76,143	44,994	33,279	21,999
	Y	C	C	C



Figure 5.48 and Fig. 5.49 show the variation of shear strain demand at the base of wall with respect to the increase in shear strength for  $R=3.5$  and  $R=5.0$  respectively. These figures show how the shear strain demand at the base of wall reduced as the wall was strengthened by adding horizontal reinforcement. In Fig. 5.48, the mean shear strain demand was reduced from a shear strain at shear failure of 0.007 to a shear strain at yielding equal to 0.0035 by a 50% increase in the amount of horizontal steel at the base of wall. In Fig. 5.49 the initial value for mean shear strain demand was found to be 0.013 which was significantly larger than the ultimate shear strain of 0.007. Increasing the shear strength of wall over its height by 50% reduced the shear strain demand to 0.007 and a further 50% increase in shear strength resulted in a shear strain at the base equal to 0.0044.

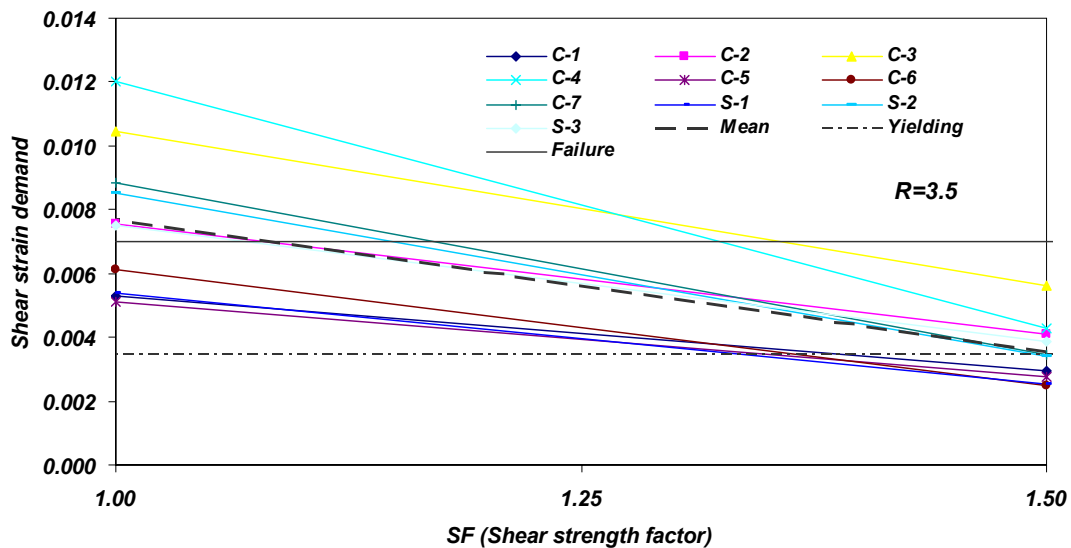


Figure 5.48 Shear strain vs. shear strength factor applied on initial design base shear for  $R=3.5$ .

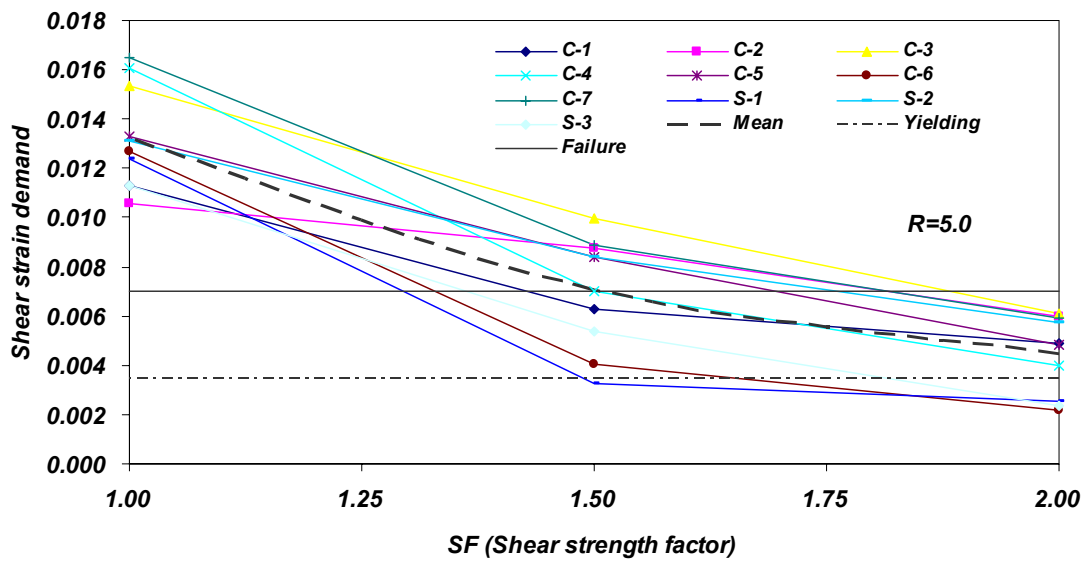


Figure 5.49 Shear strain vs. shear strength factor applied on initial design base shear for  $R=5.0$ .

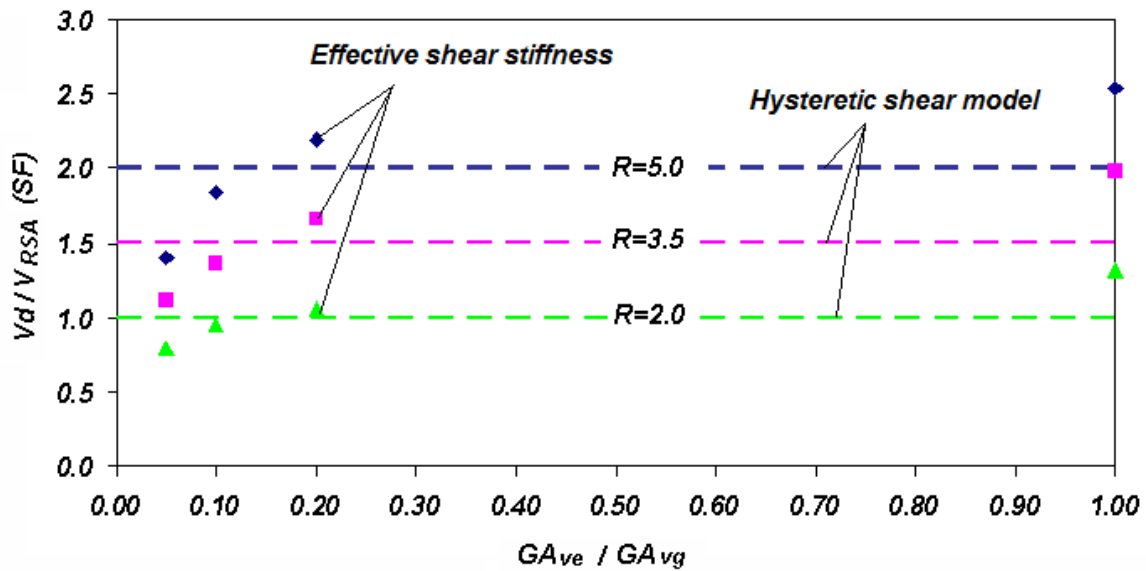


Figure 5.50 Design shear force ratio vs. uniform effective stiffness used in the simplified analysis.

Figure 5.50 shows a comparison of shear force demand at the base of wall based on reduced effective shear stiffness method and nonlinear hysteretic shear model. These two different procedures are described in Sections 5.7 and 5.8 respectively. For design purpose, it is more convenient to avoid sophisticated hysteretic shear models while using

hysteretic models for flexural behaviour that has long been used for NTHA. The complex nonlinear shear model can be accounted for by using the reduced effective shear stiffness,  $G_c A_{ve}$  as a fraction of gross shear stiffness  $G_c A_{vg}$ . In Fig. 5.50 dashed lines present the mean shear strength demand at the base of wall when appropriate hysteretic shear model was used. In the figure, data dots present the shear force demand predicted by simplified effective shear stiffness method. According to results obtained from NTHA using the hysteretic shear model, an acceptable seismic performance at the base of wall was achieved by increasing the horizontal reinforcement. The amount of increase in shear strength to reach an acceptable level of shear strain in the wall was 50% for the case of  $R=3.5$  and 100% for the case of  $R=5.0$ . In the case of  $R=2.0$  wall seismic performance was acceptable for the initially provided strength.

According to the results shown in Fig. 5.50, a reasonable estimate of shear force demand at the base of wall through simplified reduced effective stiffness method can be achieved by choosing a range of effective shear stiffness between  $0.1G_c A_{vg}$  and  $0.2G_c A_{vg}$  for the model of high-rise wall used in this study.

## 5.10 Summary and Conclusions

The scope of this study was to understand the appropriate nonlinear shear response in a high-rise concrete wall subjected to ground motion. The example of wall used in this study was similar to a core wall used as the primary lateral resisting system in high-rise concrete buildings built in the Western Canada and particularly Vancouver city.

The nonlinear flexural behaviour in high-rise walls is relatively well known and use of hysteretic flexural models such as degrading Takeda model (1970) has been long recognized as an effective way of simulating nonlinear flexural behaviour in reinforced concrete walls. Unlike flexural model, a reliable nonlinear shear model for reinforced concrete walls was not developed for many years. Gérin and Adebar (2004) proposed a tri-linear relationship which is appropriate for modeling the complicated stress-strain response for shear. This state-of-the-art model was used to investigate the seismic shear demand in high-rise concrete walls in the present work.

A set of ten ground motions were selected to run the nonlinear time history analyses on a 30-storey model of high-rise shear wall. Ground motions were scaled to match the target design spectrum for Vancouver site class C in a range between  $0.2T_l$  and  $1.5T_l$ . Seven of earthquake records used were selected from the complete set of crustal ground motions for site class C used in ATC-40 (*FEMA-440*) project. Three other earthquakes used in this study include the influence of subduction type earthquakes in dynamic analysis and were selected from recorded accelerations during the Tokachi-Oki event in Japan.

Three different  $R$  factors were used in studying the wall's nonlinear dynamic response.  $R$  was defined as the ratio between linear bending moment to the flexural strength at the base of wall. Wall's shear strength was set to match the shear force demand predicted by response spectrum analysis as the wall strength was reduced from the base toward upper levels. In most of previous studies, the nonlinear flexural behaviour was limited to the plastic hinge at the base while the rest of wall above the plastic hinge zone was assumed to remain elastic. The study on the model of wall showed that the flexural yielding may occur not only at the base but also along the entire height depending on how the flexural strength is set at different elevations. Yielding at mid-

height can cause the shear force demand at upper levels to reduce significantly; therefore it becomes important to model the flexural nonlinearities along the entire height of wall. According to the analysis results, it was observed that modeling the flexural hinge only at the base of wall would result in overestimation of the seismic shear force demand.

The influence of nonlinear shear behaviour was considered in two different ways: First, the shear cracking effect was accounted for in a simplified way by reducing the wall's effective shear stiffness over the entire height in which four different levels of effective shear stiffness were considered as a fraction of gross shear stiffness. The second way was to use the hysteretic shear model for the concrete wall.

According to the obtained results from analysis of the simplified model of 30-storey wall, the shear stiffness reduction can reduce the seismic shear force demand when diagonal cracking is severe. The reduction however was not significant until  $G_c A_{ve} = 0.2 G_c A_{vg}$ .

After considering the reduced shear stiffness in a simple way, a more appropriate hysteretic shear behaviour was considered. Nonlinear response history analysis was performed for different ground motions considering three different  $R$  factors. Localized shear deformations were observed over the wall's height. The shear strains were largest at the base in all cases. Large shear strain at upper levels where there is a sudden change in strength was noticeable.

Increasing the shear capacity of the wall by adding horizontal steel was considered as an alternate solution to improve the wall's performance for the model that was analyzed. This solution lead to a safer design in most of analysis cases , however in one case the shear demand was so high that a very large amount of strength was required in order to prevent shear failure. As the basis for performance based seismic design, the wall should be designed to maintain adequate amount of ductility in regions where localized damage is significant. These regions include the base of wall and the zones where there is sudden change in strength over the wall height.

A comparison between the results obtained from hysteretic shear model and results obtained from the simplified effective shear stiffness model confirmed that a good estimate of shear force demand can be achieved by using effective shear stiffness equal to 20% of the gross shear stiffness for the considered model of high-rise wall in this study.

## **Conclusions and recommendations for future studies**

### **6.1 Introduction**

Concrete walls are a popular seismic force resisting system for high-rise buildings as they provide good drift control and are simple to construct. Linear dynamic (response spectrum) analysis is commonly used to estimate seismic design forces in tall buildings. For many buildings, it is the only method of seismic analysis used. When nonlinear response history analysis is used in design to ensure collapse prevention requirements are satisfied, the results of response spectrum analysis are usually still used to first design the structure for life safety requirements.

Nonlinear response of reinforced concrete walls during strong ground motions is very complicated. Lateral deformation of a high-rise concrete wall under influence of earthquake is due to two distinctive behaviours in flexure and shear. While flexure dominates the overall lateral response of a high-rise shear wall, shear deformations become extremely important at the lower heights of the wall and particularly at levels below the base.

Nonlinear flexural response in a reinforced concrete wall associated with formation of horizontal cracks and yielding of vertical reinforcement is generally a well-known behaviour. The actual moment-curvature backbone for a given reinforced concrete

section can be determined with great accuracy by use of available sectional analysis tools (i.e., Response-2000, Bentz 2000). Furthermore, hysteretic models to simulate nonlinear flexural response that account for degradation in strength and energy dissipation are readily available (i.e., Takeda model 1970).

Unlike flexural response, the shear response in concrete walls is much less known in practice. One of the most significant shortcomings of the previous studies on seismic demand of high-rise concrete walls has been the lack of a reliable nonlinear shear model. Majority of nonlinear analyses for high-rise concrete walls do not account for any nonlinearity in shear at all. Gross shear stiffness ( $G_c A_{vg}$ ) is used for most of nonlinear dynamic analyses performed on concrete walls. Some designers account for diagonal cracking of concrete walls by a reduction in effective shear stiffness used in the model. Shear response of reinforced concrete is often thought to be linear elastic until brittle shear failure occurs as the shear strength is reached. In reality, there are large shear deformations when diagonal cracks form and when reinforcement yields. An appropriate nonlinear shear model that accounts for reduced shear rigidity after diagonal cracking and accounts for the shear strain capacity of a wall beyond yielding of horizontal reinforcement was not readily available until recently.

Gérin and Adebar (2004) presented the nonlinear shear force – shear strain envelope for concrete walls which they validated by comparing with a variety of tests on wall elements subjected to reverse cyclic shear such as those conducted by Stevens et al. (1991). The model accounts for initial uncracked shear rigidity, reduced shear rigidity after diagonal cracking, and shear strain capacity of a wall with yielding horizontal reinforcement. Prior to diagonal cracking, the shear rigidity is equal to  $G_c A_{vg}$ . Gérin (2004) also presented an expression for shear strain capacity of a concrete wall  $\gamma_u$ , which depends on the level of shear stress as a ratio of concrete compression strength and shear strain at yielding.

In the present study the state-of-the-art nonlinear shear model for concrete walls developed by Gérin (2004) was used to investigate three important issues related to seismic design of concrete shear wall buildings. These issues will be described in the following sections.

## **6.2 Summary and conclusions of present study**

All the recommendations presented here are based on the results obtained from analysis of simplified models of high-rise concrete walls which were developed specifically for the purpose of present study. Recommendations presented in this study apply to typical high-rise concrete buildings constructed in Western Canada which are twenty to forty stories tall. The nonlinear static analysis was used in some sections of this research and it is recognized that further study using nonlinear dynamic analysis is required to validate the conclusions based on nonlinear static analysis. Limitations of numerical models used in this work (i.e. two-dimensional analysis) shall be considered in drawing out practical recommendations.

### **6.2.1 Seismic shear demand below ground in high-rise concrete walls**

High-rise concrete shear walls are usually supported below ground by floor diaphragms connected to perimeter foundation walls, which may result in reverse shear forces below the flexural plastic hinge that are much larger than the base shear above the plastic hinge. The magnitude of the wall reverse shear force below ground in tall buildings is dependent on parameters such as foundation wall size, diaphragm stiffness below ground, the developed maximum moment and shear at the base and the degree of wall fixity at footing. Among the parameters influencing the shear reversal, the effect of overturning moment at the base has the most significant influence. The overturning moment at the base of wall is carried by the combined action of diaphragms and the wall section in two different ways. A part of seismic induced overturning moment at the base is carried by the bending behaviour of the wall section below ground and the rest is carried by coupled shear forces developed in diaphragms below ground.

In order to investigate the problem of shear reversal in depth, a simplified model of the core wall and attached diaphragms below ground was developed in Chapter 3 of the presented study. Results obtained from NTHA, showed that the magnitude of the developed reverse shear force at the below-ground levels is dependent mainly on the



magnitude of base moment. The seismic base shear has an inverse influence on the magnitude of the reverse shear force to a lesser extent.

Nonlinear shear response of the core wall at the levels below ground was investigated by using the tri-linear shear model (Gérin 2003) for the shear stress-shear strain backbone. The nonlinear shear performance of the wall section was studied by monitoring the developed shear strain. The developed shear strain at the end of nonlinear analysis was compared with the capacity of concrete section to undergo shear deformations.

The dynamic analysis of the model of wall showed that the maximum developed base moment with a combination of minimum shear at the base will result in the largest reverse shear force at the levels below ground. Based on the findings from nonlinear time history analysis, a simplified nonlinear analysis procedure was developed to investigate the nonlinear shear behaviour at the core wall below ground.

Based on this study, a complete analysis/design procedure was proposed for seismic design of the core walls at levels below ground. In this procedure, all the steps required to design a wall for seismic shear demand is clearly explained. The unique feature of this approach is that it builds up gradually from simplified analysis methods toward more advanced analysis procedures in which the influence of nonlinear shear behavior in reinforced concrete walls has been account for.

The study showed that a large increase in wall dimension is required in order to reach the acceptable level of shear strain in the wall. A more convenient solution to this problem would be allowing the diaphragm below ground to crack during strong earthquakes. Cracking of the diaphragms below ground would reduce the reverse shear force demand significantly. An appropriate design to allow cracking of diaphragm requires ductile detailing of diaphragm at weak joints and avoiding using oversized below-ground slabs in design of high-rise concrete buildings. In practice, when encountering huge shear reversal demand in the high-rises, one needs to keep the diaphragm's thickness below ground as thin as possible to satisfy design requirements. Any flexural damage to the below ground section of wall which would result in a reduction of wall effective stiffness would cause an increase in the shear force demand.

### 6.2.2 Seismic shear force distribution between connected high-rise walls

In high-rise buildings, concrete walls are tied together by rigid floor slabs at numerous levels, which significantly influences the seismic shear force distribution in walls. In Chapter 4 of the present dissertation, nonlinear static analysis was used to examine how nonlinear behaviour of walls influences shear force distribution. Linear, bi-linear and tri-linear models were used to determine both flexural and shear rigidity of the walls. When the traditional bi-linear model is assumed for bending and strength is made proportional to stiffness, the shear forces in all walls increase proportionally until all walls yield at the same displacement. If a more realistic tri-linear bending moment – curvature model is used, the shear force distribution becomes more complex, and the shear force will be higher in some walls than predicted by a linear analysis. When the influence of diagonal cracking is accounted for, the variation from linear analysis becomes greater.

Additional shear deformations due to diagonal cracking significantly influence the displacement when walls yield in flexure. A shorter length wall will actually yield in flexure at a smaller top wall displacement than a longer wall due to the increased shear deformations in the longer wall causing a local redistribution of shear forces near the base of the wall. This phenomenon was subsequently confirmed by Bohl and Adebar (2007) using nonlinear finite element analysis of cantilever concrete shear walls. Adebar et al. (2005) have demonstrated that when high-rise cantilever walls are tied together by rigid floor slabs at numerous levels, all walls yield at the same displacement (the system yield displacement) regardless of wall length. The results presented in this study demonstrate that when diagonal cracking is included in the analysis, all walls do not necessarily yield at the same displacement due to the differing shear deformations; however the results do reaffirm that the yield displacement of the walls is a system phenomenon and is not proportional to wall length.

It is common practice to increase the shear demand proportional to any flexural over-strength using the results from linear analysis. See for example Mitchell and Paultre (2006). The results from the nonlinear analysis summarized in Chapter 4 suggest that this may be unconservative as the increase in shear demand can be larger than the increase in flexural capacity.

According to the results obtained from this study if RSA is used to estimate the seismic shear demand on a system of two-connected walls, the horizontal reinforcement arranged for the base of shorter wall should be extended to a few upper levels (e.g. 25% of lower height should be designed for the shear force demand at the base) so that the weaker wall at the first lower levels above base maintain enough capacity in shear to withstand extra shear demand caused by nonlinear action of the system.

### **6.2.3 Dynamic shear demand on high-rise concrete walls**

Many high-rise concrete wall buildings are designed in North America by using only response spectrum analysis (RSA) to determine the seismic forces acting on the walls such as the bending moment and shear force envelopes. These buildings are designed using ductility force reduction factors of up to 5. Thus the maximum bending moment at the base of the wall determined by RSA is reduced by up to a factor of 5 because the wall has adequate ductility, which means the displacement capacity of the wall after a plastic hinge forms at the base is greater than the displacement demand. The design shear force at the base of the wall has traditionally been reduced from the elastic shear force determined from RSA by the same force reduction factor used to determine the design bending moment.

Nonlinear dynamic analysis has shown that flexural yielding of a cantilever wall does not limit the shear force in the wall. The shear force tends to increase as the magnitude of ground motion is increased. This increase in shear force is often referred to as “dynamic shear amplification”. The dynamic shear amplification factor is the ratio of shear force demand obtained from nonlinear analysis to shear demand obtained from a linear analysis procedure such as pseudo-static procedure or response spectrum analysis. The amplification, which is attributed to the influence of higher modes on a cantilever wall with a hinge at the base, can be as large as 3 or even more.

In Chapter 5, the influence of flexural yielding at multiple locations over the wall's height and influence of shear deformations due to diagonal cracking of the wall were investigated. The results indicate that both significantly reduce the maximum shear force in the wall. It was observed that the flexural yielding can also occur at upper levels

in addition to the base of wall. This phenomenon would cause the shear force demand at upper levels to drop significantly, therefore it is important to model the nonlinear behaviour along the entire height where seismic force demand is large.

The influence of different effective shear stiffness for the wall section was examined through the nonlinear time history analysis. This was done by using different section shear stiffness ( $G_c A_{ve}$ ) as a fraction of gross shear stiffness ( $G_c A_{vg}$ ). According to the obtained results from analyses, using the effective shear stiffness reduces the seismic shear force demand when the diagonal cracking is severe. The reduction was not noticeable for minor diagonal cracking in the wall.

An appropriate nonlinear shear behaviour was not previously used in studying the nonlinear dynamic performance of concrete walls. Based on results from experimental testing of reinforced concrete panels, the state-of-the-art hysteretic shear model (Gérin-2003) was used in order to investigate the effect of higher modes on dynamic response of high-rise concrete walls.

Results obtained from nonlinear dynamic analysis using the hysteretic shear behaviour for the wall indicated localized shear deformation over the wall's height while diagonal cracking occurred over the entire height of wall. The shear strains were largest at the base for all analysis cases and the magnitude of shear strain was noticeable particularly where a sudden change in strength takes place over the height. Yielding in flexure occurred at various heights in addition to the base of wall. Excessive shear deformation of the section beyond yielding of horizontal reinforcement resulted in an undesirable shear failure at the base of wall for some of analysis cases.

Because of the complexity of using the hysteretic shear model, a simplified approach to account for nonlinear shear response was adopted in this study. For simplification of the nonlinear shear response, and based on the current study of the model of high-rise walls,  $G_c A_{ve} = 0.2 G_c A_{vg}$  may be used to account for nonlinear shear behaviour in the sections of high-rise concrete walls above the ground level. This recommendation applies to the walls which possess similar properties to the numerical example used in the present work.

### **6.3 Recommendations for future studies**

The shear-flexure interaction is a complicated phenomenon that needs further investigations through peer studies. The interaction between flexural and shear response in concrete walls has not yet been quantified into a simplified and practical model. Once a reliable model is developed, shear-flexure interaction should be used in future studies to present the most accurate nonlinear model for reinforced concrete walls.

Fiber-section modeling is an appropriate way of considering the flexural-axial force interaction in reinforced concrete walls. This model is able to capture the flexural yielding over the entire height of reinforced concrete walls. The hysteretic model can be separately defined for concrete and steel bar material and the resultant hysteretic model for the component should be verified by the results of experimental testing on reinforced concrete elements.

Using a 3-D model of the high-rise building has several advantages compared to 2-D models. An appropriate 3-D model of the high-rise building accounting for the effect of diaphragms at every level can improve the results obtained from this study further. A 3-D model can also account for the higher modes of vibration associated with torsion. A comprehensive inspection is required to ensure all the assumptions in 3-D modeling are reasonable and lead to a better estimate of seismic response.

## References

- ACI Committee 318, 2005. Building code requirements for structural concrete (ACI 318-05) and commentary (318R-05), American Concrete Institute, Farmington Hills, Mich., 430 pp.
- Adebar, P. and A.M.M. Ibrahim. 2002. Simple non-linear flexural stiffness model for concrete shear walls, *Earthquake Spectra*, EERI, 18(3), 407-426.
- Adebar, P. Mutrie, J. and DeVall, R. 2005. Ductility of concrete walls: the Canadian seismic design provisions 1984 to 2004, *Canadian Journal of Civil Engineering*, 32: 1124 – 1137.
- Aoyama, H. 1987. Earthquake resistant design of reinforced concrete frame building with flexural walls, *Proceedings of second U.S.-Japan workshop on improvement of seismic design and construction practices*, ATC 15-1, Applied Technology Council, Redwood city, CA, pp. 101-129.
- ASCE-2000: FEMA 356 Prestandard and commentary for seismic rehabilitation of buildings, FEMA 356. Washington, DC., Federal Emergency Management Agency (FEMA).
- ATC-55, 2005. FEMA 440 Improvement of nonlinear static seismic analysis procedures, Washington, DC., Federal Emergency Management Agency (FEMA).
- Bevan-Pritchard, G. L., Man, E. and Anderson, D.L. 1983. Force distribution between the core and subgrade structure of high rise buildings subjected to lateral load induced forces, *Proceeding of 4th Canadian conference on Earthquake Engineering*, Vancouver, pp.210-219.
- Blakeley RWG, Cooney RC, Megget LM. 1975. Seismic shear loading at flexural capacity in cantilever wall structures. *Bulletin of the New Zealand National Society for Earthquake Engineering*; 8(4):278–290.
- Bohl, A. and Adebar, P. 2007. Plastic hinge length in high-rise concrete shear walls, 9th Canadian Conference on Earthquake Engineering, Ottawa, June.
- Canadian Standard Association (CSA). 2004. A23.3-05 Design of Concrete Structures, Rexdale, Ontario, Canada.
- Carr, A. J. 2003. Ruaumoko-3D [computer program] (December 2003), Department of Civil Engineering, University of Canterbury, Christchurch, New Zealand.
- Chaallal, O. and D. Gauthier. 2000. Seismic shear demand on wall segments of ductile coupled shear walls, *Canadian Journal of Civil engineering*. Vol. 27, pp: 506-522.

- Collins, M. P. and D. Mitchell. 1991. *Prestressed Concrete Structures*, New Jersey: Prentice Hall.
- Collins, M. P., D. Mitchell, P. Adebar and F. J. Vecchio. 1996. A general shear design method , *ACI Structural Journal* 93, No.1.
- Collins, M. P. 1979. Investigating the stress-strain characteristics of diagonally cracked concrete, *IABSW colloquium on the plasticity in reinforced concrete* 27-34.
- Computers and Structures Inc. 2005. *SAP2000* [computer program]. Version 9.1.0., Berkeley, California.
- Computers and Structures Inc. 2006. *SAP2000* [computer program]. Version 11.1.0., Berkeley, California.
- CSI Analysis Reference Manual. 2006. Computers and Structures Inc, Berkeley, California.
- Dowell, R. K., F. Seible and E. L. Wilson. 1998. Pivot hysteresis model for reinforced concrete members, *ACI Structural Journal* 95 (5), pp. 607–617.
- Eberhard, M. O., and M. A. Sozen. 1993. Behaviour-based method to determine design shear in earthquake-resistant walls, *Journal of Structural Engineering* Vol.119, No. 2:619-639.
- Bentz, E. C. and M. P. Collins. 2000. *Response-2000* [Computer program]: Reinforced concrete sectional analysis using the modified compression field theory. Version 1.0.5.
- Federal Emergency Management Agency. 2000. *Prestandard and Commentary for Seismic Rehabilitation of Buildings*, FEMA 356, Washington, DC.
- Filiatrault, A., Aronco, D. and Tinawi, R. 1994. Seismic shear demand of ductile cantilever walls: a Canadian code prospective. *Canadian Journal of Civil Engineering* Vol. 21,pp: 363-376.
- Gérin, M. 2003. *Reverse-cyclic shear in reinforced concrete elements*, Ph.D. thesis, Department of Civil Engineering, The University of British Columbia, Vancouver, BC.
- Gérin, M. and Adebar, P. 2002. Rational approach to seismic shear in reinforced concrete, *Proceedings of the Seventh U.S. National Conference on Earthquake Engineering* , Boston, CD-ROM.

- Gérin, M. and Adebar, P. 2000. A rational model for reinforced concrete membrane elements subjected to seismic shear, Proceedings of the 12th World Conference on Earthquake Engineering, Auckland.
- Gérin, M. and P. Adebar. 2004. Accounting for shear in seismic analysis of concrete structures, 13th World Conference on Earthquake Engineering., Vancouver, BC, CD Rom Paper No. 1747, 13 pp.1.
- Ghosh, S. K. and Markevicius, V. P. 1990. Design of earthquake resistant shear walls to prevent shear failure, Proceedings of the 4th US National Conference on Earthquake Engineering, Palm Springs, Vol. 2, 905–913.
- Ghosh, S. K. 1992. Required shear strength of earthquake-resistant reinforced concrete shear walls. Nonlinear Seismic Analysis and Design of Reinforced Concrete Buildings, Krawinkler, H. and Fajfar, P., Elsevier: New York.
- Humar, J. L. and Rahgozar, M. A. 2000. Application of uniform hazard spectra in seismic design of multi-storey buildings. Canadian Journal of Civil Engineering; 27:563–580
- IBC 2000. International Building Code, International Code Council, Falls Church, Virginia.
- Kanaan, A. E. and Powell, G. H. 1973. DRAIN-2D: General purpose computer program for dynamic analysis of inelastic plane structures, UCB/EERC Report No.73-6, University of California at Berkeley, Berkeley, CA.
- Keintzel, E. 1984. Ductility requirements for shear wall structures in seismic areas. Proceedings of the 8th World Conference on Earthquake Engineering, Vol. 4, pp. 671–677, San Francisco.
- Keintzel, E. 1992. Advances in the design of shear for RC structural walls under seismic loading. Nonlinear Seismic Analysis and Design of Reinforced Concrete Buildings, Krawinkler, H. and Fajfar, P., Elsevier: New York.
- Kelly, T. 2004. Nonlinear analysis of reinforced concrete shear-wall structures, Bulletin of New Zealand Society for Earthquake Engineering, Vol.37.
- Meyboom, J. 1978. An experimental investigation of partially prestressed orthogonally reinforced concrete element subjected to membrane shear. Department of Civil Engineering , University of Toronto, Ontario, Canada.
- Mitchell, D. and Paultre, P. 2006. Chapter 21: Seismic Design, Concrete Design Handbook, 3rd edition, Cement Association of Canada, pp. 125 -156.



- Moehle, J. P. 1992. Displacement-based design of RC structures subjected to earthquakes, *Earthquake Spectra*, EERI, Vol. 8, No. 3, pp.403-428.
- Moehle, J. P. 2005. Nonlinear analysis for performance-based earthquake engineering, *Journal of the Structural Design of Tall and Special Buildings*, Vol.14, pp: 385-400.
- Naeim, F. and Lew, M. 1995. On the use of design spectrum compatible time histories, *Earthquake Spectra*, Vol. 11, 1, EERI.
- Newmark, N. M. 1959. A method of computation for structural dynamics, *Proc. ASCE* 85, EM3, pp. 67-94
- New Zealand Standards Association. NZS 3101 Code of Practice for the Design of Concrete Structures (Parts 1 & 2) 1982 and 1995. Standards Association of New Zealand, Wellington.
- Panneton, M., P. Leger and R. Tremblay. 2006. Inelastic analysis of a reinforced concrete shear wall building according to the national building code of Canada 2005. *Canadian Journal of Civil Engineering*. Vol. 33, pp: 854-871.
- Paulay, T. 2001. Seismic Response of Structural Walls: Recent Developments, *Canadian Journal of Civil Engineering*, Vol. 28, pp. 922-937.
- Priestley, N. and A. Amaris. 2003. Dynamic amplification of seismic moments and shear forces in cantilever walls, *Proceedings, fib symposium, concrete structures in seismic regions*, Athens, Greece.
- Tremblay, R., Leger, P. and Tu, J. 2001. Inelastic response of concrete shear walls considering P-delta effects, *Canadian Journal of Civil Engineering*. Vol. 28, pp: 640-655.
- Rutenberg, A. and E. Nsieri. 2006. The seismic shear demand in ductile cantilever wall systems and the EC8 provisions, *Bulletin of Earthquake Engineering* Vol. 4, pp: 1-21.
- Rutenberg, A. 2004. The seismic shear of ductile cantilever wall Systems in Multi-storey structures, *Earthquake Engineering and Structural Dynamics*, 33: 881-896.
- Ozcebe, G. and Saatcioglu, M. 1989. Hysteretic shear model for reinforced concrete members, *ASCE Journal of Structural Engineering*, Vol.115, No.1, January, pp.132 - 148.
- Saatcioglu, M. and J. M. Humar. 2003. Dynamic analysis of buildings for earthquake resistant design, *Canadian Journal of Civil Engineering*, 30: 338-359.

- Senevratna, G. D. and H. Krawinkler. 1994. Strength and displacement demands for seismic design of structural walls, Proceedings of 5th U.S. National conference on Earthquake Engineering, Chicago, pp: 181-190.
- Stevens, N. J., M. P. Collins and S. M. Uzumeri. 1991. Reinforced concrete subjected to reversed-cyclic shear: experiments and constitutive model. ACI Journal 88, No. 2:135-146.
- Takeda, T., Sozen , M. A., and Nielsen, N. N. 1970. Reinforced concrete response to simulated earthquakes. ASCE Journal of Structural Division pp.2557-2573.
- Vecchio, F. J. and M. P. Collins. 1982. The response of reinforced concrete to in-plane shear and normal stresses, 82-03. Department of Civil Engineering, University of Toronto.
- Villani, D. R. 1995. Reinforced concrete subjected to cyclic Loads: A pilot study. BASc thesis, Department of Civil Engineering, University of Toronto, Ontario.
- Wallace, J. W. 1994. New methodology for seismic design of RC shear walls, Journal of Structural Engineering, ASCE Vol.120, No. 3: 863-884.

# Appendices

## Appendix A: Ground motions used for dynamic analysis

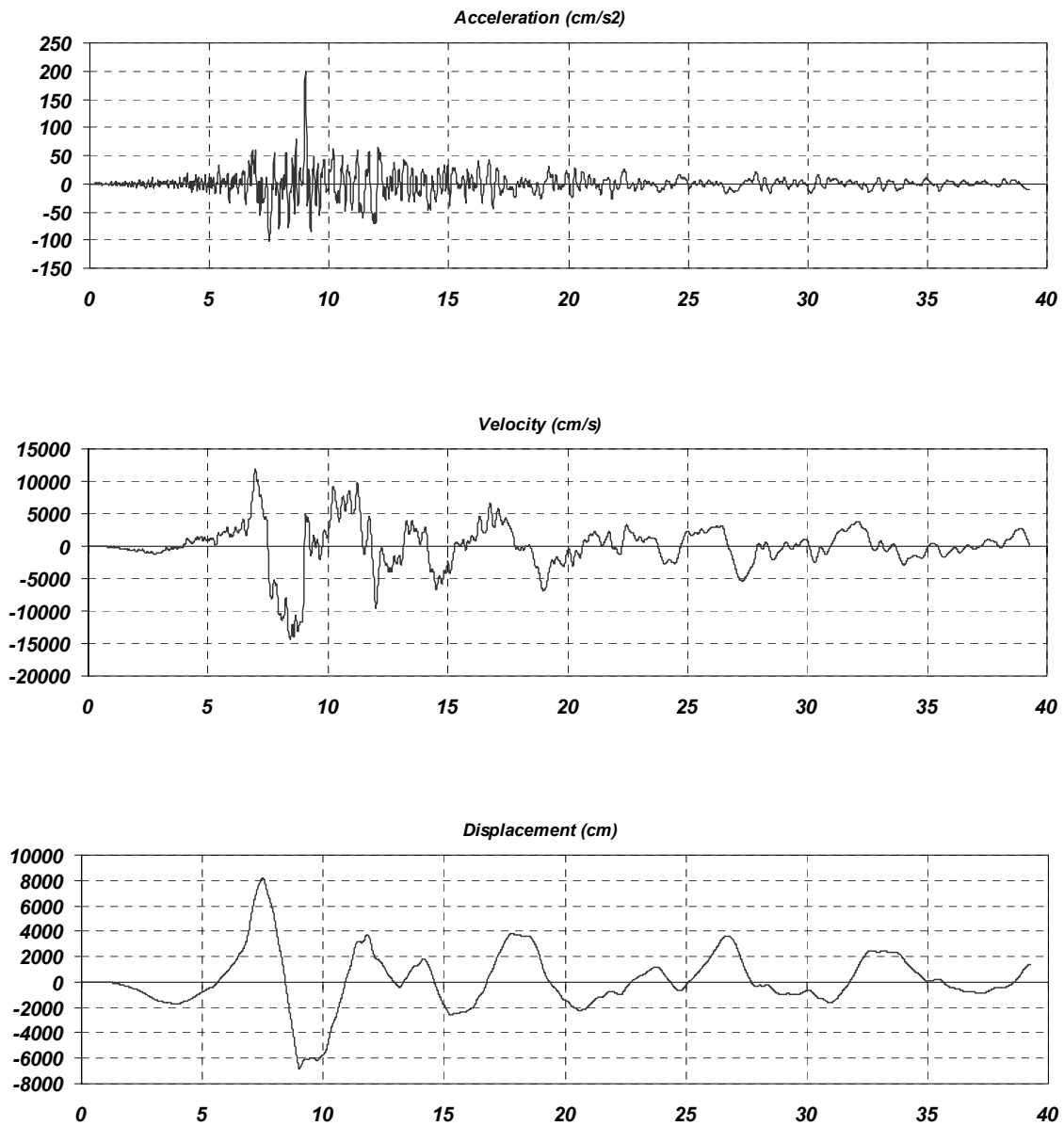


Figure 1: Acceleration, velocity and displacement for Crustal record C-1.

## Appendix A: Ground motions used for dynamic analysis

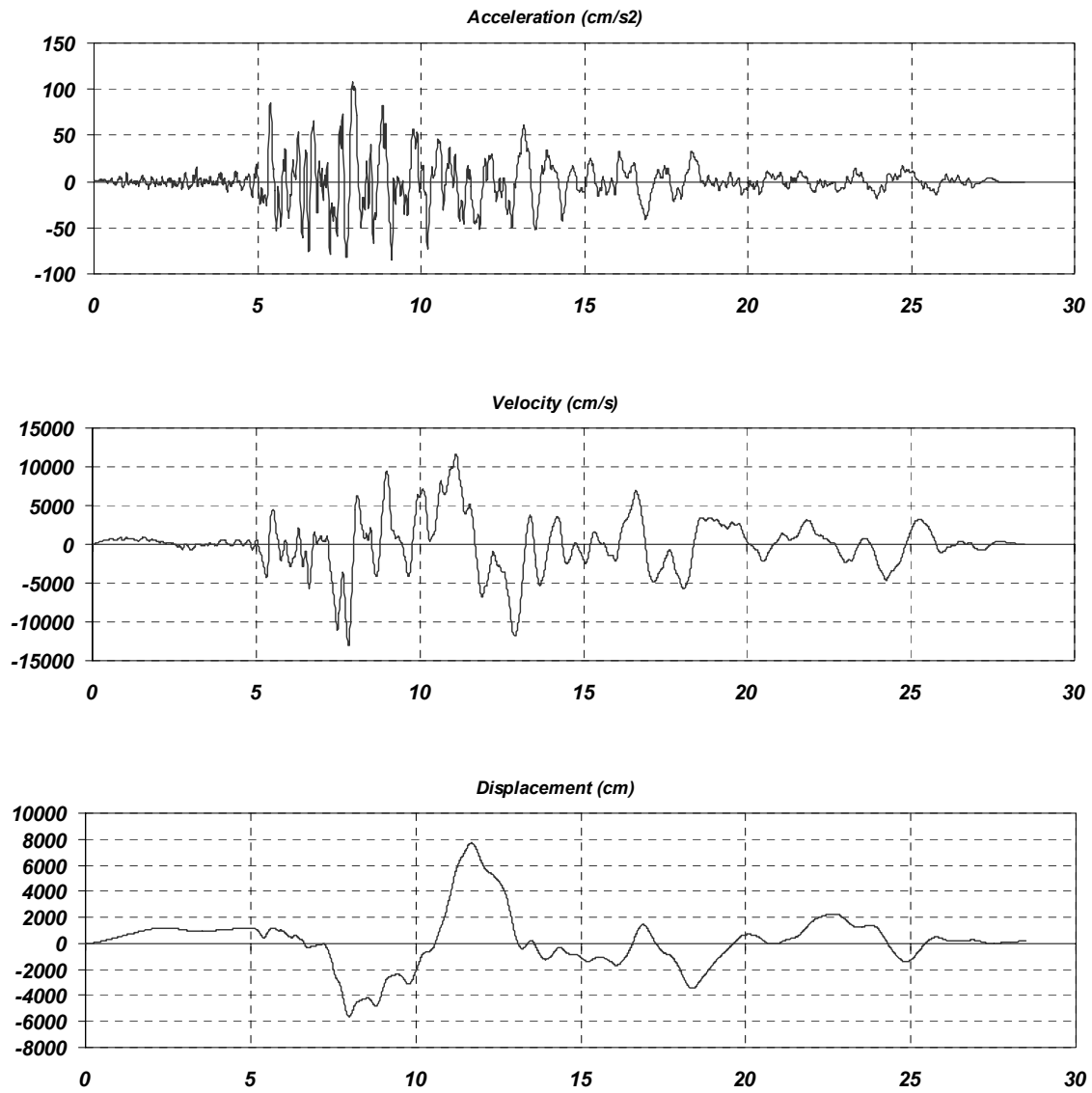


Figure 2: Acceleration, velocity and displacement for Crustal record C-2.

## Appendix A: Ground motions used for dynamic analysis

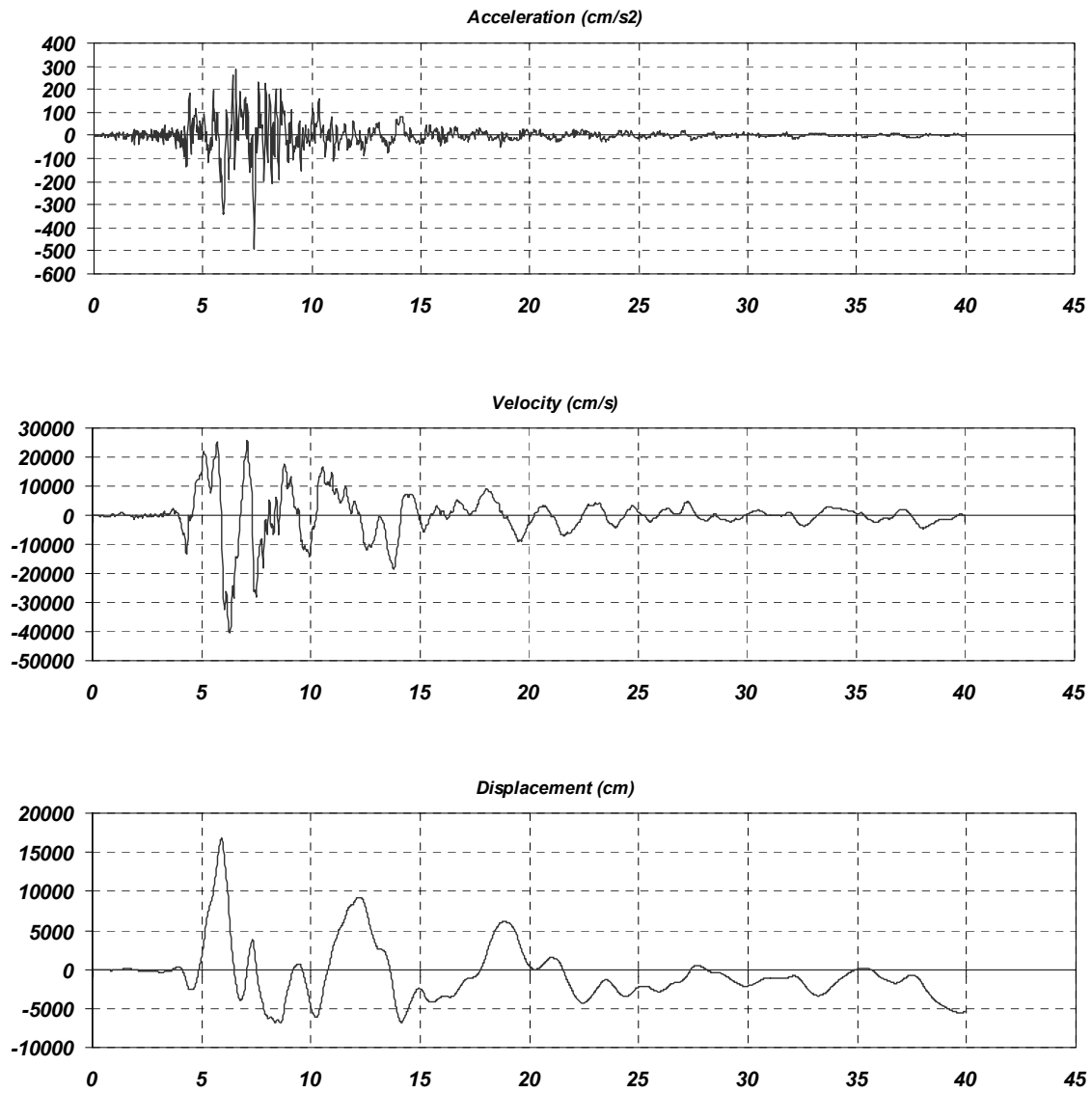


Figure 3: Acceleration, velocity and displacement for Crustal record C-3.

## Appendix A: Ground motions used for dynamic analysis

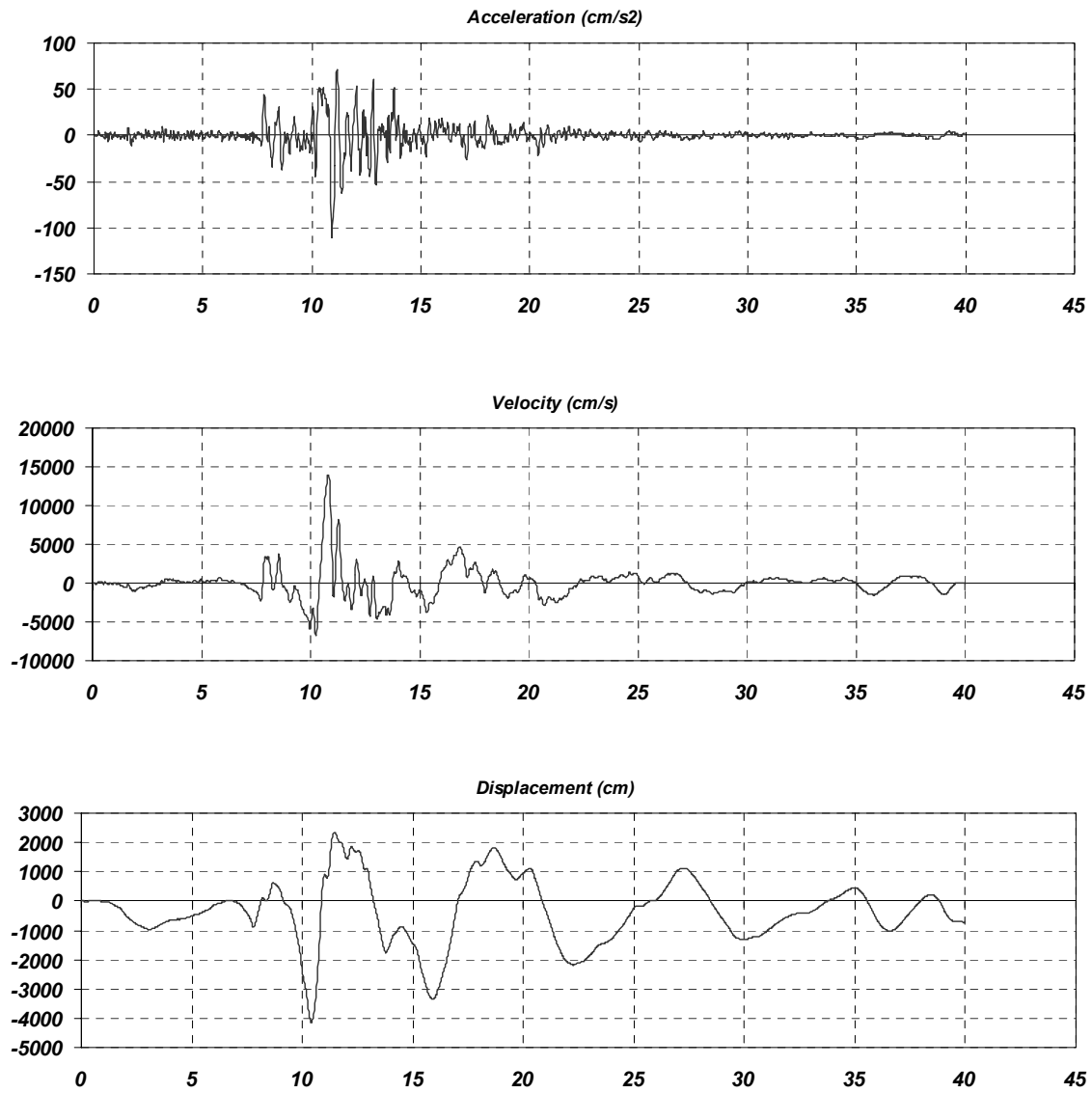


Figure 4: Acceleration, velocity and displacement for Crustal record C-4.

## Appendix A: Ground motions used for dynamic analysis

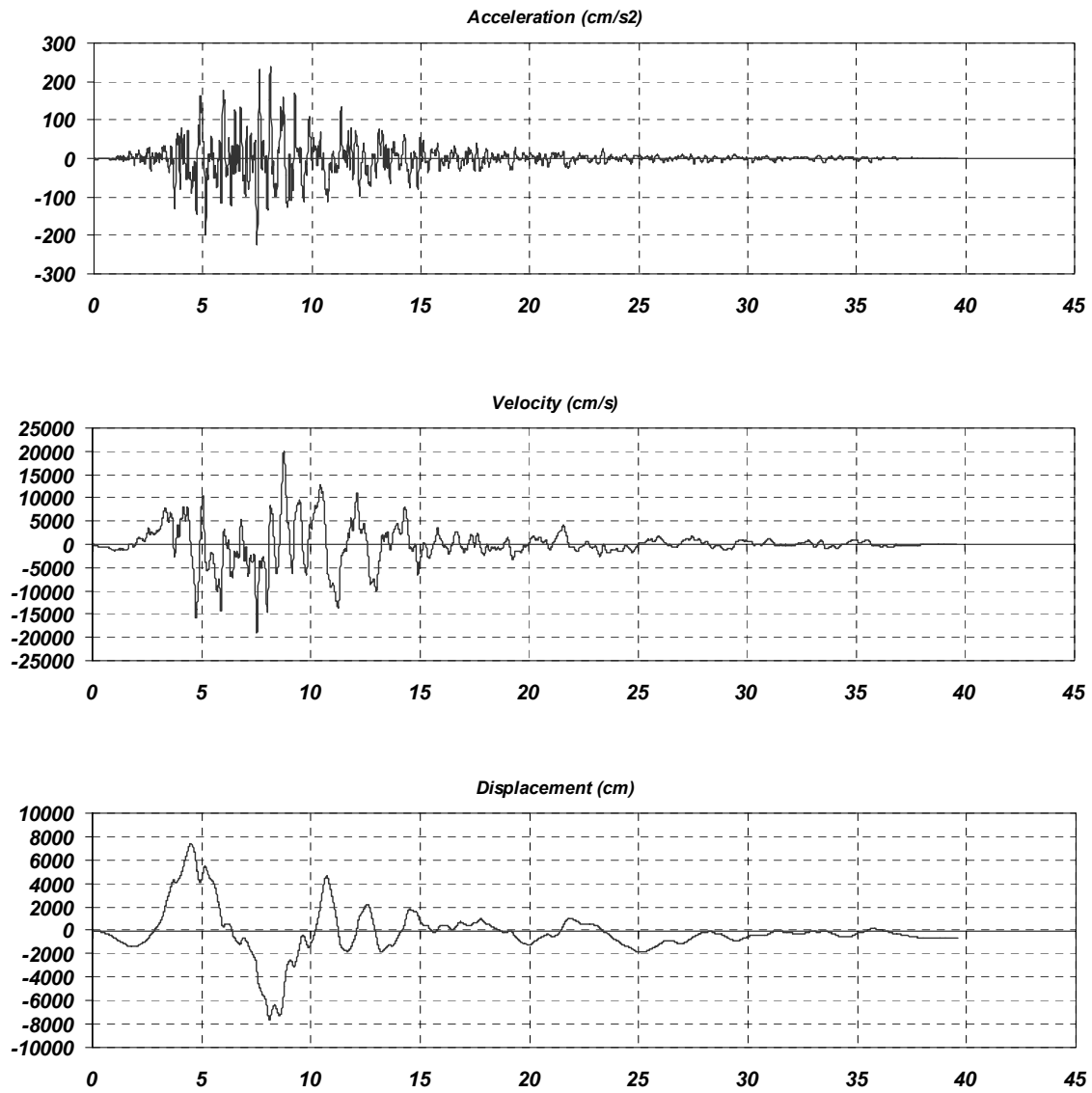


Figure 5: Acceleration, velocity and displacement for Crustal record C-5.

## Appendix A: Ground motions used for dynamic analysis

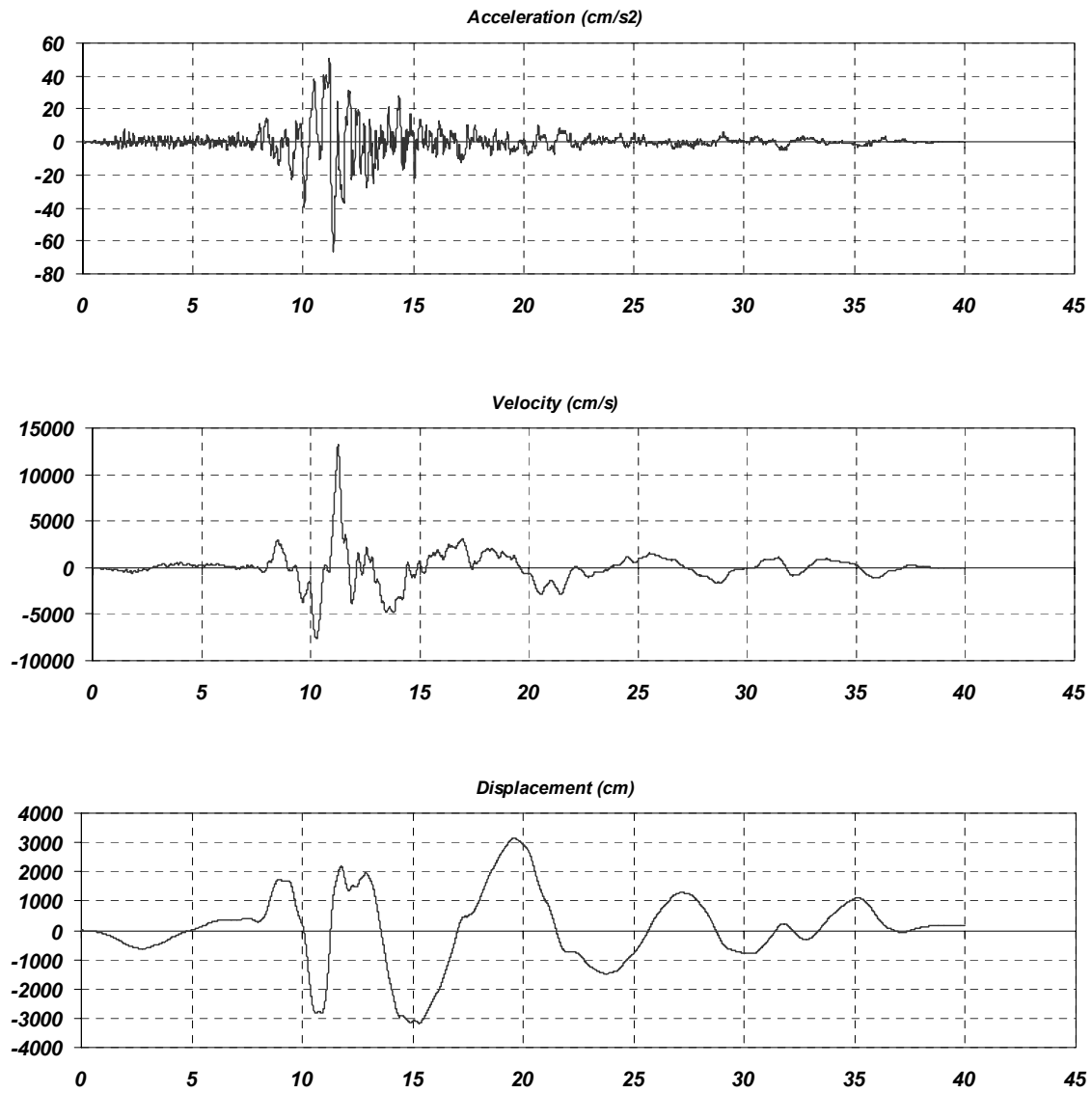


Figure 6: Acceleration, velocity and displacement for Crustal record C-6.



Appendix A: Ground motions used for dynamic analysis

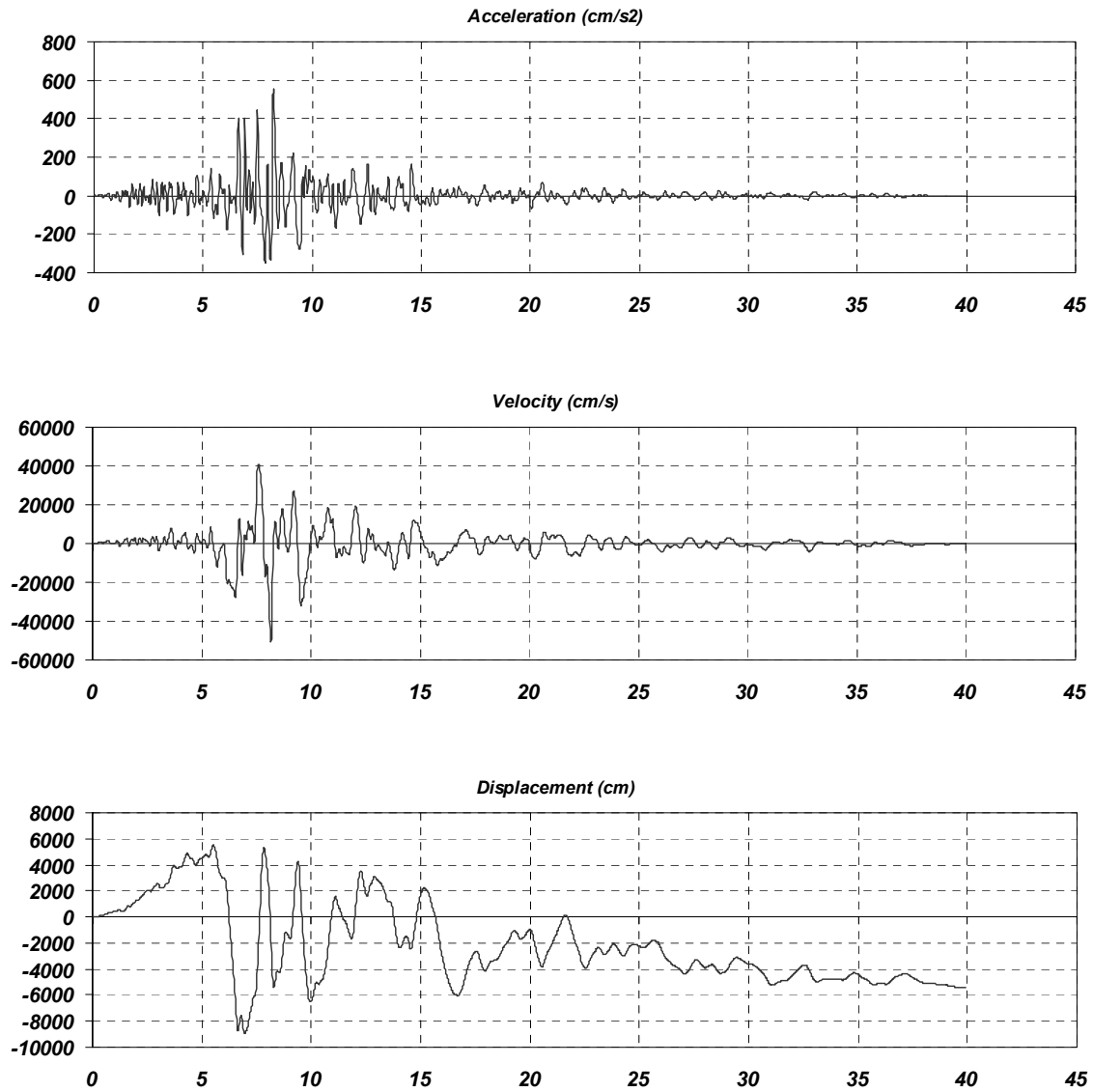


Figure 7: Acceleration, velocity and displacement for Crustal record C-7.

## Appendix A: Ground motions used for dynamic analysis

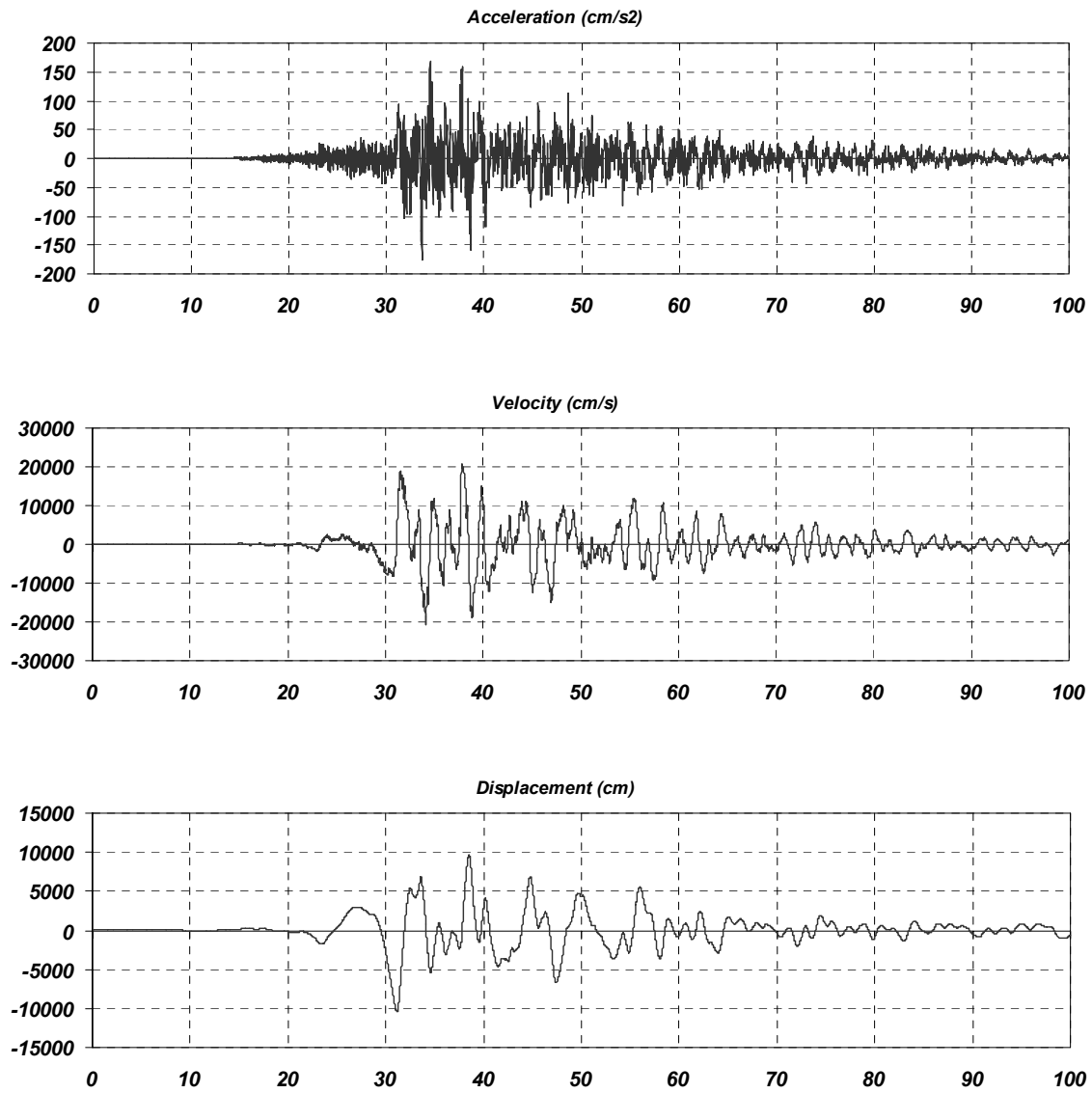


Figure 8: Acceleration, velocity and displacement for Crustal record S-1.

## Appendix A: Ground motions used for dynamic analysis

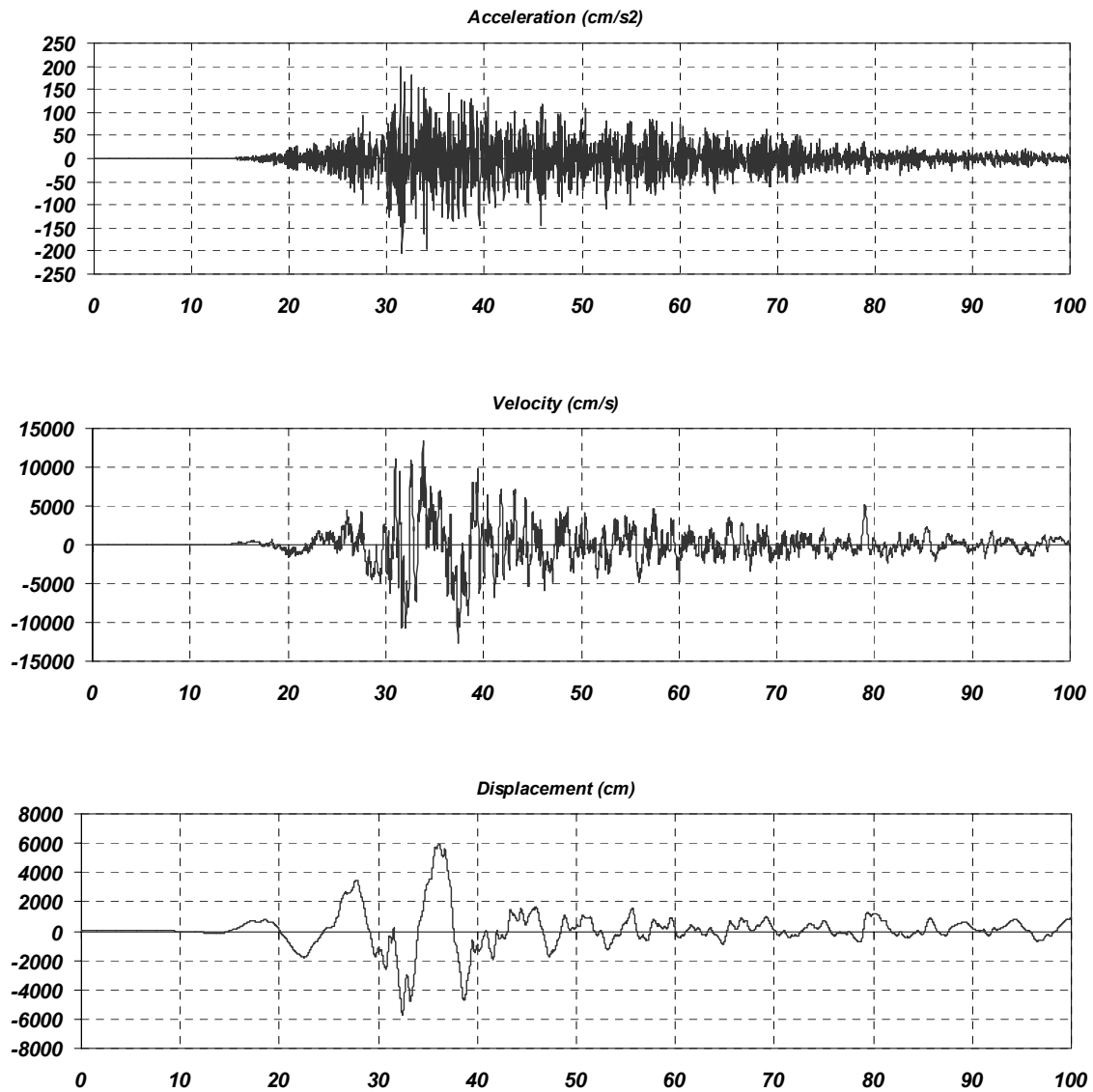


Figure 9: Acceleration, velocity and displacement for Crustal record S-2.

## Appendix A: Ground motions used for dynamic analysis

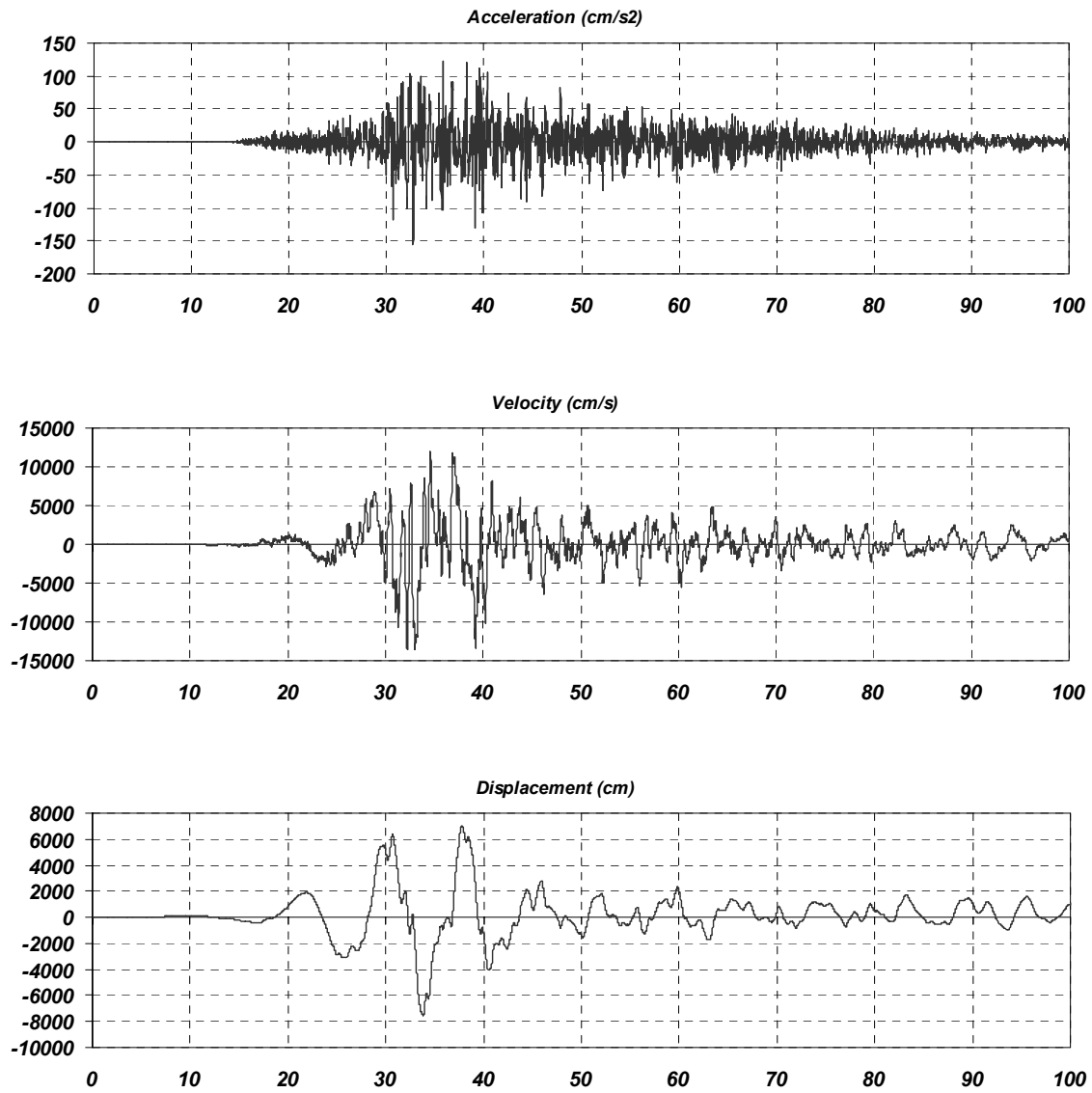
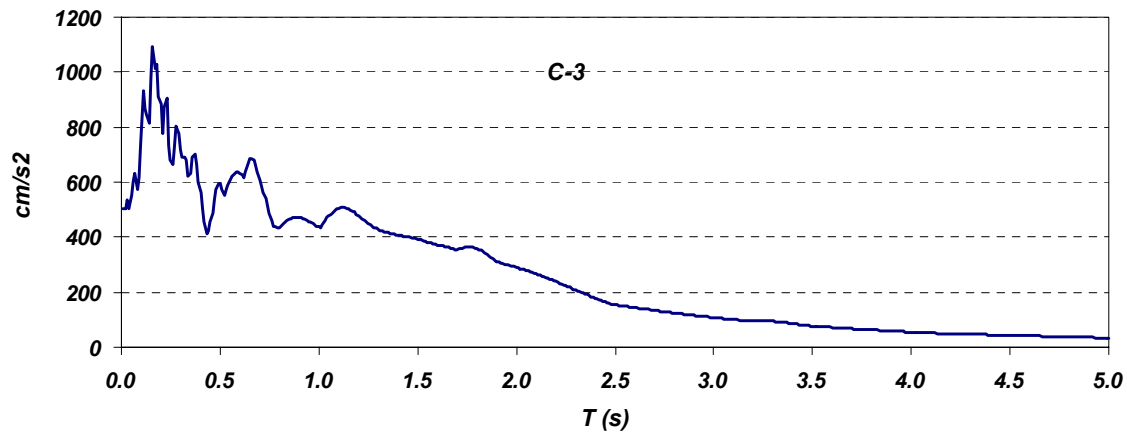
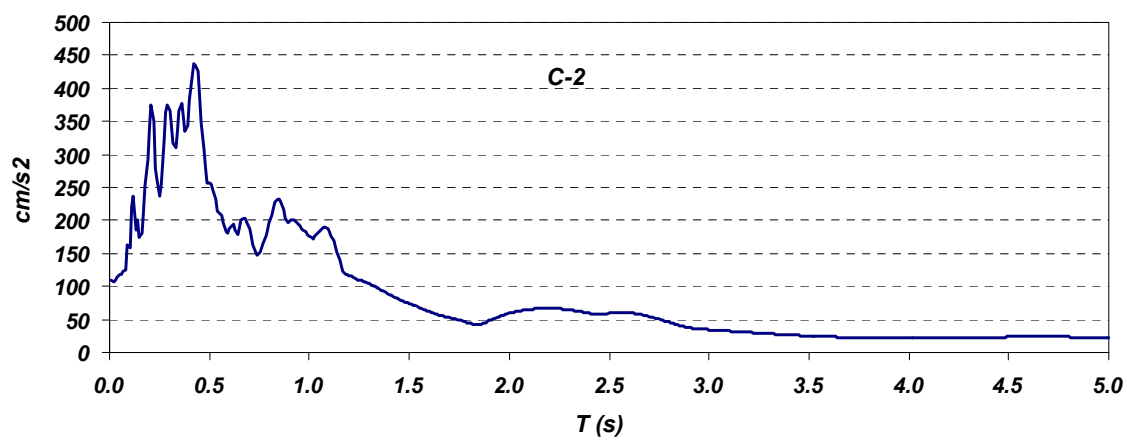
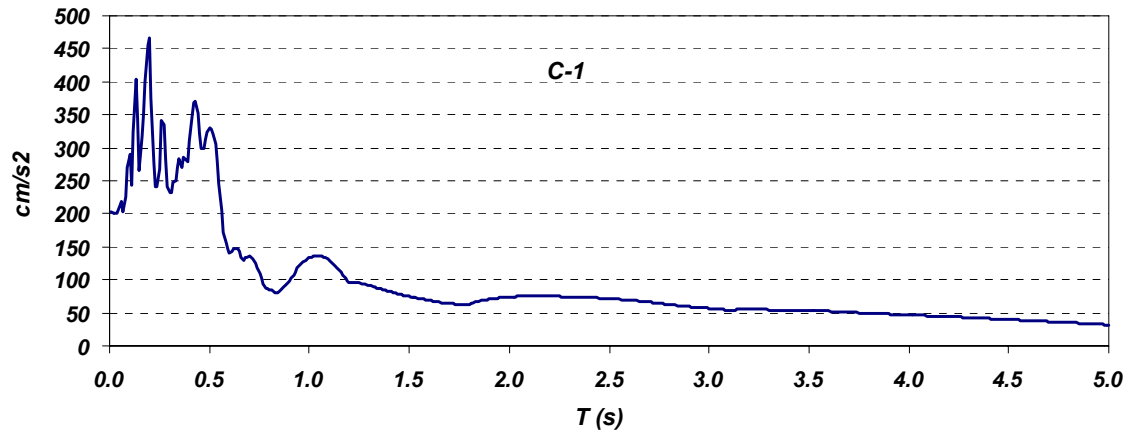


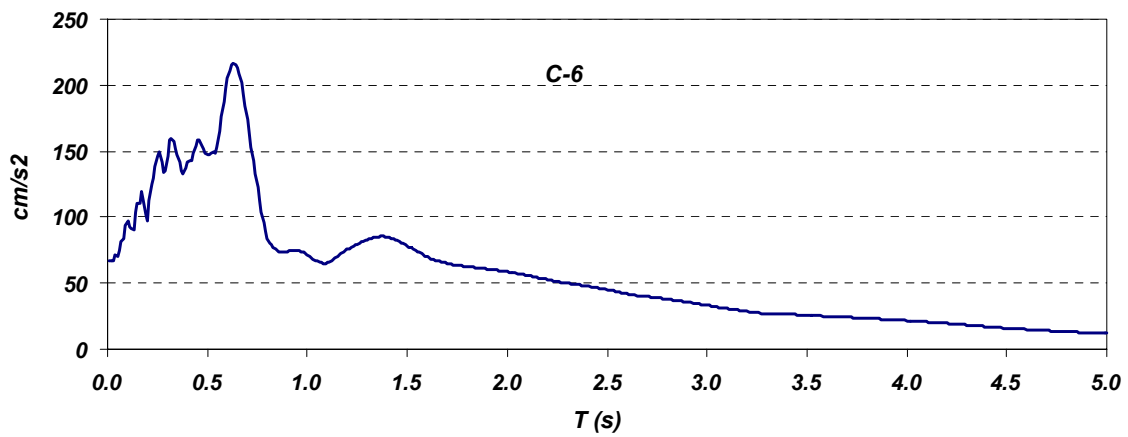
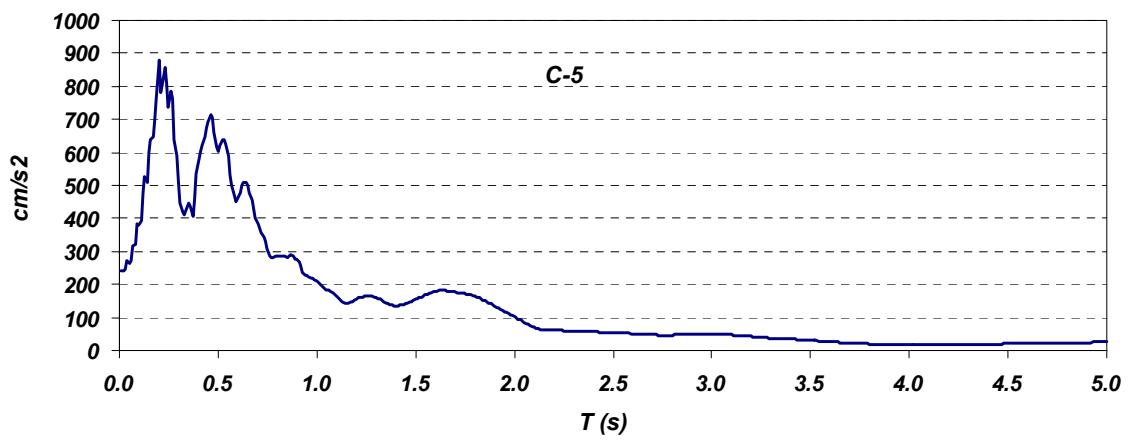
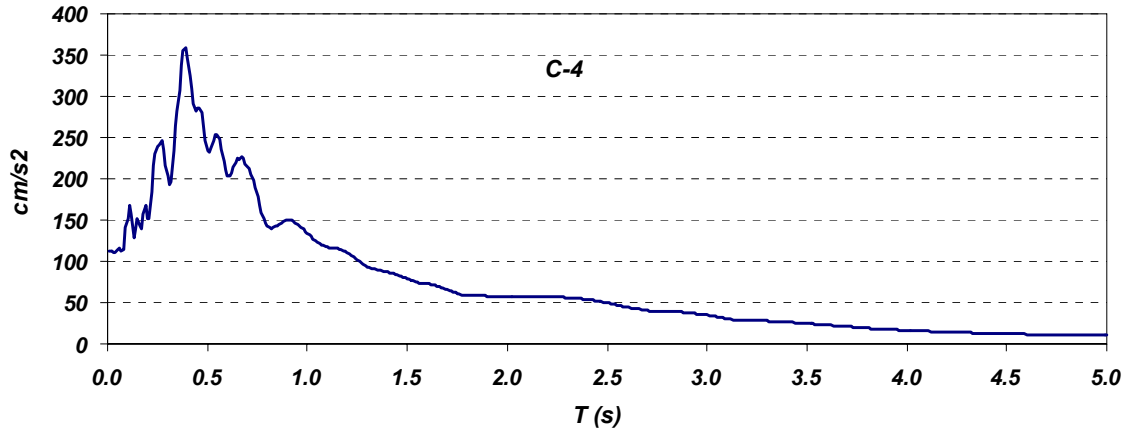
Figure 10: Acceleration, velocity and displacement for Crustal record S-3.

**Appendix B: Response spectra for selected ground motions**



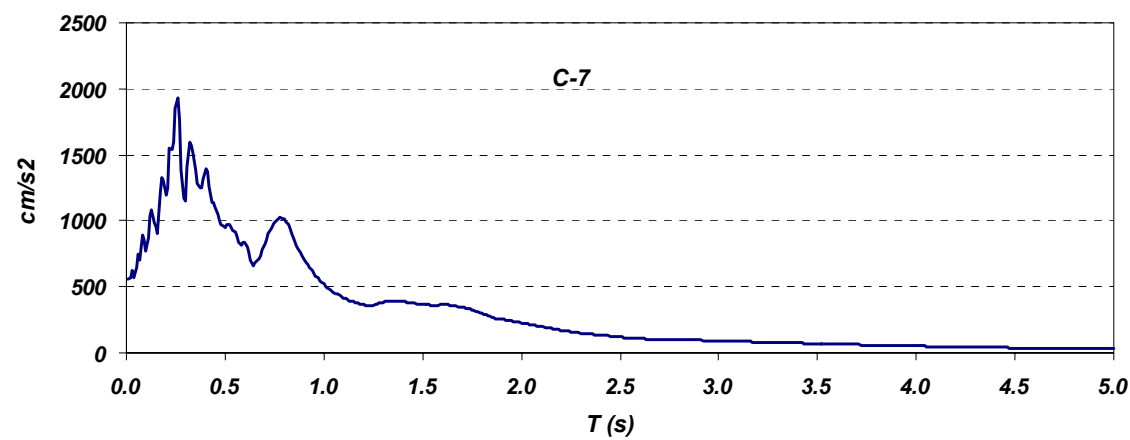
5% damped response spectra for records C-1, C-2 and C-3.

## Appendix B: Response spectra for selected ground motions



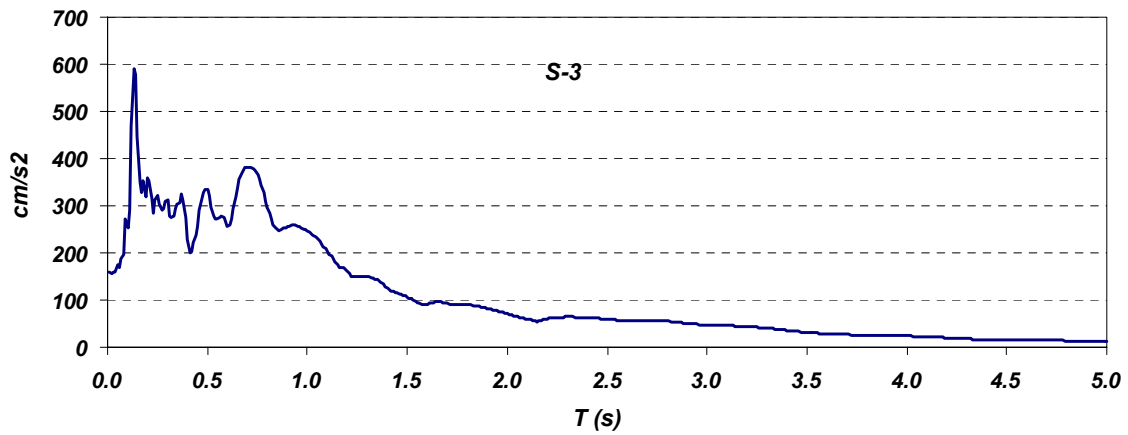
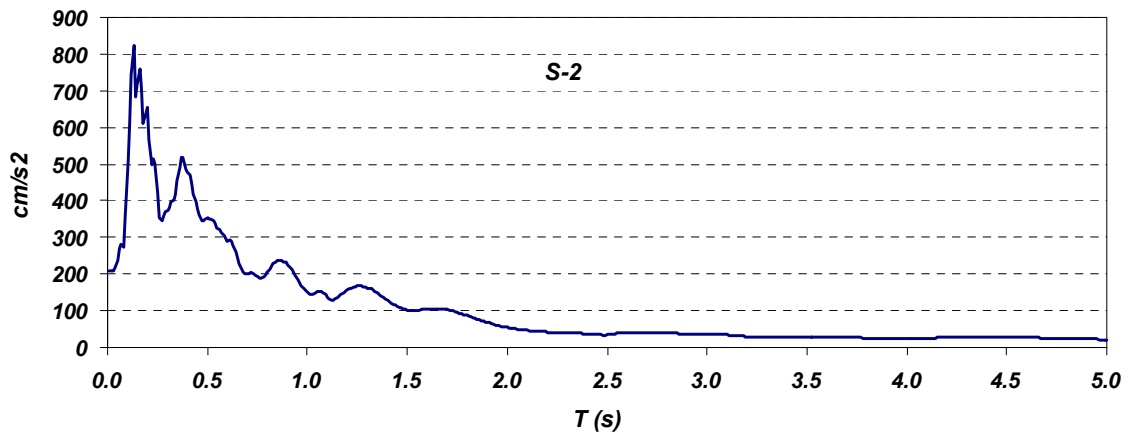
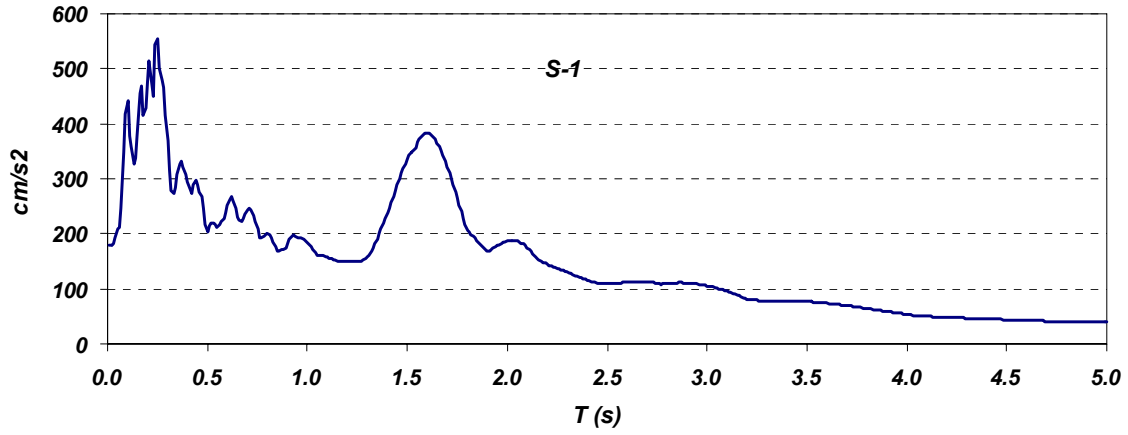
5% damped response spectra for records C-4, C-5 and C-6.

Appendix B: Response spectra for selected ground motions



5% damped response spectra for records C-7.

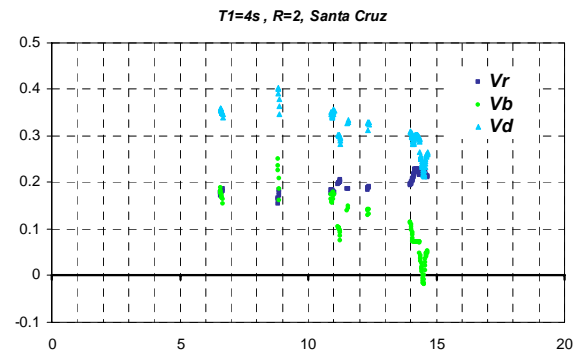
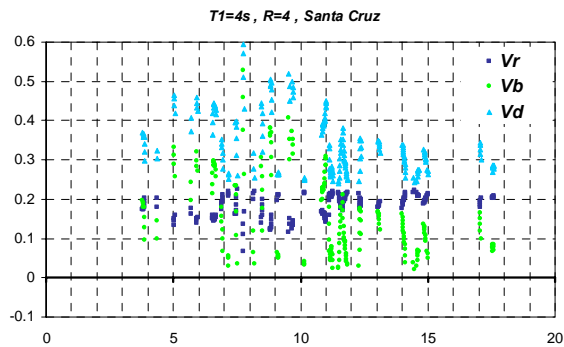
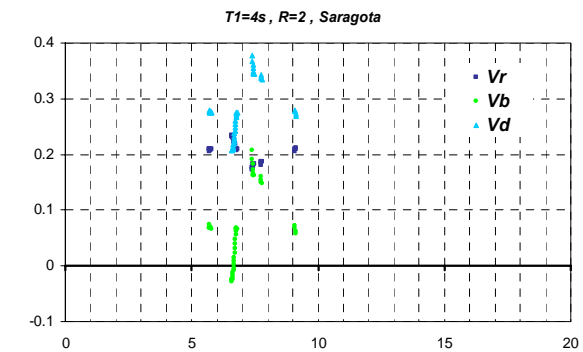
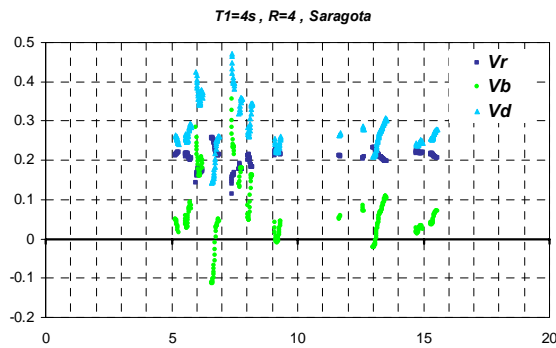
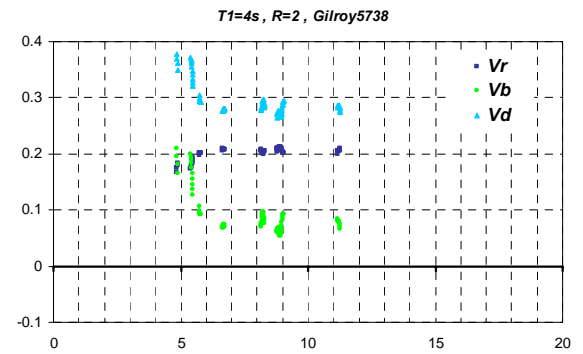
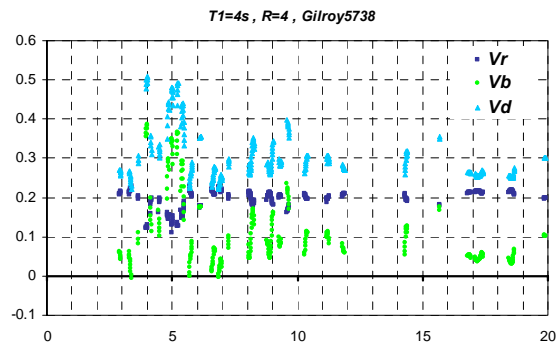
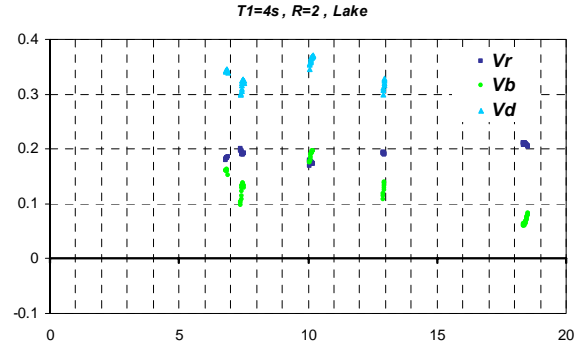
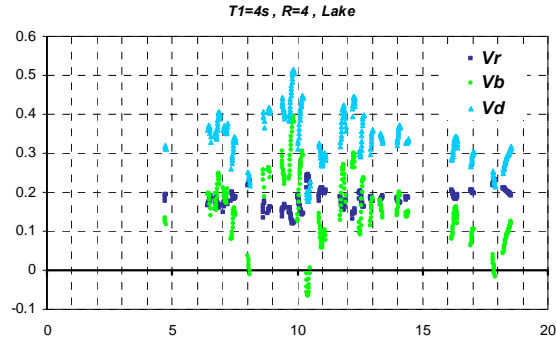
## Appendix B: Response spectra for selected ground motions

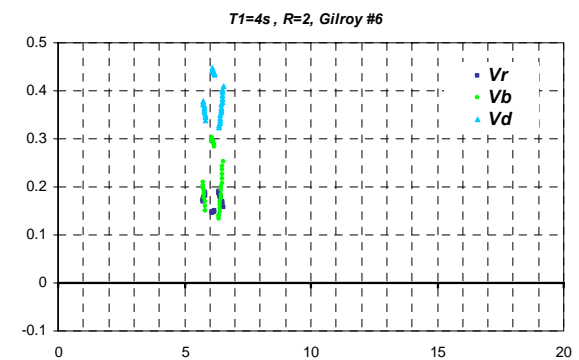
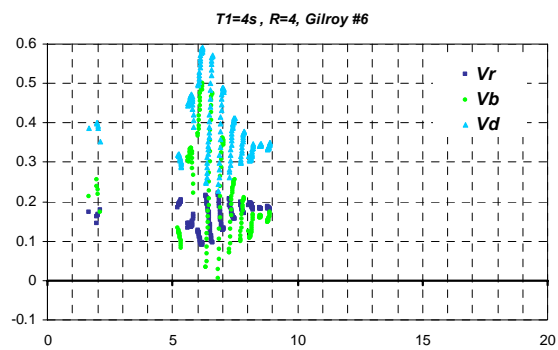
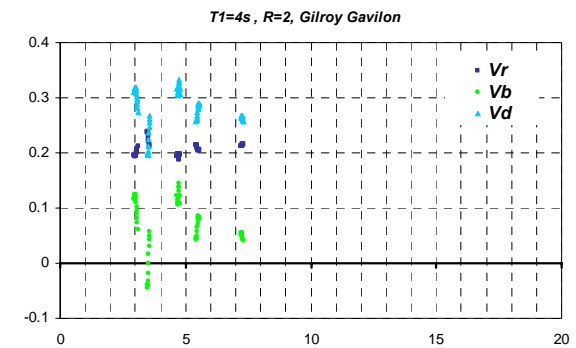
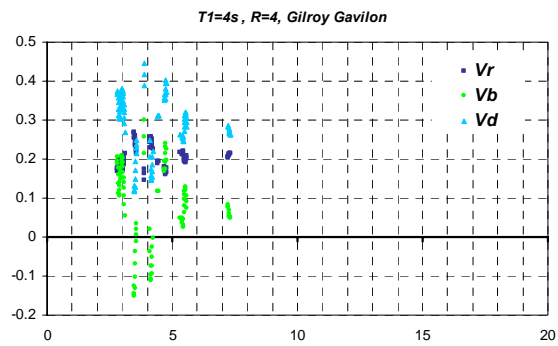
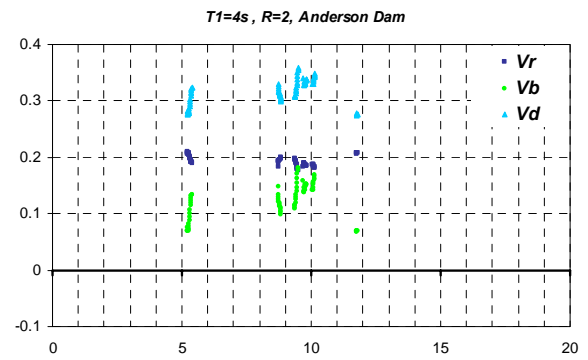
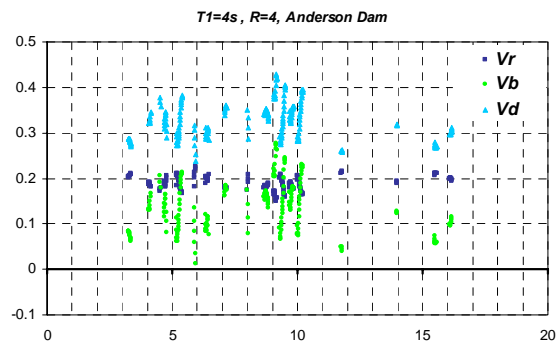
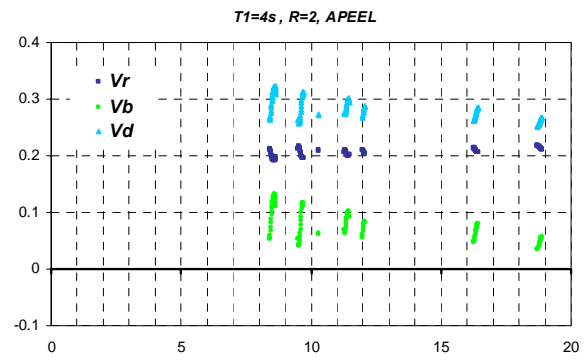
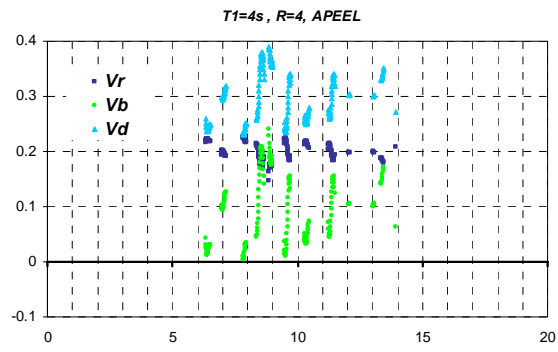


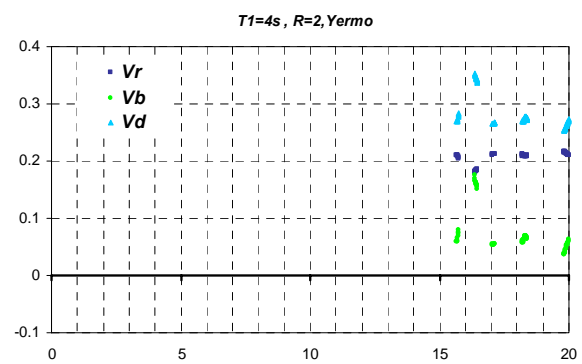
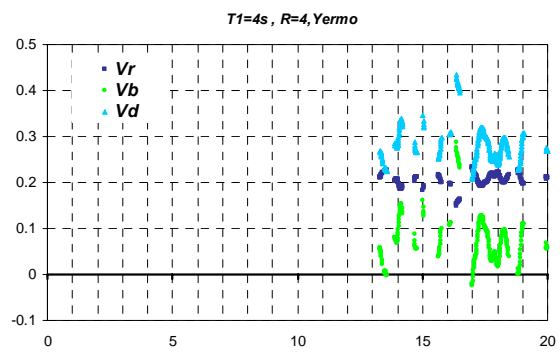
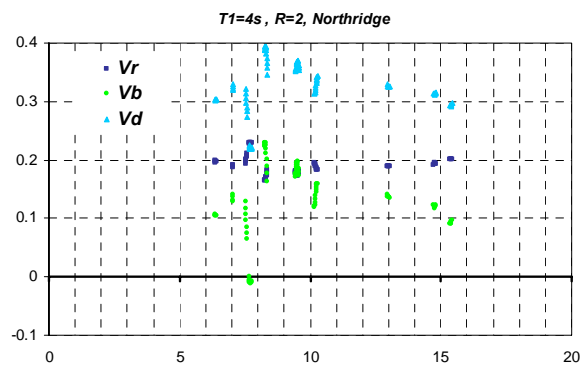
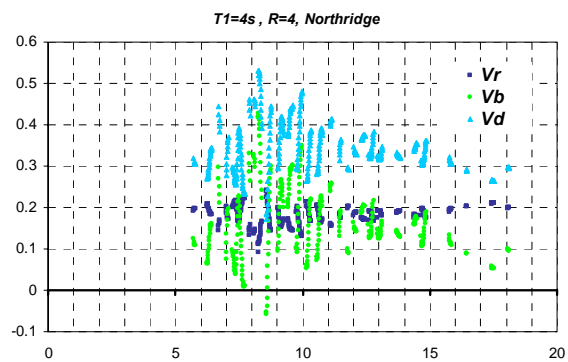
5% damped response spectra for records S-1, S-2 and S-3.

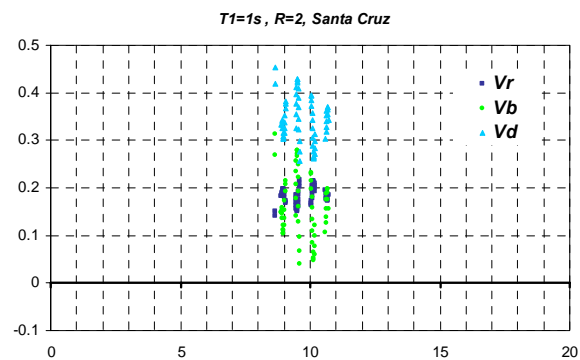
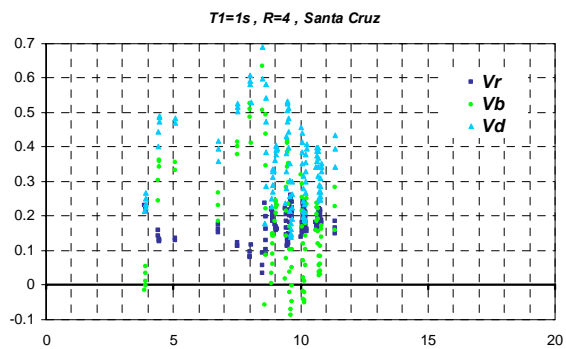
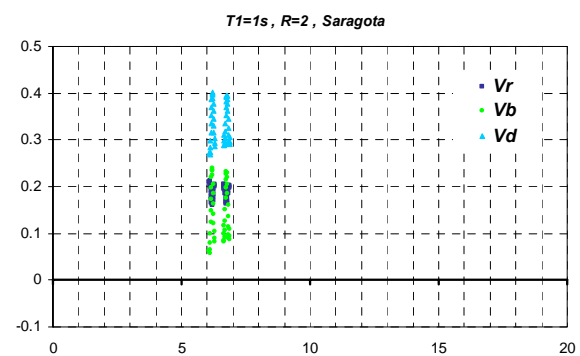
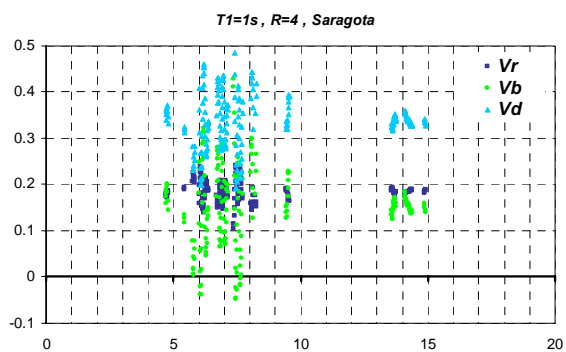
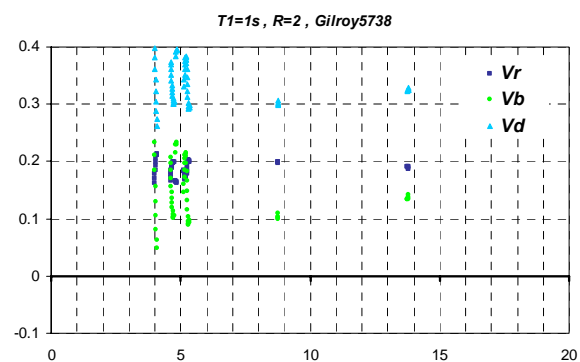
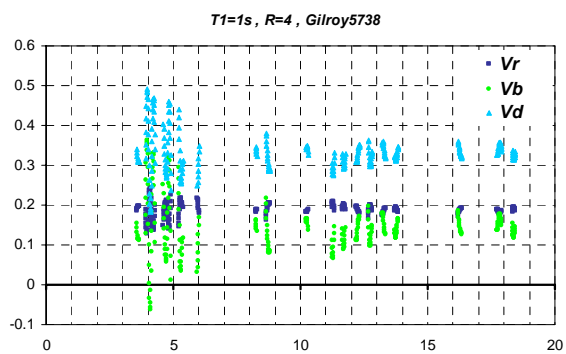
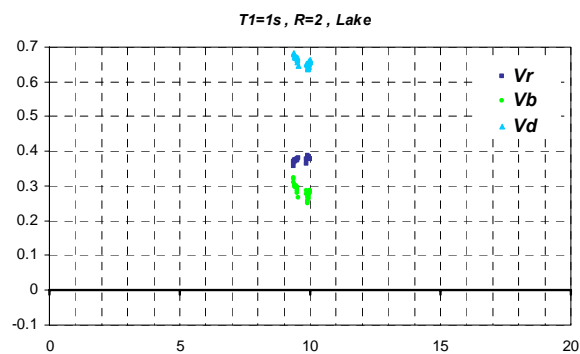
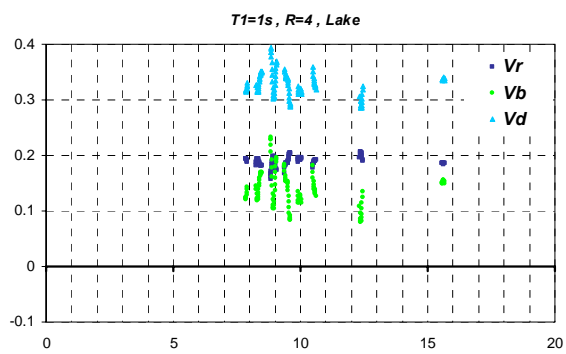


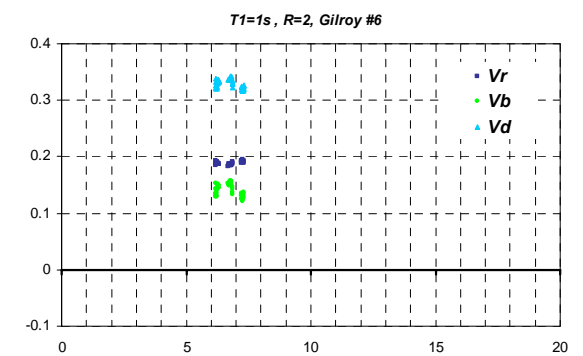
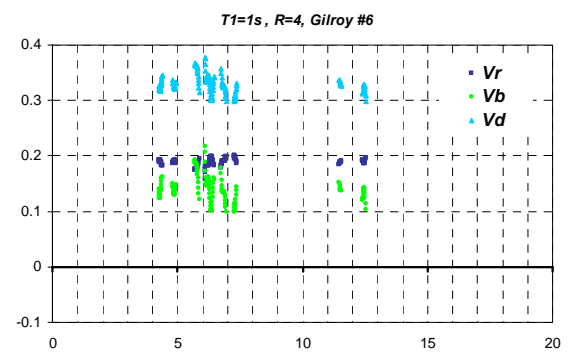
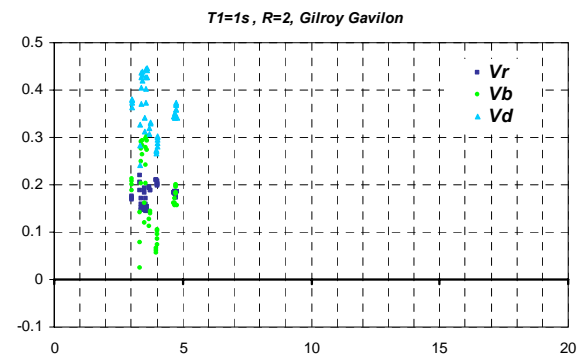
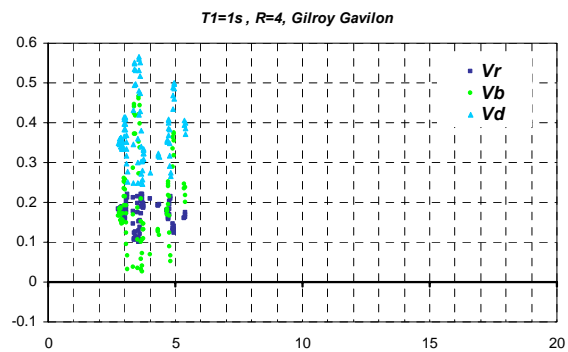
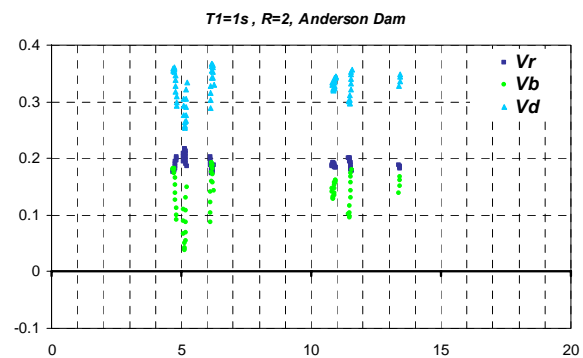
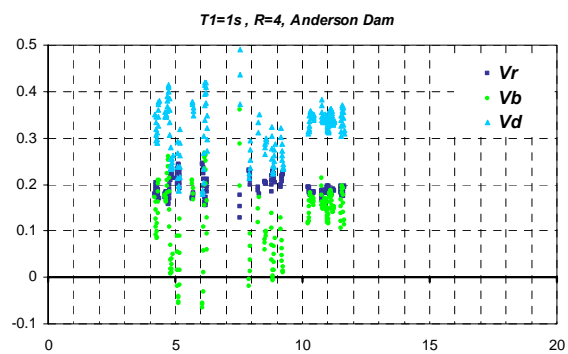
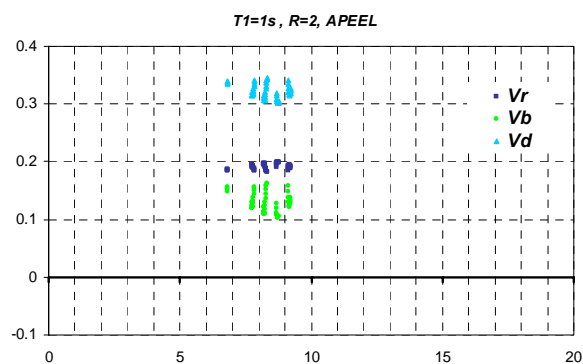
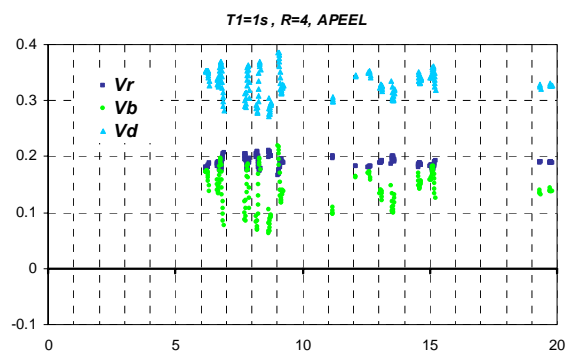
## Appendix C: Nonlinear time history analysis results (See Section 3.3.2)

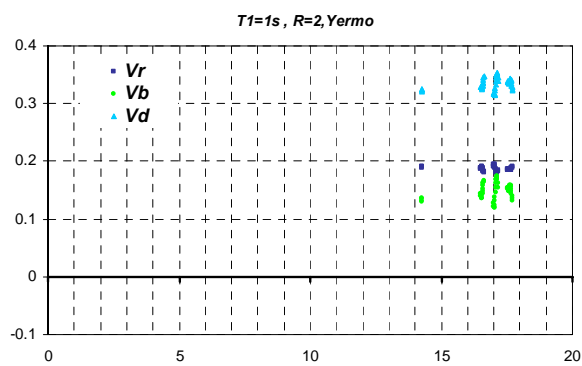
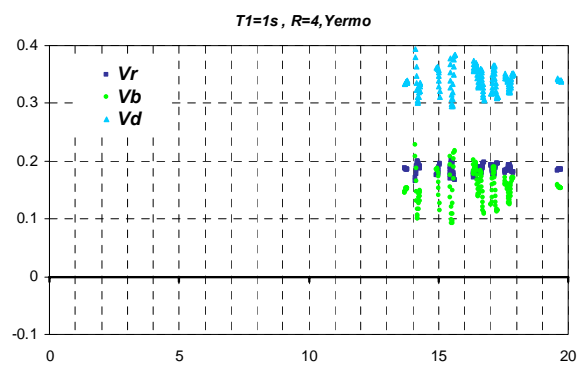
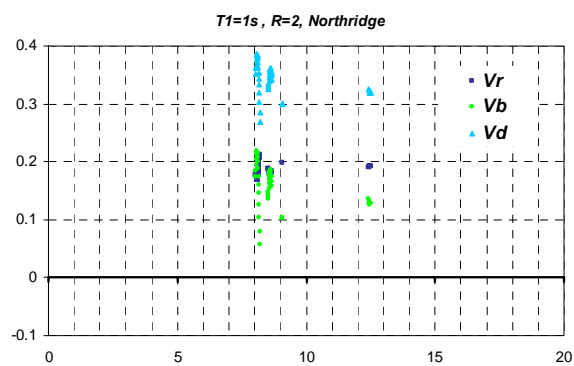
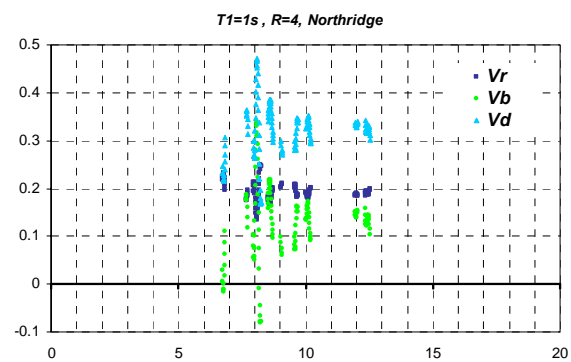




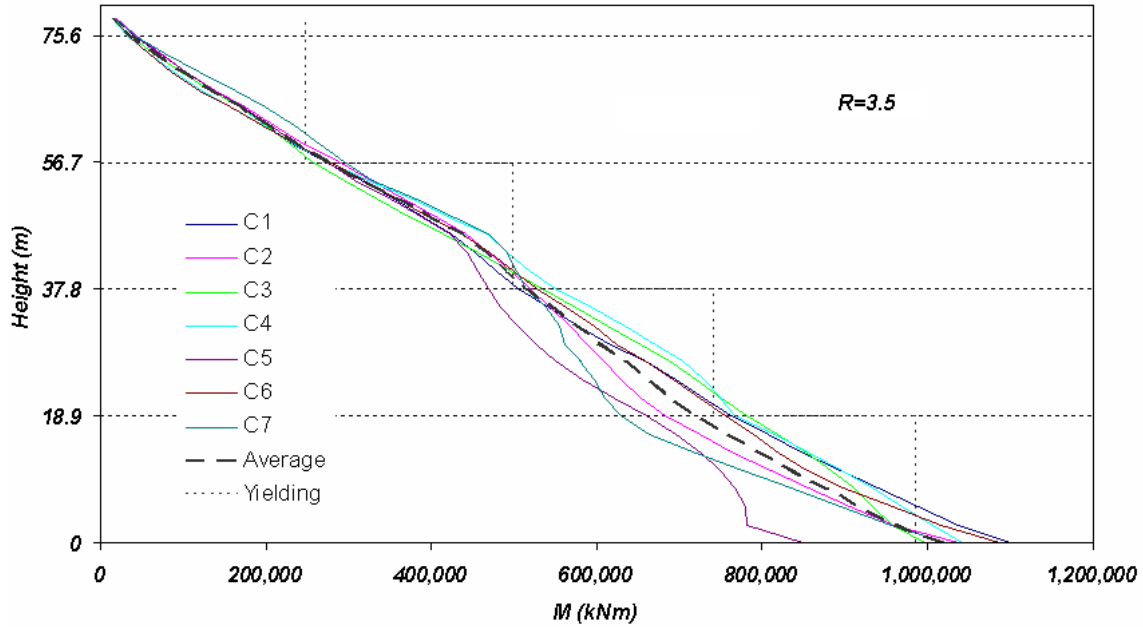




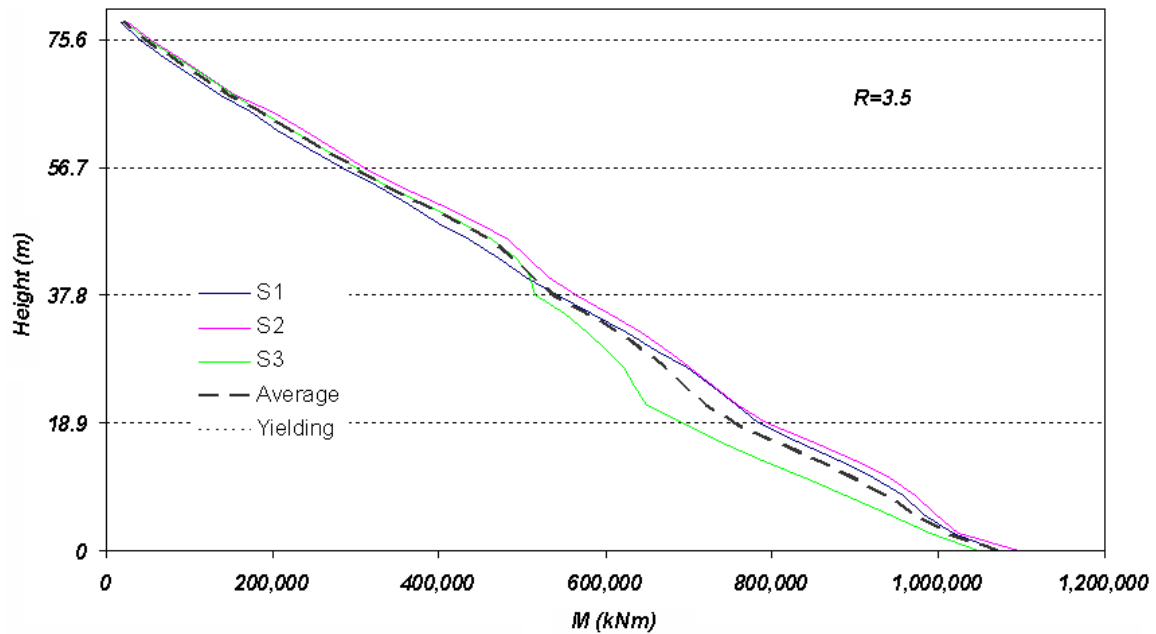




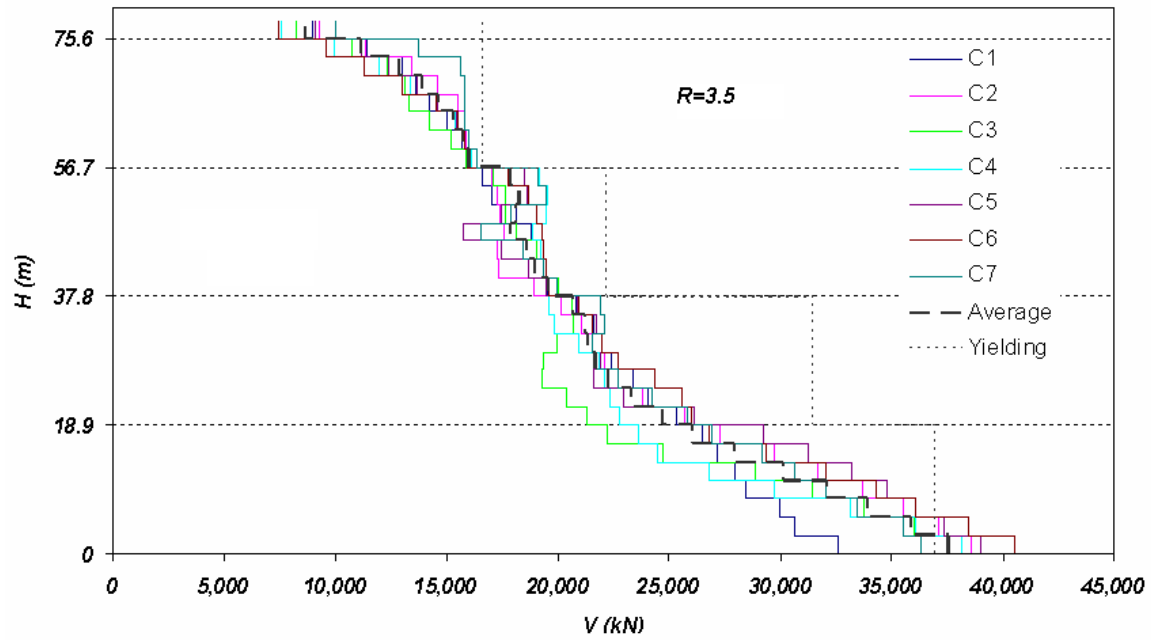
## Appendix D: Nonlinear time history analysis envelopes (See Section 5.8)



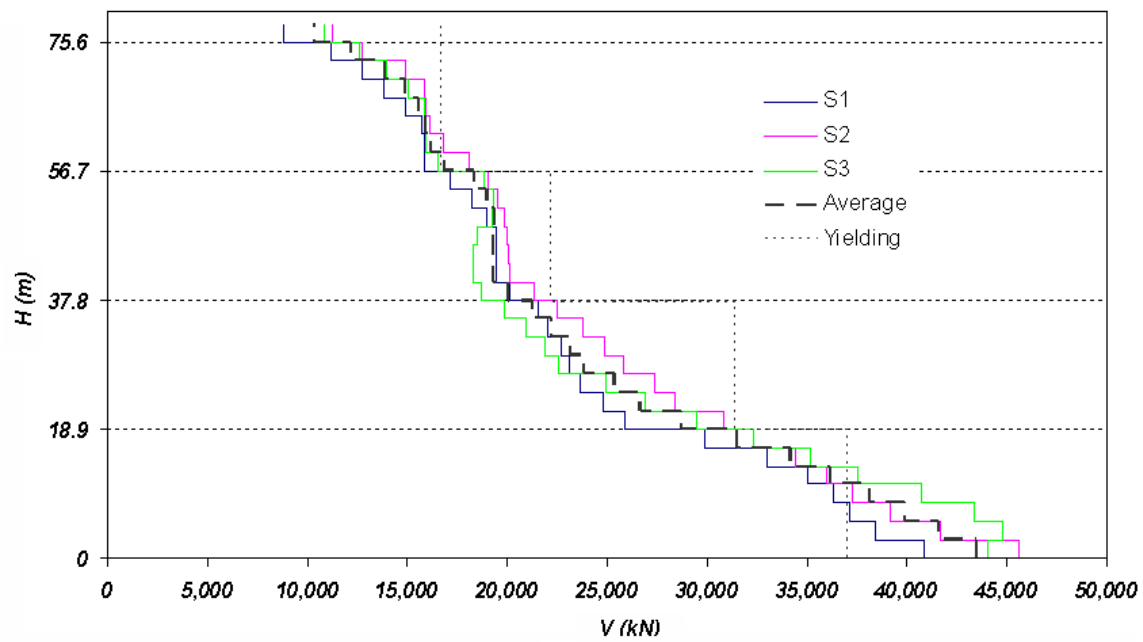
Nonlinear response envelope of bending moment for crustal events( $R=3.5$ ,  $SF=1.0$ ).



Nonlinear response envelope of bending moment for subduction events( $R=3.5$ ,  $SF=1.0$ ).

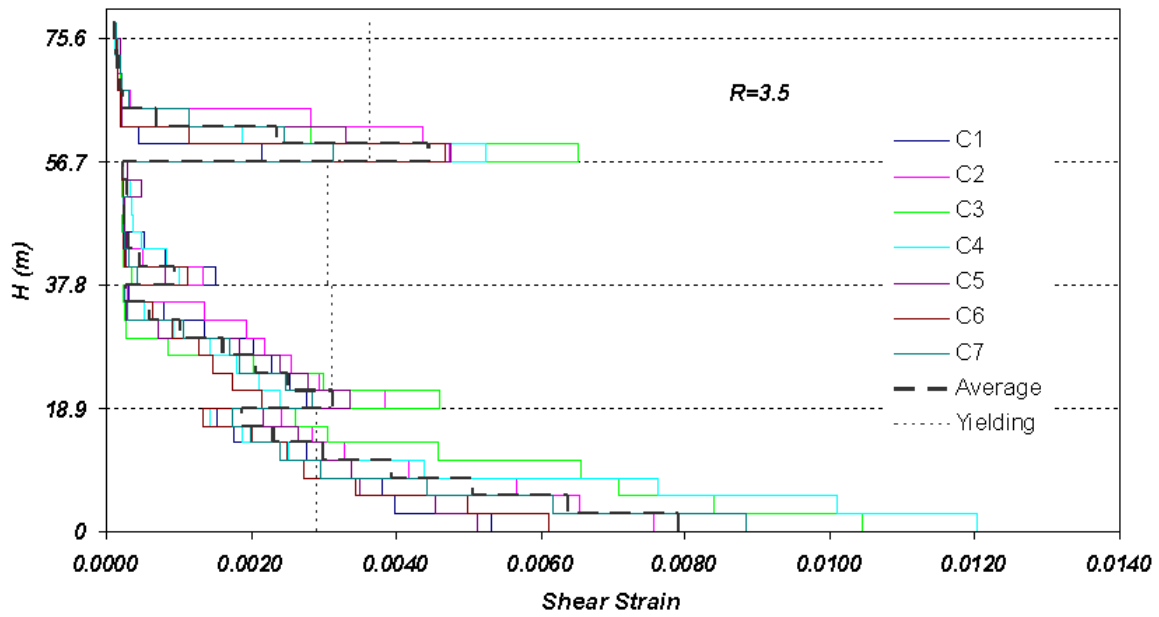


Nonlinear response envelope of shear force for crustal events( $R=3.5$ ,  $SF=1.0$ ).

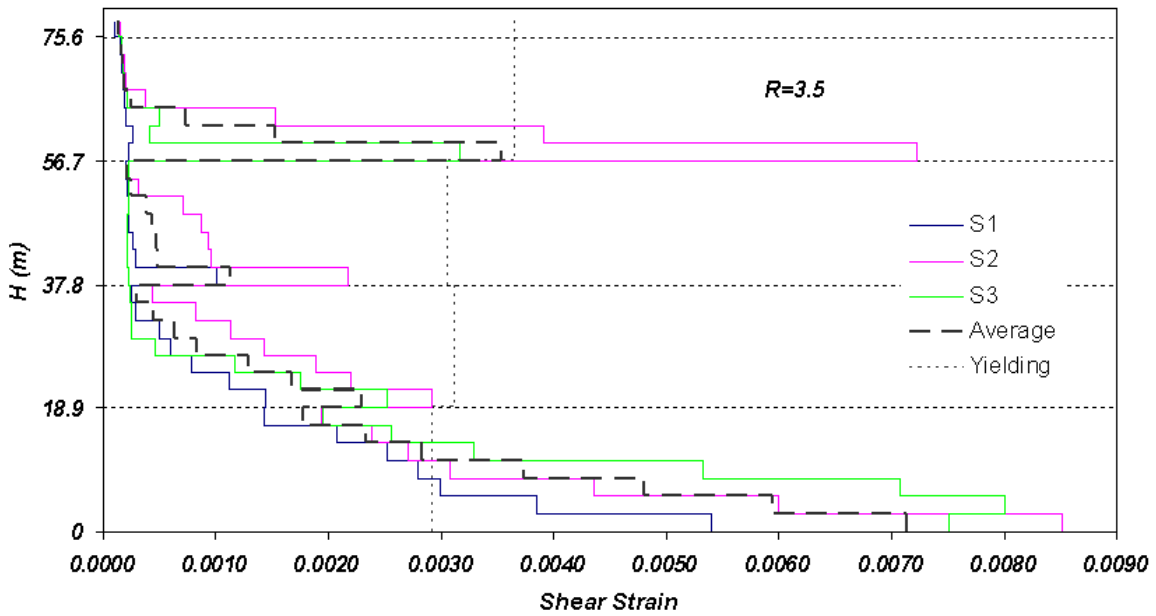


Nonlinear response envelope of shear force for subduction events( $R=3.5$ ,  $SF=1.0$ ).

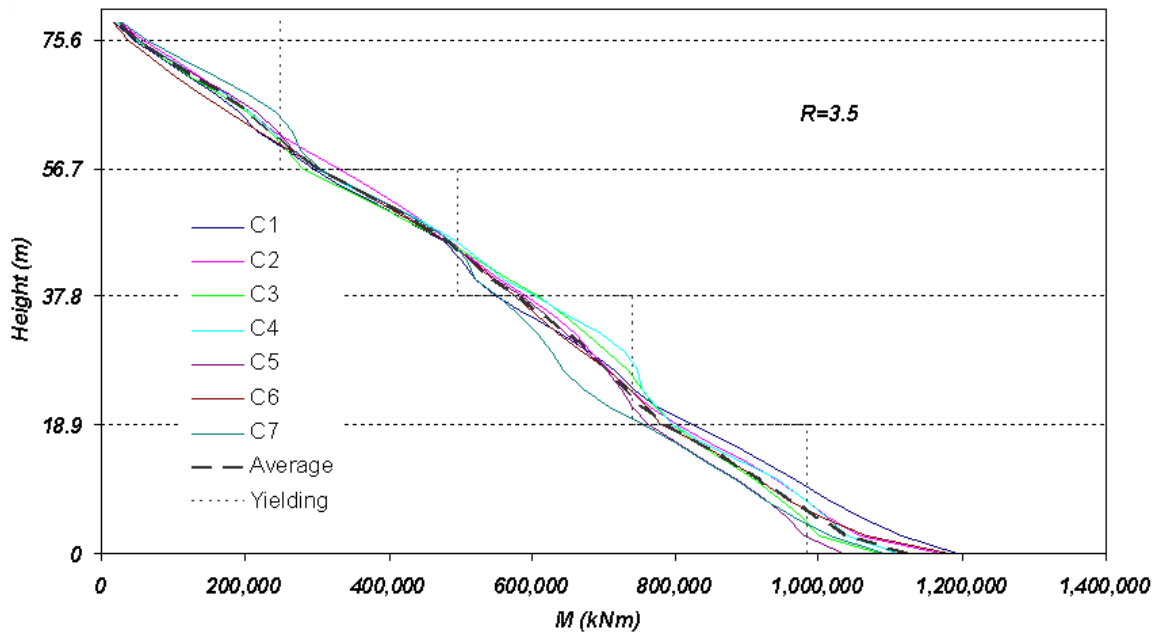




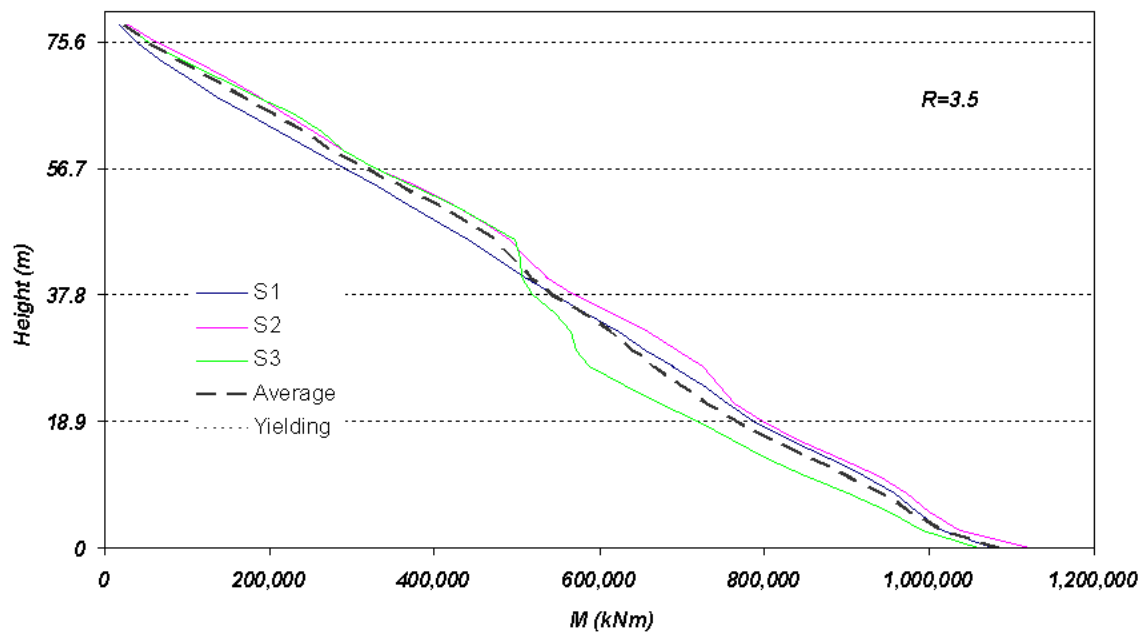
Nonlinear response envelope of shear strain for crustal events( $R=3.5$ ,  $SF=1.0$ ).



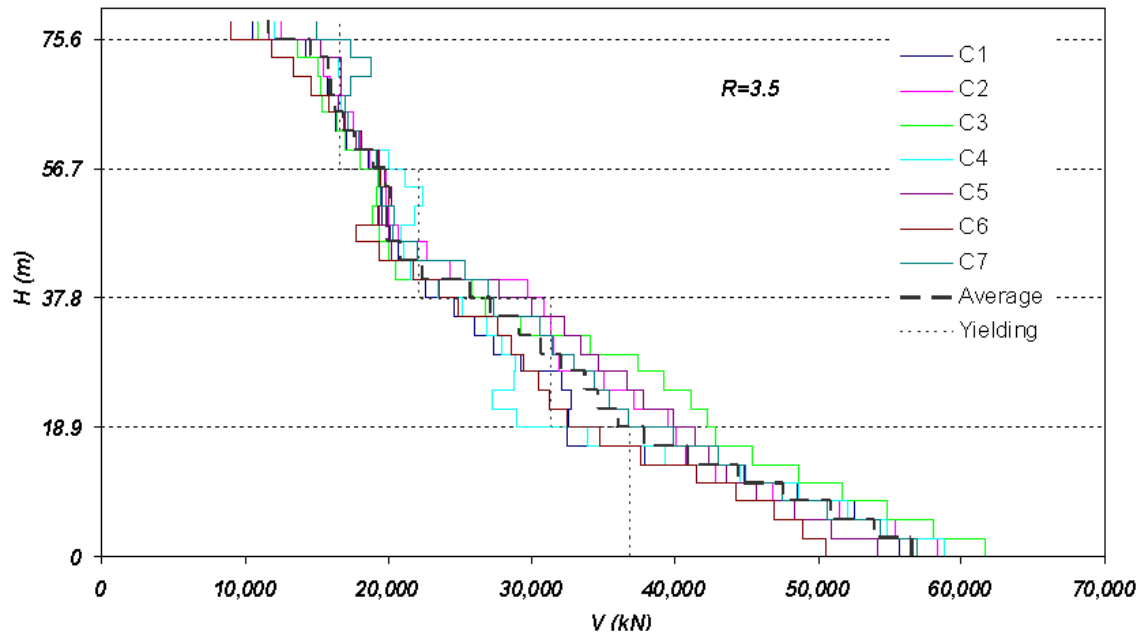
Nonlinear response envelope of shear strain for subduction events( $R=3.5$ ,  $SF=1.0$ ).



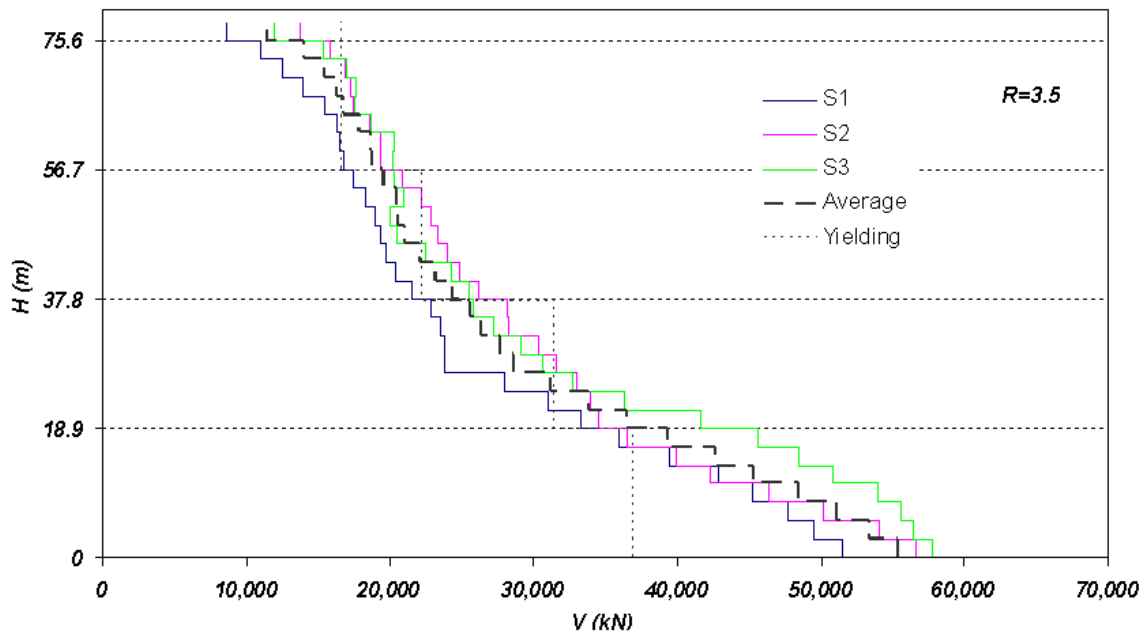
Nonlinear response envelope of bending moment for crustal events( $R=3.5$ ,  $SF=1.5$ ).



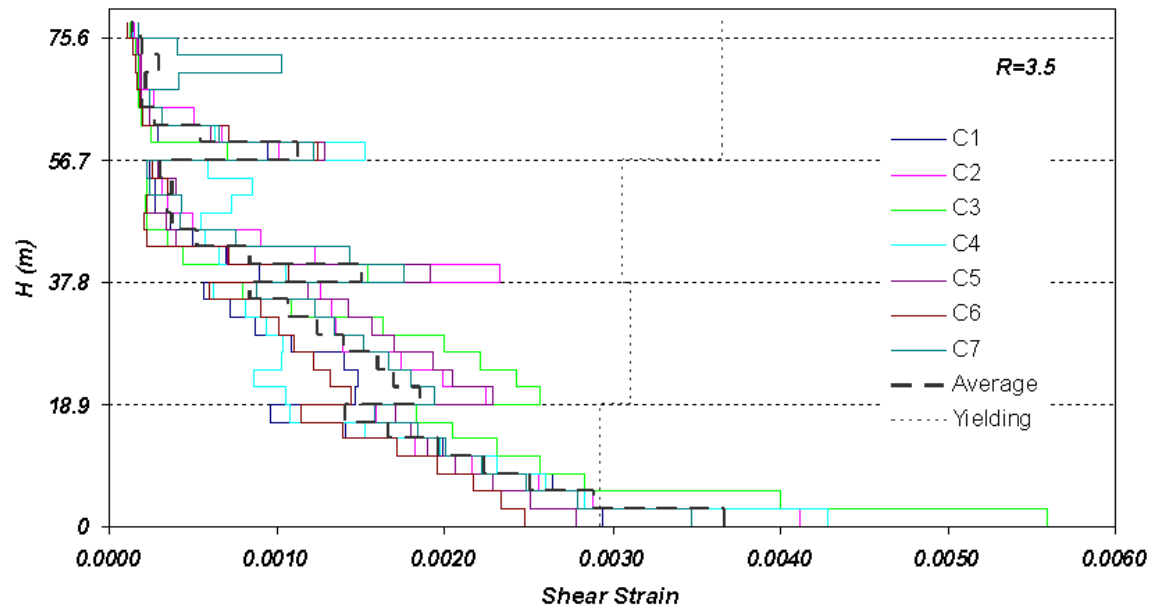
Nonlinear response envelope of bending moment for subduction events( $R=3.5$ ,  $SF=1.5$ ).



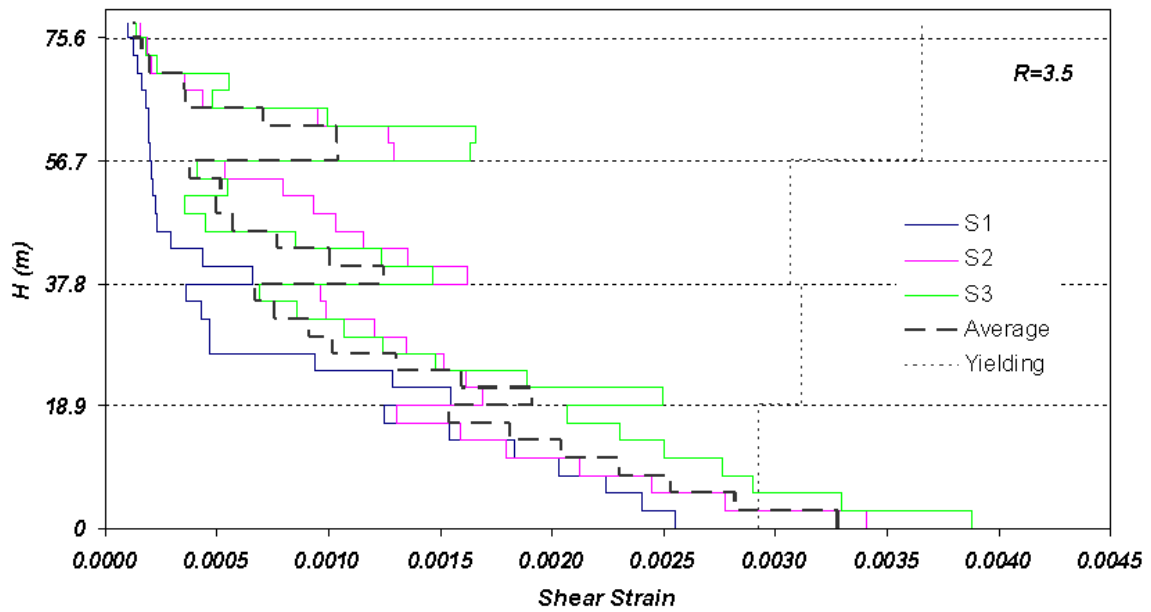
Nonlinear response envelope of shear force for crustal events( $R=3.5$ ,  $SF=1.5$ ).



Nonlinear response envelope of shear force for subduction events( $R=3.5$ ,  $SF=1.5$ ).



Nonlinear response envelope of shear strain for crustal events( $R=3.5$ ,  $SF=1.5$ ).



Nonlinear response envelope of shear strain for subduction events( $R=3.5$ ,  $SF=1.5$ ).